ABSTRACT

Title of Document: FOULING IN FORWARD OSMOSIS MEMBRANE PROCESSES: CHARACTERIZATION, MECHANISMS, AND MITIGATION

Yaolin Liu, Ph.D., 2013

Directed By: Assistant Professor Baoxia Mi, Department of Civil and environmental engineering

As a potential solution to the increasingly severe global water crisis and energy shortage, forward osmosis (FO) membrane process has attracted growing attention in many applications such as desalination, water purification, wastewater reuse, food processing, and sustainable power generation. However, the advancement of the FO membrane process is greatly hampered by a long-standing problem of membrane fouling. Membrane fouling is caused by the accumulation of foreign substances on the surface or within pores of the membrane. Membrane performance, such as energy consumption, water flux, and effluent quality, can be severely deteriorated by fouling. Therefore, developing fouling-resistant membranes is key to more efficient use of FO membrane technologies.

The objectives of this research are to fundamentally understand membrane fouling mechanisms at the molecular level and to develop novel antifouling materials for FO membrane process. Three major research tasks were performed in this study. The first task was to systematically characterize FO membrane fouling behavior by performing microscope-assisted online monitoring experiments to study the kinetics of fouling layer formation and flux decline. The second task was to combine nanoscale characterization experiments (e.g. interfacial force measurement by atomic force microscope) and molecular simulation to understand membrane fouling mechanisms. The third task was to develop novel membrane modification strategies by using hydrophilic materials, such as polydopamine and zeolite nanoparticles, to improve the membrane's antifouling properties in FO membrane process.

Major research achievements are summarized below. (1) A microscope-assisted direct observation FO system was developed to provide critical information on the morphology and formation kinetics of fouling layer for various types of fouling, including organic fouling, scaling, biofouling, and combined fouling. (2) The successful combination of experimental characterization and molecular simulation gave insights into the role of membrane surface characteristics (such as functionality and charge) in FO membrane fouling, thus providing critical information to develop new antifouling FO membranes. (3) Polydopamine and zeolite nanoparticles were successfully grafted onto FO membrane surface. The surface modification proved to greatly increase membrane surface hydrophilicity and to reduce fouling propensity in FO membrane process.

FOULING IN FORWARD OSMOSIS MEMBRANE PROCESSES: CHARACTERIZATION, MECHANISMS, AND MITIGATION

By

Yaolin Liu

Dissertation submitted to the Faculty of the Graduate School of the
University of Maryland, College Park, in partial fulfillment
of the requirements for the degree of
Doctor of Philosophy
2013

Advisory Committee:
Assistant Professor Baoxia Mi, Chair
Professor Allen P. Davis
Professor Peter Kofinas
Professor Alba Torrents
Dr. Christopher M. Stafford

© Copyright by
Yaolin Liu
2013

Acknowledgements

My sincerest appreciation goes to my advisor Professor Baoxia Mi. Professor Mi has been a very dedicated mentor from whom I have learned a great deal and who has continued to offer encouragement and competent advice throughout the entire course of my study and research. I am very grateful for all the opportunities she has given me. It is my hope that I will be able to pass on the knowledge I have gained from her down in my future work.

I would like to express my sincere thanks to my committee members: Professors Allen Davis, Peter Kofinas, Alba Torrents, and Dr. Christopher M. Stafford for their guidance and support. Special thanks to Professor Alba Torrents for kindly letting us borrow her lab for the past two years.

I would also like to extend my sincere gratitude to all the previous and current research group members: Eric Rosenfield, Christopher Allison, Samantha Aiello, Maryam Dadabhoy, Amrita Mehta, Ryan Taylor, Vicky Zhu, Yan Kang, Haiyin Yu, Yong Gao, Meng Hu, and Taqsim Husnain for their great help and assistance in the research work. Their scientific spirit and passion for science have greatly inspired me at work. I would like to specially thank Ms. Catherine Birney for her dedicated hard work and continuous support.

I have worked closely with Professors Yongsheng Leng (GWU) and Dongxia Liu (UMD) on collaborative projects. They both have contributed greatly to my learning and research experience in a broad field.

This research was supported by the National Science Foundation under Grant Number CBET-1158601 and was administered by the Department of Civil and

Environmental Engineering at the University of Maryland. I have also been supported in part by a National Water Research Institute-American Membrane Technology Association (NWRI–AMTA) Fellowship for Membrane Technology. These supports are gratefully acknowledged.

Table of Contents

List of Tables

List of Figures

Chapter 1: Introduction

1.1 Motivation

Water scarcity is a rising problem in many regions of the world. Around one-fifth of the world's population, or 1.1 billion people, live in areas lacking access to safe drinking water [1]. Due to problems such as water pollution, overexploitation of groundwater aquifers, uneven water resource distribution and population growth, the need for technologies to use alternative water resources, such as seawater/brackish water desalination and wastewater reclamation, has gained worldwide attention [2-4]. Membrane technologies, such as reverse osmosis (RO) and nano-filtration (NF), have been proved to be reliable methods to produce freshwater from alternative water resources. Currently, RO membrane process is one of the most commonly used desalination technologies due to its reliable performance and relatively low operation cost compared to traditional thermal processes, which requires excessive thermal energy with a low feed-water recovery. However, RO membrane process requires a high pressure to operate the system and is relatively energy intensive [5]. This high energy consumption has been a major obstacle to the wide application of RO membrane technology despite numerous efforts attempting to improve its energy efficiency [6]. Moreover, limited recovery (typically 35–50% for seawater) and brine disposal are also problems we are facing to further advance RO membrane technologies.

The emerging forward osmosis (FO) membrane process is considered a promising alternative technology for wastewater reuse and sea/brackish water desalination. Different from the conventional pressure-driven membrane processes (e.g., RO and NF), FO membrane process uses natural osmotic pressure generated by concentrated draw solutions as driving force to pull water molecules through a semi-permeable membrane from the feed solutions. The diluted draw solution is then re-concentrated to reuse the draw solution and also to produce purified water. FO membrane process may offer advantages such as high rejection of wide range of contaminants, less energy consumption and reduced brine discharge.

In recent years, FO membrane process has attracted more and more research attentions in membrane field. Attempts to develop new membranes, characterize fouling behavior, elucidate membrane fouling mechanisms, optimize draw solutes, and improve membrane surface properties have been made[7-9]. FO has also been applied in many fields, such as seawater/brackish water desalination [10, 11], landfill leachate treatment [12], and liquid food processing [13]. These studies suggested that FO can be a promising technology to extract fresh water due to its low energy consumption and low membrane fouling propensity.

However, the advancement of FO membrane process still faces major challenges. One of the important challenges prohibiting the applications of FO membrane processes is membrane fouling. Although efforts have been made to investigate FO membrane fouling with different foulants [14-28], the fouling

mechanisms in FO membrane processes still remains largely unknown. Studies are needed to gain a better understanding of FO membrane fouling and to develop new FO membrane materials with improved flux, solute selectivity, and enhanced resistance to fouling.

In view of the above challenges in FO membrane technology, this study aims to understand membrane fouling mechanisms in FO membrane process and explore surface modification strategies to improve membrane antifouling properties. FO membrane fouling behavior was analyzed by a microscope-assisted, online-monitoring tool. The foulant-membrane interactions were characterized by atomic force measurements. Molecular simulation was conducted to understand foulant-foulant and foulant-membrane interactions at molecular level. A few membrane surface modification strategies were explored to improve the fouling-resistance of FO membrane. The results from this study will pave the way for the advancement of FO membrane processes to enhance water and energy sustainability.

1.2 Objective and Scope of Work

The overall objectives of the study are to fundamentally and systematically understand FO membrane fouling mechanisms and develop effective surface modification strategies to facilitate the design of antifouling FO membranes with high permeability and reduced fouling propensity. These innovative FO membranes will greatly contribute to the advancement of FO membrane technology towards reducing the energy consumption and costs for water

purification and seawater/brackish water desalination. Knowledge gained from this research can also be applied to the development of antifouling microfiltration, ultrafiltration, NF, and RO membranes.

The specific research objectives are as follows:

- To obtain knowledge on the fouling behavior in FO membrane process for different types of fouling, including organic fouling, inorganic scaling, bifouling, and combined fouling;
- To gain a molecular-level understanding of fouling mechanisms in FO membrane processes;
- To develop innovative membrane surface modification strategies to mitigate FO membrane fouling.

The scope of this research includes:

I. A microscope-assisted direct observation FO system was developed to online monitoring membrane fouling layer formation and flux decline for various types of fouling, including organic fouling, scaling, biofouling, and combined fouling;

II. Nanoscale experimental characterization (e.g., atomic force measurements) and molecular simulation were combined to help us gain insights into the role of membrane surface characteristics such as functionality and charge in FO membrane fouling, thus providing critical information to develop new antifouling FO membranes; and

III. Membrane surface modification strategies such as grafting hydrophilic materials (e.g., polydopamine and zeolite nanoparticles) were explored to enhance the antifouling properties of FO membranes. The effects of surface modification on membrane surface properties and fouling behavior in FO membrane process were thoroughly evaluated.

1.3 Dissertation Organization

This dissertation presents my research on the characterization of membrane fouling behavior, understanding of fouling mechanisms, and development of membrane fouling mitigation strategies in FO membrane processes. The background information and literature review, which show the necessity and importance of the study, are presented in Chapters 1 and 2, respectively. The major results and discussion were presented in Chapter 3-8 in journal manuscript format. Major conclusions from this study and recommendations for future study are presented in Chapter 9.

Chapter 2: Literature review

2.1 Forward Osmosis (FO) Membrane Process

In recent years, membrane technologies have gained wide acceptance and made significant progress against competing technologies in the field of water and wastewater treatment. Membranes have gained attention because of their reliable performance, flexible design and competitive cost [29-31]. Currently, water treatment processes employ four types of membranes: microfiltration (MF), ultrafiltration (UF), nanofiltration (NF), and reverse osmosis (RO). As shown in Figure 2.1, the pore size of a membrane determines the size of the particle that will be rejected by it. MF membranes have the largest pore size and reject particles and microorganisms. As UF membranes have smaller pores than MF, they reject smaller bacteria and macromolecules such as proteins. NF membranes have pore size on the order of 10 Å; they further filter out low molecular weight solutes (with MWCO values of 100 to 1000 Daltons). RO membranes are non-porous membranes and, therefore, reject many low molar mass solutes such as monovalent salt ions.

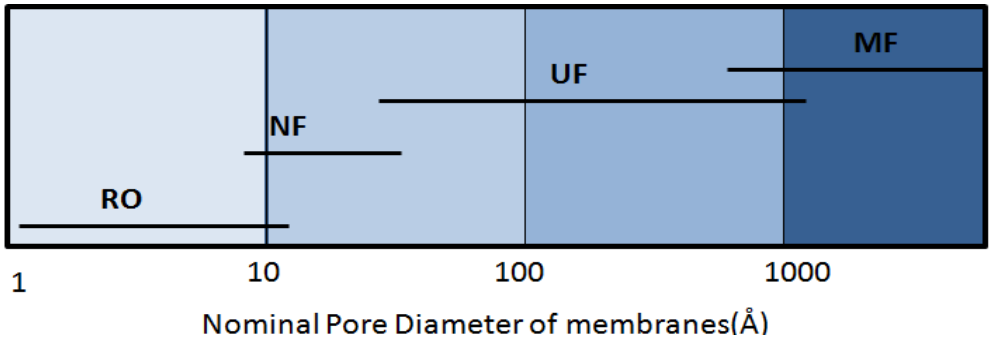

Figure 2.1 Nominal pore size of different membrane types [32].

Currently, RO is widely used for producing freshwater from alternative water resources such as seawater/brackish water and wastewater [33-35]. RO uses selective membranes which are permeable to water molecules but highly impermeable to salts, dissolved organic macromolecules, and other particulate matters. A RO process can produce relatively stable water with a high operation performance. However, RO is an energy intensive process as the system requires high applied pressure (300-500 psi) to operate [36, 37]. Numerous efforts have been made to improve the energy efficiency of RO membrane processes and the cost to produce 1m3 fresh water from seawater has been reduced to $0.50 in current RO plants [38]; however, high energy consumption is still a major disadvantages for the RO membrane process [6, 39-43]. Recently, the emerging membrane process, forward osmosis (FO), has received increasing attention. FO is considered a promising membrane process and potentially a sustainable alternative to RO membrane process for

wastewater reuse and sea/brackish water desalination.

Human beings started using osmosis even before they fully understood the mechanisms of the process; for years, osmosis has been used in many food preservation methods. These methods rely on the fact that the cell membranes of most bacteria, fungi, and other pathogenic organisms function as semi-permeable membranes. So, when the environment's salinity increases during the food preservation process, osmotic dehydration takes place and the cell will either die or temporarily become inactive [44]. In spite of this, the use of osmosis as an engineered separation process in the field of water/waste water treatment is a relatively young technology. Historically, hydraulic pressure was used during filtration processes. But, instead of using hydraulic pressure, FO uses the natural osmotic pressure generated by a concentrated draw solution as its driving force. Water molecules are drawn from the feed solution through a semi-permeable membrane to the draw solution side, as shown in Figure 2.2. The semi-permeable membrane has a similar particulate rejection range as RO membranes and, in addition to producing purified water; the diluted draw solution is concentrated to recycle the draw solutes. Thus, FO may offer the following advantages: a high rejection of a wide range of contaminants, a reduction in energy consumption, lowered brine discharge, and lowered membrane fouling propensity compared to pressure-driven membrane processes [45-47].

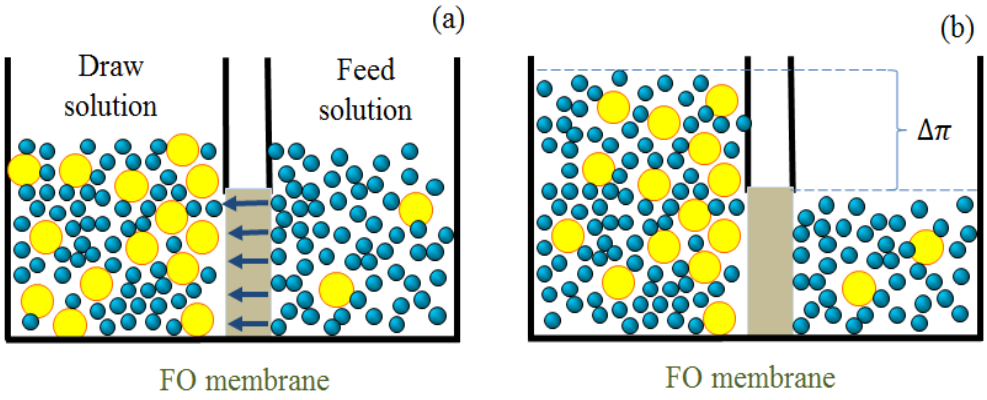

Figure 2.2 Schematic diagram of FO process, (a) water molecules diffuse from feed solution to draw solution driven by osmosis pressure; (b) the process ends when the hydraulic head difference between two solutions equals the osmotic pressure difference, $\Delta\pi$.

In literature, this process is referred to as FO or direct osmosis (DO) for most applications. The concept was first introduced in engineered systems in the 1970s [48-52]. Initially, these studies mainly focused on utilizing FO as a potential alternative for extracting freshwater from seawater. However, the research was hindered by lack of suitable membrane materials. In the 1980s, the superior separation performance of FO was continuously studied in the field of liquid food processing [13, 53, 54]. Until recently, the major developments in membrane materials greatly increased FO flux and, as flux increased, a wide array of interests was drawn to the applications of this technology. Studies on FO are ongoing; currently, progress has been made in fields as diverse as food processing[55-57], sea/brackish water desalination [10, 58, 59], RO pretreatment [60-62], and waste water treatment [28, 47, 63-65], etc. The main problems hindering the advancement of FO include the lack of FO membrane with high permeate flux, the lack of suitable draw solute with high osmotic

pressure, and the lack of effective strategies for controlling the deterioration of membrane performance due to membrane fouling and concentration polarization. A review of attempts in solving these problems is provided in the following sections.

2.2 FO Membrane Materials

Early studies on FO started by testing RO membrane performance under FO operating conditions and commonly used cellulose triacetate (CTA) RO membranes or polyamide (PA) RO membranes. The representative chemical structures of these two membrane materials are shown in Figure 2.3.

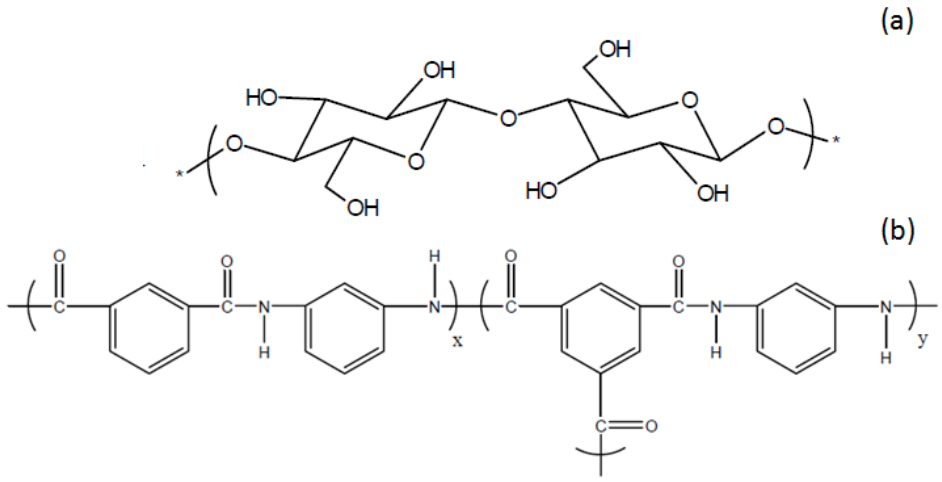

Figure 2.3 Representative chemical structure of two RO membrane materials: (a) cellulose triacetate membrane (CTA), and (b) polyamide membrane (PA).

The first CTA-RO membrane was made by Loeb and Sourirajan in 1962 and proved to have a relatively high water flux with a high salt rejection rate [66]. A CTA-RO membrane is formed by casting a thin film of cellulose triacetate on

a smooth and hard support by dissolving it in an acetone based solution and allowing the acetone to evaporate. During the evaporation, a phase inversion process takes place, resulting in a CTA membrane with an asymmetric structure: a dense surface layer with sub-nanometer pore size and a thick, porous layer with macro scale pores. The dense surface layer is responsible for salt rejection; and the remaining thick, spongy and porous layer provides mechanical strength to the membrane.

A PA-RO membrane is also known as a thin film composite (TFC) membrane. This type of membrane also has an asymmetric structure with a dense thin film layer (200-500 nm in thickness) and a thick, porous support layer (200-300 μm in thickness). The dense surface layer is made of cross-linked aromatic PA and is responsible for salt rejection and separation. The PA layer is formed *in situ* on a porous polysulfone (PSf) support by an interfacial polymerization reaction.

Compared with CTA-RO membrane, the PA-RO membrane has a higher flux, a higher salt rejection rate, and can work in a wider PH range. However, early attempts at using RO membranes for FO applications failed because the membrane flux was much lower than expected. Recent studies revealed that the reduced membrane flux is caused by concentration polarization (CP). When CP happens inside the thick support layers of the RO membranes (internal CP (ICP)), it acts as a diffusive boundary layer which greatly reduced the osmotic driving force for water flux [67]. Detailed information on CP and its effects on membrane flux will be discussed in Section 2.4. In FO membrane process, ICP adversely affects the performance of membranes with a thick support, such as

the CTA-RO and PA-RO membranes. For this reason, the following characteristics are required for a suitable FO membrane: (1) a dense, ultrathin, and uniform active surface layer that provides high solute rejection rate and high permeate flux; (2) a very thin, porous supporting layer in order to reduce ICP and increase membrane flux, but at the same time should be strong enough to provide sufficient mechanical strength to the membrane; and (3) a membrane material with high hydrophilicity to enhance water flux and reduce membrane fouling [68].

In RO membrane process, the thick and porous support layer is indispensable because the membrane must withstand high operational pressures. Since the FO process is solely driven by osmotic pressure differences, the requirement on mechanical strength is lowered for FO membranes. Therefore, modifications can be made to reduce the thickness and adjust the structure of the support layer to mitigate the ICP phenomenon.

In the 1990s, a special CTA membrane for FO was developed by Osmotek Inc. (Albany, Oregon; currently known as Hydration Technology Innovations (HTI))[46]. This membrane was made by casting a thin film of a water-absorbent cellulose triacetate on a nonwoven mesh support. It had an asymmetric structure and reduced support layer thickness. The mechanical strength of the membrane was provided by the embedded fabric support backing. These improvements to the membrane's characteristics made it suitable for the FO process. A variety of FO applications have successfully used this HTI CTA membrane. Currently, it is used in commercialized

applications such as emergency water supply and water purification [47, 60, 61, 69, 70].

Progress has also been made to modify PA membranes to make it suitable for FO membrane process. In 2010, Yip *et al*. reported a high performance thin-film composite PA-FO membrane with structure and performance suitable for FO process [71-73]. For this membrane, the support layer was fabricated on a nonwoven polyester fabric by a phase inversion process with PSf casting solutions. The PSf solution composition was optimized and the synthesis conditions were carefully controlled to obtain an optimal support layer. The resulting support layer has an asymmetric structure with a thin, dense and sponge-like surface layer that is favorable for the formation of a polyamide layer. It also has a loose, finger-like structure on the bottom which provides mechanical support, effectively reduces ICP, and increases permeate flux in FO situations. This new PA-FO membrane offers high chemical and biological stabilities, which mitigate membrane degradation for long-term operations. Draw solutions with higher or lower pH conditions, such as ammonia-carbon dioxide, can be used with this membrane. J. Wei *et al*. observed enhanced FO membrane flux in membranes with the finger-liked structure [74]. Natalia *et al*. [75] investigated the effects of sulphonated materials on PA-FO membranes by using a sulphonated copolymer (PESU-co-sPPSU) made of polyphenylsulfone (PPSU) blended with polyethersulfone (PESU) to fabricate the support layer. The high hydrophilicity of this material allows the formation of a dense, thin (40μm) support layer that results in increased permeate flux [76]. Materials

other than PSf were also tested to fabricate support layers. For example, Song, *et al*. [77] reported that an FO membrane made using PES nanofibers creates a scaffold-like support layer which provides three times higher flux than the HTI membrane. Studies on other materials such as cellulose ester [78] and PES [79] also produced FO membranes with a thin porous support and a thin, dense selective layer. All of these membranes resulted in a low internal ICP and a relatively high water flux.

2.3 Draw Solutes

Draw solution refers to the concentrated solution on the permeate side of the FO membrane. It provides the driving force for the process. An optimal draw solution is generally based on three major criteria. First, the draw solution must have a higher osmolality than the feed solution to produce high osmotic driving force, which produces high water flux. Usually, draw solutes with high solubility and low molecular weight are able to achieve a high concentration, thus producing high osmotic pressures. Second, the draw solution should have a relatively low viscosity in order to reduce concentration polarization. Third, the draw solutes must be easily separable from the solution so that it can be easily reused and purified water can be produced. Developing effective draw solutions is a key for the further advancement of FO membrane technology.

Osmotic pressure

The osmotic pressure of a solution can be calculated by using the Morse equation. This equation is based on Van't Hoff's work on osmotic pressure and

only applies to solutions with dilute concentrations (i.e. <0.5M).

$$\Delta\pi = i * \phi * M * R * T \tag{1}$$

where, i is the dimensionless Van't Hoff factor; ϕ is the osmotic coefficient; M is the molar concentration of all dissolved species (units of mol/L); R is the ideal gas constant (0.08206 L atm mol^{-1} K^{-1}); T is the absolute temperature (K).

From this equation, we see that, for a certain solute, osmotic pressure is lineally proportional to the solute concentration, i.e. the higher the solute concentration, the higher the osmotic pressure of the solution. However, this equation cannot be applied for solutions with high concentrations (usually > 0.5M). To calculate the osmotic pressure of solutions with high concentrations, other factors, such as the viscosity, must be considered. Commercial software is available for the osmotic pressure calculations. An example is given in Figure 2.4 with osmotic pressure calculated by OLI Stream Analyzer 2.0 (OLI Systems Inc., Morris Plains, NJ) [80] for both inorganic and organic solutes.

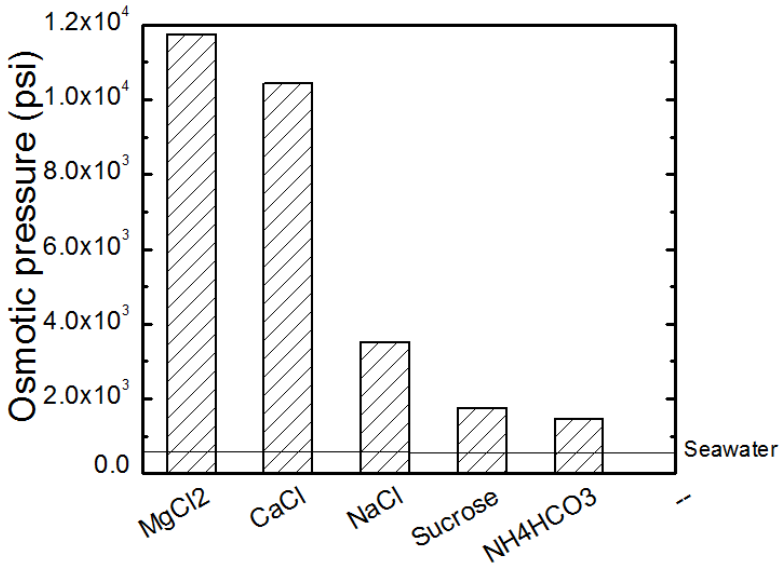

Figure 2.4 Osmotic pressure calculated using OLI Stream Analyzer 2.0for different solutions at a concentration of 4M[46, 81].

Although MgCl2 and CaCl2 demonstrate relatively high osmotic pressure at high concentrations, they are not practical as draw solution due to their low solubility and potential membrane fouling effects. Currently, sodium chloride is widely used in FO processes because of its relatively high solubility and low cost. However, difficulty in separating sodium chloride hampers its application as an optimal draw solution. Ammonium bicarbonate demonstrates high osmotic potential and can be removed from water simply by changing solution conditions such as temperature or pressure [9, 58, 82, 83]. However, using ammonium bicarbonate as draw solution requires the membrane to withstand high pH conditions and the residual ammonium in produced water causes health concerns. Many other attempts have been made to find a suitable draw solution from different materials. Some organic macromolecules with high molecular

weight, such as dendrimers [84] and polypropylene glycol [85], may provide high osmotic pressure. Furthermore, studies show that the nanoscale magnetoferritin [86, 87] may provide high osmotic pressure. In a recent study, concentrated fertilizer solutions were used as draw solution for desalination; the diluted fertilizer draw solutions were used directly as fertilizer [81].

2.4 Concentration Polarization (CP)

One of the major drawbacks of FO process is the inevitable flux decline resulted from concentration polarization (CP). CP is a phenomenon in which the solute or particle concentration in the vicinity of the membrane surface varies from the bulk solution due to water permeation [88-91]. As shown in Figure 2.5 (a), in the immediate neighborhood of the membrane surface, the solute concentration increases on the feed solution side and decreases on the draw solution side. This results in a reduced concentration gradient and thus a reduction in the osmotic pressure difference between the two solutions. As shown in Figure 2.5 (b), the real driving force across an FO membrane, $\Delta\pi m$, is lower than the osmotic pressure difference of bulk solutions, $\Delta\pi$ *bulk*. Therefore, the presence of CP inhibits permeate flow due to the decreased osmotic pressure across the membrane barrier.

In FO, CP can occur on both sides of the membrane. On the feed solution side, solute accumulates near the membrane's surface and results in a higher concentration than that in the bulk. On the draw solution side, solute is removed from the membrane's surface by permeation and, thus, the solution in this region is diluted. When the membrane has an asymmetric structure, CP can

even happen inside the porous support layer. We refer to CP within membrane support layer as internal concentration polarization (ICP) and CP near the membrane surface as external concentration polarization (ECP). Both ICP and ECP reduce FO flux.

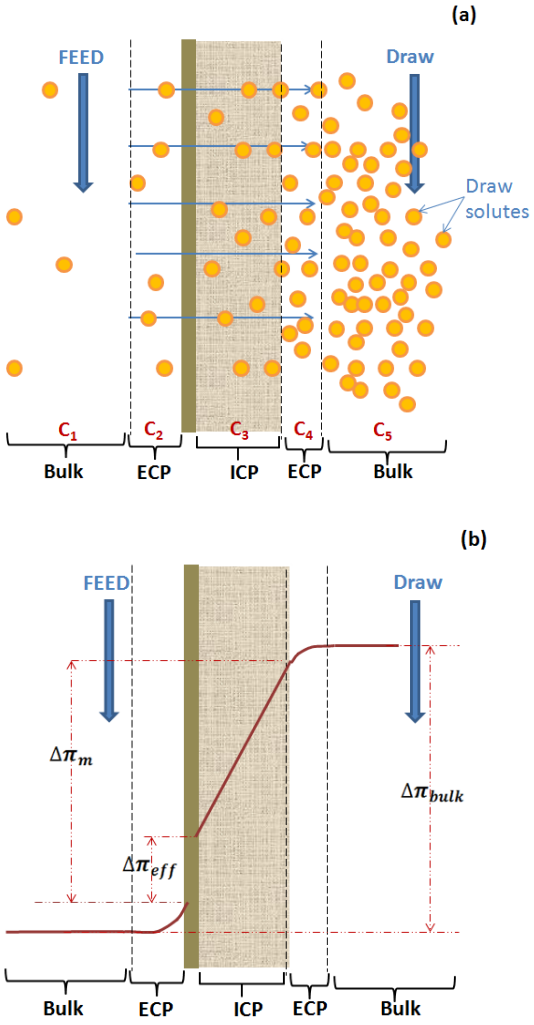

Figure 2.5 Schematic illustration of dilutive concentration polarization across an asymmetric FO membrane, (a) solute concentration polarization phenomenon, (b) CP effects on osmotic pressure.

External concentration polarization (ECP)

External concentration polarization (ECP) can be further divided into two categories: concentrative external concentration polarization (CECP) and diluted external concentration polarization (DECP). CECP occurs in the feed solution side on the active layer of the membrane's surface. This occurs because of the accumulation of the solute and causes an increase in the feed concentration. DECP takes place on the draw solution side and is caused by permeate dilution. Because of DECP, the effective osmotic pressure of the feed solution increases from πF,b to πF,m and that of the draw solution decreases from πD,b to πD,m.

In FO, the standard equation describing FO permeate flux is derived as a function of the difference in the bulk solution's osmotic pressure [92], which is:

$$J_w = A * \Delta\pi = A * (\pi_{D,m} - \pi_{F,m}) \quad (2)$$

where A stands for the pure water permeability coefficient;

$\pi_{F,m}$ is the osmotic pressure of feed solution on the membrane surface;

and, $\pi_{D,m}$ is the osmotic pressure of draw solution on the membrane surface.

The method for modifying the membrane flux model was first published by McCutcheon & Elimelech [67] in 2006.

$$\frac{\pi_{F,m}}{\pi_{F,b}} = \exp\left(\frac{J_w}{k}\right) \tag{3}$$

$$\frac{\pi_{D,m}}{\pi_{D,b}} = \exp\left(-\frac{J_w}{k}\right) \tag{4}$$

Where *Jw* is the permeate flux and *k* is the mass transfer coefficient; and, *k* is related to Sherwood number (*Sh*) solute diffusion coefficient and hydraulic diameter of the flow channel.

$$k = \frac{Sh * D}{d_h} \tag{5}$$

Sh is calculated using the following equation that depends on the flow regime.

$$Sh = 1.85 * \left(Re * Sc * \frac{d_h}{L}\right)^{0.33}, \qquad (laminar\ flow) \tag{6}$$

$$Sh = 0.04 * Re^{0.75} * Sc^{0.33}, \qquad \text{(turbulent flow)} \tag{7}$$

If salt back-diffusion does not take place across the membrane and the standard FO permeates flux equation is modified by taking CECP and DECP into consideration, equation (2) can be transformed to:

$$J_w = A * (\pi_{D,b} * \exp(-\frac{J_w}{k}) - \pi_{F,b} * \exp(\frac{J_w}{k})) \quad (8)$$

However, ECP is not considered the major reason for the reduction in membrane flux in the FO process [9, 67]. Furthermore, ECP can be alleviated by adjusting flow conditions, e.g. ECP effects on membrane flux can be minimized by increasing cross-flow rate and introducing turbulence [46].

Internal concentration polarization (ICP)

Most FO membranes have an asymmetric structure with a thin active layer and a thick porous support layer. When CP takes place inside the porous support layer, it is referred as internal concentration polarization or ICP[93]. It is sometime also referred as Diluted ICP or DICP because the draw solution is greatly diluted by the permeate water within the porous support of the membrane[94]. In FO, as water permeates through the active layer of the membrane, the draw solution is diluted within the porous support structure of the membrane and the structure of the support layer greatly hinders the diffusion of solutes from the bulk solution into the support layer.

The resistance coefficient, K, to solute diffusion inside the porous support layer can be derived from the equations presented by Loeb *et al* [95] for DICP.

$$K = \frac{1}{J_w} * \ln\left(\frac{B + A * \pi_{D,b}}{B + J_w + A * \pi_{F,m}}\right) \quad (9)$$

where B is salt back diffusion coefficient.

If salt back-diffusion is neglected, equation (9) can be simplified to:

$$K = \frac{1}{J_w} * \ln\left(\frac{A * \pi_{D,b}}{J_w + A * \pi_{F,m}}\right) \quad (10)$$

To include DICP, we correct $\pi_{D,b}$ using equation (11).

$$\frac{\pi_{D,t}}{\pi_{D,b}} = \exp(-J_w * K) \quad (11)$$

If we substitute both equation (3) and (11) into (10) and rearrange the equation, the following equation for the permeate water flux is obtained:

$$J_w = A * (\pi_{D,b} * \exp(-J_w * K) - \pi_{F,b} * \exp(\frac{J_w}{k})) \quad (12)$$

Equation (12) models water flux across an asymmetric FO membrane with both internal and external concentration polarization effects considered. Among all types of CP introduced so far, DICP is the key factor responsible for the flux reductions [94, 96]. Earlier studies on testing RO membranes in FO situations

showed a water flux decrease of more than 80% [97]caused by DICP. Furthermore, DICP cannot be mitigated by simply increasing shear force or turbulence in the flow channel; instead, possible mitigation methods must modify the support layer thickness or support layer morphology.

Cake enhanced concentration polarization (CECP)

Hoek & Elimelech discovered the existence of a new source of flux decline for salt-rejecting membranes, named cake-enhanced concentration polarization[98]. Similar studies were conducted by Chong [99, 100] and Sim [101]. During filtration, the accumulation of foulants forms a cake layer on the active surface layer of FO membrane. The cake layer results in a loss of effective osmotic pressure difference (as shown in Figure 2.6) due to hindered solute back-diffusion. Solute back-diffusion resistance is greatly increased due to the lengthened pathway. This means solute back-diffusion is hindered, CP is enhanced, osmotic pressure is reduced and permeate flux is suppressed[102].

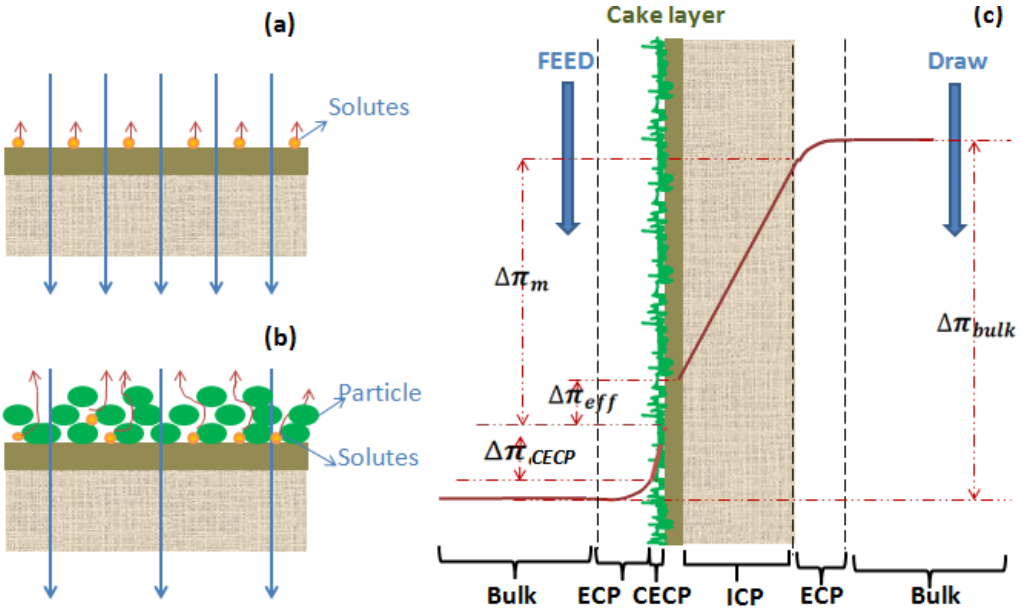

Figure 2.6 Schematic illustration of cake-enhanced concentration polarization across an asymmetric FO membrane, (a) solute back-diffusion without cake layer, (b) solute back-diffusion inside cake layer, and (c) CECP effects on effective osmotic pressure.

2.5 Membrane Fouling

Membrane fouling is the accumulation of foreign substances onto membrane surfaces or into membrane pores which degrades membrane performance (i.e. permeate flux and product water quality), shortens membrane life, and increases system maintenance cost [103-105]. Membrane fouling is a major concern for virtually every membrane process and is widely perceived to be the most significant issue affecting the design of membrane facilities. Membrane fouling is a broad term that includes the accumulation of all kinds of substances on the membrane surfaces. There are four types of membrane fouling: (1) organic fouling, (2) inorganic scaling, (3) biofouling, and (4) colloidal/particulate fouling.

2.5.1 Organic fouling

Organic fouling refers to the adsorption of organic compounds such as humic substances, protein, and grease onto the membrane's surfaces. Organic matter is a major source of membrane fouling as organic matter is prevalent in all natural water sources (e.g. surface runoff, groundwater, and seawater). These natural organic matters (NOMs) in source water are significant factors affecting performance of membrane systems. NOM accounts for a large portion of flux decline for both low and high pressure driven membrane processes [106-108], even if the NOM concentrations are small.

The mechanisms of organic fouling are complicated due to the wide variety of organic foulants existing in natural waters. Most NOMs have no unique composition or structure and their fouling behavior varies in different membrane applications. NOMs interact with minerals in source water (e.g. calcium ions) to form NOM-metal ion complexions which cause severe membrane flux decline [109, 110]. Most NOMs are negatively charged, but naturally existing calcium ions in water neutralize the negative charge of NOM and increase the adsorption of NOM onto membranes [111]. The most important property of NOMs is that adsorption of NOMs reconditions the membrane surface greatly altering membrane surface characteristics and severely affecting the fouling behaviors of other types of foulants [112]. Cleaning removes organic foulants from the membrane's surface and recovers the membrane flux to an extent, especially for FO membranes [24, 27]; however, the accumulation of organic matter on the membrane's surfaces is

almost unavoidable.

2.5.2 Mineral scaling

Membrane fouling caused by mineral scaling is a major problem in membrane processes. CP results in the increased concentration of mineral salt ions in the immediate neighborhood of the membrane's surface. The precipitation of the minerals will occur when their concentration exceeds the salt's solubility. In this case, sparingly soluble inorganic compounds such as calcium sulfate dihydrate (gypsum, CaSO4.2H2O), calcium carbonate (CaCO3) and barium sulphate (BaSO4) are concerns for the pressure driven membrane process [113, 114]. Mineral salt crystal deposition from bulk solutions, as well as direct crystallization onto membrane surfaces, forms a scaling layer that leads to membrane flux decline. Numerous efforts have been made to discover anti-scaling methods. Currently, scaling mitigation strategies mainly focus on reducing concentration polarization by operational optimization and using anti-scalants to hinder mineral salt crystallization [90, 115]. Among all mineral salts, gypsum is the most common scaling source in seawater/ brackish water desalination [91, 116-118]. Furthermore, gypsum scaling is very difficult to control. Gypsum's solubility is not pH sensitive, so gypsum scaling cannot be mitigated by adjusting the solutions' pH [119]. Gypsum scaling usually results in irreversible membrane flux decline and cannot be efficiently recovered by acid cleaning.

2.5.3 Biofouling

Membrane biofouling is a critical problem for all membrane filtration systems

[120-122]. Compared to other types of membrane fouling, biofouling is inherently more complicated for many reasons. A variety of microorganisms, including bacteria, fungi and yeasts, are involved in membrane biofouling and the microorganisms involved depend on the type of source water and the type of pretreatment. In biofilms, the most commonly occurring microorganisms are *Pseudomonas* and *Coryne bacterium* and the fungal genera *Penicillium* and *Trichoderma* [123, 124]. Furthermore, since microorganisms are living cells; they grow, multiply, and relocate on the membrane's surfaces after the initial deposition and attachment [125-128]. Microorganisms in biofilms are held together and protected by a matrix of excreted polymeric organic compounds and extracellular polymeric substance (EPS) which serve as a scaffolding to hold the biofilm together. The result is a formation of complex biofilm structure. Biofouling inevitably occurs in all membrane systems even with the use of pretreatment systems and disinfectant ions such as chlorination.

Table 2.1 Common microorganisms identified in membrane biofilm[123]

Bacteria	*Corynebacterium, Pseudomonas, Bacillus, Artrobacter, Flavobacterium, Aeromonas*
Fungi	*Penicillium, Trichoderma, Mucor, Fusarium, Aspergillus*
Yeasts	Occasionally identified in significant numbers

Biofilms occurring in membrane systems may cause severe loss of performance, requiring the use of costly cleaning procedures to maintain output and quality. The attachment of bacteria and subsequent biofilm growth on the membrane's surface strongly effect membrane system productivity and reliability. When the acceptable operation can no longer be maintained, membrane replacement is

needed. Biofouling has the following adverse effects on membrane systems: (1) membrane flux decline due to the formation of a biofilm of low permeability on the membrane surface; (2) damage to the membrane or membrane biodegradation caused by concentrated acidic by-products that are produced by microorganisms on the membrane surface; and, (3) decreased salt rejection rate caused by the hindered back-diffusion of salt in the neighborhood of the membrane surface.

Theoretically, biofouling can be separated into four stages: (1) Initial attachment and detachment, (2) irreversible attachment, (3) initial biofilm formation; and, (4) biofilm growth. The control of bacteria cell transportation, deposition and permanent attachment to membrane surfaces is essential for controlling biofilm formation. The transportation and deposition of bacteria are affected by system hydrodynamic conditions as well as solution chemistry. As a bacterium approaches the membrane's surface, bacteria-membrane surface interactions start to play an important role [129, 130]. Membrane surface characteristics such as surface hydrophobicity, surface charge, surface functional groups, and surface roughness may play a role in bacteria-membrane interactions. Research shows that bacteria cells prefer to attach to hydrophobic surfaces over hydrophilic surfaces [131]. Bacterial characteristics such as surface charge (related to solution pH), growing phase, and flagella motility play also an important role in bacteria attachment [132, 133]. The lipopolysaccharides (LPS) and extracellular polymeric substances (EPS) on bacteria cell surfaces affect bacteria-membrane surface interactions [134].

2.5.4 Colloid fouling

Numerous colloidal particles, such as clay minerals, colloidal silica, iron/aluminum oxides, manganese oxides, organic colloids and suspended matter, and calcium carbonate precipitates, exist in natural waters. These colloidal particles have ubiquitous characteristics. Colloids cover a wide size range (radius 1 nm-1 μm) and have a large specific surface area where chemicals are adsorbed. Most colloids carry a negative surface charge in natural waters. For the salt rejection membrane process, colloids accumulate on the membrane surface and adversely affect both the permeate flux and solute rejection rate [135, 136]. Colloidal fouling is caused by the accumulation of particles on the membrane surface and the formation of a cake layer. Hydraulic resistance and cake enhanced concentration polarization from this cake layer greatly reduces the water flux [99, 100, 137]. Colloidal fouling is controlled primarily by the surface forces between the particles and between particles and the membrane. These surface forces introduce an energetic barrier which determines the probability of effective particle collisions [138]. This energetic barrier is greatly influenced by water composition, ionic strength and surface characteristics of membrane [139-144].

2.6 Membrane Fouling Mitigation Strategies.

Membrane surface characteristics play an important role in foulant deposition and fouling layer formation. The performance of membrane materials relies largely on surface properties. Altering membrane surface characteristics by membrane surface modification may effectively control membrane fouling.

Membrane surface modification is, therefore, a key area of research for the development of high-performance membrane materials in the membrane industry [145]. Surface modification using either coating or grafting of a hydrophilic polymer onto the membrane surface is a possible route to improving the fouling propensities of FO membranes. A variety of surface modification strategies are found in literature. The aim of these strategies represents the basic philosophy, namely, improving fouling resistance includes decreasing membrane surface roughness; increasing membrane surface hydrophilicity; introducing negatively charged surface groups; and, adding steric repulsion effects to membrane surface[137, 138] (Figure 2.7).

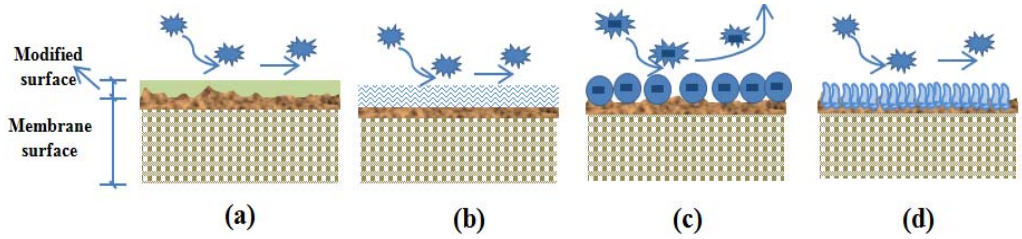

Figure 2.7 Schematic diagrams of surface modification mechanisms: (a) smoother surface; (b) hydrophilic layer; (c) negative charged surface; and (d) hydrophilic polymer brush.

There are two main categories of surface modification methods: coating and grafting. Coating is a process in which coating materials form a functionalized thin-film layer which physically adheres to the membrane surface. Grafting is a method where organic monomers or inorganic particles with surface functional groups are covalently bonded onto the membrane's surface to form a new surface through a composite formation process. Techniques to initiate free

surface radicals for grafting include: (a) Chemical, where free radicals are produced chemically and transferred to the membrane surface to initiate polymerization and form grafted-copolymers [146, 147]; (b) Photochemical and radiation initiation techniques, where free radicals are generated by absorbing lights; and, (c) Plasma initiation technique, where free radicals are generated by plasma irritation. Plasma initiation technique usually refers to a plasma reaction that either results in modification of the molecular structure of the surface or atomic substitution [43, 148, 149].

As a salt rejection membrane process, the integrity of the active salt rejection layer is critical for the operation FO process. Therefore, efforts are needed to develop a surface modification method that does not require harsh conditions.

Polydopamine (PDA) coating

Polydopamine PDA coating is a novel bio-inspired hydrophilic polymer coating method which can increase surface hydrophilicity and enhance membrane flux. PDA has similar properties to that of the secretions of mussels [150, 151]. It polymerizes from dopamine in a pH range of 8.5-9.0 on almost any kind of surfaces. PDA coating shows dramatic improvement in permeate flux performance in both RO process [152-154]and PRO processes [153]. The formation of an adhesive thin film on the support layer side also introduces coating into the inner pore structure of the membrane support layer, which increases the hydropholicity of membrane support layer and wettability of the pores. Thus, the PDA modified membrane exihbits reduced internal

concentration polarization and improved water flux. The membrane antifouling properties also improve with PDA coating [155-157] due to the increased hydrophilic properties.

Nano-particle grafting

Incorporating nanomaterials into membrane structure have drawn significantly attention and have been considered as a promising strategy to tailor membrane surface characteristics and reduce fouling [158-161]. Many attempts have been made to incorporate nanomaterials such as carbon nanotube [160-162], nanosilver [163-165], silicon nano particles [166-168] and zeolite [159, 169, 170] into membrane structure or onto membrane surfaces. The incorporation of nanomaterials may offer a number of advantages such as improved antimicrobial abilities, manufacturing scalability, and the non-depleting by irreversible binding.

Among all the nanoparticles, zeolite nanoparticles are particularly attractive for membrane surface modification because of it allows high water permeability and high surface hydrophilicity. Zeolite material has well-defined, three-dimensional and cage-like structure with uniform microspores ranged from 1-20 Å diameter[171]. The unique structure of zeolite led to their use as molecular sieves and separation barrier. Zeolite membranes have been studied extensively focusing on gas separation [172-174] and liquid pervaporation processes [175, 176]. Theoretical calculations and molecular dynamics simulation [177]have shown that zeolite membranes can be complete reject ions

by size exclusion, which implies its application for desalination. However, the attempts of using zeolite membrane as reverse osmosis membrane for directly salt rejection are not quite successful. Most membranes showed relatively low salt rejection rate and low water flux for practical use. Experimental results showed that the filtration mechanism is not only dependent on size exclusion, but also on Donnan exclusion which reduce the rejection rate of monovalent ions in the presence of divalent ions[178].

The development in nanotechnologies allows other methods of utilizing zeolite materials in membrane technologies. Research shows that the incorporation of zeolite nano-particles into membrane structure provides the opportunity to combine the selectivity of inorganic molecular sieving materials and the processability of polymer membranes [179]. Zeolite nanocomposite membranes have been widely researched in membrane processes such as reverse osmosis [159, 170] ultrafiltration [180-184], and forward osmosis [185] to facilitate rejection and improve flux.

Zeolite nanocomposite reverse osmosis membranes exhibits improved salt rejection rate because of the size exclusion and Donnan exclusion effects of zeolite nanoparticles. Water molecule is more likely to flow through the hydrophilic nanoparticle pores, while salt ions rejected by both polyamide layer and zeolite nanoparticles. NaA-type zeolite nanoparticle with size range of 50 – 150 nm, and a Si/Al ratio of 1.5, and entrance pores of approximately 4 Å were used in the interfatial polymerization process and formed a high

performance thin-film nanocomposite (TFN) reverse osmosis membrane [186]. NaX-type zeolite nanoparticle with larger pores size (7.4 Å) was added to the polyamide layer with similar method and showed higher water permeater flux and reasonable salt rejection rate [159]. NaY-type zeolite nanoparticles with size range of 40 to 150 nm were also added to the polyamide layer of a FO membrane, which exhibited an improve ermeate water flux of 50% [185]. Research on adding Linde type A (LTA) type zeolite nanocrystals with different size of 100 nm, 200nm and 300 nm in polyamide film showed that lower size of nanocrystals kept the integrity of the polyamide film and generated higher water flux and salt rejection rate.

Chapter 3: Combined Fouling of Forward Osmosis Membranes: Synergistic Foulant Interaction and Direct Observation of Fouling Layer Formation

3.1 Abstract

This study investigated the combined fouling by organic and inorganic foulants in forward osmosis (FO) membrane processes. Alginate and gypsum were used as model foulants for organic and inorganic fouling, respectively. A synergistic effect between alginate fouling and gypsum scaling was observed in the combined fouling experiment: the coexistence of foulants caused faster flux decline than the algebraic sum of flux declines due to individual foulants. It was found that the synergistic effect was mainly a result of the aggravated gypsum scaling in the presence of alginate molecules: alginate molecules acts as nuclei in gypsum crystal growth, thus significantly increasing the size of gypsum crystal and accelerating crystallization kinetics. Besides, in the presence of alginate, the dominating scaling mechanism switched from bulk crystallization to surface/heterogeneous crystallization. In order to better understand the effect of alginate on the kinetics of gypsum crystal growth, a membrane window cell coupled with a microscope was used to directly observe crystal formation on the FO membrane surface during the fouling experiments. The direct observation results confirmed the hypothesis that alginate shortens the nucleation time, increases the gypsum growth rate, and changes the morphology of gypsum crystals. Finally, cleaning experiments were performed by rinsing the fouled FO membranes with pure water and continuously introduced air bubbles. It was found that the cleaning efficiency for membranes

fouled by combined foulants was lower than that for membranes fouled by individual foulants.

3.2 Introduction

Due to the increasingly severe interrelated crisis of water and energy, developing low cost methods for wastewater reclamation and seawater desalination has gained worldwide attention [2-4]. As one of the membrane technologies for water treatment, the reverse osmosis (RO) process requires a high pressure to operate the system and therefore is relatively energy intensive [5]. This high energy consumption has been a major obstacle to wide application of RO technology despite numerous efforts attempting to improve its energy efficiency [6].

The emerging forward osmosis (FO) membrane process has received increasing attention as a promising technology for wastewater reuse and sea/brackish water desalination. FO utilizes natural osmotic pressure generated by a concentrated draw solution as driving force to pull water molecules from the feed solution through a semi-permeable membrane to the draw solution. The diluted draw solution is then re-concentrated to recycle the draw solutes as well as to produce purified water. Compared to pressure-driven membrane processes, FO offers a number of potential advantages including high rejection of various contaminants, reduction of energy consumption and brine discharge, and low membrane fouling propensity [45-47] .

Nevertheless, similar to other membrane processes, the FO process suffers from the enduring problem of membrane fouling. Fouling occurs when solutes or particles in the solution deposit onto surfaces or into pores of the membrane.

There are four major types of fouling: (1) organic fouling, which is caused by macromolecular organic compounds such as alginate, protein, and natural organic matters [187]; (2) inorganic fouling, which is due to crystallization of sparingly soluble mineral salts when the salt concentration exceeds saturation; (3) biofouling, which involves bacteria deposition, attachment, and subsequent growth to form biofilm [188] [189]; and (4) colloidal fouling, which results from the deposition of colloidal particles [190, 191]. Depending on its severity, fouling can have varied degree of adverse impact on membrane performance, such as deceasing water flux, deteriorating product water quality, and increasing maintenance burden [192, 193].

Mechanisms of fouling in pressure-driven membrane processes have been investigated extensively [9, 13-15]. In contrast, only a few studies have so far been targeting FO membrane fouling [8, 16-20]. Holloway et al. demonstrated a slow flux decline and high flux recovery rate in the FO process, compared to the RO process, in treating anaerobic digester centrate; the better fouling behavior of FO was hypothetically contributed by less compaction of fouling layer due to the lack of hydraulic pressure [47, 194]. Similar conclusion was drawn by Achilli et al. who compared fouling/cleaning behaviors of an FO membrane bioreactor and a conventional membrane bioreactor [47]. In order to elucidate the fouling mechanisms in the FO process, Mi and Elimelech used atomic force microscopy (AFM) force measurements to study the role of membrane-foulant and foulant-foulant interactions in organic fouling and gypsum scaling of FO membranes [27, 195, 196]. They discovered that (1)

foulant-foulant interactions significantly affect the rate and extent of FO organic fouling; and (2) membranes made of different materials exhibit different gypsum scaling behavior and have different mechanisms. Mi and Elimelech also systematically studied the cleaning behavior of FO membranes [27, 195, 196]. They found that, depending on specific membrane materials, membranes fouled by organics or gypsums could even be thoroughly cleaned by simple water rinsing without using any chemical cleaning reagents. Recently the effects of critical flux and internal concentration polarization on the flux decline behavior of FO membrane were also investigated [197].

It is emphasized that previous studies on FO membrane fouling have focused on single foulants. To the best of the authors' knowledge, there has been no reported study on combined fouling of FO membranes. However, in real-world situations, different types of foulants almost always coexist in natural waters. In addition to organic fouling by the prevalent natural organic matters, gypsum scaling is also possible due to membrane permeation-induced supersaturation of calcium and sulfate ions, which are common in ground or brackish water. Therefore, membranes are most likely fouled by different foulants simultaneously. The individual fouling behaviors alone are already very complex. The co-existence of organic foulants and sparingly soluble inorganic minerals may lead to even more complicated, unique fouling behavior in membrane processes. Fouling studies on RO membranes have demonstrated that, compared to fouling by individual foulants, combined fouling often exhibits dramatically different behavior and involves different mechanisms

[198-201]. Different organic foulants could interfere with each other or one foulant affects the interactions between another foulant and membrane surface. On the other hand, organic fouling could also be affected by other types of foulants. For instance, it has been shown that the presence of inorganic calcium ions may accelerate organic fouling by bridging organic molecules to form a network structure in pressure-driven membrane processes [193, 202, 203].

The objective of this study is to investigate factors that govern the combined organic and inorganic fouling of FO membranes and to elucidate mechanisms that underlie the combined fouling. Alginate and gypsum are used as model organic and inorganic foulants, respectively. A microscopic direct observation method is developed to characterize the fouling layer growth and to understand the effects of cake-enhanced concentration polarization on membrane flux decline not only due to individual organic/inorganic fouling but also caused by combined fouling. The cleaning efficiencies for FO membranes fouled by individual and combined foulants are also investigated and compared.

3.3 Materials and Methods

3.3.1 FO membrane and its characterization

A commercially available cellulose triacetate (CA) membrane from Hydration Technology Innovations (Albany, OR) was used in this study. Membrane samples were stored in deionized (DI) water at 4 °C and soaked in DI water at room temperature for 24 hours before each experiment. The

hydrophobicity/hydrophilicity of the FO membrane was evaluated by measuring water contact angle using sessile drop approach (Kruss G10 goniometer, Kruss, Germany). The pure water permeability of the membrane was determined in a cross-flow RO membrane system. The membrane surface morphology was characterized by AFM (Asylum Research, Santa Barbara, CA). In order to avoid changes in morphology as the CA membrane becomes dried, the AFM images were taken in a fluid cell filled with test solution. The test solution, containing 20 mM NaCl and 45 mM Na2SO4 with total ionic strength of 0.14 M and pH 7.5, has the same components as was used in the corresponding baseline experiments. Before the imaging, a fresh membrane sample was cut and attached to the bottom of a fluid cell with the active layer facing up and soaked in the test solution.

3.3.2 Bench-scale FO membrane system

The fouling and cleaning behavior of the FO membrane was investigated in a bench-scale cross-flow system, as schematically shown in Figure 3.1. A similar system was used in a previous study [27]. This system includes a cross-flow membrane cell with two symmetric flow channels each of 77 mm × 26 mm × 3 mm in dimension. Membrane coupons were placed in the membrane cell between the two channels for draw and feed solutions, respectively. In order to reduce pressure on the suspended FO membrane, co-current flow was introduced into the two channels. Two variable speed gear pumps (Cole-Parmer, Vernon Hills, IL) were used to pump draw and feed solutions into separate closed loops. The cross flow rates of draw and feed solutions were monitored

by flow meters. Both draw and feed solutions were kept at an almost constant temperature (20±1°C) by a refrigerated water bath (Thermo Neslab Inc., Newington, NH). The feed solution was constantly stirred to avoid precipitation of foulants. Change in the weight of draw solution was monitored by a digital balance (Denver Instruments, Denver, CO) and recorded in a computer by data acquisition software (TAL tech, Philadelphia, PA).

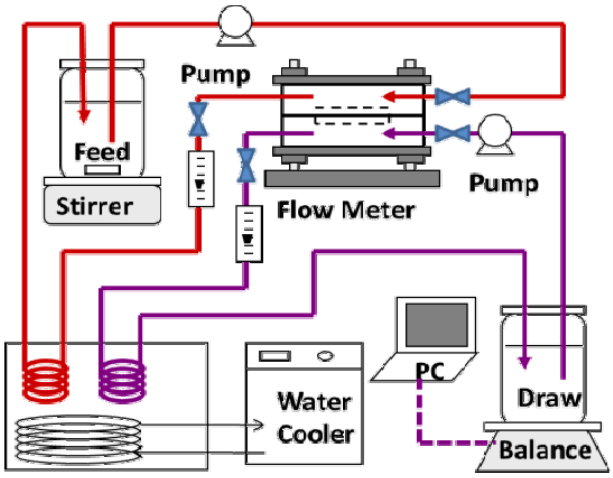

Figure 3.1. Schematic diagram of the laboratory-scale FO system.

3.3.3 Direct observation system

As schematically shown in Figure 3.2, a cross-flow FO membrane direct observation system was employed to monitor in real time the formation of fouling layer during filtration experiments. This system is equipped with a window cell and an Olympus BX51 microscope (Olympus, Japan). A 16 mm × 38 mm glass window is built into the upper plate of the membrane cell to allow direct observation of foulant deposition on the membrane surface. The thickness of the flow channel on the feed side is 1 mm. The rest of the direct

observation system closely resembles the cross-flow FO membrane system previously used in fouling and cleaning experiments [27].

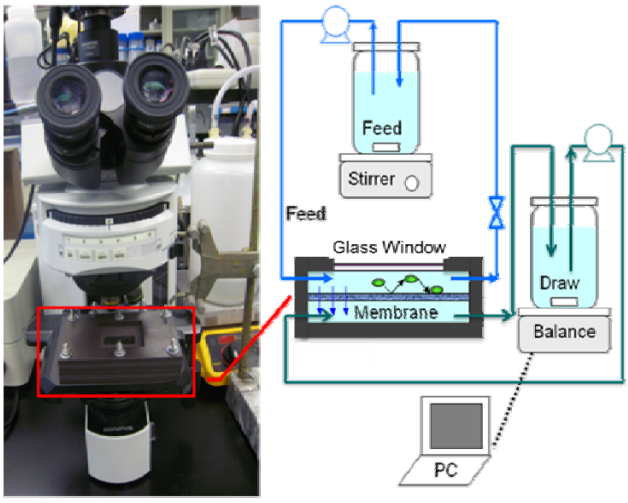

Figure 3.2. Schematic diagram of the direct observation system.

3.3.4 Draw and feed solutions

A 4 M NaCl solution was used as the draw solution in both fouling and baseline experiments. Sodium alginate (12-80 kDa) and gypsum ($CaSO_4 \cdot 2H_2O$) were selected as the model organic foulant and model mineral (inorganic) scaling agent, respectively. Alginate was added into the fouling solution from a concentrated sodium alginate stock solution with a concentration of 10 g/L and stored at 4 °C. Gypsum was added into the fouling solution from stock solutions of 3.5 M $CaCl_2$ and 1 M Na_2SO_4. The concentration of alginate in the feed solution was 200 mg/L. With a saturation index of 1.3, the concentrations of Ca^{2+} and SO_4^{2-} in the feed solution were made slightly higher than the solubility of gypsum. All the chemicals were obtained from Sigma-Aldrich (St. Louis, MO). Detailed composition of feed solutions is

listed in Table 3.1. During the fouling and baseline experiments, the feed solution chemistry was carefully controlled to maintain a relatively constant osmotic pressure.

Table 3.1. Feed solution composition in fouling and baseline experiments.

Foulants	NaCl (mM)	Alginate (mg/L)	Na_2SO_4 (mM)	$CaCl_2$ (mM)	$NaHCO_3$ (mM)	Ionic strength (M)
Alginate	20	200	45	1	1	0.14
Gypsum	20	0	20	35	1	0.14
Alginate + Gypsum	20	200	20	35	1	0.14
Baseline	20	0	45	0	1	0.14

3.3.5 Protocols of fouling and cleaning experiments

The procedure to conduct FO membrane fouling and cleaning experiments is described as follows. First, a fresh FO membrane coupon was sealed in the membrane cell with the active layer facing the feed solution channel. Then, the whole membrane system was stabilized with DI water on both sides of the membrane at 20± 1 °C for 30 minutes. Baseline experiment was performed for one hour to obtain the initial membrane flux. Fouling experiment started with 2 L of feed solution and 2 L of draw solution. It continuously ran for 48 hours at a cross flow rate of 8.5 cm/s, pH 7.5, and temperature of 20±1 °C. The permeate water was collected in the draw solution tank. The corresponding changes in the weight of draw solution were monitored, recorded, and later converted to changes in membrane flux. Typically, the feed solution volume was around 1.1 ± 0.2 L at the end of the fouling experiment. After the fouling experiment, membrane permeate flux was shut down and the membrane was immediately rinsed using DI water. In order to enhance physical scrubbing, air

bubbles were introduced into the rinsing water at an interval of 5 minutes. The temperature was kept at 20±1 °C and the cross flow rate was increased to 21 cm/s in the cleaning experiment. After membrane cleaning, baseline experiment was conducted again to determine the membrane flux recovery ratio.

The baseline experiment that was conducted before fouling experiments aimed to eliminate the membrane flux decline due to the decreasing of osmotic driving force. Such a decline was caused by the continuous decrease of concentration difference between draw and feed solutions due to permeation of water from feed to draw. The baseline experiment followed the same protocol as that for the fouling experiment except that there was no foulant in the feed solution.

3.3.6 Protocols of direct observation experiments

In the direct observation experiments, a microscope-equipped window cell FO membrane system was adopted to conduct the fouling experiments. The protocol was similar to what has been described in the previous section, except that a microscope was used to observe the membrane surface through the glass window on the membrane cell. Images of the membrane surface were taken with an objective of 10× magnification and captured by a digital camera connected to the microscopy computer. In the first hour of the experiment, images were taken at a ten-minute interval to capture the initial deposition of foulants. After that, images were taken every hour until the membrane surface was fully covered by foulants. During membrane cleaning, images were taken every five minutes to directly observe the cleaning efficiency. The Image J software was used for image processing [29].

3.4 Results and Discussion

3.4.1 FO membrane properties

The CA membrane used in this study has an asymmetric structure that includes a porous support layer and a relatively smooth active layer. AFM images of the FO membrane active layer are shown in Figure 3.3. The mean roughness of the membrane surface in an area of 10 μm ×10 μm is 25 nm, as determined by image analysis software of IGRO Pro (Lake Oswego, OR). It is observed that the membrane surface is often rougher in areas right above or near the embedded mesh support. The membrane surface is relatively hydrophilic with a water contact angle of around 75± 3°, which was measured under ambient conditions using a KRUSS G10 Goniometer (Matthews, NC). The pure water permeability of the FO membrane measured in an RO operation mode is 9.7×10-13 m/(s·Pa).

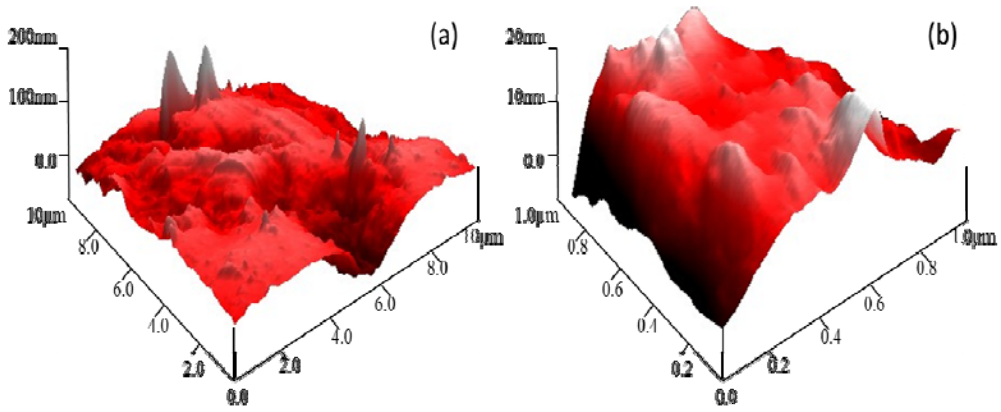

Figure 3.3. AFM images of the FO membrane surface (active layer). The scanning area is 10 μm x 10 μm for image (a) and 1 μm x 1 μm for imiage (b). Note that vertical scales of the two images are different.

3.4.2 Synergistic effects between organic fouling and inorganic scaling

In order to identify any possible synergistic effects between organic fouling and inorganic scaling, FO fouling experiments with single foulants were performed prior to the combined fouling experiments. As mentioned earlier, sodium alginate was used as a model foulant for organic fouling, and gypsum (CaSO4.2H2O) for inorganic scaling. The total ionic strength of fouling solution was kept the same in order to maintain a constant osmotic pressure and initial flux in all fouling experiments.

Figure 3.4 shows the results of FO membrane flux decline caused by individual foulants. No significant flux decline is observed in the alginate fouling experiment, indicating that the initial flux is already below the critical flux associated with alginate fouling. In contrast, the flux decline during gypsum scaling undergoes two stages: the flux decreases at a relatively low rate until at around 2000 minutes when the flux quickly drops below 1 μm/s. The rapid flux decline after 2000 minutes is most likely caused by the concentrating effect, because the concentration of gypsum ions in feed solution almost doubled, which can potentially shorten nucleation time and increase the rate of gypsum crystal growth. Note that the scaling experiment was started with 2000 mL of feed solution, and around 900 mL of water had permeated from feed solution to the draw solution by the end of 2000 minutes.

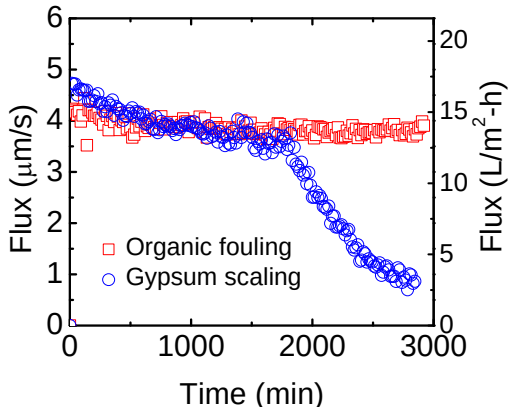

Figure 3.4. Comparison of FO membrane flux declines during single-foulant experiments. Experimental conditions were: 4 M NaCl as draw solution in both experiments; feed solution total ionic strength kept at 0.14 mM by adjusting the concentration of Na2SO4; feed solution pH kept at 7.5 by adding 1 mM NaHCO3; temperature of 20±1oC; cross-flow rate of 8.5 cm/s; 200 mg/L sodium alginate used as the organic foulant, with 1 mM Ca2+ added; the gypsum (CaSO4·2H2O) saturation index equal to 1.3 in the scaling experiment, with 35 mM CaCl2, 20 mM Na2SO4, and 20 mM NaCl in the solution.

A combined fouling experiment was then conducted with both sodium alginate and gypsum in the feed solution to study whether synergistic effect exists between the two different types of fouling. As shown in Figure 3.5, when both alginate and gypsum are present in FO membrane process, a rapid flux decline occurs even at the beginning of the fouling experiment. In contrast, superposition of the flux decline curves associated with individual foulants leads to a much slower initial decline.

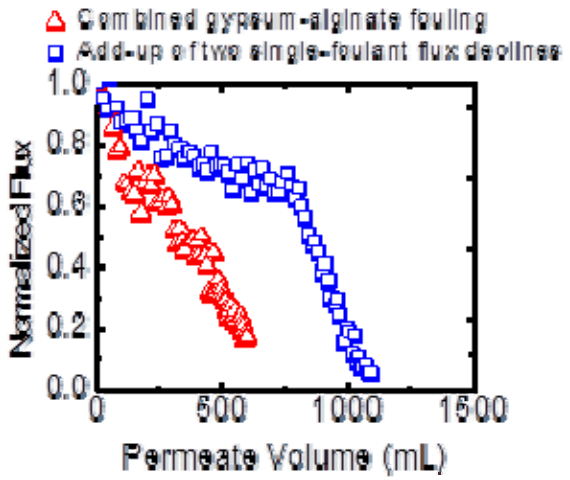

Figure 3.5. Flux of FO membrane subjected to combined organic fouling and gypsum scaling. Conditions in the combined fouling experiment were the same as described in Figure 3. 4, except that feed solution contained 200 mg/L sodium alginate, 35 mM CaCl2, 20 mM Na2SO4, and 20 mM NaCl, with a saturation index of 1.3. Algebraic sum of individual flux declines due to organic fouling and gypsum scaling is also presented to highlight the synergistic fouling effect.

The faster initial flux decline in the combined fouling experiment clearly indicates that a synergistic effect exists between alginate fouling and gypsum scaling. That is, the effect of the co-existence of these two types of foulants on flux decline is greater than the algebraic sum of their individual effects. Accordingly, it is important to understand mechanisms that underlie the synergistic effects in order to develop effective strategies for controlling the combined fouling. In the following sections, detailed elucidation of these mechanisms is presented.

3.4.3 Mechanisms controlling the synergistic interactions between gypsum and alginate

Gypsum and alginate in the solution may interact in one or several of the following possible ways: (1) the presence of gypsum (i.e., calcium and sulfate) ions affects the kinetics of alginate deposition and/or structure of alginate fouling layer; (2) the presence of alginate molecules affects the growth or deposition of gypsum crystals; and (3) the deposition of one type of foulants modifies surface characteristics of the membrane and thereby affects the subsequent deposition of the other type of foulants.

Effects of gypsum on alginate fouling

In order to initiate gypsum scaling, elevated concentration of calcium and sulfate ions was used in the combined fouling experiments. It is unlikely that sulfate ions would directly interact with alginate molecules, which mainly contain negatively charged carboxylate functional groups. However, the presence of calcium ions may significantly aggravate alginate fouling. This is because calcium ions are able to bridge alginate molecules together by forming a zigzag structure, eventually resulting in a dense gel layer of alginate on membrane surfaces [204, 205]. Previous study has demonstrated that FO membrane flux decline due to alginate fouling is much faster in the presence of 0.5 mM calcium ions than in the absence of calcium [197]. However, there has been no reported research on the alginate fouling behavior of FO membrane in the presence of very high concentration (for example, 35 mM as used in the present study) of calcium ions.

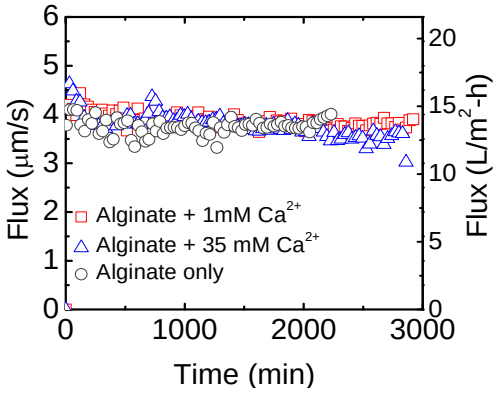

Figure 3.6. Effects of divalent cations on FO membrane organic fouling behavior. 200 mg/L sodium alginate was introduced to feed solution as model organic foulant; Ca2+ ion was added in two sets of experiment at a concentration of 1 mM and 35 mM, respectively (same concentration as used in the combined fouling experiment). Other fouling experiment conditions were the same as those described in Figure 3. 4.

In order to study the effects of calcium ions on alginate fouling behavior, three different concentrations (0 mM, 1 mM and 35 mM) of calcium ions were used in alginate fouling experiments. As shown in Figure 3.6, there is no significant flux decline in any of the three experiments, an apparent difference from the results of a previous study where the addition of 0.5 mM of calcium considerably decreased flux in alginate fouling [197]. This difference is caused by different initial fluxes used in the fouling studies. Compared to an approximate 8 μm/s in the previous study, the initial flux in the present study is 4.5 μm/s, which is most likely below the critical flux for alginate fouling, prohibiting the deposition and accumulation of alginate molecules on the membrane surface. The results indicate that the addition of calcium does not aggravate alginate fouling when the initial membrane flux is below the critical

point.

Effects of alginate on gypsum scaling

Gypsum scaling in membrane processes can be governed by one of the two different mechanisms: (1) heterogeneous or surface crystallization, during which crystals grow directly on membrane surface, and (2) homogeneous crystallization, where crystals are formed in the bulk solution and then deposit on membrane surface [197]. However, it was found in the previous study that variation in membrane materials/surface properties may alter the dominating gypsum scaling mechanism from homogeneous to heterogeneous crystallization [197]. Similarly, alginate may affect gypsum scaling in two different ways: (1) to interfere with homogeneous crystallization by directly interacting with calcium or sulfate ions in bulk solution, or (2) to modify membrane surface properties through adsorption and thereby initiate crystal growth on membrane surface.

In order to elucidate the dominating effect of alginate, the flux declines and fouling layer morphologies from three well-controlled fouling experiments were studied and compared. These experiments were gypsum scaling on clean membrane (i.e., no alginate was added in feed solution), combined gypsum-alginate fouling on clean membrane (i.e., alginate was added in feed solution), and gypsum scaling on alginate conditioned membrane (i.e., alginate was pre-coated on membrane surface but not added in feed solution). Note that the alginate conditioned membrane was obtained by performing an alginate fouling

experiment for 24 hours to allow a thin alginate layer to be evenly coated on the membrane surface, without causing noticeable flux decline. After the coating treatment, the feed solution was replaced by a new gypsum scaling solution to perform the scaling experiment.

Figure 3.7(a) compares the flux decline curves resulting from these three experiments. It shows that the presence of alginate aggravates gypsum scaling, regardless of whether alginate exists in the feed solution or it is pre-coated on the membrane surface. Despite the fact that alginate was mainly present in the bulk solution during the combined fouling experiment, it is unlikely that the worsened flux decline was mostly caused by the direct interaction between alginate molecules and gypsum ions in bulk solution. This is because the most severe flux decline was observed when alginate was present on membrane surface only but not in bulk solution. In fact, when alginate was added in bulk solution, the adsorption of alginate molecules on membrane surface possibly modified membrane surface properties and subsequently stimulated heterogeneous crystallization, which became the dominating mechanism of gypsum scaling, as opposed to homogeneous crystallization in the absence of alginate for the CA membrane.

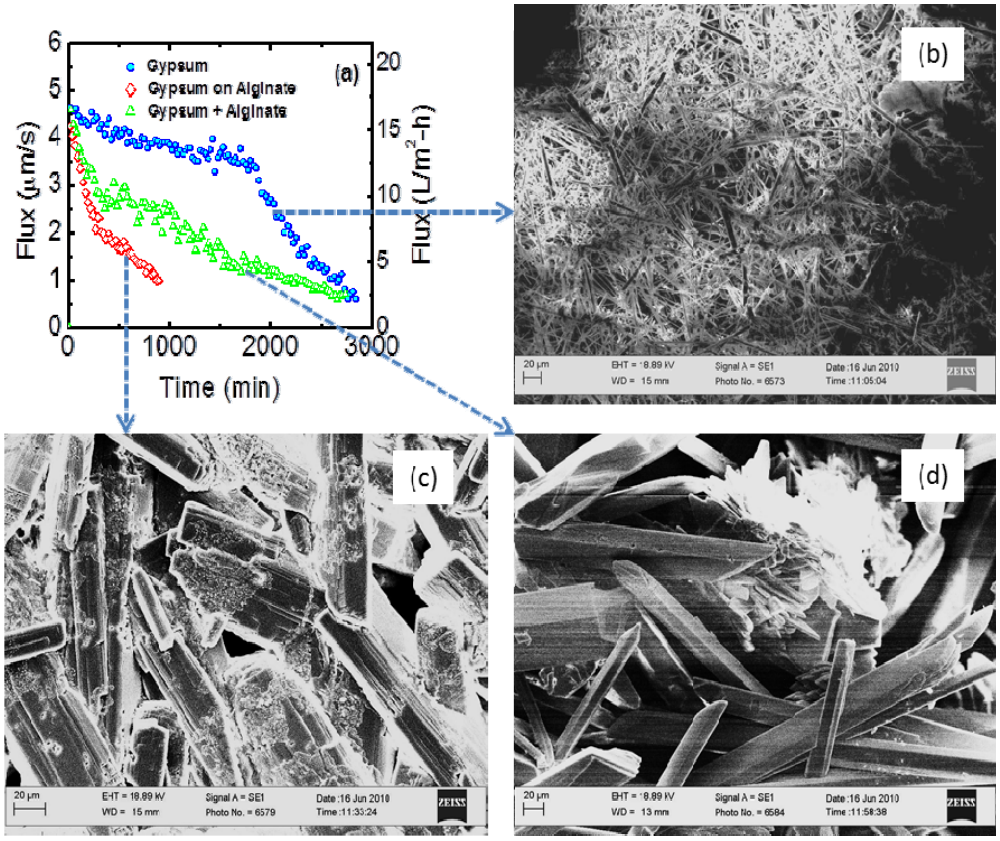

Figure 3.7. Effects of organic foulant on FO membrane scaling behavior: (a) Flux decline in FO scaling with or without alginate; (b) SEM image of gypsum scale on the FO membrane surface; (c) SEM image of gypsum scale on the alginate conditioned membrane surface; and (d) SEM image of combined gypsum-alginate foulant layer on the FO membrane. All images were taken at the same magnification. Scaling experiment conditions were the same as those described in Figure 3.4.

Effects of alginate on the size of gypsum crystals In order to understand how alginate affects the morphology of gypsum crystals, the membrane coupon with intact fouling layer was taken out from the membrane cell after each fouling experiment and analyzed by Scanning Electron Microscopy (SEM). The SEM images of fouling layer samples are shown in Figure 3.7(b-d). Figure 3.7(b)

exhibits the gypsum crystals formed in the absence of alginate; in this case, only relatively small gypsum crystals are observed. Figure 3.7(c) shows gypsum crystals that growed on the alginate conditioned membrane surface; in this case, much larger crystals are observed. As indicated in Figure 3.7(d), the size of gypsum crystals formed during the combined fouling experiment is similar to that of gypsum crystals growing on the alginate coated membrane surface. These comparisons reveal that the presence of alginate molecules, either in solution or on membrane surface, significantly increases the size of gypsum crystals.

Effects of cake-enhanced concentration polarization (CECP) in gypsum scaling on the alginate conditioned membrane

CECP can also play a role in gypsum scaling on the alginate conditioned membrane. CECP takes place when a cake layer formed on the membrane surface hinders the back diffusion of solute, causing an elevated concentration at the membrane surface compared to the bulk solution concentration. In the experiment with the alginate conditioned membrane, a thin gel layer was deposited on membrane surface before the scaling experiment. Although this thin gel layer itself was unable to cause noticeable flux decline, the associated CECP led to elevated calcium and sulfate concentration at the membrane surface, causing gypsum crystallization to start earlier on the membrane surface (i.e., under the alginate gel layer) than in the bulk solution. Therefore, gypsum crystals grow underneath the preexisting alginate layer but not on top of it. This effect is clearly shown in Fig. 7(c): pieces of alginate gel layer appear on top of

a layer of gypsum crystals growing underneath.

3.4.4 Direct observation of the kinetics of gypsum crystallization on FO membrane surface

Direct observation experiments were conducted to observe the kinetics of gypsum crystal formation on membrane surfaces during the fouling experiments. The experimental conditions in the direct observation experiments were kept the same as those in the fouling experiments. The results are presented in Figure 3.8. The upper three images (Figure 3.8(a1-c1)) were taken when gypsum crystal was first detected on membrane surfaces. Figure 3.8(a1) shows that it took two hours for gypsum crystals to appear on a clean membrane surface. In contrast, as shown in Figure 3.8(b1), it only took ten minutes for the first crystal to be spotted on the surface of the alginate conditioned membrane. Figure 3.8(c1) indicates that, in the combined fouling experiment, gypsum crystal appeared after the first hour. Comparison of these three images reveals that the presence of alginate shortened the nucleation time for gypsum crystal formation. Moreover, the nucleation time was much shorter when alginate pre-existed on membrane surface (i.e., in the alginate conditioned fouling experiment) than when alginate was in solution (i.e., in the combined fouling experiment). This is probably because of the CECP effect in the alginate conditioned experiment and also the slow adsorption of alginate on membrane surface in the combined fouling experiment.

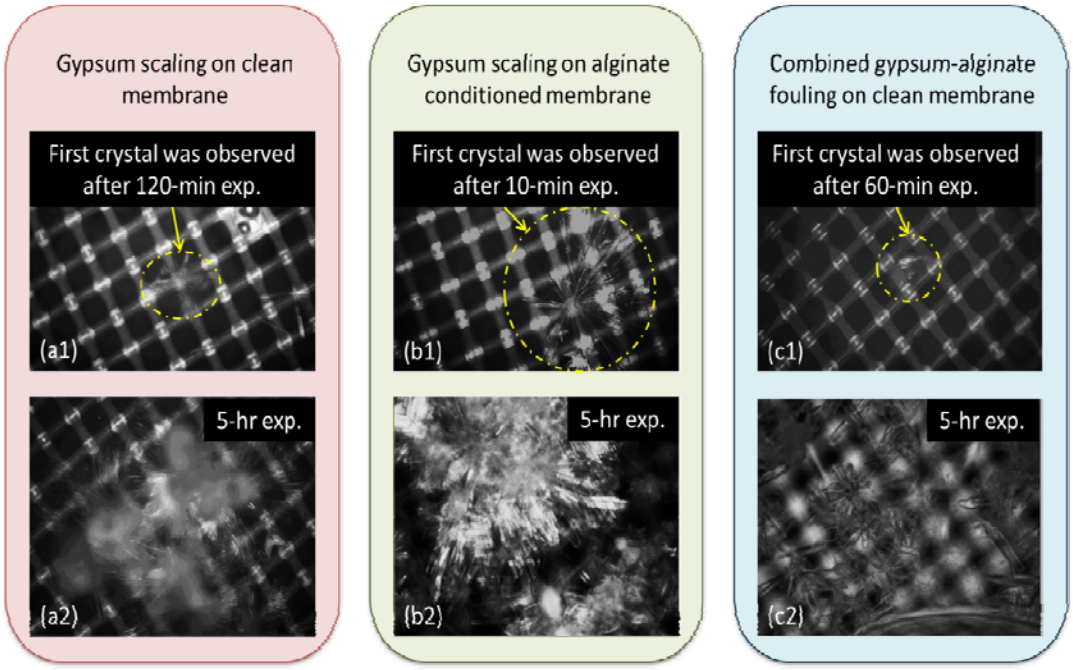

Figure 3.8. Images of the FO membrane surface from direct observation of scaling experiments. The upper three images (a1, b1, c1) were taken when the first gypsum crystal was observed on membrane surfaces. The lower three images (a2, b2, c2) were taken after five hours of fouling experiments. Experimental conditions were detailed in Figure 3.4.

The lower portion of Figure 3.8 gives the images of gypsum crystals formed on each membrane surface after five hours of fouling experiment. Figure 3.8(a2) is the surface image of gypsum crystals growing on clean membrane surface in the absence of alginate. Obviously these crystals have relatively thin branches and form a loose gypsum cluster. In contrast, the gypsum crystals observed on top of the alginate conditioned membrane surface have a much thicker and denser structure, as shown in Figure 3.8(b2). Figure 3.8(c2) presents the gypsum crystals found on clean membrane surface in combined fouling (i.e., alginate was present in solution). In this case, single crystals appear to be thick

but scattered within a gel-like network. Generally, higher surface coverage and thicker crystals were observed when alginate was present, indicating that alginate did increase the growth kinetics of gypsum crystals.

3.4.5 Dominating mechanisms for the combined gypsum and alginate fouling of FO membrane

The synergistic effect observed in the combined gypsum and alginate fouling is mainly caused by alginate significantly affecting the morphology and formation kinetics of gypsum crystals. The specific interactions between alginate molecules and calcium ions play a key role in the process. Gypsum crystal is composed of repeating layers of calcium ions and sulfate ions, while alginate is generally in the form of a long chain molecule with a large number of negatively charged carboxylate functional groups along the chain. Carboxylate groups have a strong tendency to form complexes with calcium ions. As a result, when alginate is introduced into a gypsum scaling solution, the alginate molecule may trap a layer of Ca2+ immediately around its surface. Due to charge effects, this Ca2+ layer could then attract a layer of SO42-, initiating crystal growth around the alginate molecule. As illustrated in Figure 3.9, the crystal formed around a long-chain alginate molecule, which acts as a nucleus, is much bigger than a pure gypsum crystal (such a difference in crystal size is demonstrated by the SEM images in Figure 3.7(b-d)).

In addition, since alginate behaves as the nucleus for crystallization, the time needed for nucleation before crystal starts growing could also be shortened, thereby changing the kinetics of gypsum crystallization, as demonstrated in the

direct observation experiments. Therefore, the combined gypsum and alginate fouling is dominated by the adsorption of alginate molecules on membrane surface followed by heterogeneous crystallization around alginate nuclei, resulting in a combined network of gypsum crystal and alginate gel, as illustrated in Figure 3.9(b). In contrast, although the gypsum scaling on alginate conditioned membrane is also controlled by heterogeneous crystallization with alginate as nucleus, crystals grow from the bottom of the alginate gel layer due to CECP.

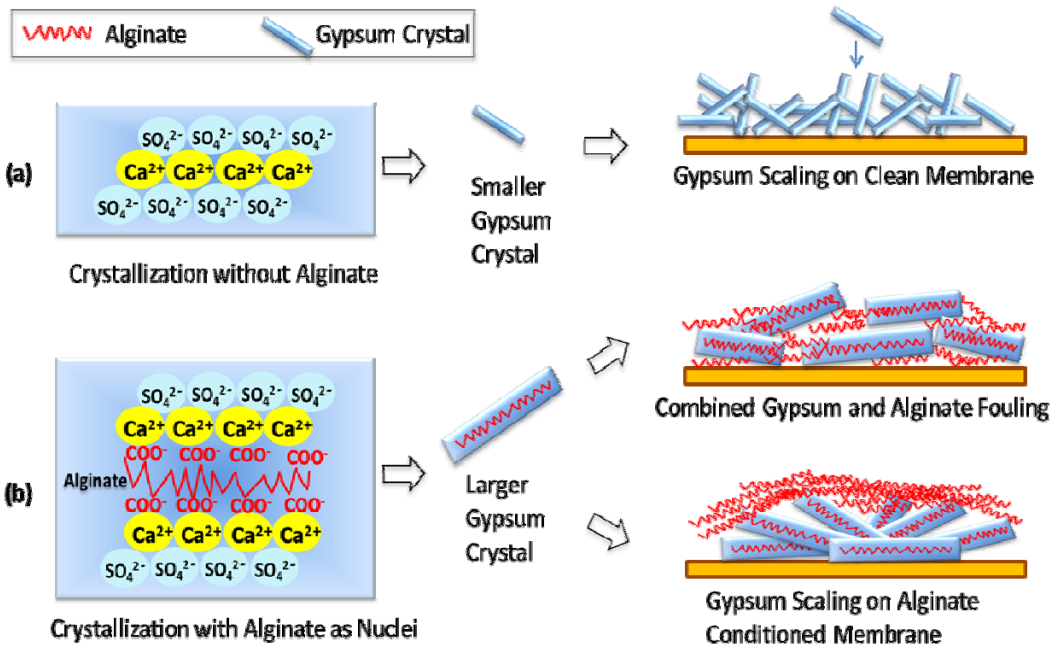

Figure 3.9. Illustration of gypsum scaling mechanism: (a) Gypsum crystal formation in the absence of alginate; and (b) Gypsum crystal formation in the presence of alginate.

3.4.6 FO fouling reversibility by cleaning

Membrane cleaning experiments were performed immediately after each

fouling experiment to test fouling reversibility. Cleaning experiments were conducted by rinsing the membrane with DI water for 20 minutes at a cross-flow rate of 21 cm/s in the absence of permeate flux; air bubbles were continuously introduced to enhance cleaning. Membrane flux was tested under the baseline experiment condition after the cleaning experiment. Results of membrane fluxes before and after cleaning are presented Figure 3.10. These fluxes are normalized by the clean membrane flux obtained from the baseline experiment before each fouling experiment. It is seen that, for gypsum scaling on clean membrane, fouling is almost fully reversible by pure water cleaning. However, when alginate is present either in the solution or on membrane surface, the flux of membrane subjected to gypsum scaling can no longer be fully recovered by the physical cleaning with pure water. However, the results do not necessarily indicate that the combined fouling in FO is irreversible, as it is still possible to fully recover the membrane flux by appropriate chemical cleaning, a topic that deserves further investigation.

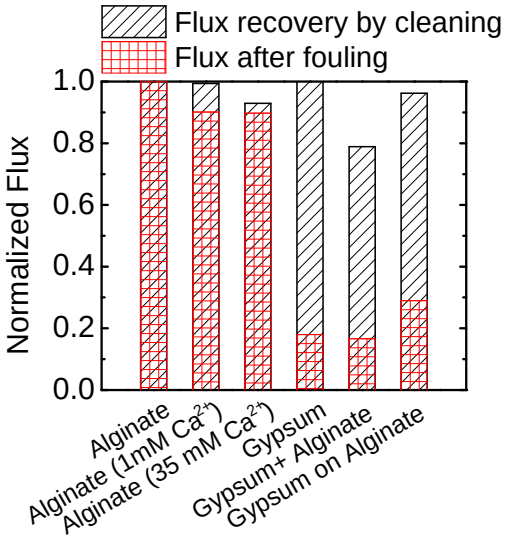

Figure 3.10. Cleaning efficiencies of FO membranes after different fouling experiments. Experimental conditions were detailed in Figure 3.4. Cleaning experiments were conducted by rinsing the membrane with DI water for 20 minutes at a cross-flow rate of 21 cm/s in the absence of permeate flux, with air bubbles continuously introduced. Membrane flux was tested under the baseline experiment condition after each cleaning experiment. The membrane flux presented is normalized by the clean membrane flux obtained from the baseline experiment.

3.5 Concluding Remarks

This study investigated combined organic and inorganic fouling of FO membranes using alginate and gypsum as model foulants. A synergistic effect between alginate fouling and gypsum scaling was observed in the combined fouling experiment. That is, the coexistence of foulants resulted in more severe flux decline than the algebraic sum of flux declines caused by individual foulants. It was found that this synergistic effect was mainly due to the aggravated gypsum scaling in the presence of alginate molecules. However, the

effect of gypsum on alginate fouling was negligible under the present experimental condition where membrane initial flux in the fouling experiment was below the critical point.

Analysis of flux decline results and SEM images indicate that alginate molecules act as large nuclei in gypsum crystal growth, thus significantly increasing the size of gypsum crystal and shortening the initiation time for crystallization. It is also revealed that the dominating scaling mechanism switches from bulk crystallization (in the absence of alginate) to surface/heterogeneous crystallization (in the presence of alginate). In the combined gypsum and alginate fouling, alginate molecules are first absorbed onto membrane surface, and then used as nuclei for heterogeneous crystallization, resulting in a combined network of gypsum crystal and alginate gel. In contrast, although the gypsum scaling on alginate conditioned membrane is also controlled by heterogeneous crystallization with alginate as nucleus, crystals grow from the bottom of the alginate gel layer due to CECP.

In order to better understand the effects of alginate on the kinetics of gypsum crystal growth, a membrane window cell coupled with a microscope was used to directly observe crystal formation on the FO membrane surface during the fouling experiments. The direct observation results confirmed that alginate shortened the nucleation time, increased the rate of gypsum growth, and changed the morphology of gypsum crystals.

The cleaning efficiencies of fouled FO membranes were tested by rinsing the

membrane surface with pure water plus continuously introduced bubbles. It was found that cleaning efficiency for combined fouling was lower than that for individual fouling. The results, however, do not necessarily indicate that the combined fouling in FO is irreversible, as it is still possible to fully recover the membrane flux by appropriate chemical cleaning.

3.6 Acknowledgements

This material is based upon work supported by the National Science Foundation under Grant No.s CBET-1158601 and CBET-1154572. The opinions in this paper do not necessarily reflect those of the sponsor. The first author is also supported in part by an NWRI-AMTA (National Water Research Institute – American Membrane Technology Association) Fellowship for Membrane Technology. These supports are gratefully acknowledged. The authors would also like to thank Dr. Ed Beaudry of Hydration Technology Innovations (HTI) for providing the FO membrane.

Chapter 4: Effects of Absorbed Organic Macromolecule on Gypsum Scaling of Forward Osmosis Membranes

4.1 Abstract

This paper analyzes the effects of organic macromolecule absorption on gypsum scaling in the forward osmosis (FO) process. The base membrane used in the study was a commercially available cellulose acetate FO membrane. The membrane surface was conditioned with a variety of organic macromolecules, including sodium alginate, bovine serum albumin (BSA), and Aldrich humic acid (AHA) prior to performing gypsum scaling experiments. The absorbed organic macromolecules significantly changed the membrane flux-decline behavior under gypsum scaling. Organic macromolecules (AHA and alginate) with a high density of carboxylate functional groups led to increased gypsum crystal size, shortened crystal nucleation time, and faster flux decline, while BSA with its low carboxylate density did not show any significant effects on gypsum scaling. Further characterization of the foulant layer structure and composition suggest that the presence and density of carboxylate functional groups on membrane surface greatly accelerate gypsum crystallization. In addition, fouling-enhanced concentration polarization within the adsorbed organic layer also plays a role in gypsum scaling. Quartz Crystal Microbalance with Dissipation (QCM-D) was used to investigate the behavior of calcium ion adsorption on different organic molecule conditioned layers. The results suggest that the conditioning layer of BSA hindered the adsorption of calcium ions.

4.2 Introduction

Forward osmosis (FO) is an emerging membrane technology ideally poised at the nexus of water and energy. There has been a growing interest in the use of FO as an alternative process for reverse osmosis (RO) or nanofiltration (NF) in a wide range of applications, such as seawater/brackish water desalination [9-11, 81, 206, 207], wastewater treatment[12, 208], and liquid food processing [13, 209]. Unlike conventional pressure driven membrane processes, FO uses natural osmotic pressures generated by concentrated draw solutions as the driving force to pull water molecules through a semi-permeable membrane from the feed solution. This results in a diluted draw solution which can then be reused by concentrating the draw solute and extracting pure water. The advantages of FO over RO membrane processes are low hydraulic pressure with similar rejection rate of a wide range of contaminants. Low hydraulic pressure provides benefits such as the reduction of energy consumption and reduced membrane fouling [12, 210].

There are, however, still some challenges faced by FO such as improving membrane performance and advancing the application of this process. The most important of these challenges is the mitigation of membrane fouling and the improvement membrane flux. Membrane fouling is the accumulation of foreign substances onto membrane surfaces or into membrane pores which degrades membrane performance (i.e. permeate flux and product water quality), shortens membrane life, and increases system maintenance cost [103, 105]. Membrane fouling is a broad term that includes the accumulation of all kinds of

substances onto the membrane surfaces and can be generally divided into four groups: organic fouling, inorganic scaling, microbial fouling, and colloidal/particulate fouling.

Organic foulants such as natural organic matters (NOMs) are prevalent and unavoidable in natural water sources (e.g., seawater, surface water, and groundwater) [106-108]. The adsorption of organic foulants onto the membrane surface not only results in a direct decline in membrane flux, but also changes the membrane surface characteristics, thus greatly affecting the behaviors of other types of fouling. NOMs have a wide range of chemical formulas with no unique structure or composition. Therefore, organic fouling and their effect on subsequent fouling are naturally complicated. Our previous study [211] found that the coexistence of alginate and gypsum in FO membrane processes can result in faster flux decline than the flux declines caused by a single foulant. The most severe flux decline was found when alginate was pre-coated on the membrane surface. Membrane cleaning can remove the adsorbed foulants and recover the membrane flux to a certain degree, especially for FO membranes [24, 27]; however, overtime, the conditioning of membrane surfaces by the accumulation of organic matter is almost unavoidable. Therefore, it is important to understand the fouling behavior of organic macromolecules conditioned membranes in order to develop effective fouling control strategies.

Gypsum scaling is the most common and troublesome scaling found in membrane processes for seawater/brackish water desalination. [91, 116-118] It

is very difficult to control gypsum scaling because gypsum's solubility is not pH sensitive and cannot be mitigated by adjusting the solution's pH. Gypsum scaling usually results in irreversible membrane flux decline and cannot be efficiently removed by acid cleaning. Mechanisms of gypsum scaling in pressure-driven membrane processes are well investigated [117, 118, 212]; however, only a few studies focus on gypsum scaling in FO process. Mi and Elimelech [119] investigated the gypsum scaling behaviors in FO by conducting both macro-scale fouling experiments and micro-scale atomic force measurement experiments. They found that, in bulk solutions, gypsum scaling of cellulose acetate (CA) membrane is dominated by crystallization and subsequent crystal deposition. While in our previous study [211], we found that, when alginate is added to the system, the dominant scaling phenomenon on the CA membrane changed to surface crystallization.

The objective of this study is to investigate how different organic macromolecules, after they absorb onto a membrane surface, may change the membrane surface characteristics and subsequently affect the behaviors of gypsum scaling in an FO membrane process. Three types of organic molecules - sodium alginate, bovine serum albumin (BSA), Aldrich humic acid (AHA) - were used as model organic foulants. Membrane flux was constantly monitored during membrane scaling and cleaning experiments. We also employed a direct observation method to characterize the gypsum scale formation and elucidate scaling mechanisms with different organic macromolecules. Scanning electron microscopy (SEM) and energy-dispersive X-ray spectroscopy (EDS) analysis

were used to characterize gypsum scaling layers formed with each organic macromolecule. QCM-D experiments were conducted to investigate calcium ion adsorption behavior on different organic molecule conditioned layers.

4.3 Materials and Methods

4.3.1 FO membranes

The FO membranes tested in the present study were provided by Hydration Technology Innovations (Albany, OR). The membrane is made of cellulose acetate (CA) and supported by embedded polyester mesh to enhance the mechanical strength of the membrane [12]. The CA membrane has an asymmetric structure with a total thickness of approximately 50 μm based on the examining of SEM images [24]. The pure water permeability of this CTA membrane was tested in RO mode as 9.7×10-13 m/ (s·Pa). More information on the CA membrane can be found in a previous study [211].

4.3.2 Organic and inorganic foulants

All the chemicals needed to prepare fouling solution were obtained from Sigma-Aldrich (St. Louis, MO) and used as received. Three organic macromolecules – bovine serum albumin (BSA), Aldrich humic acid (AHA), and sodium alginate – were used as model organic foulants to represent protein, NOM, and extracellular polysaccharides, respectively, which are three common types of organic macromolecules in natural waters. The properties of the three representative organic foulants are provided in Table 4.1.

Table 4. 1. Characteristics of three organic macromolecules

	MW (kDa)	Surface Functional groups	Carboxylic acidity (meq/g)
Alginate	75-100	-COOH	3-3.5[26]
AHA	20-50	-COOH, -C=O, -NH-, -OH	3.5[27]
BSA	66.4	-C=O, -NH-	1-1.5[26]

Stock solutions of the organic macromolecules (10 g/L) were prepared by dissolving solids in deionized (DI) water with continuously stirring at room temperature for over 24 h. Then, the stock solutions of alginate and BSA were each transferred to sterilized glass bottles and stored at 4 °C, while the AHA stock solution was further purified to decrease ash content in solution following a purification procedure [27, 109]. Stock solutions of CaCl2 (3.5 M) and Na2SO4 (1 M) were prepared for gypsum (CaSO4•2H2O) scaling experiments.

Prior to each scaling experiment, the stock solutions were diluted to desired concentrations for use as the feed solutions in the baseline, organic conditioning, and gypsum scaling experiments, respectively. Chemical composition of the feed solutions is listed in Table 2. Note that the concentrations of Ca2+ and SO42- in the feed solution were made slightly higher (with a saturation index of 1.3) than those of the solubility product of gypsum so that scaling can take place at a reasonable speed [119].

Table 4.2. Chemical composition of the feed solution used in the baseline, organic deposition, and gypsum scaling experiments

Fouling Experiments	NaCl (mM)	Organic matter (mg/L)	Na_2SO_4 (mM)	$CaCl_2$ (mM)	$NaHCO_3$ (mM)	PH	Total Ionic Strength(M)
Baseline Experiment	20	0	45	0	1	7.5	0.14
Gypsum Scaling	20	0	20	35	1	7.5	0.14
Alginate Deposition	20	200	45	1	1	7.5	0.14
BSA Deposition	20	200	45	1	1	7.5	0.14
AHA Deposition	20	200	45	1	1	7.5	0.14

4.3.3 FO membrane system

The scaling and cleaning experiments were conducted in parallel using two bench-scale membrane cross-flow systems (an FO system and an FO direct observation system), which have been previously used for FO fouling study [213]. Basically, the FO system comprises a custom-built cross-flow membrane cell with identically structured rectangular channels (77 mm long, 26 mm wide, and 3 mm deep) on both sides of the membrane. Two variable speed gear pumps were used to generate cross flows that form separate closed loops for feed and draw solutions, respectively. The draw solution tank was placed on a digital scale (Denver Instruments, Denver, CO) so that weight change was monitored by a computer to record the permeate flux. The feed solution tank was placed on a stir plate and feed solution was continuously stirred to avoid foulant precipitation. A constant temperature of 20±1 °C was maintained for both feed and draw solutions using a water bath (Neslab, Newington, NH). The FO direct observation system has a similar set up as the FO system, except that a built-in glass window was created in the membrane cell to allow the online monitoring of scaling layer formation on membrane surface during filtration experiments.4.3.4 Membrane fouling and cleaning protocols

We ran two identical conditioning/scaling experiments for each organic foulant: Experiment (a) investigated the foulant layer formation by direct observation and SEM examining; and Experiment (b) tested the cleaning efficiency by DI rinsing (with air bubbles introduced). Membrane flux declines were monitored in both Experiment (a) and (b) (Figure 4.1).

Each membrane conditioning/scaling experiment was conducted in the following five steps: (1) place a fresh membrane coupon in the membrane cell with the active layer facing the feed solution side; (2) stabilize the system with DI water on both sides of the membrane for 30 min to remove the impurities from membrane surface; (3) test virgin membrane flux under baseline conditions (Table 2)so that the effect of draw solution dilution on membrane flux could be corrected; (4) continuously perform the organic conditioning experiment with freshly prepared feed solution and draw solution for 24 h to introduce an organic conditioning layer on membrane surface; and (5) immediately perform the gypsum scaling experiment by switching the organic conditioning and draw solutions to newly prepared gypsum scaling and fresh draw solutions. Note that all the conditioning and scaling experiments were performed with a cross-flow rate of 8.5 cm/s, pH 7.5 (controlled by adding NaHCO3), and temperature of 20±1 °C. The permeate water flux was monitored throughout the conditioning and scaling experiments by a digital balance connected to a PC.

During Experiment (a), a digital camera connected to a microscope computer was used to capture images of the membrane surface at a magnification of 10×.

Within the initial hour of the experiment, photos were taken every 10 min in order to assess the initial deposition of foulants. After the first hour, images were taken every hour until the full coverage of membrane surface by foulants. At the end of the experiment, the fouled membrane was immediately taken out of the membrane cell and dried in vacuum desiccator for the subsequent SEM analysis.

Experiment (b) was very similar to Experiment (a) except that, as the final stage of the experiment, membrane cleaning was performed immediately following gypsum scaling. Conditions for the cleaning experiment included a cross-flow rate of 21 cm/s, DI as the cleaning solution with air bubble introduced every 5 min, and a cleaning duration of 20 min. The membrane flux was tested after the cleaning experiment to determine the flux recovery. Conditions for the flux test were the same as those for the initial pure water flux test on the virgin membrane.

4.3.5 Quartz crystal microgravimetry with dissipation (QCM-D) experiment for adsorption and cleaning protocols

QCM-D is an effective tool to measure with nanoscale sensitivity the changes in mass, thickness, structural, and/or viscoelastic properties of the adsorbed layer on top of a quartz sensor [214]. The working mechanism of QCM-D is briefly described as follows. When an alternating current is applied to the quartz sensor, it starts to oscillate at its resonant frequency. The adsorption of mass onto the sensor surface is then sensed as a change in sensor frequency (Δf).

In addition, the change in system energy dissipation (ΔD) reveals information about the viscoelastic properties of the adsorption layer. For a rigid adsorption layer (i.e., ΔD < 1), the adsorbed mass can be calculated by the following Sauerbrey equation [215-217]:

$$\Delta m = -C(\Delta f)/n \quad (1)$$

where Δm = the change in adsorbed mass (ng/cm2), C = a constant for the crystal (e.g., 17.7 ng/Hz-cm2 for a 4.95 MHz quartz crystal), and n = the overtone number. If the adsorbed layer exhibits viscoelastic properties (i.e., ΔD > 1), a viscoelastic model can be used to fit the ΔD vs. Δf curve to obtain data for the adsorbed mass (Δm) and other parameters of the adsorbed layer (e.g., thickness, elastic modulus, and viscosity) [214, 218].

In the present study, QCM-D (E4, Q-Sense, Glen Burnie, MD) was used to quantitatively assess the effects of organic conditioning on the adsorption of calcium ions. First, the sensor surface was conditioned using a solution containing 1 g/L organic macromolecules (i.e., BSA, AHA, or alginate). After the adsorption of target organic macromolecules reached equilibrium, the membrane surface with stabilized conditioning layer was rinsed with DI water. Then, 1mM CaCl2 solution was pumped through the system until a new equilibrium was attained. In the end, the system was rinsed with DI water for 20 min. The cross-flow rate in the QCM-D experiments was fixed at 0.15 μL/min.

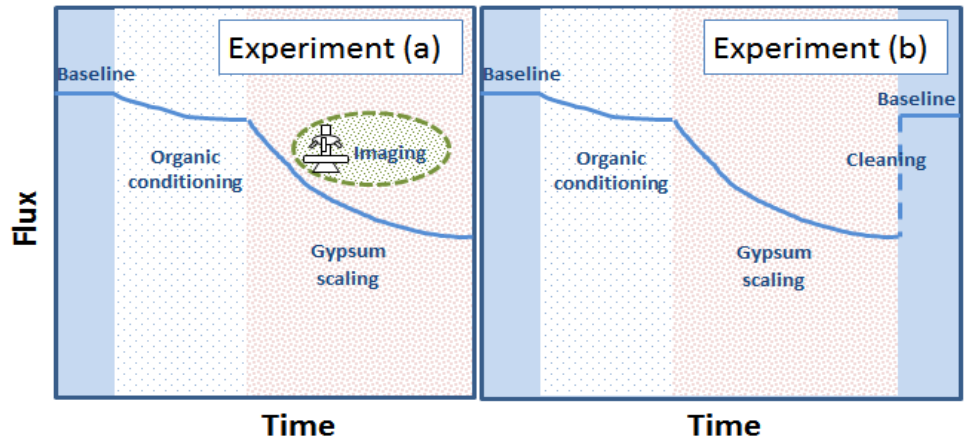

Figure 4.1. Experimental protocols for the conditioning and gypsum scaling experiment.

4.4 Results and Discussion

4.4.1 Membrane conditioning by organic macromolecules

The water flux of the FO membrane was monitored during organic conditioning experiments. The addition of organic foulants (BSA, AHA, and alginate) introduced a layer of organic macromolecules onto membrane surface without significantly reducing the permeability of the membrane. As shown in Fig. 4.2, organic conditioning only resulted in very slow, insignificant (less than 5%) flux decline over the entire conditioning experiments. Severe membrane flux decline typically happens when the fouling experiments were conducted above critical [219-221]. For our experiments, the CTA membrane has a relatively low initial flux due to the internal concentration polarization which takes place in the support layer even with a high draw solution concentration [222]. Under this flux condition, the organic foulants are unlikely to cause severe fouling on the CTA membrane.

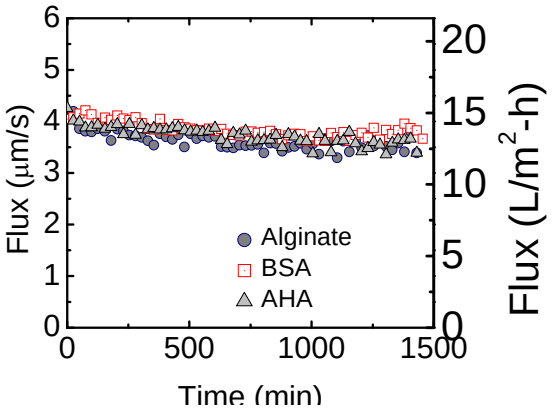

Figure 4.2. Fouling behavior of FO membranes under various organic fouling conditions. Experimental conditions of fouling experiments: 4 M NaCl is used as the draw solution in all experiments; 200 mg/L organic foulant was added to the feed solution; 1 mM Ca2+ is added; feed solution total ionic strength is kept at 0.14 mM by adjusting the concentration of NaCl and Na2SO4; and, feed solution pH is kept at 7.5 by adding 1 mM NaHCO3. The experimental temperature is 20 ± 1ºC and the cross-flow rate is 8.5 cm/s for both draw and feed solutions. Note, the membrane flux presented here has been normalized by the clean membrane flux which is obtained by baseline experiment to eliminate effects of the draw solution dilution.

4.4.2 Effects of organic macromolecule conditioning on gypsum scaling

The effect of organic conditioning on membrane flux decline was studied over the long-term (48 h) scaling experiment, as shown in Fig. 4.3. Note the membrane flux presented in the figure is normalized by the clean membrane flux obtained in the baseline experiment in order to eliminate the effect of dilution of the draw solution. It is seen that, for gypsum scaling on the virgin membrane surface, the flux did not decline severely at the beginning of the experiment while it dropped quickly to less than 20% of the initial flux (J0) after 1000 mL water permeated through the membrane. Such significant flux drop toward the end of the experiment is most likely due to an increase in feed solution concentration, which was almost doubled after 1000 mL water

permeated into the draw solution. In contrast, conditioning of the membrane by different organic macromolecules affected the flux decline to various degrees. Specifically, the alginate conditioned membrane exhibited a much faster flux decline during gypsum scaling: the flux decreased to less than 20% of the initial flux after only 200 mL water permeated through the membrane. For the AHA conditioned membrane, although the flux decline during gypsum scaling was slower than that of the alginate conditioned membrane, such flux decline was still very fast compared with that of the virgin membrane. Of the three conditioning types, the conditioning by BSA led to the slowest flux decline.

The above observations indicate that surface conditioning by alginate and AHA each greatly accelerates gypsum scaling, while the conditioning by BSA slightly inhibits gypsum scaling. Such a difference suggests that the effect of organic conditioning on gypsum scaling may largely depend on the properties of the specific type of organic macromolecules. Therefore, it is important to identify such properties that can lead to more severe scaling.

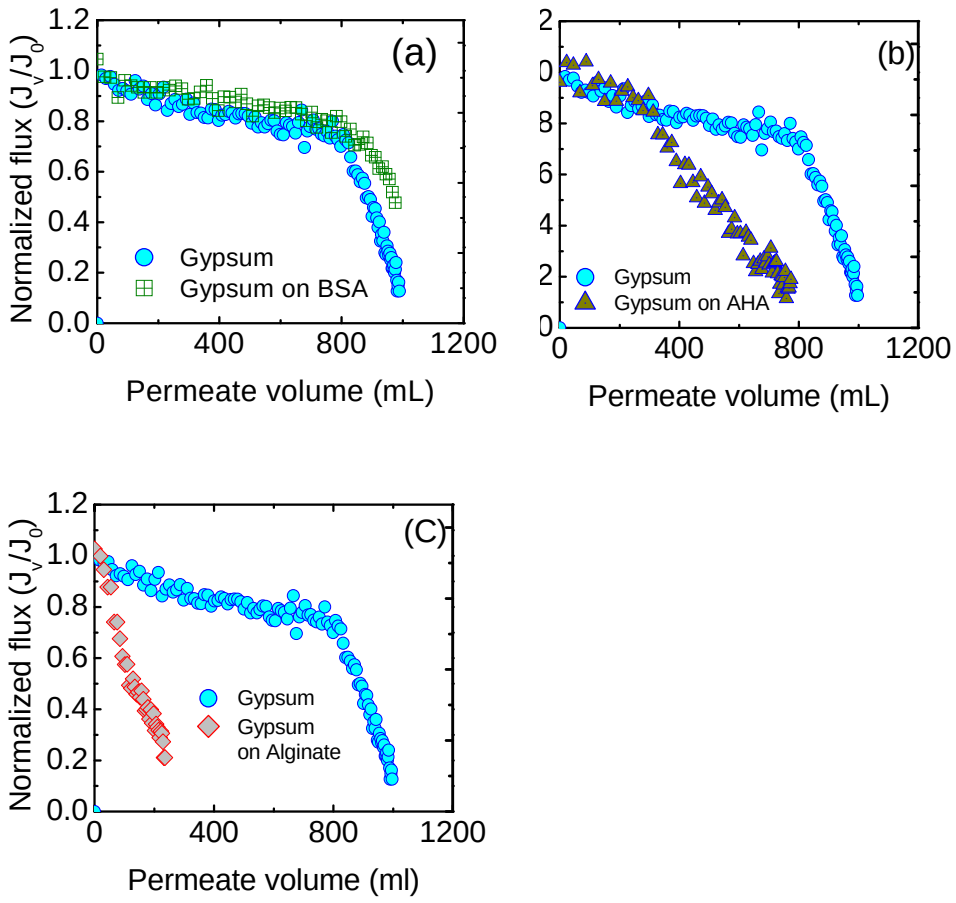

Figure 4.3. Influence of organic conditioning layers on gypsum scaling. Membrane flux decline of gypsum scaling on (a) BSA-conditioned membrane, (b) AHA-conditioned membrane, and (c) alginate-conditioned membrane. Gypsum ($CaSO_4 \cdot 2H_2O$) saturation index (SI) in the scaling experiment is 1.3 with 35 mM $CaCl_2$, 20 mM Na_2SO_4, and 20 mM NaCl in the solution. Other experimental conditions of fouling experiments are the same as those described in Figure 4.2.

The dramatically different flux decline rates of gypsum scaling on conditioned membrane surfaces demonstrate that the adsorption of organic compounds on membrane surfaces could have significant effects on gypsum scaling behavior. The severity of this effect largely depends on the properties of the organic macromolecules. Our results show that the surface conditioning by alginate

and humic acid greatly accelerates gypsum scaling while the conditioning by BSA slightly inhibits gypsum scaling. A better understanding of the sophisticated interactions between organic macromolecules, inorganic ions, and FO membrane surfaces will be of critical importance in order to develop effective FO membrane fouling control strategies.

4.4.3 Effects of organic macromolecule conditioning on flux reversibility

A membrane cleaning experiment was performed immediately after gypsum scaling in order to test the flux reversibility. Membrane fluxes before and after cleaning are compared in Fig. 4.4. It is seen that for gypsum scaling of a virgin membrane, flux is almost fully reversible by simple physical cleaning. In contrast, the flux of an organically conditioned membrane when subjected to gypsum scaling cannot be completely reversed by cleaning. Such a relatively low flux recovery by physical cleaning suggests that the adsorbed organic macromolecules interact with gypsum crystals, resulting in stronger binding between the scalants and scalants or salants and membrane surface.

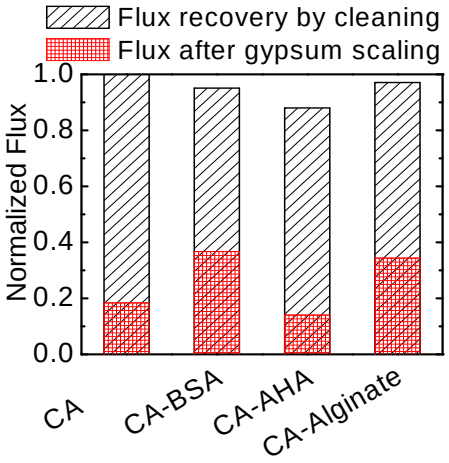

Figure 4.4. Cleaning efficiency of FO membranes after various fouling experiment conditions. Experimental conditions are detailed in Figure 4.2. Cleaning experiments were conducted by rinsing membranes with DI water for 20 minutes at a cross-flow rate of 21 cm/s in the absence of permeate flux and with air bubbles continuously introduced. Membrane flux was tested under the baseline experiment after the cleaning experiment. Note, the membrane flux presented here is normalized by the clean membrane flux obtained under baseline conditions before each experiment.

4.4.4 Effects of organic macromolecule on scaling kinetics and scalant morphology

A membrane cleaning experiment was performed immediately after gypsum scaling in order to test the flux reversibility. Membrane fluxes before and after cleaning are compared in Fig. 4.4 It is seen that for gypsum scaling of a virgin membrane, flux is almost fully reversible by simple physical cleaning. In contrast, the flux of an organically conditioned membrane when subjected to gypsum scaling cannot be completely reversed by cleaning. Such a relatively low flux recovery by physical cleaning suggests that the adsorbed organic macromolecules interact with gypsum crystals, resulting in stronger binding

between the scalants and scalants or salants and membrane surface.

Figure 4.5. Microscopic images (10 x) of membrane surfaces during scaling experiments. All images were taken after 2 hours of the experiment. The red arrows point out where gypsum crystals grow on membrane surfaces. The images show gypsum crystal growing on (a) clean membrane surfaces; (b) BSA-conditioned membrane surface; (c) AHA-conditioned membrane surfaces; and, (d) alginate-conditioned membrane surface. Note, the bright grid structure shown in the first two images is the background noise caused by the membrane supporting mesh.

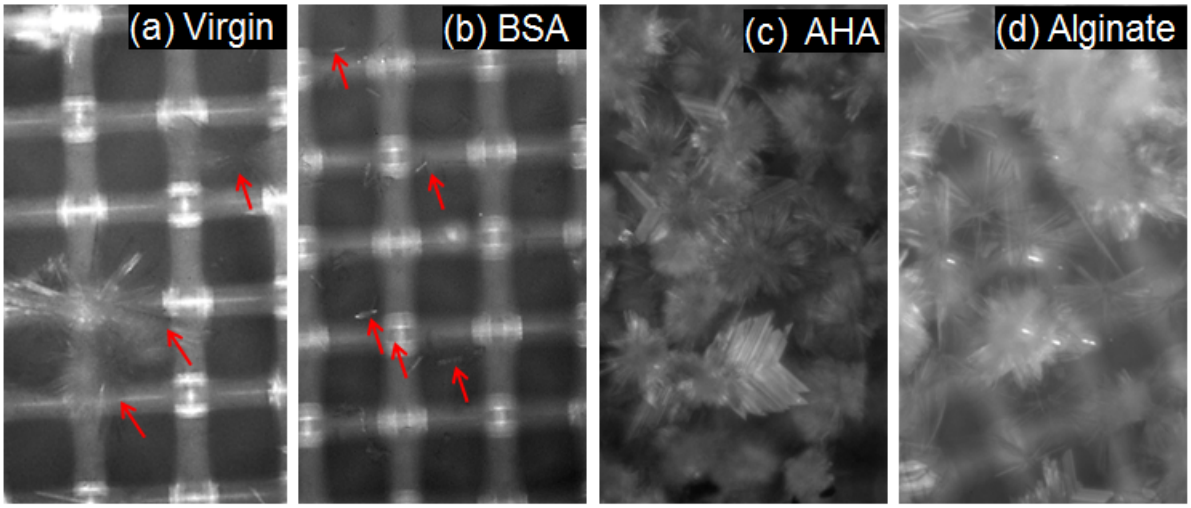

After each scaling experiment, the membrane was taken out of the membrane cell and analyzed by SEM (Carl Zeiss, Thornwood, NY, and Hitachi, JAPAN). The surface and cross-sectional images of the scaling layers are provided in Figs. 4.6 and 4.7, respectively. These images demonstrate that the size and morphology of gypsum crystals can be greatly affected by the conditioning of membrane surface by the specific type of organic macromolecules. Gypsum crystals developed on the virgin membrane surface have a rod-like shape and are relatively small and uniform in size. In contrast, the gypsum crystals on the BSA conditioned membrane appear to be much smaller particles, the crystals on the AHA conditioned membrane have a jelly, cake-like structure, and the

crystals formed on the alginate conditioned membrane are very large in size,. Such observations suggest that the interactions between organic macromolecules and inorganic calcium ions may play a very important role in crystal formation and gypsum scaling on different membrane surfaces. Meanwhile, mechanisms underlying such interactions are most likely different.

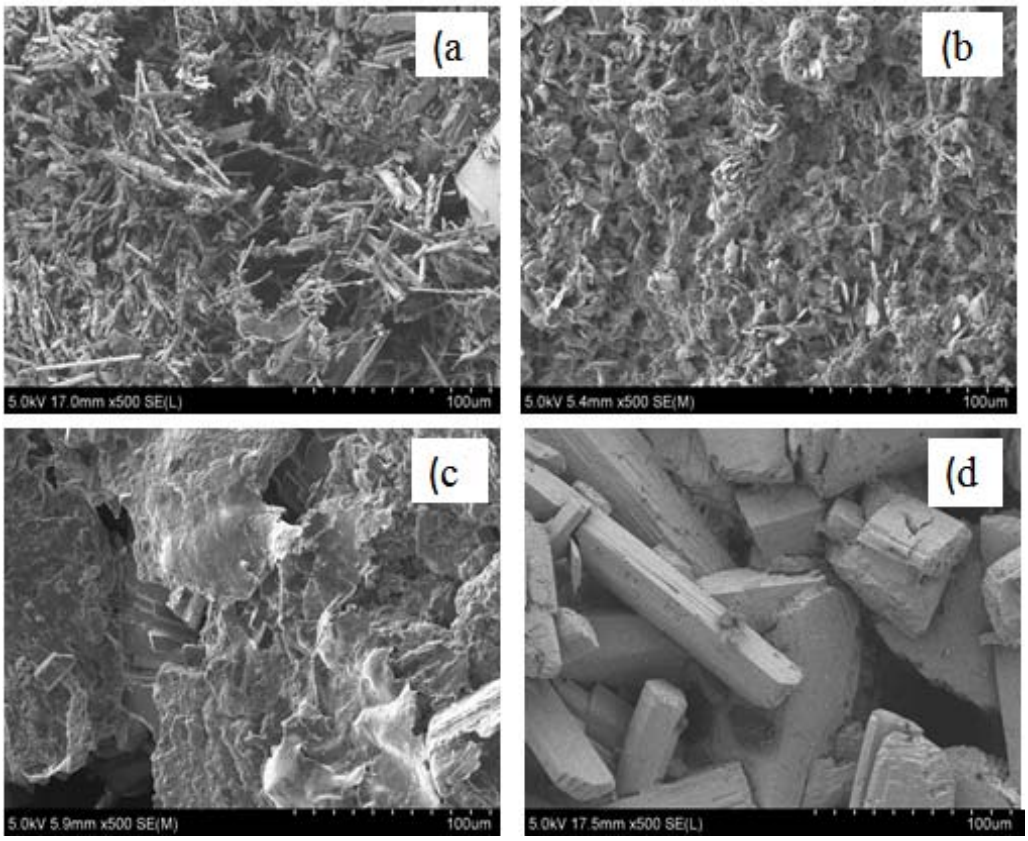

Figure 4.6. SEM images of the top surfaces of (a) gypsum scaling on unmodified membrane, (b) gypsum scaling on BSA-conditioned membrane, (c) gypsum scaling on AHA conditioned membrane, and (d) gypsum scaling on alginate conditioned membrane.

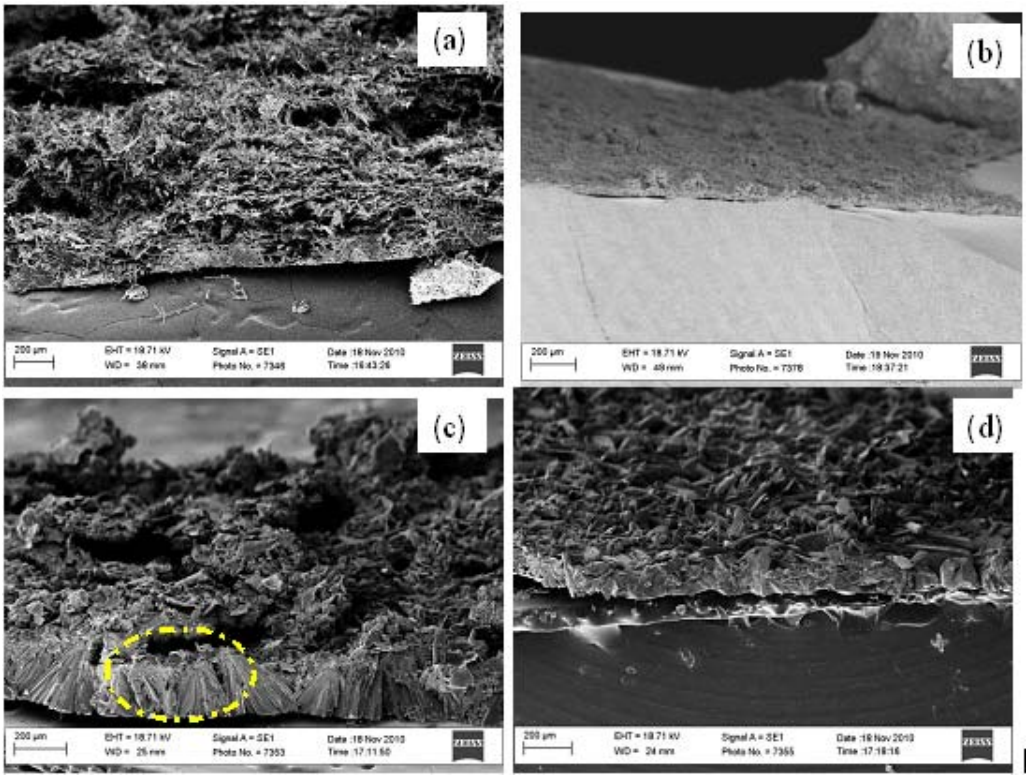

Figure 4.7. SEM images of the cross section of foulant layers (a) gypsum scaling on unmodified membrane, (b) gypsum scaling on BSA-conditioned membrane, (c) gypsum scaling on AHA-conditioned membrane, and (d) gypsum scaling on alginate-conditioned membrane.

QCM-D was used to test the hypothesis that the interactions between carboxylate functional groups and calcium ions play an important role in initiating gypsum scaling on an organically conditioned membrane surface. The oscillation frequency and the energy dissipation of the sensor changes were presented as the properties of the absorbed layer vary during conditioning and adsorption experiments. The mass of the conditioning layers were obtained by Saubrey equation (section 2.5) (Fig4.9 10 (a)), switching to a calcium solution produced an increase in frequency, indicating that there was a loss of mass on the sensor surface. The energy dissipation of the sensor remained relatively low,

suggesting the film rigidity/softness did not change. For the AHA conditioned surface (Fig.4.9 (b)), the exposure to calcium solution resulted in a decrease in frequency and an increase in dissipation, indicating more mass was deposited on the sensor surface and at the same time the AHA layer became softer. The increased softness was most likely caused by greater water content in the AHA layer after calcium ion adsorption. Therefore, the increase in mass on the AHA conditioned sensor can be attributed to the adsorption of not only calcium ions but also water molecules. For the alginate conditioned surface (Fig. 4.9 (c)), the decrease in frequency after the exposure to calcium solution confirmed the adsorption of calcium ions onto the alginate layer. Note that the originally adsorbed alginate layer appeared to be softer than the absorbed AHA and BSA layers, as demonstrated by its relatively higher dissipation. However, the exposure to calcium solution decreased the dissipation, indicating the alginate layer became more rigid after the adsorption of calcium ions (Fig. 4.9 (c)). This observation confirms that the egg-box structure formed in calcium-alginate complex made the alginate film denser and more rigid.

The frequency and dissipation data were further analyzed to compare the mass changes during calcium absorption on and subsequent DI rinsing of the three conditioned membrane surfaces. The mass change was normalized by the original mass of the BSA, AHA and alginate conditioning layers, respectively. As compared in Fig. 4.9 (d), the calcium solution slightly reduced the mass on the BSA conditioned surface while it drastically increased the mass on the AHA conditioned surface and slightly so on the alginate conditioned surface. This

comparison demonstrates a lack of interaction between calcium ions and BSA molecules but strong adsorption of calcium ions to the AHA conditioning layer and less so to the alginate conditioning layer. The subsequent DI rinsing reduced the masses on both BSA and AHA conditioned surfaces, suggesting that the two conditioning layers can easily detach from the surface even though AHA has strong adsorption of calcium ions. In contrast, for the alginate conditioned surface, the DI rinsing did not detach any alginate layer, indicating the strong interactions between alginate and calcium ions not only resulted in an elevated calcium concentration in the conditioning layer but also made the layer more rigid and more difficult to rinse off.

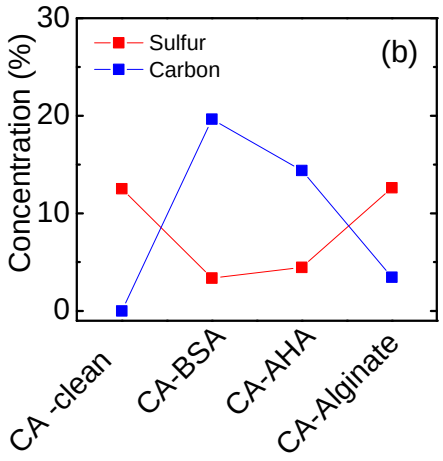

Figure 4.8. Energy-dispersive X-ray spectroscopy (EDS) data of four types of foulant layers including foulant layers on a clean membrane, a BSA-conditioned membrane, an AHA-conditioned membrane, and an alginate-conditioned membrane, respectively. Carbon and sulfur were presented here to represent the organic and inorganic content in fouling layers.

4.4.5 Effects of organic macromolecule conditioning on calcium ion adsorption

QCM-D was used to test the hypothesis that the interactions between carboxylate functional groups and calcium ions play an important role in initiating gypsum scaling on an organically conditioned membrane surface. The oscillation frequency and the energy dissipation of the sensor changes were presented as the properties of the absorbed layer vary during conditioning and adsorption experiments. The mass of the conditioning layers were obtained by Saubrey equation (section 2.5) (Fig4.9 10 (a)), switching to a calcium solution produced an increase in frequency, indicating that there was a loss of mass on the sensor surface. The energy dissipation of the sensor remained relatively low,

suggesting the film rigidity/softness did not change. For the AHA conditioned surface (Fig.4.9 (b)), the exposure to calcium solution resulted in a decrease in frequency and an increase in dissipation, indicating more mass was deposited on the sensor surface and at the same time the AHA layer became softer. The increased softness was most likely caused by greater water content in the AHA layer after calcium ion adsorption. Therefore, the increase in mass on the AHA conditioned sensor can be attributed to the adsorption of not only calcium ions but also water molecules. For the alginate conditioned surface (Fig. 4.9 (c)), the decrease in frequency after the exposure to calcium solution confirmed the adsorption of calcium ions onto the alginate layer. Note that the originally adsorbed alginate layer appeared to be softer than the absorbed AHA and BSA layers, as demonstrated by its relatively higher dissipation. However, the exposure to calcium solution decreased the dissipation, indicating the alginate layer became more rigid after the adsorption of calcium ions (Fig. 4.9 (c)). This observation confirms that the egg-box structure formed in calcium-alginate complex made the alginate film denser and more rigid.

The frequency and dissipation data were further analyzed to compare the mass changes during calcium absorption on and subsequent DI rinsing of the three conditioned membrane surfaces. The mass change was normalized by the original mass of the BSA, AHA and alginate conditioning layers, respectively. As compared in Fig. 4.9 (d), the calcium solution slightly reduced the mass on the BSA conditioned surface while it drastically increased the mass on the AHA conditioned surface and slightly so on the alginate conditioned surface. This

comparison demonstrates a lack of interaction between calcium ions and BSA molecules but strong adsorption of calcium ions to the AHA conditioning layer and less so to the alginate conditioning layer. The subsequent DI rinsing reduced the masses on both BSA and AHA conditioned surfaces, suggesting that the two conditioning layers can easily detach from the surface even though AHA has strong adsorption of calcium ions. In contrast, for the alginate conditioned surface, the DI rinsing did not detach any alginate layer, indicating the strong interactions between alginate and calcium ions not only resulted in an elevated calcium concentration in the conditioning layer but also made the layer more rigid and more difficult to rinse off.

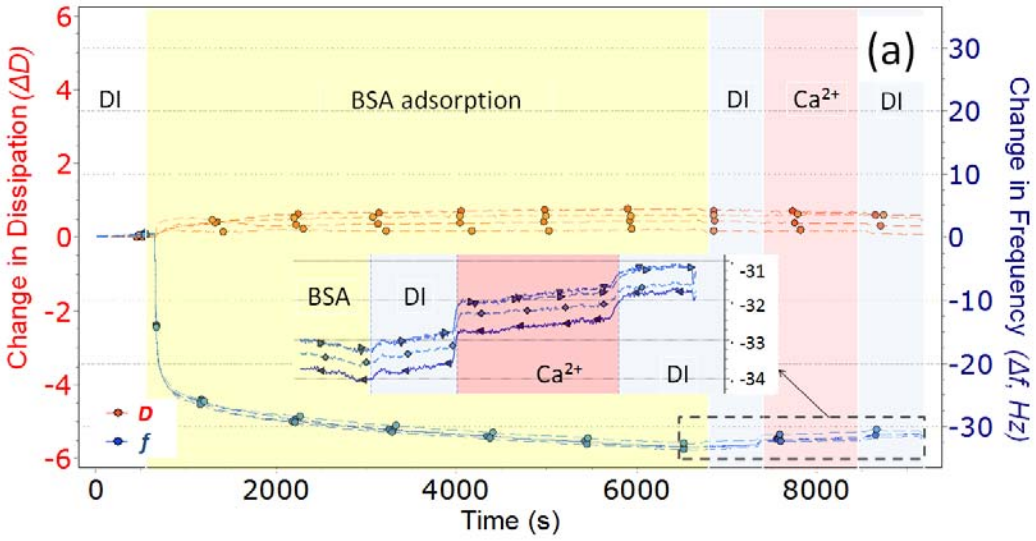

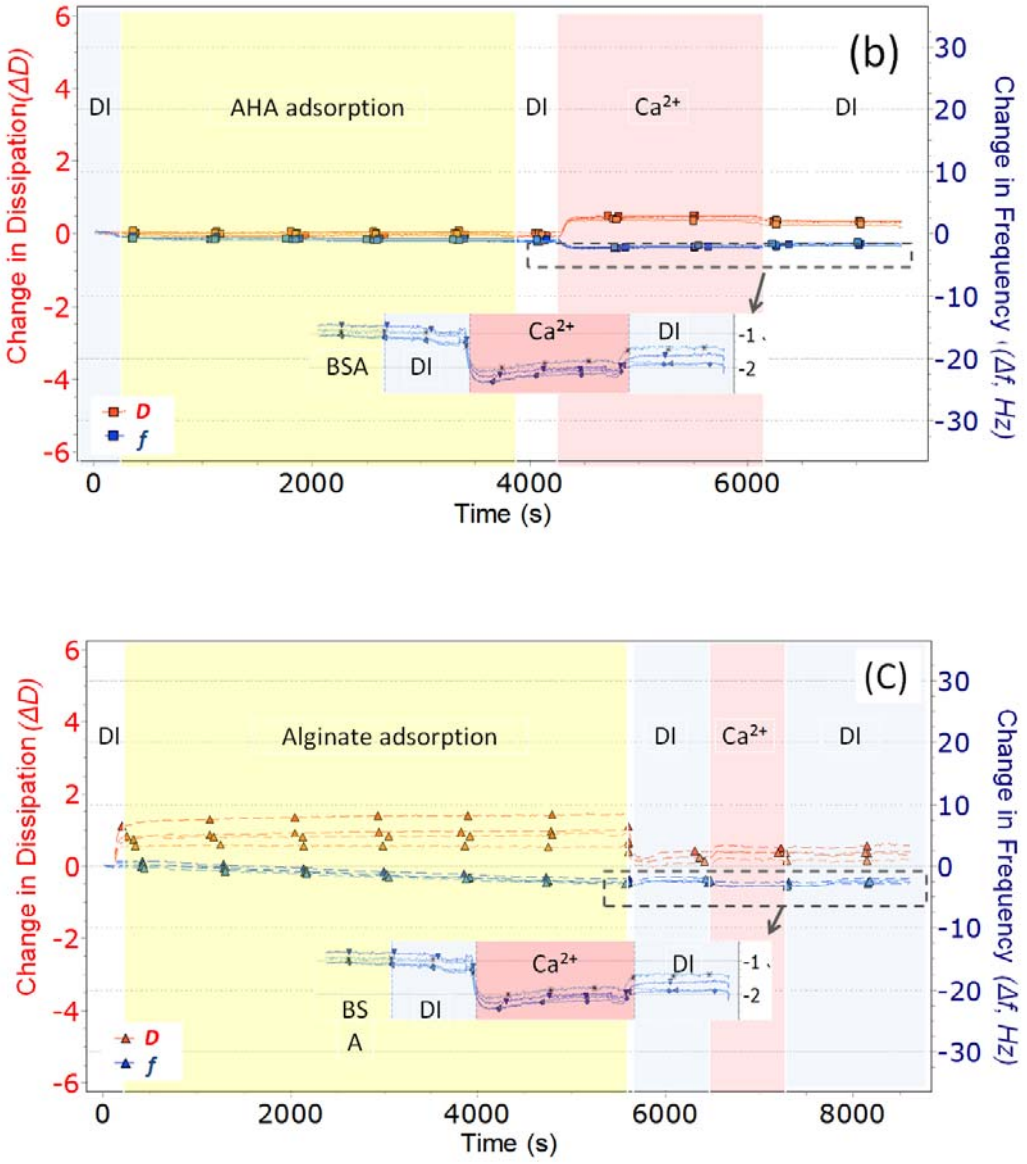

Figure 4.9. QCM-D data for three organic molecule conditioning experiments. The blue lines represent the change in frequency and the orange lines represent change in dissipation: a) effects of BSA conditioning on calcium absorption; (b) effects of AHA conditioning on calcium absorption; and, (c) effects of alginate conditioning on calcium absorption.

4.4.6 Understanding the role of organic macromolecule conditioning

Effects of organic molecule surface functional groups

As illustrated in Fig. 4.10, three organic macromolecules forms different

condition layers on CTA membrane surfaces and forms different gypsum scaling layers. It has been found previously that alginate macromolecules can act as the nucleus in gypsum crystal formation due to the calcium bridging effects (or egg-box effects) [223, 224] among carboxylate functional groups on alginate macromolecular chains [211]. For the alginate conditioned membrane surface, the absorbed alginate macromolecules introduced a dense layer that contained abundant carboxylate functional groups onto the membrane surface and thus provided active nucleation sites for gypsum crystallization on membrane surface. Hence, alginate macromolecules greatly changed gypsum crystallization by shortening the nucleation period, enlarging the crystal sizes, and thus enhancing gypsum scaling, eventually directly resulting in the fastest flux decline.

Similarly, there exists a strong interaction between AHA and Ca2+. AHAs are considered natural polyelectrolyte organic compounds with a complex structure that involves a proportion of condensed aromatic rings with a large number of surface hydroxyl, phenoxyl, and carboxylate reactive groups [225, 226]. In a neutral environment, AHA macromolecules are predominantly negatively charged, with a tendency to adsorb cations and form metal-humic acid complexes due to the calcium bridging effect among AHA macromolecules [130, 227]. In the present experiment, the AHA conditioning introduced a thick AHA layer with enhanced Ca2+ adsorption capability of accelerating the surface crystallization of gypsum, thereby leading to a faster flux decline.

In comparison, BSA has a heart-shaped structure (at neutral pH) with fewer

carboxylate functional groups [228, 229]. This particular shape can cause an steric effect that interferes with the interaction between BSA molecules and calcium ions. Overall, the gypsum scaling was inhibited by the BSA conditioning due to the lower density of carboxylate functional groups and also the steric effect of the BSA molecular structure.

Effects of cake enhanced concentration polarization

Cake enhanced concentration polarization (CECP) refers to a phenomenon that during filtration, foulants accumulate to form a cake layer on the active surface layer of an FO membrane [98]. CECP may result in an elevated salt concentration in the cake layer by hindering the back diffusion of salts from the membrane surface to bulk solution. As a result, CECP can significantly deteriorate water flux due to the increased osmotic pressure in the cake layer and thus decrease driving force for flux [100, 101, 230]. During the conditioning experiments, a thin layer of organic macromolecules was deposited on membrane surface. Even though the thin layer itself did not result in an apparent flux decline, it could still increase the calcium and sulfate ion concentrations at the bottom of the conditioning layer (i.e., at the membrane surface) during gypsum scaling experiments. Because gypsum crystallization is faster with higher calcium and sulfate concentrations (higher SI value), gypsum scaling would initiate at the bottom of the conditioning layer where an elevated ion concentration was present. This hypothesis 4.6(c), gypsum crystals grew underneath the AHA conditioning layer and formed uniform gypsum clusters. Similarly, the gypsum crystallization was initiated at the bottom of the alginate

layer 4.7 (d)).

4.5 Concluding Remarks

This study demonstrates that the adsorption of organic foulants on membrane surfaces could have dramatic effects on gypsum scaling in FO membrane process. Organic macromolecules with different properties show different effects on gypsum scaling behaviors. Membrane surface conditioning by organic compounds affects not only the kinetics of gypsum crystal growth or rate of flux decline, but also the morphology of gypsum crystals. It is necessary to further study the sophisticated interactions between organic macromolecules, inorganic ions, and FO membrane surfaces to reveal the underlying mechanisms in order to develop effective FO membrane fouling control strategies.

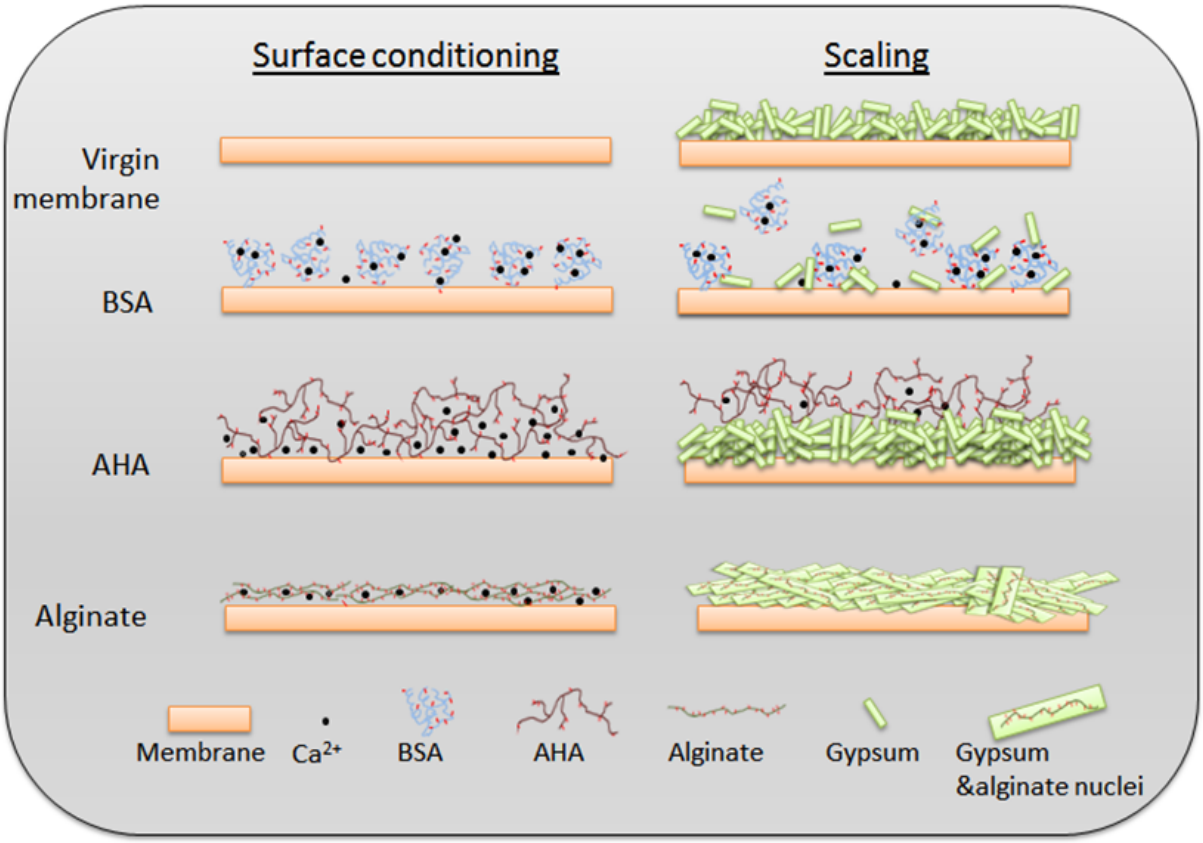

Figure. 4.10. Illustration of gypsum scaling mechanism on different organic macromolecule conditioned membrane surfaces.

4.6 Acknowledgements

This material is based upon work supported by the National Science Foundation under Grant Nos. CBET-1154572 and CBET-1158601. In addition, the first author is partially supported by an NWRI – AMTA (National Water Research Institute – American Membrane Technology Association) Fellowship for Membrane Technology. These supports are gratefully acknowledged. The authors would like to thank Hydration Technology Innovations for providing the FO membrane.

Chapter 5: Online Monitoring the Initial Stage of Biofouling in Forward Osmosis Membrane Process

5.1 Abstract

This paper presents the application of a non–intrusive microscopic direct observation technique for the study of initial microbial cell deposition and release onto/from the forward osmosis (FO) membrane surface. A commercial cellulose triacetate CTA-FO membrane was tested in this study. *Escherichia coli (E. coli)* K12 MG1655 with green fluorescence protein were used as the model bacteria to allow the real-time monitoring of bacteria deposition on the membrane's surface. The effects of bacteria concentration, ionic strength, pH and membrane surface conditions on bacteria deposition and detachment were systematically investigated. The results of this study provided insight into the interactions between bacteria-bacteria and bacteria-membrane surfaces. CTA-FO membrane demonstrated relatively low fouling propensity to bacteria adherence. The initial microbial deposition rate is relatively slow and solution chemistry shows no significant effects on deposition rate. Furthermore, more than 50% cells deposited on the FO membrane surfaces can be easily removed by simultaneously increasing the cross-flow rate and stopping permeate flux. This high removal efficiency indicates a weak bond between bacteria and the membrane's surface. Membrane surface properties such as hydrophilicity played an important role in bacteria deposition. Dopamine coating on CTA-FO membrane further increased surface hydrophilicity and greatly reduced fouling.

5.2 Introduction

Forward osmosis (FO) is an emerging osmotic-driven membrane process where water molecules are pulled from a feed solution to a draw solution through a semi-permeable membrane by the osmotic pressure difference between the two solutions [12]. FO is considered a promising new technology; it has many advantages over existing membrane processes [231-234] like reverse osmosis (RO) and nanofiltration (NF) in producing clean water from seawater/brackish water [9, 10, 235] and wastewater[236]: low membrane fouling potential, high cleaning efficiency, low hydraulic pressure requirements, and low energy consumption. FO also shows great potential to enhance sustainability when combined with current membrane technologies. For example, studies show that integrating FO into microbial fuel cells [208, 237] improves energy output while simultaneously accomplishing wastewater treatment and electricity generation. Pairing FO with reverse osmosis contributes to a high degree of safety for the use of impaired water and reduces energy requirements for membrane cleaning and maintenance [60, 61, 207, 238].

One of the major issues in the application of FO process is membrane fouling. Typically, there are four types of fouling: organic fouling, inorganic scaling, colloid fouling and biofouling. Membrane fouling can severely deteriorate membrane performance, shorten membrane life, and greatly increase the operational cost of the system [239]. Existing FO fouling studies have focused on FO performance with organic fouling [24, 27, 240], colloidal fouling [18], and gypsum scaling [15, 119, 241]. Investigations of FO biofouling are still

lacking. Studies on FO membrane bioreactors demonstrated that FO membranes (cellulose triacetate membrane) are less sensitive to biofouling and that membrane flux can be recovered by simple physical rinsing [26, 242]. However, these studies all focused on the membrane flux behavior and cleaning efficiency when the FO membrane was facing a variety of microorganisms, rather than on biofouling mechanisms. Therefore, systematic study is still needed to understand the dominant mechanisms of biofouling and their interactions within the FO process.

Membrane biofouling is a multistep process in membrane filtration systems [243-245]. It is initiated by the adhesion of bacterium to the membrane surface and followed by microbial biofilm growth on the membrane's surface. One of the important steps in the formation of a microbial biofilm in a membrane system is the transport and subsequent adhesion of microorganisms to the membrane surface. The use of both invasive and noninvasive microscopic methods for the examination of biofilm formation has increased in recent years. Among the various noninvasive biofouling characterization methods, direct microscopic observation has been widely used to study the development of biofilms in pressure-driven membrane systems [246, 247]. This method allows real-time visualization of the progress of microbial deposition on membrane surfaces and provides a qualitative understanding of membrane biofouling mechanisms. Several past studies used direct microscopic observation to study bacterial adhesion and detachment in pressure driven membrane systems. These studies [246, 247] found that biofouling can

be influenced by system hydrodynamic conditions, solution chemistry, microbial properties, and the surface properties of the membrane.

The objective of this study was to develop a procedure enabling the quantitative determination of the mechanisms governing the initial deposition and release of microbes in a cross-flow forward osmosis process. We have applied microscopic observation of organic fouling and scaling that occurs within a FO system [16, 248]. This allowed us to obtain valuable information about the kinetics of foulant formation. In this study, the system was slightly modified and *Escherichia coli* (*E. coli*) K12 MG1655 with green fluorescence protein served as the model microbial particles. Two membranes including a commercial cellulose triacetate membrane and a polydopamine-modified cellulose triacetate membrane were tested as model FO membranes. Various physicochemical conditions of the feed solutions were used during direct microscopic observation experiments to systematically study the effects of interactions on bacterial adhesion. A novel image analysis procedure enabled rapid quantification of net deposition rates.

5.3 Materials and Methods

5.3.1 Microbial suspension preparation

E. coli K12 MG1655, which was labeled with enhanced green fluorescing protein, was first streaked from a frozen stock in a mixture of LB broth and glycerol and grown overnight (12-14 hours) at 37 °C on a agar plate. The plate was then kept in fridge (4 ºC) for future use. Several colonies on the agar plate were inoculated into 50 ml LB broth and incubated at 37 °C in shaking water

bath (120 rpm) for 12 hours. 0.1 ml of this preculture was used to inoculate a second culture that was grown in shaking water bath again for approximately 4 hours (at 37 °C, with shaking speed of 180 rpm). The bacteria from the second culture were harvested by centrifugation when the optical density reading reached 0.3 at 600 nm and after they were washed three times with sterile 154 mM NaCl solution. To prepare the feed solution for direct observation experiment, the cleaned bacterial cell suspension was diluted in a salt solution (varies between experiments) to a targeted concentration. All the chemicals and reagents used in the experiments are of analytical grade. Sterilized dionized (DI) water was used in all the experiments for solution preparation.

5.3.2. FO direct observation systems

A cross-flow FO direct microscopic observation system was employed in this study to monitor the microbial deposition and release onto/from membrane surface. The schematic drawing of the direct observation system is illustrated in Figure 5.1. The cross-flow system closely resembles the FO membrane system used in our previous studies [16, 24, 27], which includes two loops circulated separately on both sides of the membrane, i.e. a feed solution loop and a draw solution loop. The cross flow rate was controlled by a digital gear pump (Cole Parmer, Vernon Hills, IL) and the temperature of the experiment was stabilized at 20 ºC by a digital cooler (Thermo Neslab Inc., Newington, NH). Draw solution tank was placed on a balance (Denver Instruments, Denver, CO) to record the weight changes for flux monitoring. A stir plate was used to continuously mix feed solution to avoid microbial settlement.

The membrane chamber was specially designed to provide a defined, constant laminar flow (Re~24) in the system. As shown in Figure 5.1, two identical flow channels were separated by the inserted membrane with a dimension of 77 mm×26 mm×3 mm (L×W×H). A glass window (38 mm × 16 mm) was built in the middle of the upper plate to enable real-time monitoring. The entire membrane chamber was placed on the stage of Olympus BX51 microscope (Olympus, Japan) equipped with a 10× objective with an ultra-long working distance (10 mm). A CCD camera (Olympus, Japan) is mounted on top of the microscope and is coupled to an image analyzer (Qcapture, QEM, BC, Canada).

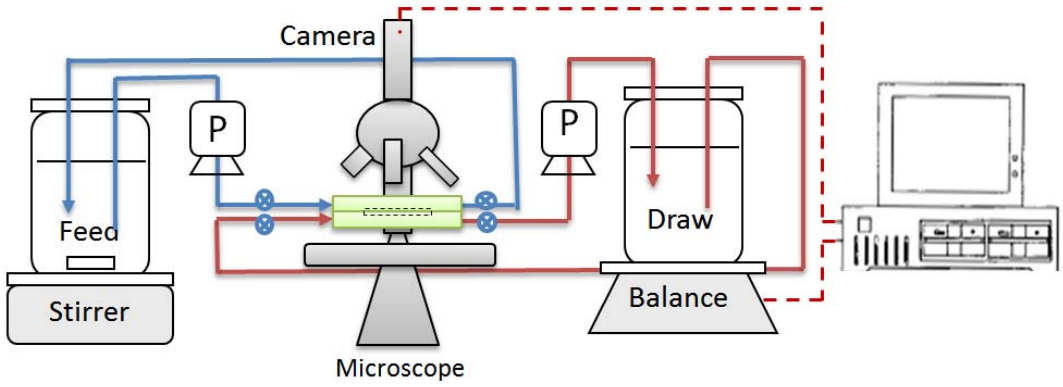

Figure 5.1. Direct observation system for bacteria deposition and detachment experiment.

5.3.3. Microbial deposition and rinsing protocols

FO direct observation experiments consists of two parts including microbial deposition experiment and physical rinsing experiment. In both experiments, microbial suspension was circulated in the feed solution loop to allow contact with the active side of the membrane. A concentrated NaCl solution was used as draw solution to provide the driving force for water permeation. The weight

changes of draw solution were measured by a digital balance and the readings were recorded by computer for on-line flux monitoring.

For the microbial deposition experiment, a cross-flow rate of 100 mL/min was used to generate. *E. coli* seed solution was added after 30 minutes of experiment. Images were taken on the membrane's surface at a fixed spot in 1 minute intervals at the beginning (20 minutes) and then every 5 minutes till the end of the experiments (60 minutes).

In the end of deposition experiment, the draw solution was switched to a new NaCl solution (with same concentration as feed solution) to stop permeate flow. Cross-flow rate was increased to 1000 mL/min to enhance shear stress. Images were taken every 1 minute. The rinsing experiment lasted 10 minutes.

The system (both draw solution and feed solution loops) was then thoroughly cleaned and sterilized using the following protocols [145]: (1) sterilization by circulating NaOCl (0.5%) for 2 hours and rinsing by DI water for 0.5 hours, (2) dissolving and removal of organic matter by circulating EDTA (5 mM) at pH 11 for 0.5 hours and rinsing by DI water for 0.5 hours, (3) removal of trace organic matter by circulating SDS (2 mM) at pH 11 for 0.5 hours and rinsing by DI water for 0.5 hours, (4) Final sterilization by circulating ethanol (95%) for 1 hours, (5) rinsing the unit three times with fresh made DI water.

5.3.4 Image analytical methods

In order to keep consistency, all images were obtained on same spot in the middle of the membrane surface. To distinguish between the deposited bacteria

and moving bacteria, the lens were carefully focused on the membrane surface. All images were saved in a Tagged-Image File Format (TIFF) of 1600 ×1200 pixels, with each pixel representing one byte. The total field of view is 1mm2 and the area of one bacterium equals approximately 1×10-5 mm2.

To eliminate artifacts caused by the background noise, image processing software was employed to edit the images by subtracting background noise impact and obtain the attached accurate bacteria cell density (Figure 5.2).

Enumeration of the total number of adhering bacteria as well as the determination of the deposition rate was achieved by image processing (Image J). The total count of bacteria on the surface was normalized by membrane surface area (N). The net deposition rate constant, kd, was calculated with the following equation[248]:

$$k_d = \frac{\Delta N}{\Delta T}\frac{1}{N_0} \quad (1)$$

Where, ΔN is the increased bacteria cell density in time period ΔT; and N0 is the initial bacteria cell density in the solution.

And the removal rate kr by rinsing is calculated by:

kr= (1-N60mins/Nrinsing, 1min) ×100% (2)

Where N0 was the bulk feed cell concentration.

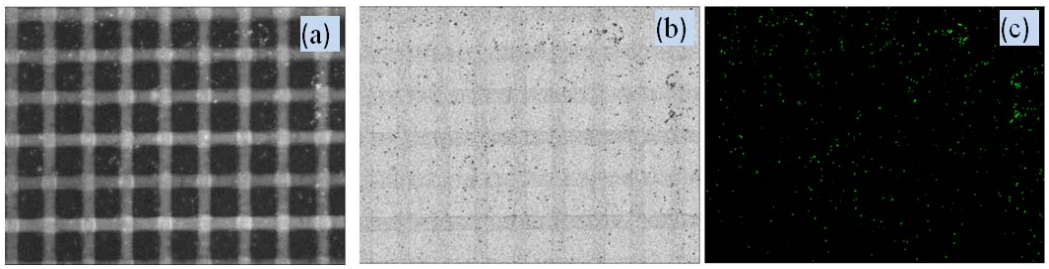

Figure 5.2 Image processing example, (a) original image, (b) image with reduced background noise, and (c) image for cell counting. Images were taken with a 10× objective lens by CCD camera with a resolution of 1600×1200 pixels. The membrane area shown in the image is 1 mm2.

5.4 Results and Discussion

5.4.1 Impact of initial cell concentration on deposition and release

The influence of bacteria concentrations on initial bacterial deposition and release rate was presented in Figure 5.3. In these experiments, the initial total ionic strength of the feed solution was kept constant at 100 mM. The draw solution concentration was adjusted between 3.5 M and 4.0 M to achieve same initial flux (3.0 μm/s) and maintain same permeate drag force for all experiments. The effect of initial cell concentration on initial stage of biofouling was studied at concentrations of 104, 105, and 106 CFU/ml, respectively.

As shown in Figure 5.3 (a), the increase in bacterial concentration (from 104 to 106 CFU/ml) in the feed solution increased the total number of bacteria deposited on the membrane surface. Higher bacterial concentration resulted in a higher surface coverage. However, if the three curves were plotted with different vertical axis scales (Figures 5.3 (b), (c), and (d)), they appear to be quite similar in shape. In the first 20 minutes, the rate of microbial cell

deposition was relatively quick and the cell density appeared to be linear with time in all three experiments. The net deposition rate constants in the three experiments (104, 105, and 106 CFU/ml) were 5.56, 8.27, and 6.79 um/s, respectively. The deposition rates are quite similar, considering the magnitude of concentration difference. The linear increase of attached cell density and the similarity in net deposition rates between experiments with different cell concentrations indicated that bacteria-membrane interactions play an important role for initial bacteria deposition. Initial cell concentration has negligible effects on initial stage of bacteria deposition rate. However, the release rate by rinsing at low cell concentration is quite low (34%). This may be explained by the cell aggregation on the membrane surface due to increased cell density. These small aggregates are more easily to be carried away by cross-flow.

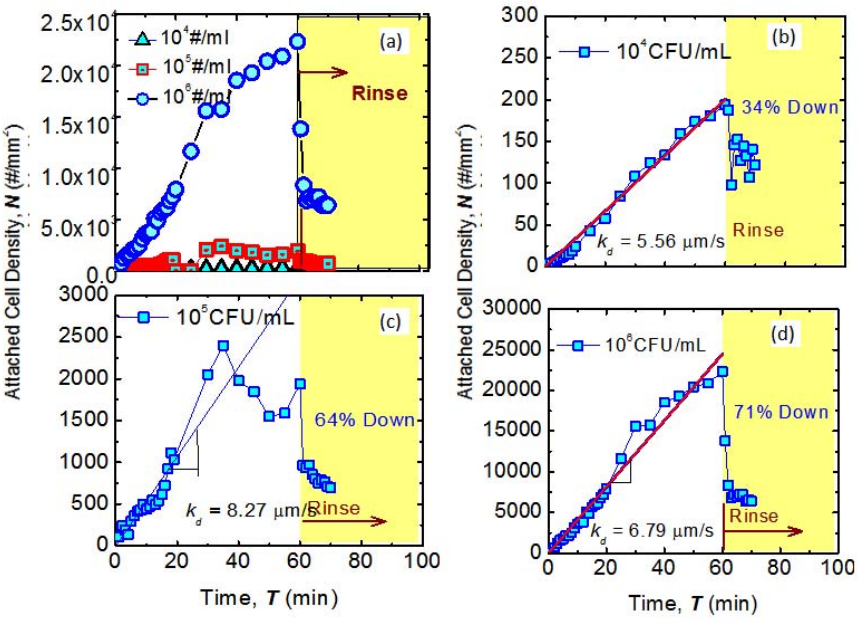

Figure 5.3. Effects of *E. coli* concentrations on initial bacteria deposition and release rate, (a) a comparison of three feed solution concentrations (106, 105, and 104 CFU/ml), (b) feed solution with *E. coli* concentration of 104 CFU/ml, (c) feed solution with *E. coli* concentration of 105 CFU/ml, and (d) feed solution with *E. coli* concentration of 106 CFU/ml. The operation conditions for the attachment experiment were: 4 M NaCl solution as draw solution and 100 mM NaCl as feed solution (which resulted in a permeate flux of 3.0 μm/s), pH 7.0, a cross-flow rate of 100 ml/min. The operation conditions for the rinsing experiments were: 100 mM NaCl as draw and feed solutions, and a cross-flow rate of 1000 ml/min.

5.4.2 Impact of ionic strength on bacteria deposition rate

The effects of ionic strength on deposition kinetics of bacteria onto membrane surface are investigated in this part of study. Draw solution concentrations were controlled to provide same permeate flux for all experiments. Feed solution concentration was adjusted at 1mM and 100mM by adding NaCl solution. Solution pH was adjusted to pH 7.0 by adding NaOH solution. The experiments were conducted at temperature of 20±1°C.

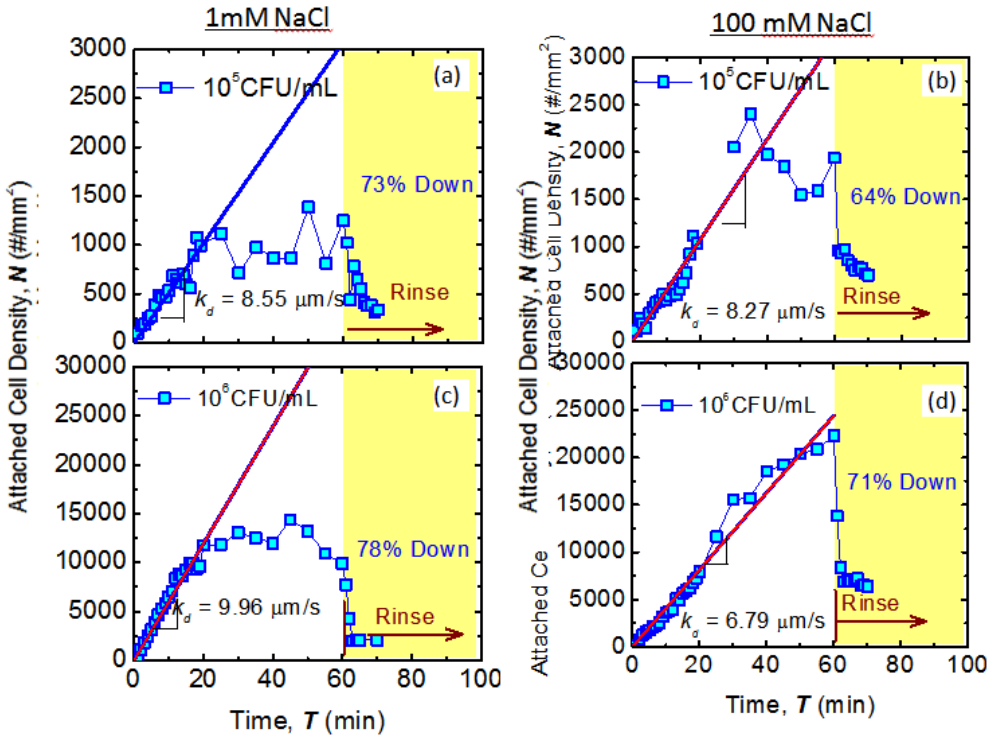

Figure 5.4 Effects of ionic strength on bacteria deposition and release with different cell concentrations. The experiments were conducted at different conditions, (a) 1mM , NaCl, 105CFU/ml, (b) 100 mM NaCl, 105CFU/ml, (c) 1mM , NaCl, 106CFU/ml, and (d) 100 mM NaCl, 106CFU/ml. The other operation conditions for the deposition experiment were the same as listed in Figure 5.3.

The deposition rates for *E. coli* with a concentration of 105 and 106 CFU/ml, at ionic concentrations of 1 and 100 mM NaCl were plotted in Figure 5.4. For lower cell concentration (105 CFU/ml), the deposition rate at 1mM is slightly higher than that at 100mM (Figure 5.4 (a) and (b)). For higher concentration (106 CFU/ml), an increase in the net deposition rate was observed at lower ionic strength. A possible explanation is that bacteria aggregation in bulk solution was enhanced because of electrostatic double-layer compaction effects

at higher ionic strength and higher cell concentration [249]. The surface charge of bacteria decreased due to compression of the electrostatic double layers at higher ionic strength. The electrostatic repulsive force between bacteria and bacteria was decreased as well. With higher cell concentration and lower repulsive force, bacteria cells were more easily to accumulate and form aggregates. The aggregates of bacterial cells have larger size are more strongly affected by the cross-flow rate than the interactions between cells and membranes than single bacteria cells. More effective collisions between cells happen at higher cell concentration and higher ionic strength, so *E. coli* with a concentration of 106 CFU/ml at ionic strength of 100mM has the lowest deposition rate.

5.4.3 Impact of pH on bacteria deposition rate

In this part of the study, the influence of pH on bacteria adhesion to CTA membrane surface is presented in Figure 5.5. Zeta potential measurement showed that a CTA membrane surface is negatively charged in solution at pH 5.5 and pH 7.0[250]. And at pH 7.0, membrane surface carried slightly higher charge density than that of pH 5.5. Most of the bacteria in the solution are slightly negatively charged in the solution as well. Therefore, electrostatic repulsion between the CTA membrane surface and bacteria could be a factor to determine bacteria deposition rate. At higher pH, the higher charge density results in higher repulsive force between bacteria and membrane surface and, thus, reduce the overall adhesive force. The repulsive force effects between

bacteria-and-bacteria and bacteria-and-membrane surface resulted in higher deposition rates at pH 5.5.

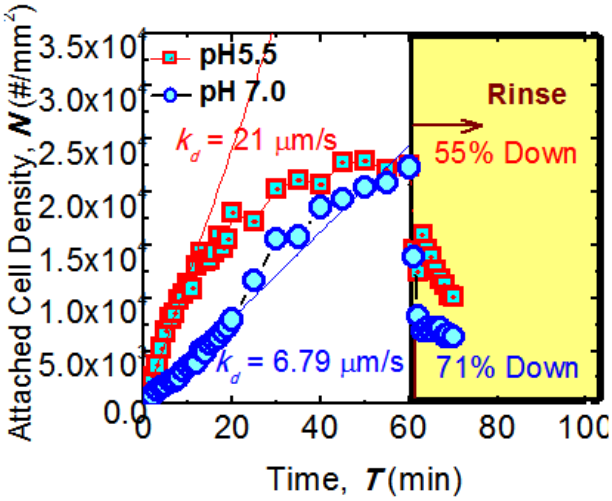

Figure 5.5. Comparison of attached bacteria cell density and deposition rate under different feed solution pH conditions,

5.4.4 Impact of membrane materials on bacteria deposition rate

In this part of study, we used dopamine (DOPA) to modify the CA membrane's surfaces and to study the biofouling properties of this DOPA-CA membrane. DOPA coating is a bio-inspired surface modification method, it has been recently used to mimic a mussels adhesive [251, 252]. In alkaline solution environment, DOPA self-polymerize (polydopamine) and bond to virtually any surface. It is very simple approach, as it does not involve any complicated chemicals or harsh treatments. DOPA coating has been proven to be very effective on polymeric membrane materials, including PA-RO membranes [152-154]. DOPA was found to increase membranes surface hydrophilicity and therefore increase its resistance to fouling.

We used a dip-coating approach to attach DOPA to the CA membrane surface, as shown in Figure 5.6. We soaked the membrane active layer in DOPA solution for 1 hour and then thoroughly rinsed the surface with DI water. The membrane was submerged in DI for 3 hours to remove the residues before the experiment.

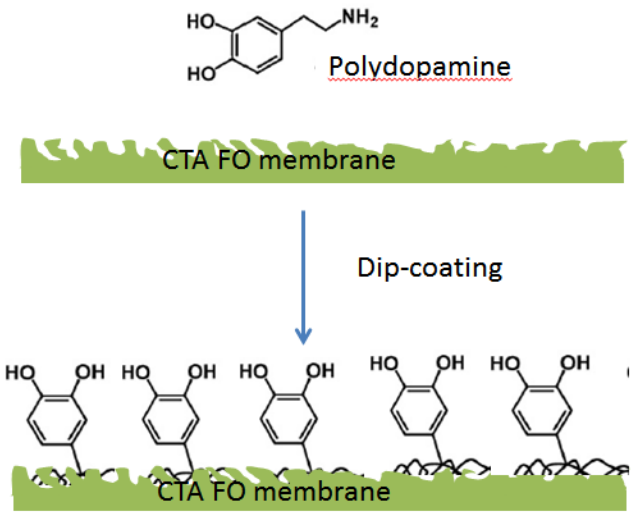

Figure 5.6. The scheme of coating polydopamine on CTA membrane surfaces.

X-ray photoelectron spectroscopy (XPS) was used to evaluate the effectiveness of DOPA coating. As shown in Table 5.1, the nitrogen content increased from 0.6 to 0.8 %, and the ratio of oxygen and nitrogen decreased from 54.7 to 38.2%. These results indicate a layer of DOPA was successfully coated on the CTA membrane surface.

Table 5.1 XPS results of CA membrane surface

	C %	N %	O %	Si %	O:N
CA Neat	64.3	0.6	33.2	1.9	54.7
CA+DOPA	66.0	0.8	32.0	1.3	38.2

The biofouling results are presented in Figure 5.7. As shown in Figure 5.7(a), dopamine coating on a membrane surface significantly slows down the bacteria deposition rate. An explanation for this occurrence is the increased surface hydrophilicity due to dopamine coating [253, 254], which inhibits hydrophobic attraction between bacteria and membrane surface.

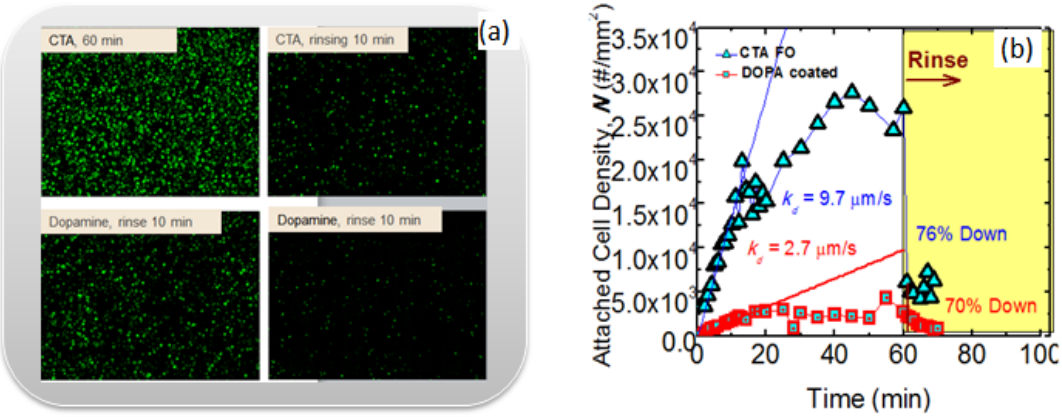

Figure 5.7. Comparison of dopamine coating effects on bacteria attachment density during deposition and rinsing experiments, (a) bacteria deposition and release rate, and (b) representative images of bacteria attachment density during deposition and rinsing experiments on CTA membrane surface and polydopamine coated membrane surfaces. The initial cell density in feed solution is 106 CFU/ml and 10 mM NaCl was added to feed solution. The other experiment conditions were the same as in Figure 5.3.

5.5 Concluding Remarks

This study demonstrates that CTA-FO membrane exhibits relatively low fouling tendency subjected to bacteria adherence. The initial microbial deposition rate is relatively slow and solution chemistry shows no significant effects on deposition rate. Furthermore, more than 50% cells deposited on the FO membrane surfaces can be easily removed by simultaneously increasing the crow-flow rate and stopping permeate flux. This high removal efficiency indicates a weak bond between bacteria and the membrane's surface. Membrane surface properties such as hydrophilicity played an important role in bacteria deposition. Solution chemistry shows more effects on bacteria-bacteria than bacteria-membrane interaction. The change in solution ionic strength and pH affects bacteria surface charge and aggregation behavior which slightly changed bacteria deposition rate.

A hydrophilic composite CTA-FO membrane was successfully fabricated by dopamine self-polymerization and on CTA-FO substrate. Compared to the original membrane, the hydrophilicity of the resultant DOPA CTA-FO NF membranes was improved and antibiofouling properties were significantly improved.

Chapter 6: Effects of Solution Chemistry on Initial Bacterial Deposition and Detachment in Forward Osmosis Process

6.1 Abstract

Bacterial deposition and subsequent biofilm growth in membrane processes are often inevitable. In order to understand the mechanisms of biofouling in membrane processes, it is critical to understand the specific contributions of various factors that affect bacteria-membrane interactions at the molecular level. This paper presents both experimental and molecular simulation results for our current study on biofouling in a forward osmosis (FO) process. In this study, we employed a non–intrusive microscopic direct observation technique to examine real-time bacterial deposition and release in a cross-flow FO membrane process. A flat sheet polyamide FO membrane (synthesized in our lab) was tested in this study. *Escherichia coli* (*E. coli*) K12 MG1655 tagged with a plasmid coding for green fluorescence protein was used as the model bacterial strain. To determine the interfacial forces between a single bacterium and the membrane surface, a carboxylate functionalized particle probe was used as a surrogate for the functional groups in the extracellular polymeric substances of bacteria. The data from bacterial deposition experiment was combined with the interfacial force data and molecular simulation data to elucidate the mechanisms of the initial stage of biofouling. This study showed that an increased adsorption of bacteria originated at a pH of 5.5 and was probably due to a reduction in deprotonated chemical functional groups that are

in charge of repulsive electrostatic interactions. Calcium ions were found to enhance the rate of bacterial deposition, especially in high pH environments. The results of atomic force microscopy measurements and simulations showed higher adhesive force in the presence of calcium ions than that without calcium, thus further confirming our findings from the deposition experiments.

6.2 Introduction

With its different applications such as water purification, seawater/brackish water desalination, and wastewater reclamation, membrane technology has proven to be a reliable technique for supplying clean water. Forward osmosis (FO), which is an emerging membrane technology, is particularly attractive because it has the potential to reduce the energy consumption for filtration. Significant efforts have been made in the development of thin-film polyamide (PA) FO membranes [71, 72, 185, 255] in order to improve performance in areas such as high selectivity and water permeability. However, PA membranes have relatively high fouling propensity because of the inherent physicochemical properties of their surface. Among all types of membrane fouling, biofouling is the major challenge in the operation of PA membrane [120-122].

Biofouling is a complicated phenomenon which inevitably occurs in all membrane systems, even with the use of pretreatment and disinfection systems such as chlorination [256, 257]. Membrane biofouling starts when the membranes are exposed to water sources that contain microorganisms, such as bacteria, fungi, and yeasts. After the initial deposition and adsorption, these microorganisms migrate, grow, and multiply. They are held together by a

matrix of polymeric organic compounds excreted onto a membrane surface and form a very complicated system - biofilm [125-128]. The formation of a biofilm in a membrane system is very problematic as it results in the reduction in membrane water flux due to establishment of a gel-like diffusion barrier. Increases in solute concentration polarization are accompanied by lower solute rejection along with an increase in the module differential pressure and the biodegradation / biodeterioration of the membrane or other membrane module materials [258].

Bioflouling can be described as a four-phase process which includes (1) initial attachment and detachment, (2) irreversible attachment, (3) initial biofilm formation, and (4) biofilm growth. Initial bacterial attachment is the essential step in the biofilm formation; however, the molecular and physicochemical interactions that govern bacterial adhesion to membrane surfaces have not been understood in detail. Theoretically, the physiochemical interactions in charge of the initial attachment of microorganisms to the membrane surface may include: hydrophobic interactions [131], intermolecular interactions, hydrogen bonding, and electrostatic interactions [129, 130]. Research on biofouling in PA FO membranes shows that these interactions are greatly affected by membrane surface properties (including hydrophobicity, charge, and surface roughness), solution chemistry (such as ionic strength, divalent cations, and pH), system hydrodynamic conditions (such as permeate flux and cross-flow conditions), and the characteristics of bacteria (including surface charge, growing phase, and flagella motility) [132, 133]. These factors have been

found to affect many of the interaction forces that govern the approach and adhesion of bacterial cells to the surface. Hence, if fouling is to be minimized, it is this initial stage of bacterial adhesion that must be inhibited and these interaction mechanisms that must be understood. However, systematic studies on biofouling in forward osmosis membranes are scarce. Until recently, very few studies on FO biofouling have been reported in literature [242, 259-261]. As a result, the underlying fouling mechanisms of FO processes are basically unknown. The lack of hydraulic pressure in FO processes may alter the hydrodynamic conditions and change bacterial adhesion behavior. Therefore, fundamental research efforts are immediately needed to elucidate the biofouling mechanisms of FO membranes.

The objective of this study is to elucidate the mechanisms of FO membrane biofouling in the initial stage. Well-controlled bacterial deposition experiments with a model bacterium, *E. coli K12* MG1655, were conducted using a lab-scale direct observation system. The effects of solution chemistry (such as pH, ionic strength, and divalent ions) on bacterial adhesion were investigated by monitoring and imaging the dynamic bacterial coverage on membrane surface. Atomic force measurement and molecular simulation were conducted to further explain the electrostatic force between a single bacterium and the membrane surface.

6.3 Materials and Methods

6.3.1 FO membrane preparation

Chemicals and materials

All chemicals used were ACS grade. 1-methyl-2-pyrrolidinone (NMP, anhydrous, 99.5%), N,N-dimethylformamide (DMF, anhydrous, 99.8%), 1,3-phenylenediamine (MPD, >99%), and 1,3,5-benzenetricarbonyl trichloride (TMC, 98%) were used as received (Sigma- Aldrich, St. Louis, MO). Polyester nonwoven fabric sheet (40 μm, grade 3249) were provided by Ahlstrom, Helsinki, Finland. Polysulfone (PSf) beads (Mn: 22,000) were provided by Solvay Advanced Polymers, L.L.C (Alpharetta, Georgia).

Polysulfone support layer fabrication.

The thin, porous polysulfone (PSf) support layer was synthesized by a traditional nonsolvent-induced phase inversion process of PSf on the polyester fabric. PSf (12 wt %) was dissolved in a mixed solvent of DMF and NMP (DMF:NMP = 1:3) by continuously stirring at room temperature for 12 h. The PSf solution was then degassed in a desiccator for at least 24 h before use. To cast the membrane, the thin fabric was first taped to clean glass and then was moistened by a mixture of DMF and NMP (1:3). Excessive NMP/DMF was carefully removed using filter paper. Subsequently, the PSf solution was cast on a polyester fabric surface with a thickness of 250 μm via a casting blade. Then, the whole composite was immediately transferred to a deionized (DI) water

gelation bath with 0.25 wt % of DMF and 2.75 wt % of NMP to initiate phase inversion. After 10 minutes, the PSf membrane was peeled off from the glass plate and soaked in DI before further treatment.

Polyamide active layer formation.

PSf support membranes were fixed to a frame to provide a smooth surface for interfacial polymerization. The fixed membrane was placed in an aqueous MPD solution (3.4 wt %) for 120 s and then treated with an air knife to remove the excess MPD solution from the membrane surface. Next, the MPD-absorbed support membrane was soaked in a TMC solution (0.15 wt %, in Isopar-G) for 60 s to allow interfacial polymerization process to take place and form the PA layer. The composite membrane was then cured in DI at 95ºC for 120 s, rinsed with a sodium hypochlorite (NaClO, 200 ppm) aqueous solution for 120 s, soaked in a sodium bisulfite (NaHSO3,1000 ppm) aqueous solution for 30 s, and cured in DI at 95ºC for 120 s. The finished PA membranes were rinsed thoroughly with DI and stored in DI at 4 ºC.

6.3.2 Biofouling test systems

The membrane cell was specially designed and built with a thin glass window (16 mm × 38 mm) in the upper plate to enable real-time monitoring by an Olympus BX51 microscope (Olympus, Japan). The thickness of the flow channel on the feed side is 3 mm. The rest of the system closely resembles the cross-flow FO membrane system used in our previous study[16].

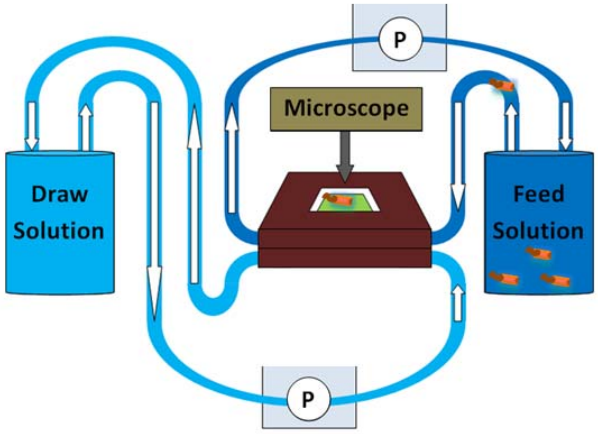

Figure 6.1 Direct observation system for the bacterial deposition and detachment experiment.

6.3.3 Model bacteria

The model bacteria used in this study were *E. coli* K12 MG1655, which was tagged with a plasmid coding for green fluorescence protein to allow visualization via microscope. *E.coli* colonies were cultured twice in Luria Bertani (LB) broth and harvested at the mid-exponential growing stage [262]. The *E.coli* solution was centrifuged (4,000 rpm for 15 mins) and cleaned three times with 154 mM NaCl solution to remove impurities before use. To make the feed solution for the direct observation experiment, the cleaned bacterial cell suspension was diluted in a test solution to a targeted concentration of 1×106 colony forming units (CFU/mL).

6.3.4. Bacterial attachment and detachment protocols

FO direct observation experiments were conducted using the following procedure: (1) sterilize the membrane system using the cleaning procedure

developed by Moshe and Menachem [145]; (2) insert a new membrane sample into the membrane cell with the active layer facing the glass window on the upper plate; (3) stabilize the system with DI for 30 min; (4) switch the DI with the test solution and start the experiment with a cross-flow rate of 400 mL/min; (5) add the *E. coli* seed solution after 30 min; (6) take images at a fixed spot on the membrane surface every minute for the first 20 min of the experiment and then every five minutes until the end of the deposition experiment; and (7) after the experiment has run for 60 min, switch the draw solution to the NaCl solution with the same concentration as the feed solution (in order to stop the permeate flow), increase the cross-flow rate to 1000 mL/min, and take an image every minute. The permeate flux was monitored during the deposition experiment.

6.3.5 Test solutions

Three electrolyte solutions were prepared and tested in bacterial adhesion and detachment experiments: 10 mM NaCl, 100 mM NaCl, and a combination of 97 mM NaCl and 1 mM CaCl2 (total ionic strength of 100mM). For the pH effects testing experiments, the pH of 100 mM NaCl solution was adjusted by adding HCl (1:10) and NaOH (0.1 N) before introducing the bacterial solutions. All the chemicals and reagents used in the experiments were of analytical grade. DI water was used in all the experiments for solution preparation.

6.3.6 AFM force measurement

Atomic force microscopy (AFM) was used to measure and quantify the adhesive forces between the foulant and the membrane surface. The force

measurement was performed in a fluid cell by a Nanoscope Multimode AFM (Digital Instruments, Santa Barbara, CA). A carboxylate modified polystyrene particle (Spherotech, Inc. Lake forest, IL) was used as a surrogate for the bacteria since the carboxylic groups are the predominant functional groups of the extracellular polymeric substances (EPS), which play an important role in initial bacterial deposition and subsequent biofilm formation [189, 263]. Using UV cured glue, the particle probe was made by attaching a single particle (5 μm in diameter) to the end of a commercial SiN tipless cantilever with a spring constant of 0.06 N/m (Veeco Metrology Group, Santa Barbara, CA) (Figure 6.2). A micro pipette controlled by a micro-manipulator was used to transfer glue/particle to the very end of the tipless cantilever. All force data were obtained by the same particle probe. The integrity and strength of the particle probe was carefully examined under a microscope before and after each experiment.

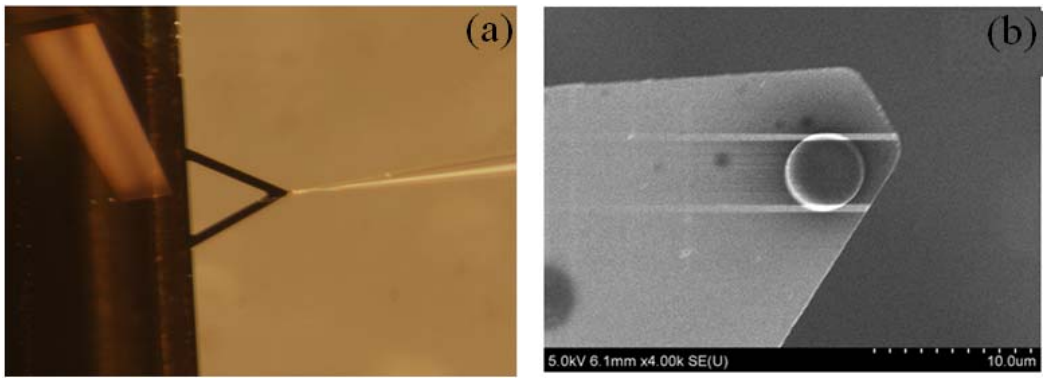

Figure 6.2 Images of particle probe preparation: (a) Transferring a particle by a micro-controlled quartz glass needle (20 ×) and (b) a SEM image of the prepared particle probe.

The force measurement experiments were performed in a fluid cell which was placed and sealed on top of a membrane coupon. Test solution was prepared under conditions similar to those used in the deposition experiment. The fluid cell was rinsed with 10 ml DI and 20 ml test solution and allowed to stabilize for 30 min before each experiment. For each experimental condition, six different measurements were taken at five different locations to avoid possible membrane surface heterogeneity effects. In total, 30 retracting force curves were obtained by the AFM. Raw force data were processed by Matlab and converted from cantilever deflection and *z*-piezo position to force vs. extension distance curves. The representative force curve was then normalized by the radius of the particle, *R,* to get the *F*/*R* ratio. In a fluid system, the *F*/*R* ratio can be viewed as a measure of the energy that is required to prevent a foulant from accumulating on the membrane surface and thus as an indicator for the

membrane fouling potential [202, 264]. The *F*/*R* ratio is presented in the Section 3.4 for comparison of the interfacial forces between the particle and membrane surface under different test conditions. Detailed experimental procedures for using the AFM particle-probe technique to quantify interaction forces relevant to organic fouling are given in our previous publications [24, 27].

6.3.7 Image analytical methods

Images were taken at 1 and 5 min intervals and saved in a Tagged-Image File Format (TIFF). Image processing software was used to minimize the impact of background noise and to obtain the total count of attached bacterial cells. The normalized the attached bacterial cell density, *N*, increased with time, *T*. The net deposition rate constant, *kd*, was calculated with the following equation [248]:

$$k_d = \frac{\Delta N}{\Delta T}\frac{1}{N_0} \quad (1)$$

Where N0 was the bulk feed cell concentration.

6.4 Results and Discussion

6.4.1 FO membrane characterization

Membrane structure information, such as surface morphology, support layer structure, surface functionality, and elemental composition, was characterized through experiments and the results of the experiments are presented here.

Membrane morphology

The Scanning Electron Microscopy (SEM) images of membrane surface and cross section are shown in Figure 6.3. The total thickness of the PA FO membrane is approximately 80 μm with straight, finger-like pores at bottom and smaller pores toward the surface. The structure of the support layer is what would be expected in a high performance FO membrane.

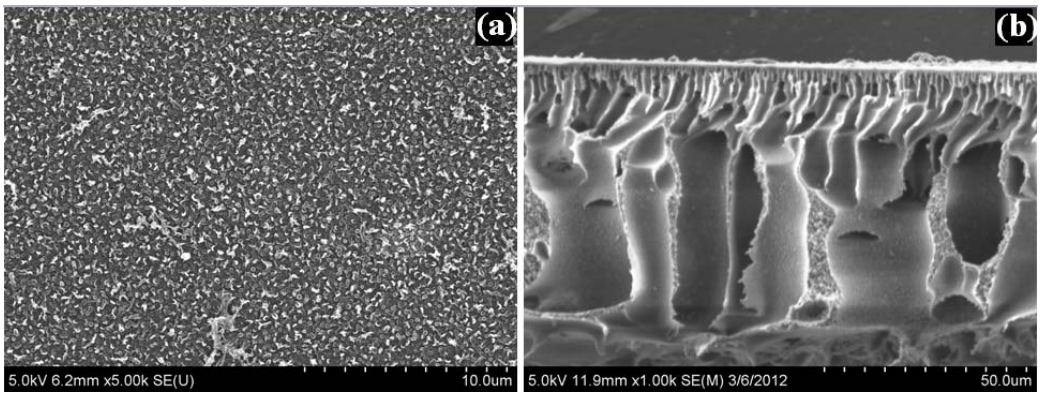

Figure 6.3. SEM images of polyamide membranes: (a) surface image and (b) cross section image.

Membrane Elementary Composition

We used X-ray photoelectron spectroscopy (XPS) to characterize the surface elemental composition of the PA membrane. Surface scans were performed using a high sensitivity AXIS 165 spectrometer (Kratos, Analytical Company, Chestnut Ridge, NY) equipped with a monochromatic Al X-ray source (1×10−9 Torr chamber pressure, 13 kV). Using a 90 degree take off angle, the spectrometer can detect carbon (1s), nitrogen (1s), and oxygen (1s) in a normal sample. XPS results showed that all the membrane surfaces contained

predominantly oxygen, nitrogen, and carbon. The relative elemental composition was determined based on the intensity of the peaks of C (1s), O (1s), and N (1s) which centered around 284 eV, 532 eV, and 399 eV, respectively. As shown in Figure 6.4, core level peaks of 1s for C, O, and N are clearly visible and a small peak of 1s for Na is also observed. Trace amount of sodium chloride (0.25%) resulting from the NaClO used during membrane synthesis was observed on the membrane surface. The O/N ratio of the PA membrane is about 1.64, indicating the existence of free carboxylate functional groups on the membrane surface.

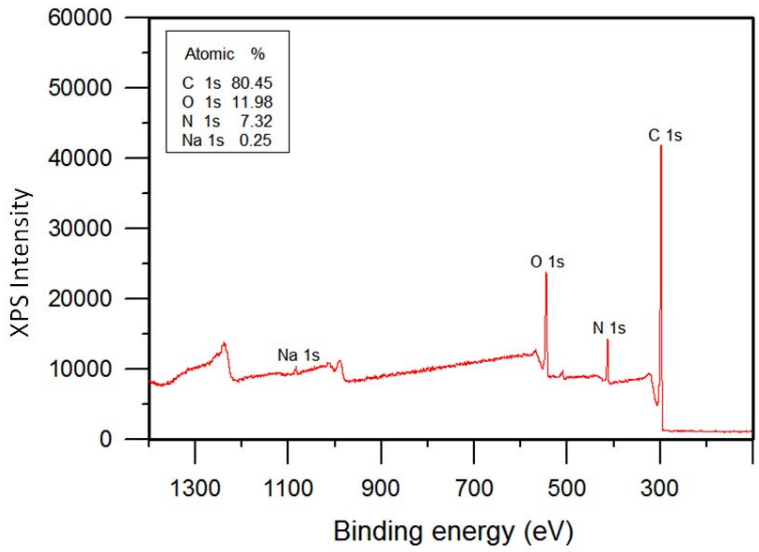

Figure 6.4. XPS spectra of the PA membrane.

Membane surface functionality

Attenuated total reflection Fourier transform infrared spectroscopy (ATR-FTIR) was used to characterize the surface chemical functional groups of the PA

membranes. ATR-FTIR spectra were obtained by a Thermo Nicolet Nexus 670 spectrometer (Waltham, MA) with a Smart ARK ATR accessory and a ZnSe crystal window (Madison, WI). Data collection and analysis was performed using the OMNIC software 6.2 provided with the instrument. Six replicate membrane samples were scanned for each membrane type and the representative spectrum was presented. All spectra (120 scans at a resolution of 4 cm−1) were recorded at room temperature. The background spectrum was obtained before each measurement. No ATR corrections were applied for the spectra obtained.

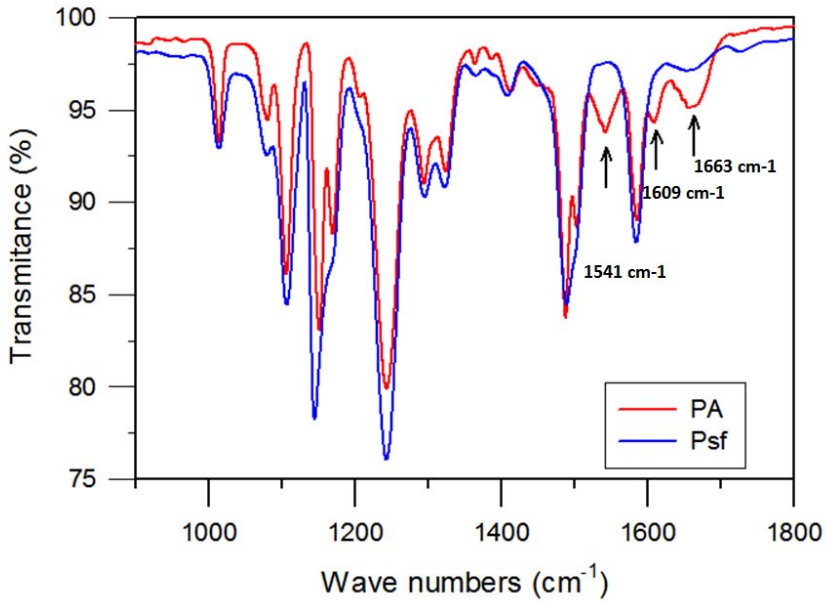

Figure 6.5. Comparison of FTIR spectra of the PA membrane and the polysulfone support. The black arrows pointed to the distinguish peaks on the polyamide membrane surface at wave numbers of 1541 cm-1,1609 cm-1,and 1663 cm-1 belong to functional groups of -CO-NH- [265, 266], -N–H[265, 267], and - C=O)[265, 268], respectively.

A comparison of the FTIR spectra of the PA membrane and the PSf support is

presented in Figure 6.5. It is observed that the PA membrane has three distinct peaks that differentiate it from the polysulfone support layer: (1) the peak at wave number 1541 cm-1 represents an amide II functional group (-N-H and -CO-NH-) [265, 266]; (2) the peak at wave number 1663 cm-1 represents amide I band (-C=O)[265, 268]; and (3) the peak at wave number 1609 cm-1 represents an aromatic amide (N–H) [265, 267].

6.4.2 Effects of pH on bacterial attachment kinetics

The influence of pH on bacterial adhesion to the PA membrane surface is presented in Figure 6.6. In these experiments, the initial total ionic strength of feed solution was kept constant at 100 mM. The concentration of the draw solution was adjusted between 3.5 M and 4.5 M to achieve the same initial flux for all experiments (3.5 μm/s). The effect of pH on initial stage of biofouling was studied at pH 4.0, 5.5, 7.0, and 8.5 (adjusted using 0.1 M NaOH). All other test conditions were kept the same between experiments. As shown in Figure 6.6a and 6.6b, bacterial deposition was strongly influenced by pH. The PA membrane exhibited lower initial bacterial deposition rates of 2.2 and 0.9 μm/S at pH values of 7.0 and 8.5, respectively. At pH 4.0 or lower, the deposition rate of the bacteria is 6.7 μm/S. Notably, the bacterial deposition rate reached 13.4μm/S at pH 5.5.

Previous studies have shown that PA membranes may have electrically charged surfaces in solutions. This surface charge is dependent not only on the dissociation and ionization of functional groups (such as carboxylic (R-COOH) and amine (R-NH2)) on the membrane surface but also the solution chemistry

[269-271]. The p*Ka* of a polyamide membrane surface is determined by the dissociation behaviors of these functional groups. The carboxyl functional groups and amine functional groups are the dominant functional group for a fully aromatic PA membrane which has p*Ka* values of 5.23 and 8.97 and the amine groups are found to have one dissociation constant (p*Ka* = 4.74) [272, 273]. At lower pH (<4.74), the membrane surface can be slightly positively charged (R-NH3+), while, at a neural pH or higher pH (R-COO-) it can be negatively charged. The characterization of the PA membrane surface charge by different methods also shows that membrane surfaces become more negative as pH increases [269, 274, 275].

Solution pH also affects bacterial surface properties. The outer cell membrane of *E. coli* is known to be covered with a layer of extracellular polymeric substances (EPS). EPS are high molecular weight substances secreted by bacteria to the environment and mainly include polysaccharides, proteins, and humic substances. Solution chemistry can greatly affect the EPS properties (such as structure, thickness, hydrophobicity/hydrophilicity, and surface charge [276-279]) and thus can affect bacterial adhesion behaviors. For example, at lower pH, increased amount of protonated carboxylic and hydroxylic functional groups reduces the negative charge and the hydrophilic nature of the EPS surrounded bacteria[280]. Studies have shown that the *pKa* of E coli is close to 5.5[280, 281].

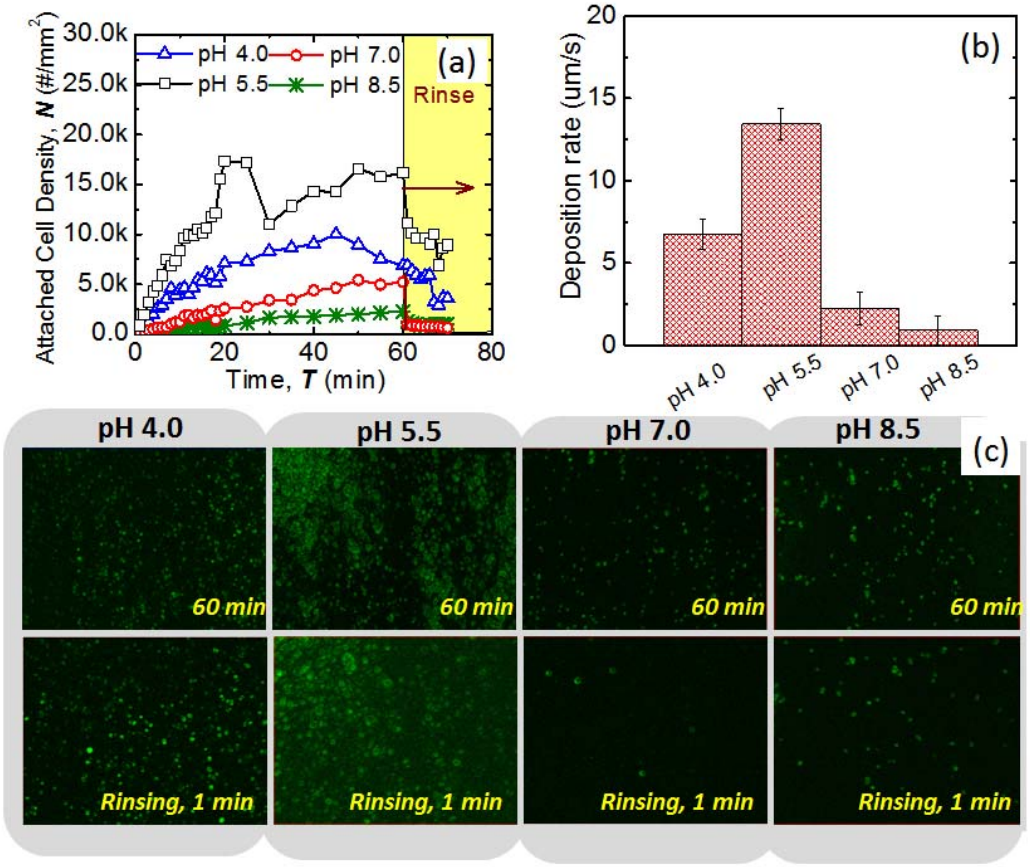

Figure 6.6. Comparison of attached bacterial cell density and deposition rate under different feed solution pH conditions: (a) density of attached bacterial cells on membrane surface during attachment and rinsing experiments, (b) deposition rates during attachment experiment, and (c) removal efficiency during rinsing experiments. The operational conditions for the attachment experiment were: 4~5 M NaCl solution as draw solution and 100 mM NaCl as feed solution (which resulted in a permeate flux of 3.5 μm/s), 1x106 CFU/ml *E. coli* K12, and a cross-flow rate of 8 cm/s. The operational conditions for the rinsing experiments were: 100 mM NaCl as draw and feed solutions, 1x106 CFU/ml *E. coli* K12 in the feed solution, and a cross-flow rate of 21.4cm/s. Four sets of experiments were conducted with different pH conditions in the feed solution, i.e. pH 4, pH 5.5, pH 7.0, and pH8.5 (adjusted by 0.1 N NaOH).

In our experiment, solution pH is found to affect the charge of both membrane surface and bacteria surface and thus affect the electrostatic force between bacteria and membrane as well as bacteria and bacteria. pH 5.5 is close to both

the p*Ka* value of and membrane *E.Coli.* In this condition, most of the bacteria in the solution are neutrally charged. Therefore, electrostatic repulsion force between the PA surface and bacteria as well as between the bacteria a in the solution and the deposited bacteria is greatly reduced, compared to the cases of pH 7.0 and pH 8.5. The reduced charge exclusion effects between bacteria and bacteria as well as between bacteria and the membrane surface resulted in a higher deposition rate at pH 5.5.

At pH above the p*Ka* of *E.Coli*, negative charge (R-COO-) in the bacterial EPS and on the PA membrane surface, and both the bacteria and membrane surface are negatively charged. Hence, the bacteria-membrane attraction is smaller due to the repelling effects that exist between the negatively charged bacteria and the membrane surface.

At lower pH (~4), the membrane surface is slightly positively charged due to the positive charge from the amine functional groups [282]. At this pH, the EPS surrounded bacterial cell surface might be slightly positively charged as well considering the protein content in the mixture of EPS. Thus, the electrostatic repulsive interactions resulted in lower bacteria deposition rate as well.

6.4.3 Ionic strength effects on bacterial attachment and detachment

In this part of study, the effects of ionic strength on deposition kinetics of bacteria onto the membrane surface under repulsive electrostatic conditions are investigated. The deposition rates for *E. coli* with ionic concentrations of 10

and 100 mM NaCl at pH 7.0 are plotted in Figure 6.7. Both the bacterial coverage and the deposition rate at 10 mM are much higher than those at 100 mM. An increase in net deposition rate with decreased ionic strength is observed.

The bacteria deposition indicated a stronger interaction between bacterial cells and membrane surfaces. As discussed in Section 6.3.1, bacterial cell aggregation and adhesion behavior is strongly influenced by the surrounding EPS. The two sets of experiments were running at neutral pH, and both the bacterial surface and the membranes surface are negatively charged. However, at the lower ionic strength, the EPS layer expands and, consequently, reduces the density of negative surface charges [277]. So at low ionic strength charge, the repulsive force between a single bacterial cell and membrane surface can be reduced. Furthermore, at higher ionic strength, cell aggregation in the bulk solutions may happen at higher chance due to a double layer compaction for the EPS layer at a higher ionic strength. The double layer compaction affects the mean charge of EPS layer and reduces repulsive force between bacterial cells. Cell aggregation happen at higher ionic strength and the aggregates are more strongly affected by the sheer force introduced by cross-flow than the electrostatic interactions between cells and membranes.

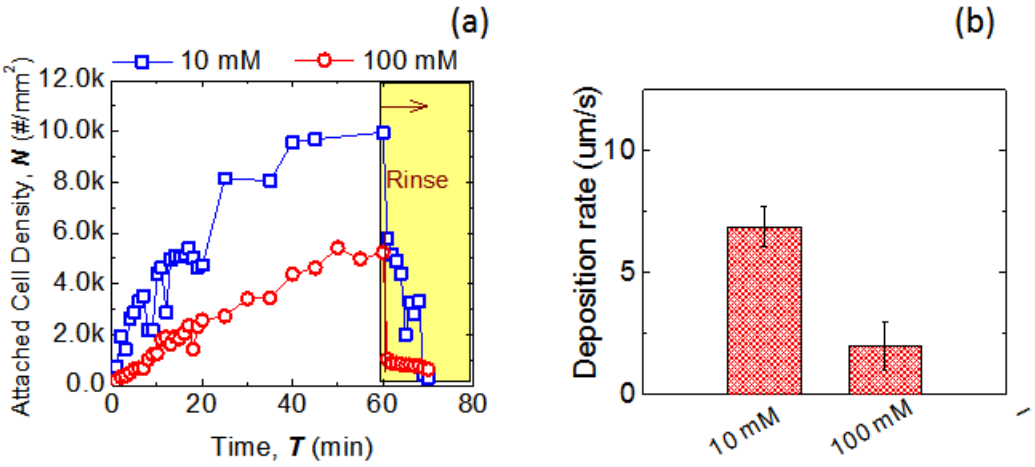

Figure 6.7. Comparison of ironic strength effects on bacterial attachment density during deposition and rinsing experiments: (a) count of attached bacterial cells on membrane surface during attachment and rinsing experiments; and, (b) deposition rates during attachment experiment. The solution ionic strength in feed solution of 10mM and 100mM was adjusted by NaCl. Solution pH was adjusted to 7.0. Other experiment conditions were the same as in Figure 6.6.

6.4.4 Calcium effects on bacterial attachment and detachment

The specific interactions between polysaccharides and calcium have a major effect on the organic fouling of FO membranes [24, 27] and also greatly affect the mechanical stability of biofilm formation [283] . Divalent cations, which are known for their involvement in bridging the functional groups on both polysaccharides and membrane surfaces, are likely to play a pivotal role in the bacterial adhesion on membrane surface. Enhancements in bacterial aggregation and adhesion by divalent cations rely on screening of surface charges and forming cationic bridges between negatively charged surface functional groups. In this study, bacterial deposition/detachment experiments were conducted in the presence or absence of calcium ions (1 mM) in NaCl

solutions adjusted to an ionic strength of 100 mM at pH 5.5 and pH 8.5. A greater bacterial deposition rate was observed when the test solution was supplemented with calcium (Figures 6.8a and b).

Our results indicate that calcium cations significantly enhanced bacterial adhesion at higher pH (pH 8.5). Very low concentrations of divalent cations (i.e., 1 mM) were added to reach a deposition rate of 7.9 μm/s, which is almost 10 times higher than the rate for non-calcium experiment. The zeta potential of the PA surface under these conditions (pH 7.0 and 8.5) is expected to have a negative value and, therefore, exhibit electrostatic repulsion to bacterial cells. At lower pH (pH 5.5 compared with pH 8.5), the increased amount of protonated carboxylic groups reduced the bridging of the negatively charged calcium between the PA surface and the bacteria as well as between the bacteria in the solution and the deposited bacteria.

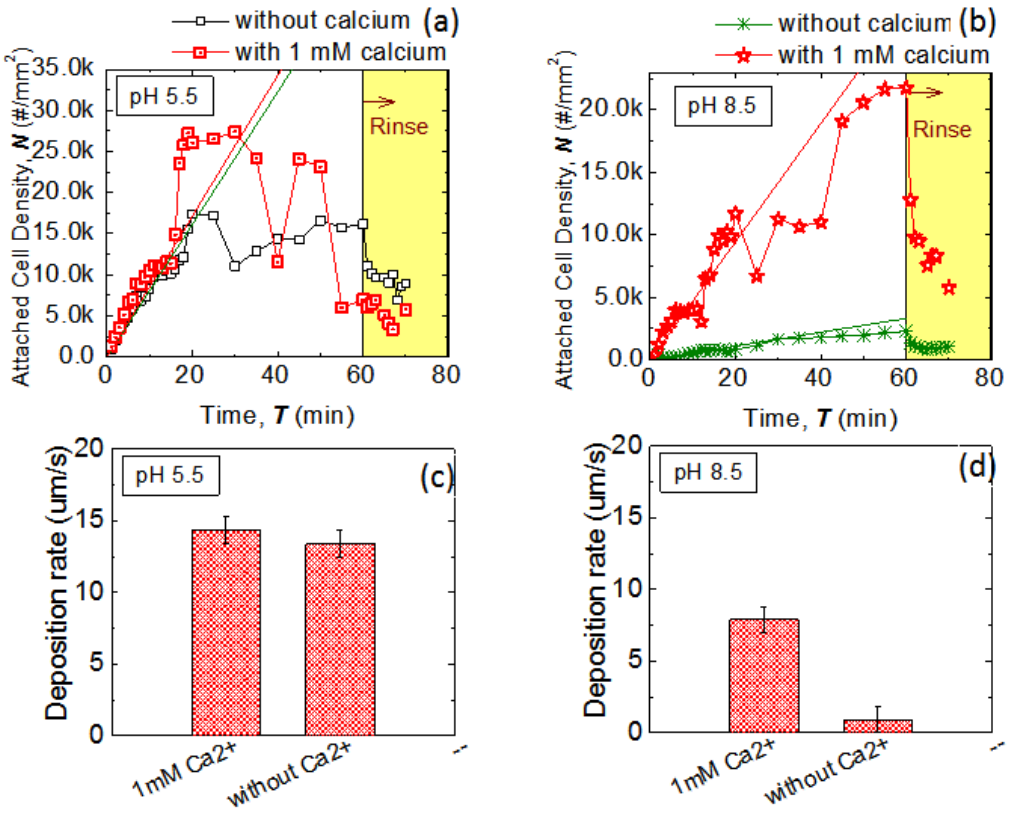

Figure 6.8. Comparison of calcium effects on bacterial attachment density during deposition and rinsing experiments: (a) Bacterial deposition at pH 5.5 with/without calcium; (b) Bacterial deposition at pH 8.5 with/without calcium; (c) deposition rates during the attachment experiment at pH 5.5; and, (d) deposition rates during the attachment experiment at pH 8.5. The experimental conditions were the same as in Figure 4 except that 1 mM calcium chloride was added to the feed solution.

6.4.5 Foulant-membrane interactions

Force measurements by AFM are presented to support the proposed biofouling mechanism of the PA-FO membrane. As shown in Figure 6.9 a, a carboxylate-functionalized polystyrene AFM particle probe was used as a surrogate for the polysaccride in bacteria EPS, The method was described in previous publications [24, 119]. Based on the analysis of the force versus distance curve obtained during retraction of the particle probe from membrane surface, we presented the adhesive force *F/R* versus the extension distance in Figure 6.9b, 6.9c, and 6.9d. All the force measurement experiments were conducted in solution. Solution ionic strength was kept constant at 100 mM by NaCl solution. Solution pH was adjusted by HCl (1:9) or NaCl (0.1 N). Calcium chloride (1 mM) was added to investigate calcium effects on adhesive force.

Our deposition results demonstrated the importance of calcium bridges between bacteria-bacteria and bacteria-membrane. Strong adhesive forces and long rupture distances are obtained in our experiments for membranes exposed to solutions with calcium ions. Furthermore, calcium bridging has more significant effects at higher pH.

In the absence of calcium ions but at the lower pH (pH 5.5), the adhesive force and rupture distance decreased remarkably from 0.79 to 0.15 mN/m and from 192 to 43 nm, respectively (Figure 6.9c). In the presence of calcium ions, the adhesive forces between the carboxylate particle probe and the PA membrane surface had a significantly wider distribution than those for experiments

involving non-calcium membranes (Figure 6.9c, 6.9d). Specifically, adhesive force as high as 1.62 mN/m were measured at pH 8.5 in the presence of calcium ions, whereas the adhesive force for a non-calcium experiment was 0.46 mN/ m. The results presented in Figures 6.9c and 6.9d provide significant evidence for the formation of calcium bridges with the PA membranes in higher pH. The AFM results are in agreement with both bacterial deposition experiments.

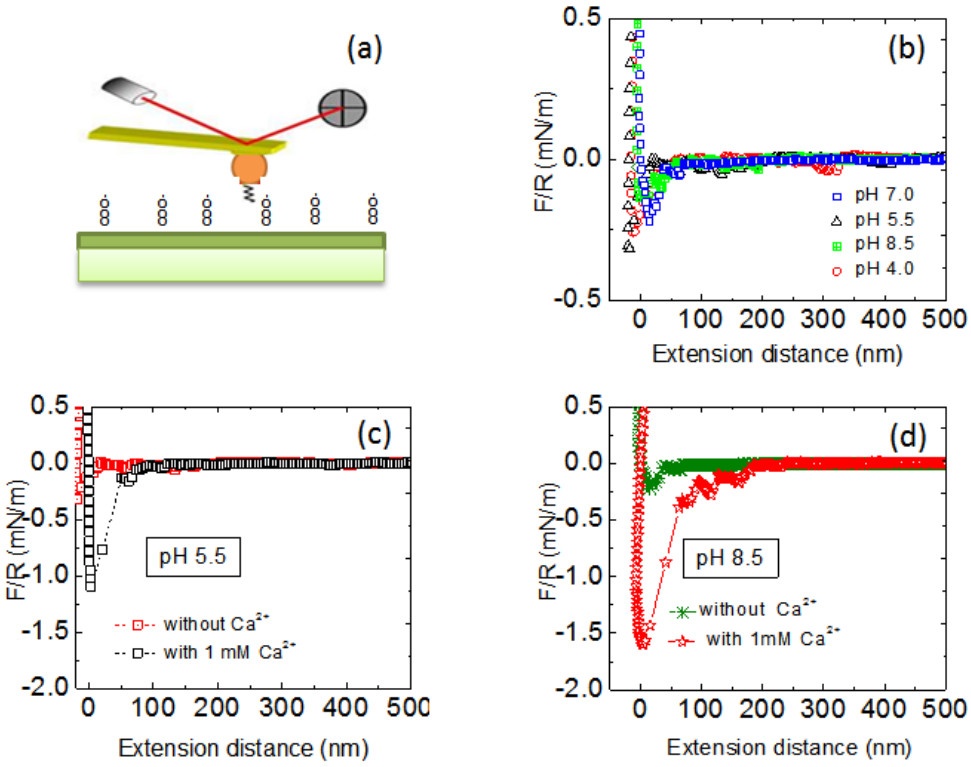

Figure 6.9. AFM results with a carboxylate functionalized particle probe: (a) schematic illustration of force measurement experiment; (b) pH effects on the adhesive forces between the PA membrane and the particle; (c) calcium effects on adhesive force under lower pH (5.5); and, (d) calcium effects on adhesive force under higher pH (8.5).

6.4.6 Interpretation by molecular dynamics simulations

Molecular dynamics simulations of membrane and foulant Interaction

Molecular dynamics (MD) simulations have contributed significantly to the membrane research by providing a way to directly investigate the microscopic detail information of the system that is not directly available by experiments. In this study, we use a method based on the configuration-bias Monte-Carlo

algorithm to build a PA-FO membrane configuration. A long chain polysaccharide molecule was built to model the behavior of bacteria EPS interacting with membrane surface (Figure 6.10a). The membrane-foulant system was placed in aqueous electrolyte solutions; the foulant, membrane, water molecules and dissolved ions were modeled using the consistent-valance force field (CVFF). We investigated the local foulant-membranes interaction via steered molecular dynamics (SMD) simulation. For detailed information regarding system modeling, please refer to our simulation paper[284].

(b) Interactions in SMD simulation

1) *Inner-sphere ionic bridge*. Inner sphere complex is a type of surface complex. Formation of inner sphere complexes occurs when ions bind directly to the surface with no intervening water molecules (Figure 6.10a). This binding structure could only be found in R-COO- (PA) – ions/ R-COO- (polysaccharide) system, ex. the neutral environment.

2) *Dipole - dipole binding.* Dipole-dipole binding could occur in both R-COO- cases and R-COOH cases (Figure 6.10b), but it is very rare in simulation. In SMD simulation, this type of binding results in adhesive force (possibly contributed by hydrogen bonding).

3) *Outer-sphere complex.* This kind of binding can be formed in both R-COO- cases and R-COOH cases. An example is illustrated in Figure 10c (within the circle). In SMD simulation, this type of binding results from small adhesions (usually less than 0.15nN). Significant force peak is rarely observed.

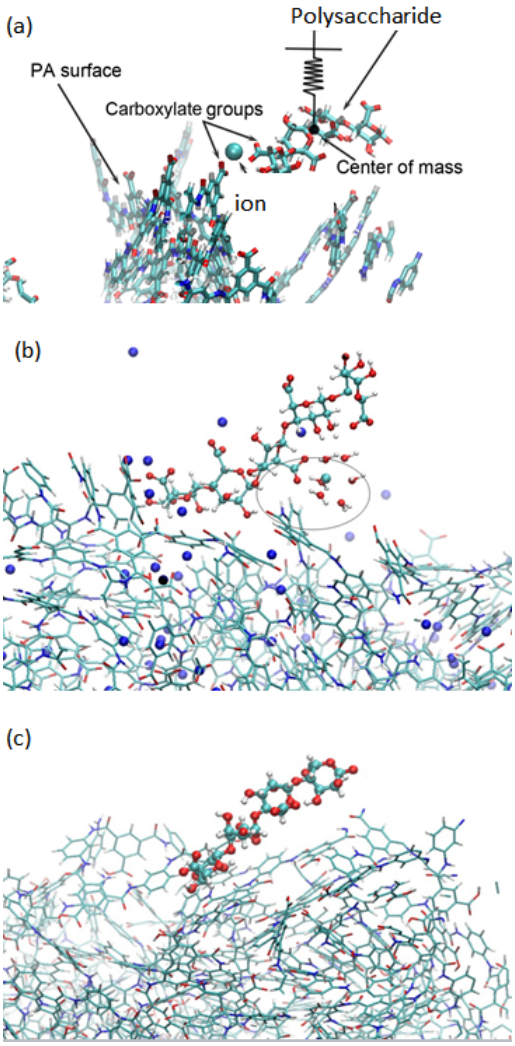

Figure 6.10. Interaction models: (a) Polysaccharide and membrane system and inner sphere ionic bridge; (b) outer sphere complex; and (c) dipole-dipole binding.

(c) Understanding of pH effects

According Henderson-Hasselbalch equation: pH=pka+log([base]/[acid])[285], we obtain the proportion of acids and their conjugate bases as shown in Table 6.1.

For a membrane in a mildly acidic environment (pH=4.0 and pH=5.5), the presence of R-COOH on membrane surface is significant and should be given

consideration. In the other cases (pH=7.0 and 8.5), R-COO- is dominant. For a polysaccharide molecule, R-COO- group is dominant under all pH conditions. As a result, in acidic environments, we consider the interactions between R-COOH, Na+, water and COO- (alginate) in the simulation system. Meanwhile, in the neutral and basic environment, the PA and alginate have the functional group of R-COO-, the significant difference observed from the experiment could be attributed to the Na+ ions bridge.

In neutral environments, a stable inner-sphere ionic bridge could form between R-COO- functional groups, so the pull-off force is much larger than that for a R-COOH case (Figure 6.10a). Some outer-sphere complex could form in R-COOH- Na+ system. However, as mentioned before, this kind of binding is rather weak and contributes little to the total pull-off force. The existence of carboxylate groups promotes the deposition of alginate and also forms a stable binding structure. This could partially explain the fact that the neutral environments (pH=5.5) have a higher deposition rate than in the acidic environment (pH=4.0).

Table 6.1 Functional group analysis in system with different pH value

	Membrane R-COO- /COOH	Membrane R-NH2/R-NH3+	Polysaccride R-COO-/R-COOH
pH=4.0	5.8/100	18/100	223/100
pH=5.5	186/100	575/100	7079/100
pH=7.0	58.9/1	182/1	2239/1
pH=8.5	1862/1	5754/1	70794/1

(d) Understanding of the effects of calcium ions

The R-COO- -Na+ force curve and the R-COO- -Ca2+ force curves in different pH conditions are plotted in Figure 6.11. In neutral and basic environment, the pull-off force of R-COO- -Ca2+ was much larger than that of R-COO- -Na+ as observed from simulation as shown in the red and green curves. This indicates a significant increase in adhesion when adding Ca2+ in the neutral or basic system. Ca2+ promoted a stronger binding than Na+ ion. In comparison, in the acidic environment (i.e. R-COOH system), slightly higher force occurs when Ca2+ ions are added since Ca2+ does not participate in the inner-sphere ionic bridge in R-COOH system. This is consistent with experimental results. Fouling study and force measurement both revealed that Ca2+ ions greatly promoted fouling in basic and neutral environments. Ca2+ also promoted the

bacteria - bacteria interactions in acid environment, which will enhance the bacteria aggregation and enhance deposition. In sum, in neutral and basic systems, the Ca2+ ions have significant effects on both PA - alginate interaction and alginate aggregation; in acidic systems, the PA - alginate interaction is not obvious, so the effect of Ca2+ ions may be weaker.

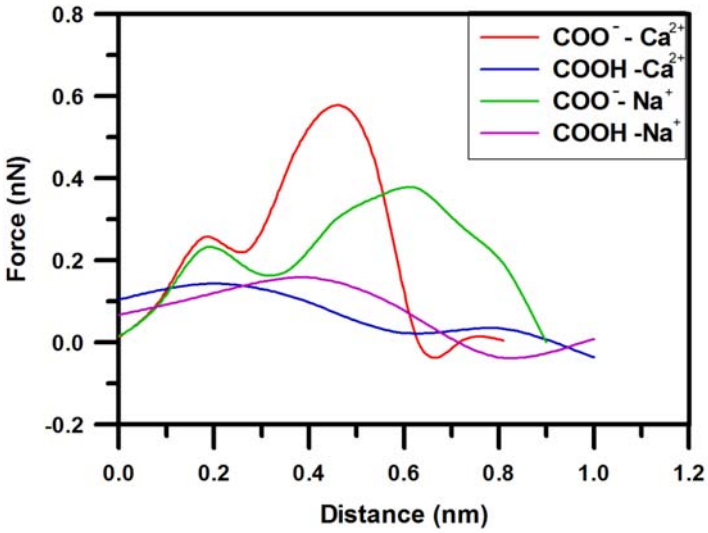

Figure 6.11. SMD results: (a) pH effects and (b) calcium effects.

6.5 Concluding Remarks

Initial bacterial deposition onto polyamide forward osmosis membranes were investigated with a focus on the effects of solution chemistry such as pH, ionic strength, and divalent ions. The experimental results of deposition rate, a, and molecular simulation were employed to elucidate the mechanisms of initial biofouling in forward osmosis process. This study demonstrated that solution chemistry had strong effects on initial bacterial deposition. Enhanced bacterial deposition rates were observed with lower solution pH, lower ionic strength, and the addition of calcium ions. Solution pH changed the membrane's surface

charge and also affected the charge and hydrophilicity of EPS bacteria, which resulted in a change of interactions between bacteria and membrane. Furthermore, the calcium bridging effects significantly increased adhesion force and bacterial deposition rate.

6.6 Acknowledgements

This work is collaborated with Prof. Yongsheng Leng and Yuan xiang from the George Washington University. This study is based upon work supported by the National Science Foundation under Grant No. CBET-1158601. In addition, the first author is partially supported by an NWRI-AMTA (National Water Research Institute – American Membrane Technology Association) Fellowship for Membrane Technology. These supports are gratefully acknowledged. The authors would also like to thank Prof. Kai Loon Chen from Johns Hopkins University for kindly providing the bacteria.

Chapter 7: Organic Fouling Behaviors and Foulant layer Viscoelastic Properties of Polyamide Forward Osmosis Membranes

7.1 Abstract

This study investigated organic fouling behavior of polyamide-forward osmosis (PA-FO) membranes subjected to alginate fouling and their relationships to foulant adsorption and fouling layer viscosity properties. Specifically, the adsorption and viscoelastic structure properties of the alginate layer on a polyamide sensor surface grew as a function of ionic strength and the presence of calcium ions was monitored by quartz crystal microbalance with dissipation (QCM-D). The PA-FO membrane was synthesized by interfacial polymerization on a polysulfone (PSf) support. The polyamide sensor was prepared by isolating the active polyamide layer from the PSf layer support and attaching it on a commercial gold sensor. This sensor provided exactly the same surface as the PA-FO membrane for alginate adsorption in QCM-D study. The properties of the adsorbed alginate layer were investigated by combining the information of the incremental adsorbed areal mass and the alginate layer's viscoelastic properties. It was found that, the absence of calcium ions, alginate adsorption behavior was strongly influenced by charge screening between the negatively charged carboxyl functional groups of the alginate molecules and the membrane surface. Enhanced alginate adsorption rates were observed as ionic

strength is increased; however, the charge screening effects at different ionic strengths had negligible effects on PA-FO membrane fouling. The presence of calcium ions induced the formation of a thick and dense alginate layer via the bridging effects between alginate - alginate and alginate - membrane surfaces and significantly changed membrane fouling behavior.

7.2 Introduction

The forward osmosis (FO) is a promising membrane process for sea/brackish water desalination and wastewater reuse [9, 10, 12, 232, 235, 286]. The FO process is considered to be an energy-friendly and cost effective method compared with traditional membrane processes. No hydraulic pressure is required for the separation process; the FO membrane uses natural osmotic pressure to pull water molecules through a semi-permeable membrane from diluted feed solutions to concentrated draw solutions; and the diluted draw solutions can be concentrated again by reverse osmosis for solute reuse and purified water production [235, 287]. One of the major drawbacks of membrane technology is membrane fouling, which significantly limits the permeate flux efficiency and increases operating costs [288, 289]. Membrane fouling remains the most restrictive and challenging factor for the application of all membrane technologies.

Among the various types of membrane fouling hindering industry implementation, organic fouling is a significant challenge. Organic fouling refers to the adsorption of organic matters such as polysaccrides, humic

substances, protein, and grease onto the membrane surfaces. Organic matter is a major source of membrane foulants, as it is prominent in all natural waters (e.g. surface runoff, groundwater, and seawater) and it has special properties that interact with other types of foulants to form complexities which can result in accelerat surfaces is almost unavoidable, the deterioration of membrane performance subjected to organic fouling is inevitable and must be considered when designing fouling control strategies.

In the FO membrane process, it has been demonstrated that FO membranes have lower fouling propensity and higher cleaning efficiency compared to RO membranes [21, 24, 25]. However, most of these studies focus on the flux behavior under different types of fouling. To date, the mechanisms behind these fouling behaviors are still unknown. Therefore, in order to develop effective fouling control strategies, it is important to develop an applicable method to investigate the relation between organic molecule adsorption and membrane fouling behavior.

QCM-D has proven to be an effective tool for studying organic micromolecule adsorption on top of a quartz sensor with nanoscale sensitivity [290, 291]. Changes of mass/thickness and structural/viscoelastic that occur on the sensor surface can be obtained and the adsorption of mass onto the sensor surface will be sensed as a change in sensor frequency. In addition, the loss of system energy to dissipation provides valuable information on the viscoelastic properties of the adsorption layer.

This chapter aims to develop an effective method for the investigation of alginate adsorption behaviors on a polyamide surface and the properties of the subsequent adsorption layer by QCM-D. An innovative sensor coating procedure was developed to attach the active polyamide film onto a commercial gold sensor surface. The effects of solution chemistry (ionic strength and divalent ions) on alginate adsorption behavior onto a polyamide sensor were studied and compared with those in actual fouling experiments, where the membrane flux was also studied and the fouling was composed of similar alginate concentrations on polyamide membranes.

7.3 Materials and Methods

7.3.1 Materials and chemicals

ACS certified 1, 3- phenylenediamine (MPD, >99%), 1, 3, 5-benzenetricarbonyl trichloride (TMC, 98%) 1-methyl-2-pyrrolidinone (NMP, anhydrous, 99.5%), and N,N-dimethylformamide (DMF, anhydrous, 99.8%) were used as received (Sigma- Aldrich, St. Louis, MO). Polyester nonwoven fabric sheets (40 μm, grade 3249) were provided by Ahlstrom, Helsinki, Finland. Polysulfone (PSf) beads (Mn: 22,000) were provided by Solvay Advanced Polymers, L.L.C (Alpharetta, Georgia).

7.3.2 Organic foulants

Alginate was selected as the model organic foulant to represent some of the common types of organic matters in water environment. Sodium alginate (Sigma-Aldrich, St. Louis, MO) with a molecular weight range from 75 to 100 kDa is extracted from brown algae. Stock solutions of sodium alginate (10g/L)

was prepared by dissolving sodium alginate into sterilized deionized (DI) water and kept at 4°C to avoid biological contamination. Diluted alginate solutions (200mg/L) were used in both the organic fouling and the QCM-D experiments.

7.3.3 FO membrane and organic fouling testing systems

The FO membrane tested in this study was prepared by interfacial polymerization of TMC and MPD on top of the pre-casted PSf support. Detailed information of the polyamide membrane fabrication and post treatment was described in Chapter 6. The FO membrane was relatively hydrophilic with a water contact angle of 61 ± 4° measured by a G10 goniometer (Kruss, Ste K Matthews, NC). The pure water permeability of the membrane was determined to be 8.86×10-13 m/(s·Pa) in RO mode. The salt rejection rate under the same test conditions was determined to be 97% with 20 mM NaCl as the feed solution.

A FO cross-flow system was used in this study to monitor the fouling behavior s of the polyamide membranes. It included a cross-flow membrane chamber with two identical flow channels (77 mm ×26 mm × 3 mm) [16] . Membrane coupons were cut and sealed in the membrane cell between the two channels. The draw solution and feed solution circulated in separate loops with co-current cross flow in the chamber to reduce pressure on the suspended FO membrane. Detailed information on this system was provided in our previous study [16].

7.3.4 Organic fouling and cleaning protocols

Organic fouling experiments were performed using the protocols similar to

Chapter 3. Basically, a freshly made membrane coupon was used for every experiment and pure water flux with 5M NaCl as the draw solution and DI as the feed solution was tested before all fouling experiments. After that organic fouling experiments with alginate (200mg/L) and NaCl (20mM) and draw solution (NaCl, 5M) was used for the fouling experiments. All of the fouling experiments were performed with a cross-flow rate of 400ml/min, at pH 7.0 (adjusted by NaHCO3), and a temperature of 20 ± 1 °C. The permeate water was collected in a draw solution tank and the weight changes were monitored throughout the fouling experiments for further flux calculations. Note that, before the fouling experiments, a baseline experiment with same ionic strength for both draw solution and feed solution was conducted to correct the solution's dilution/concentration effects on the membrane flux.

7.3.5 QCM-D experiments protocols

A QCM-D E4 system (Q-Sense AB, Gothenburg, Sweden) was utilized in this study to investigate organic molecule adsorption on a polyamide modified sensor. QCM-D experiments were performed with polyamide-coated gold sensor surfaces. The protocols of sensor fabrication and alginate adsorption experiments are documented in the following sections.

Polyamide sensor fabrication

The polyamide sensor was prepared by spin coating a thin layer of PSf and by the attaching of an isolated PA film onto the PSf layer (Figure 7.1). The gold sensor was thoroughly cleaned before the coating. Each new, clean sensor was

treated in a UV/ozone chamber (ProCleaner Chamber, Bioforce Nanoscience, Ames, IA) for 20 minutes and then heated in a mixture of DI, ammonium hydroxide (25%) and hydrogen peroxide (30%) (5:1:1) at 75°C for 5 minutes. After heating, the sensor was rinsed with DI and dried with pure nitrogen gas before being treated in the UV/ozone chamber for another 10 minutes. The newly cleaned sensor was mounted on a spin coater and coated with polysulfone solution (1%, in NMP) for 10 s at 2500 rpm. A 2 ×2 cm2 PA-FO membrane was cleaned with DI and dried in a desiccator for 24 hours before isolation. DMF was used as the organic solvent to dissolve and remove the PSf support layer from the PA surface layer. The membrane coupon was secured onto a silicon wafer with the PSf layer facing up. A dissolving and drying procedure was repeatedly performed to totally remove the PSf layer. During this procedure, 0.1 ml of DMF was dropped onto the membrane surface and any excess DMF was carefully removed by filter paper. Then, the membrane coupon was dried in air for 2 minutes. Next, another 0.1 ml of DMF was added to membrane surface. After this procedure was repeated 10 times, the polyester mesh could be peeled off using tweezers without damaging the bottom PA layer. DMF dissolving and drying was then repeated another thirty times until the PSf was completely removed. The isolated PA film was gently attached to the PSf coated sensor and dried in desiccator.

Before each measurement, the sensor was cleaned three times by repeated sonication in a Hellmanex III solution (2%). The sensor was thoroughly rinsed with DI water and dried with high-purity N2 gas.

Alginate adsorption protocol

The QCM-D instrument monitored the changes in the resonant frequency (Δf) and dissipation (ΔD) of the quartz crystals at a number of different resonance overtones. The shifts of Δf and ΔD were recorded to model the adsorbed layer properties. For each QCM-D experiment, Δf and ΔD baselines were first established in DI water before test solutions were introduced into the flow chambers. The flow rate of the pure water and the salt solutions was controlled at 100 μL/min by a high precision multichannel pump dispenser (Labinett lab AB, Goteborg) which generated a velocity of approximately 0.2 mm/s on the crystal surface. All adsorption experiments were conducted at a controlled temperature of 25 °C.

Three sets of alginate adsorption experiments were conducted to test the effects of ionic strength on alginate adsorption and also to compare sodium bridging and calcium bridging effects on alginate adsorption (Figure 7.1).

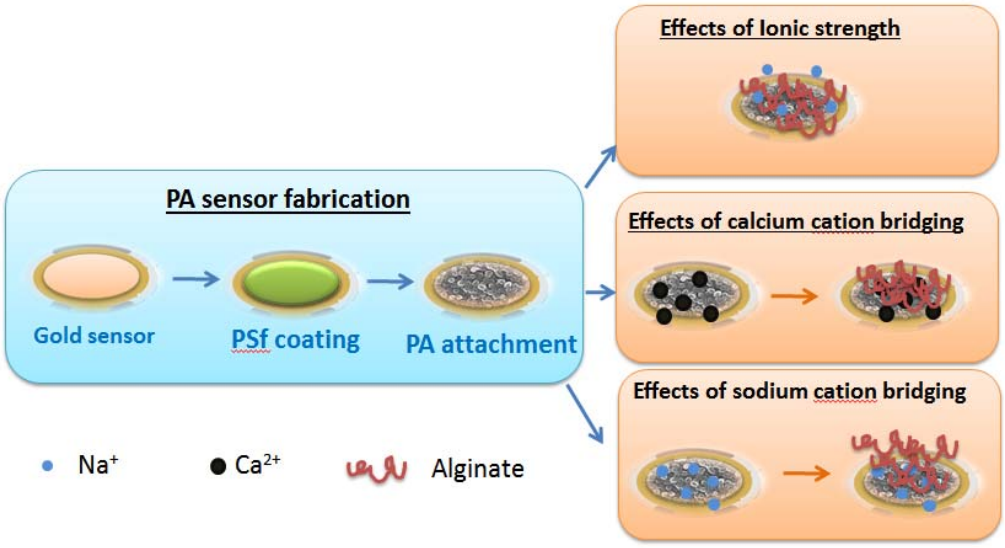

Figure 7.1 Schematic illustration of QCM-D alginate fouling experiments.

7.4 Results and Discussion

7.4.1 Influence of ionic strength on alginate fouling

The flux behaviors of FO membranes subjected to organic fouling at different ionic strengths were tested with accelerated alginate concentration (200 mg/L) over a 24 hour period. A 5 M NaCl solution was used as the draw solution and lower concentrations of NaCl solutions with total ionic strengths of 10 mM, 20 mM and 100 mM, respectively, were used as the feed solution. NaHCO3 was added to adjust the pH value of the feed solutions (pH 7.0). Sodium ions were the only cation in the feed solutions. As shown in Figure 7.2, the membrane flux declines during the alginate fouling are negligible at all ionic strengths. For all three experiments, after 24 hours, more than 95% of the clean membrane flux still remained. By visual examination of the fouling layer, alginate formed

a very thin, discontinuous, gel-like layer and covered the membrane surface. The fouling layers were not attached tightly to the membrane surface; they could be easily separated by DI rinsing. This observation indicated that total ionic strength had insignificant effects on the flux decline for a PA-FO membrane. In a neutral environment, alginate molecules are negatively charged; the increase in total ionic strength of the solution reduces the surface charge along with the number of changes in the structure of a single alginate molecule because of electrostatic double layer compression. The reduced surface charge may prompt the aggregation of alginate molecules and enhance adsorption. However, the flux decline behaviors of the PA-FO membrane confirms electrostatic double layer compression because increased ionic strength did not play a major role in alginate fouling on PA-FO membranes.

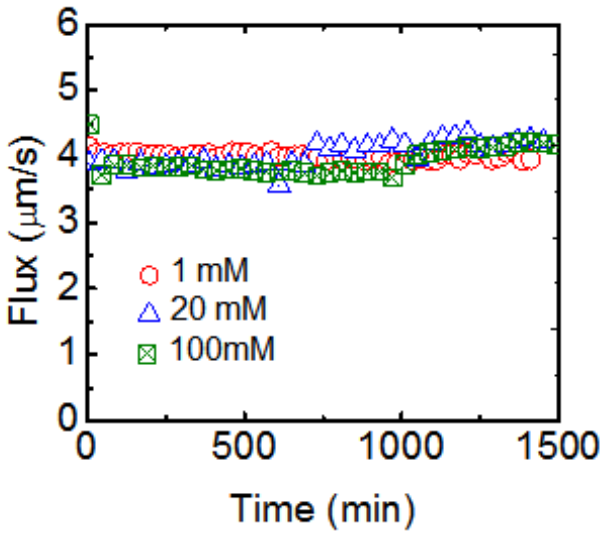

Figure 7.2. Flux behaviors of FO membrane subjected to organic fouling. Experimental conditions were as follwowing: 4 M NaCl was used as draw solution; and lower concentrations of NaCl solutions (1 mM, 20 mM and 100 mM) were used as feed solution; and feed solution pH was kept at 7.0 adjusted by NaHCO3; the temperature was kept constant at 20 ± 1ºC; the cross-flow rate was 400ml/min; and the alginate concentration used was 200mg/L. Note the membrane flux presented is normalized by the clean membrane flux which was obtained by baseline experiment.

7.4.2 Influence of divalent ions on alginate fouling

Divalent cations have been reported to enhance alginate fouling by neutralizing negative charges and providing a bridging mechanism that allows alginate–alginate and alginate-membrane complexes to form [202, 292-294]. Enhanced alginate fouling experiments with calcium were conducted at a total ionic strength of 20 mM, with 1 mM Ca2+ added in the feed solution to determine the effect of the presence of divalent cations on membrane flux decline. Ca2+ was chosen as a model divalent cation because it is one of the major divalent cations in natural waters. As shown in Figure 7.3, Ca2+ dramatically enhanced

membrane fouling. The membrane permeate flux fluctuated less than 5% over a period of 24 hours when the divalent cations were absent in the feed solution. When Ca2+ cations were present, the permeate flux decreased markedly by 40 % within 24 hours. The dramatic effects of Ca2+ on membrane fouling, compared those to Na+ ions, will be discussed later when presenting the corresponding adsorption experiments.

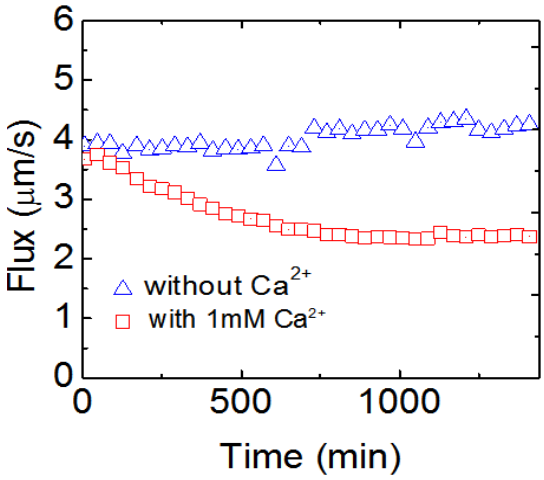

Figure 7.3. Calcium effects on flux behavior f FO membrane subjected to organic fouling. Experimental conditions were as following: 4 M NaCl was used as draw solution; and a lower concentrations of NaCl solutions (1 mM, 20 mM and 100 mM) were used as feed solution; and feed solution pH was kept at 7.0 adjusted by NaHCO3; testing temperature was kept constant at 20±1ºC; cross-flow rate 400ml/min; the alginate used was 200 mg/L. 1 mM CaCl2 was added in the calcium effects experiment. Note the membrane flux presented was normalized by the clean membrane flux which is obtained by baseline experiment.

7.4.3 QCM-D study on alginate adsorption

To study the effects of solution chemistry on alginate fouling potential, alginate adsorption kinetics and viscoelastic properties were analyzed in the experiments

with alginate adsorption to polyamide coated crystals in a QCM-D. The polyamide coated gold sensor was used as a model surface that mimicked polyamide membrane surface as a substratum for alginate to demonstrate adsorption behavior and viscoelastic characteristics.

Effects of ionic strengths on alginate adsorption

In this part of study, the ionic effects of alginate adsorption on the polyamide surface were tested in a cross-flow QCM-D chamber. The sensor was first stabilized in DI. After the sensor reached equilibrium in DI, alginate solutions (200 mg/L) with different total ionic strengths (NaCl 1 mM, 20 mM, and 100 mM, respectively) were then introduced into the system until it reached the adsorption equilibrium. In the end, the system was rinsed with DI water till stabilized. The changes in frequency and dissipation were monitored and analyzed. The cross flow rate for all adsorption experiments was fixed at 100 μl/min and increased to 300 μl/min for the rinsing experiments.

Figures 7.4 (a), (b) and (c) describe the decrease in frequency and increase in dissipation energy of the polyamide crystal due to adsorption of alginate on the surfaces at a total ionic strength of 1 mM, 20 mM, and 100 mM, respectively. When DI was replaced by alginate solution in the experiment, adsorption started immediately as demonstrated by the decrease of sensor frequency and increase of dissipation. Alginate exhibits totally different adsorption behaviors in different ionic environments. With lower ionic strength (1 mM), it takes a shorter time to reach equilibrium and DI rinsing totally removed the adsorption

layer and fully recovered sensor shifts to original status. The increase in total ionic strength (20 mM and 100 mM) resulted in more decreases in the frequency and DI rinsing could not totally remove the adsorption layer. The difference in alginate adsorption behaviors indicated that the increase in solution ionic strength changed the alginate properties as well as the surface properties, which eventually changed the alginate-membrane interactions.

The initial alginate adsorption rates expressed as a decrease in the frequency were plotted in Figure 7.4 (d). The alginate adsorption rate was increased as the solution's ionic strength increased. The highest adsorption rate was observed at ionic strength of 100 mM, which indicated a strong attraction between the membrane surface and the alginate molecules at higher ionic strengths.

In neutral environments, both the alginate molecule and the membrane surfaces are negatively charged. Charge shielding by positively charged sodium ions affects the interactions between the alginate and the membrane surface. The higher adsorption rate at high ionic strengths indicates that electrostatic interactions play an important role in initial alginate adsorption.

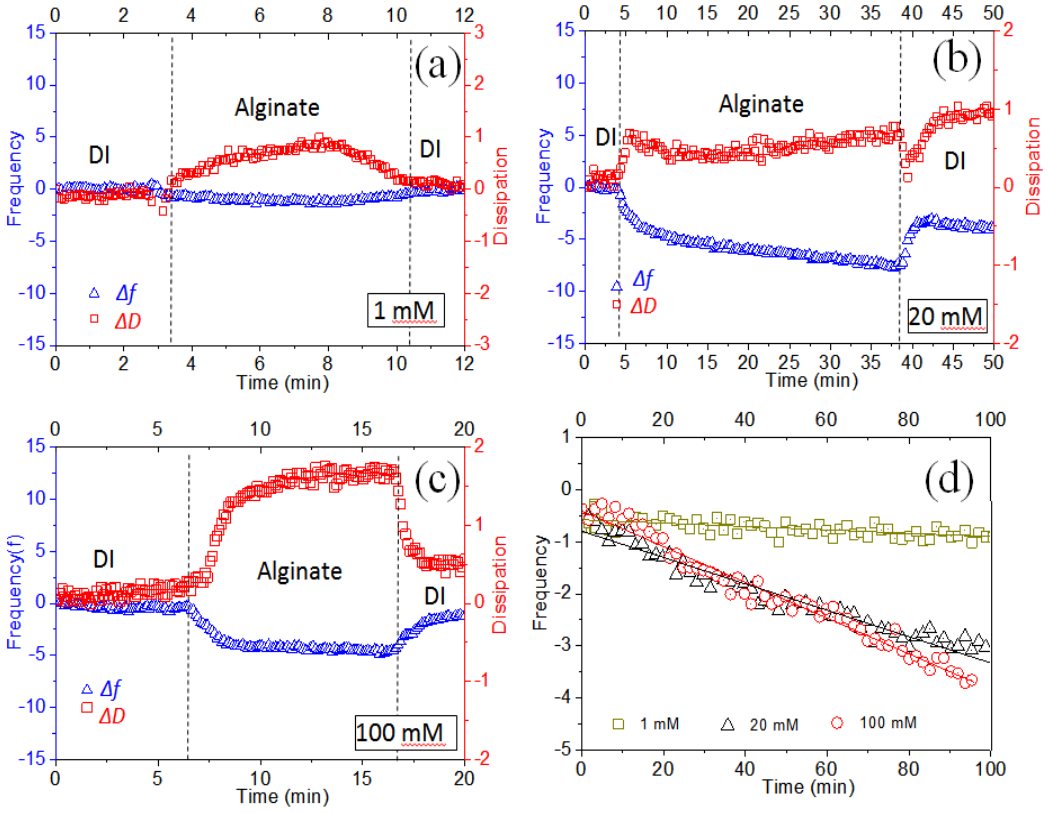

Figure 7.4. Effects of alginate adsorption in different ionic strengths on the resonance frequencies and the corresponding dissipations ((a), (b), and (c)) of the QCM-D quartz. And the frequency decrease rate in the first 100 seconds due to alginate adsorption was compared in (d). The QCM-D experiments were conducted on a polyamide coated gold sensor surface with varied NaCl concentrations (1 mM, 20 mM and 100 mM) at an ambient pH.

Calcium effects on alginate adsorption

This part of the study investigated the calcium effects on alginate adsorption. Two sets of experiments were conducted including alginate adsorption with 3mM NaCl and alginate adsorption with the addition of 1 mM CaCl2. The effects of Na+ and Ca2+ on alginate adsorption were compared. The polyamide sensors were firstly stabilized in salt solutions (3 mM NaCl or 1 mM CaCl2) to be conditioned by Na+ or Ca2+before the alginate adsorption

experiments in order to introduce a conditioning layer of ions on the negatively charged polyamide sensor surface. After the sensor reached equilibrium in salt solutions, the alginate solutions (200mg/L) with different solution compositions (3 mM NaCl, or 1 mM CaCl2) were then introduced into the system until adsorption reached the equilibrium. In the end, the system was rinsed with DI water until stabilization. The changes in frequency and dissipation were monitored and analyzed. The cross flow rate for all adsorption experiments were fixed at 100 μl/min and increased to 300 μl/min for the rinsing experiments.

As shown in Figure 7.5 (a), experiments with alginate adsorption on Na+ exhibited a small change in the shift of frequency of the polyamide-coated crystal sensor by alginate adsorption and DI rinsing fully recovered the sensor shifts. It indicated that the adsorbed sodium cations on polyamide surface did not form a strong bond between alginate molecule and polyamide surface. Significant decreases in sensor frequency of alginate adsorption was observed on Ca2+ conditioned sensor (Figure 7.5 (b)). DI rinsing did not recover sensor shifts to the original status, which indicates a layer of alginate was strongly bonded to membrane surface. The absorbed calcium ions bridged between the carboxylic functional groups on both alginate molecule and polyamide membrane surface and introduced a strong bond between them. This observation is consistent with the fouling study with calcium in the system, where the addition of calcium ions significantly changed membrane fouling behavior.

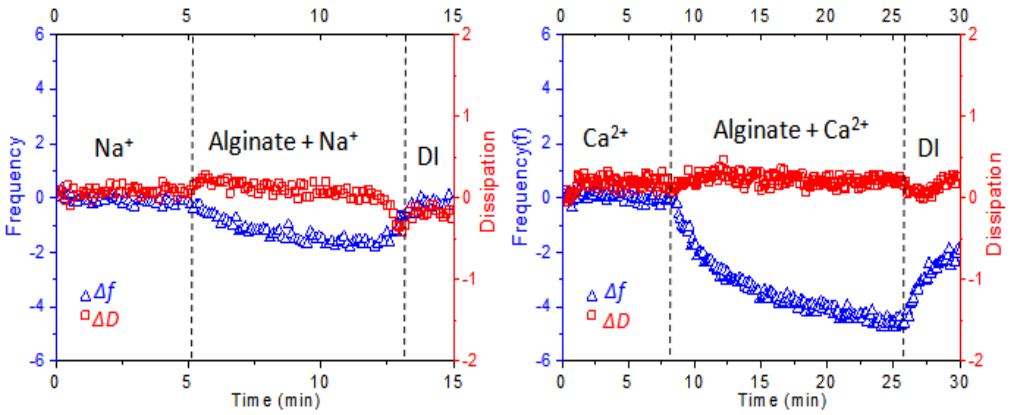

Figure 7.5. Effects of alginate adsorption with/without calcium on the resonance frequencies: (a) shifts of the QCM-D quartz frequency and the corresponding dissipations with Na+ in solution and (b) shifts of the QCM-D quartz frequency and the corresponding dissipations with Ca2+ in solution.

In Figure 7.6, the initial alginate adsorption rates expressed as the decrease rate in the frequency of two experiments were compared. At the beginning of the adsorption experiment with Na+ surface conditioning, the alginate layer appeared to increase slowly and resulted in a slow decrease in frequency. On the calcium ion conditioned sensor, alginate accumulated quickly and formed an even denser alginate film (as indicated by the lower change in dissipation).

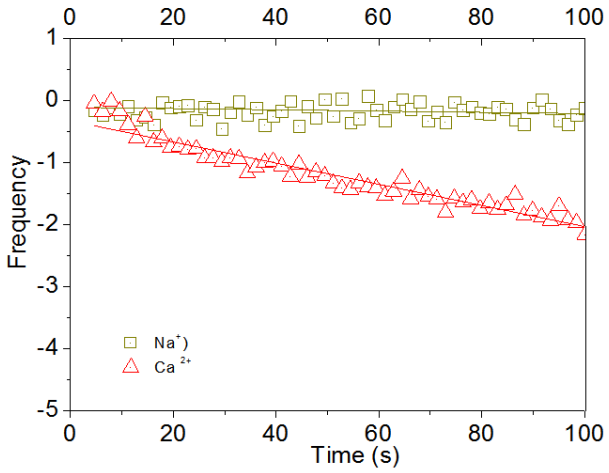

Figure 7.6. Frequency decrease rate in the first 100 seconds due to calcium bridging on alginate adsorption layer.

The adsorption of alginate molecules onto polyamide membrane surfaces was greatly affected by the presence of calcium cations. The alginate adsorption rate was accelerated by the addition of calcium and the adsorbed mass became much higher. The adsorption layer was dense and rigid compared with that in the sodium conditioning experiment. Calcium enhanced the attraction between alginate molecule and polyamide membrane surface and facilitated a strong bond after alginate is adsorbed. The enhanced adsorption of alginate eventually resulted in a dense fouling layer from accelerated fouling on the polyamide membrane surface.

7.5. Concluding Remarks

This study demonstrated that alginate adsorption behavior was strongly influenced by charge screening between the negatively charged carboxyl functional groups of the alginate molecules and the membrane surfaces.

Enhanced alginate adsorption rates were observed as ionic strength increased. However, the charge screening effects at different ionic strengths have negligible effects on PA-FO membrane fouling. The presence of calcium ions induced the formation of a thick and dense layer via the bridging effects between alginate -alginate and alginate-membrane surfaces and significantly changed membrane fouling behavior.

Chapter 8: Grafting Zeolite Nanoparticles onto Polyamide Membranes for Enhanced Fouling Resistance in Forward Osmosis Membrane Process

8.1 Abstract

In this study, we developed an innovative method for zeolite nanoparticles functionalization and grafting to enhance fouling resistance of thin film composite (TFC) membranes in forward osmosis (FO) membrane process. Linde type A (LTA) zeolite nanoparticles were modified with amine functional groups and covalently bonded to the carboxyl functional groups on the TFC membrane surface. X-ray photoelectron spectroscopy (XPS) examination of the membrane surface suggested that zeolite nanoparticles are successfully grafted onto membrane surface. And this layer of zeolite nanoparticles greatly changed the surface morphology of the TFC-FO membrane as suggested by the results from atomic force microscopy (AFM), and scanning electron microscopy (SEM). Increased membrane surface hydrophilicy, enhanced permeatibily and reduced salt back diffusion are observed after zeolite modification. Our further investigation showed that antifouling properties of the zeolite-modified membrane are significantly enhanced. FO fouling experiments showed that bacterial deposition, organic fouling, inorganic scaling were inhibited by zeolite modification, most likely due to reduced carboxyl functionality and increased hydrophilicity of the zeolite modified membranes.

8.2 Introduction

Membrane-based desalination techniques are energy-efficient and cost-effective in comparison with conventional desalination processes such as multi-stage flash distillation (MSF), multiple-effect distillation (MED) and vapor compression (VC). Among all membrane technologies, forward osmosis (FO) is very promising due to its high selectivity, reduced cost and energy feature [10, 60, 63, 83, 172, 232, 295-297]. As an essential part of the FO process, the development of FO membranes with high performance is always in need for the advancement of this technique. In recent years, many attempts have been made to synthesize new FO membrane materials. Elimelech's group reported a high performance thin-film composite FO (TFC-FO) polyamide membrane with finger like-structure support layer structure, which can effectively reduce internal concentration polarization (ICP) and increase permeate flux in FO mode [71-73]. Further studies on the performance of this membrane have shown that the TFC-FO membrane is very suitable for FO process with higher flux and salt rejection rate compared with commercial cellulose triacetate FO membranes.

However, polyamide membrane materials have shown relatively high fouling propensity in its applications such as reverse osmosis (RO), nanofiltration (NF) and FO because of its intrinsic surface physicochemical properties[24, 27, 119, 144, 298-300]. Improvements in fouling resistance of TFC-FO membranes are critical steps for further development and applications of the process.

For all types of membrane fouling, membrane surface characteristics play an important role in foulant deposition and fouling layer formation. The antifouling performance of membrane materials relies largely upon their surface properties. Therefore, optimize membrane surface characteristics such as tailored surface

functional groups, reduced surface roughness and increased surface hydrophilicity by surface modification may effectively control membrane fouling. Among all the modification methods, incorporating nanomaterials has drawn significantly attention and have been considered as a promising strategy to improve membrane surface characteristics [174, 301-303], enhance membrane mechanical strength[304, 305], improve antimicrobial abilities [306-308], and improve membrane fouling resistance[166, 309-311].

Zeolite nanomaterials have drawn great attention in membrane processes and research has shown that the incorporation of zeolite nano-particles into membrane structure provides the opportunity to combine the high selectivity of inorganic molecular sieving materials and the processability of polymer membranes [179]. The favorable properties of zeolite materials can help improve membrane characteristics including: (1) zeolite nanomaterials can reject ions by size exclusion and Donnan exclusion, which implies its application for desalination[177] [179, 312]; (2) zeolite nanomaterials may offer its vigorous characteristic such as surperhydrophilicty and potential in antifouling and antimicrobial performance[313, 314] to membrane surfaces, and (3) zeolite nanomaterials may help improve the stability of polymeric membranes against pressure. Zeolite nanocomposite membranes have been widely researched in membrane processes such as reverse osmosis [159, 170, 186, 315, 316]; ultrafiltration [180-184], and forward osmosis [185] to facilitate rejection and improve flux.

The above studies all focused on incorporating the zeolite nanoparticles into the main body of membrane materials to optimize the structure and improve

membrane flux and salt rejection rate. However, we have not found many studies utilizing the attractive superhydrophlicity of zeolite nanoparticles to enhance membrane fouling resistance. Han et.al found that the addition of NaA zeolite particle (3 wt%) into poly(phthalazinone ether sulfone ketone) composite ultrafiltration (UF) membrane can effectively reduce flux decline against titan yellow dyedue to the increased surface hydrophilicity[317]. Liao et.al. blended silver NaY zeolite nanoparticles into poly (vinylidene fluoride) (PVDF) membranes, which demonstrated superior antibacterial activity against *E. coli*. [318]. In these studies, zeolite nanoparticles demonstrated both high water permeability and high surface hydrophilicity which made it an attractive agent for membrane surface modification.

The objectives of this study are to synthesize zeolite modified TFC-FO membrane by incorporating zeolite nanoparticles onto a TFC-FO membrane surface and to evaluate the feasibility of using this fabricated zeolite TFC-FO membrane in FO process. The fouling propensity of the zeolite TFC membranes are investigated by three major types of foulants in desalination processes including organic foulant, inorganic scalant and microorganisms.

8.3 Materials and Methods

8.3.1 Chemicals

Tetramethylammonium hydroxide (TMAOH, 25 wt% aqueous solution) and aluminum isopropoxide (Al (i-pro)3, 99.99+% (metals basis)) were purchased from Alfa Aesar (Ward Hill, MA) . (3-Aminopropyl) trimethoxysilane (APTES), N-(3-Dimethylaminopropyl)-N′-ethylcarbodiimide hydrochloride (EDC), N-Hydroxysuccinimide (NHS), Sodium hydroxide (NaOH, ACS

reagent, ≥ 97.0%), 1-methyl-2-pyrrolidinone (NMP, anhydrous, 99.5%), N,N-dimethylformamide (DMF, anhydrous, 99.8%), 1,3- phenylenediamine (MPD, >99%), and 1,3,5-benzenetricarbonyl trichloride (TMC, 98%) were used as received (Sigma- Aldrich, St. Louis, MO). Polysulfone (PSf) beads (Mn: 22,000) were provided by Solvay Advanced Polymers, L.L.C (Alpharetta, Georgia). Polyester nonwoven fabric sheet (40 μm, grade 3249) were provided by Ahlstrom, Helsinki, Finland. All chemicals used were ACS grade.

8.3.2 Fabrication of zeolite nanoparticles

Deinoized (DI) water was used in the experiment. The zeolite crystals of Linde type A (LTA) were synthesized using the methods presented in recent literature [319, 320]. Briefly, the process of synthesizing includes dissolving 0.9575 g NaOH in 89.498 g DI water in a 250 mL Teflon bottle followed by the addition of 48.856 g TMAOH solution. Then, 6.76 g silicic acid is added to the resulting basic solution and the mixture is heated in a convection oven at 80°C to speed the dissolution of silicic acid. After a clear solution forms, the solution is cooled to room temperature and 7.353 g Al (i-pro)3 is added. A clear gel with a composition of 11.25SiO2/1.8Al2O3/6.7 (TMA)2O/1.2Na2O/700H2O forms after rigorous stirring at room temperature for around 1 hour. The as-obtained gel in the Teflon bottle is transferred into a preheated convection oven for 3 days of hydrothermal synthesis at 70°C. LTA samples are collected by repeated (3 times) centrifugation and washing with DI water. The as-prepared LTA nano-crystals are, then, ready for membrane fabrication.

8.3.3 PA membrane synthesis

PSf beads (Mn = 22,000 Da) was dissolved in the solvent or solvent mixture (NMP:DMF, 3:1) and cast on a PET fabric sheet moisturized by the solvent mixture (250μm in thickness) to form a support PSf membrane [71]. The PA active layer was formed on top of the PSf support membranes through interfacial polymerization following the procedures described in previous publications (PA biofouling paper). During the process, the PSf support was initially dipped in a MPD (3.4 wt% in water) solution for 120 s to create a layer of MPD covering the entire surface. Next, the PSf support was dipped in a TMC solution (0.15 wt% in Isopar- G) for 60 s and allowed to react with air to form a stable film of polyamide. The post treatment procedures for removing residue chemicals included the following steps: (1) heating in DI at 95 ◦C for 120 s; (2) Rinsing with a NaClO solution (200ppm) for 120 s; (3) rinsing in a NaHSO3 solution (1000ppm) aqueous for 30 s; and, heating at 95 ◦C in DI for 120 s. The fabricated TFC membranes were rinsed thoroughly and stored in DI at 4 ◦C before surface modification.

8.3.4 Membrane surface modification by zeolite nanoparticles

Free carboxyl functional groups at the surface of polyamide membranes were used as active sites to irreversibly bind amine functionalized zeolite nanoparticles. A simple dip coating protocol was developed to functionalize the zeolite particles and then to graft onto membrane surfaces (Figure 8.1). Amine functionalized zeolite nanoparticles were fabricated by surface modification of zeolite nanoparticles with (3-Aminopropyl) trimethoxysilane. The zeolite

solution was centrifuged and replaced with DI water to totally remove any chemical residue from the synthesis. 60 ml of zeolite solution (3%) was sonicated for 30 minutes to break down any small aggregates. After that, 5.25 g of (3-Aminopropyl) trimethoxysilane (50%) was added to the suspension. The pH of the suspension was adjusted to 5 and then kept under vigorous stirring at 60 °C for 18 h. The suspension was dialyzed in DI water using SnakeSkin tubing (7 kDa MWCO, Pierce Biotechnology) for 72 hrs. The pH of the final suspension was adjusted to pH 7 before adding EDC (2 mM) and NHS (5 mM). The active side of polyamide membranes was immersed in the nanoparticle suspension for 12 h at room temperature (23 °C). During this step, the amine functional groups on the surface of the nanoparticles react with the carboxylic groups on the surface of polyamide membranes and form an irreversible binding.

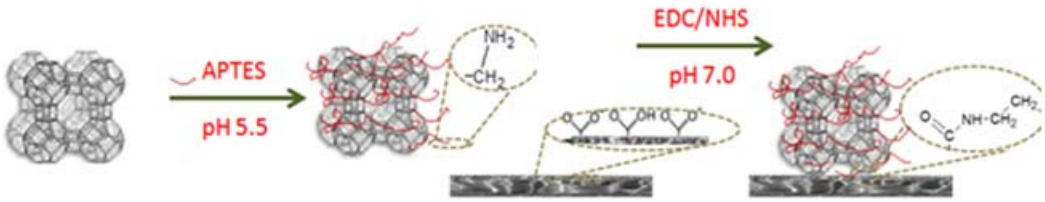

Figure 8.1. Schematic of protocol used for the zeolite nanoparticles functionalization and the PA membrane surface modification.

8.3.5. FO direct observation system and fouling experiment protocol

Cross-flow FO membrane systems were used to conduct the scaling and

cleaning experiments. Both systems contain custom built membrane cells. The feed and draw solution channels in FO have identical dimensions: 77 mm in length, 26 mm in width, and 3 mm in depth. A schematic diagram and detailed description of the system are given in our previous publications [16].

Organic fouling and cleaning protocol

The following protocol was used to run the alginate fouling and cleaning experiments. First, a new membrane coupon was placed in the membrane cell with the active side facing the feed solution channel. The membrane was stabilized with DI water as both feed solution and draw solution for 30 minutes. Next, the permeate flux of the stabilized membrane was measured for 24 hours with 5M NaCl as the draw solution and 20 mM NaCl as the feed solution. Baseline experiments were conducted to correct effects such as concentration and dilution. After that, the draw solution and the feed solution were changed for the organic fouling experiment. The organic fouling experiment was, then, performed for 24 hours. 5M NaCl was used as draw solution and the same alginate solution was used for both the PA membrane and the zeolite modified PA membrane: 200mg/L alginate, 20 mM NaCl, and 1 mM CaCl2. Other test conditions included: cross flow velocity of 8.5 cm/s, pH 7.0, and temperature of 20 ± 1 °C. Weight change of draw solution was continuously monitored throughout the fouling experiments. Membrane cleaning experiments were performed immediately after the fouling experiments. DI water was used as both draw solution and feed solution to rinse the system for 20 minutes at a cross-flow rate of 21 cm/s. The cleaning experiment was conducted at a

temperature of 20 ± 1 °C and no chemicals were added as cleaning agents. After the cleaning experiment, the membrane water flux was tested under baseline conditions. A detailed procedure can be found in our previous publications [16].

Bacterial deposition and Release Experiment

The befouling experiment protocols are similarly to the protocols used in Chapter 5 and Chapter 6. *Escherichia coli K12* MG1655 is used as model foulant. *E. coli* solutions were pre-cultured in 50 mL of LB broth in 250 mL culture flask on a shaking water bath for 12-14 hours at 37.0 °C. 0.1 mL of pre-culture was then transferred into another 250 mL culture flask with 50 mL of LB broth and incubated at 37.0 ºC in the shaking water bath until the *E. coli* reach a late exponential growth phase. The bacterial cells were then harvested and suspended in a test solution to a target concentration of 1×106 CFU/mL. 100 mM NaCl was used as the feed solution and 1 mM CaCl2 was added. 5 M NaCl solutions were used as the draw solution to provide a driving force for the permeate flow.

Membrane biofouling experiments were conducted after the system was sterilized by circulating Ethanol (>70%) for an hour and fresh DI for an hour. New membrane samples were used for every experiment. The active layer of the membrane was set against feed solution in the test. After that, membrane was stabilized in the feed solution and the draw solution for 30 minutes, bacterial cells were added into the feed tank (1×106 CFU/mL). Images were taken immediately after the permeate flow started. The same places on the

membrane's surface were monitored and imaged at an interval of every 1 minute for the first 20 minutes of the experiment; after 60 minutes, the draw solution was switched to 100 mM NaCl and the cross-flow rate was increased to 1000mL/min and image was taken every 1 minute.

8.4. Results and discussion

8.4.1. Effects of zeolite modification on surface properties

The PA membrane and zeolite modified PA membrane used in this study both have an asymmetric structure that includes a porous PSf support layer and an active polyamide layer. The surface morphology of the active layer, before and after functionalization, was analyzed by SEM and atomic force microscopy (AFM) (Figure 8.2). The SEM surface micrographs (Figure 8.2a) and the representative topographic image (Figure 8.2c) of a PA membrane showed a uniform ridge-and-valley structure, which is the typical morphology of polyamide films formed by interfacial polymerization. The characteristic surface roughness parameters of the membranes were measured by tapping-mode AFM. The PA membrane's surface had a RMS of 80 ± 30 nm, an average roughness (Ra) of 62 ± 20 nm, and a maximum roughness (Rmax) of 835 ± 30 nm. The SEM micrographs in Figure 8.2b (imaged at the surface of the zeolite modified PA membrane) showed that the surface features of the PA membrane were covered by a layer of zeolite nanoparticles. The surface roughness measurements of zeolite modified PA membrane (Figure 8.2d) indicated a slight increase in surface roughness that was due to the presence of nanoparticles. The zeolite modified PA membrane had a RMS of 89 ± 30 nm, an average roughness (Ra) of 66 ± 20 nm, a maximum roughness (Rmax) of 1,003 ± 30 nm.

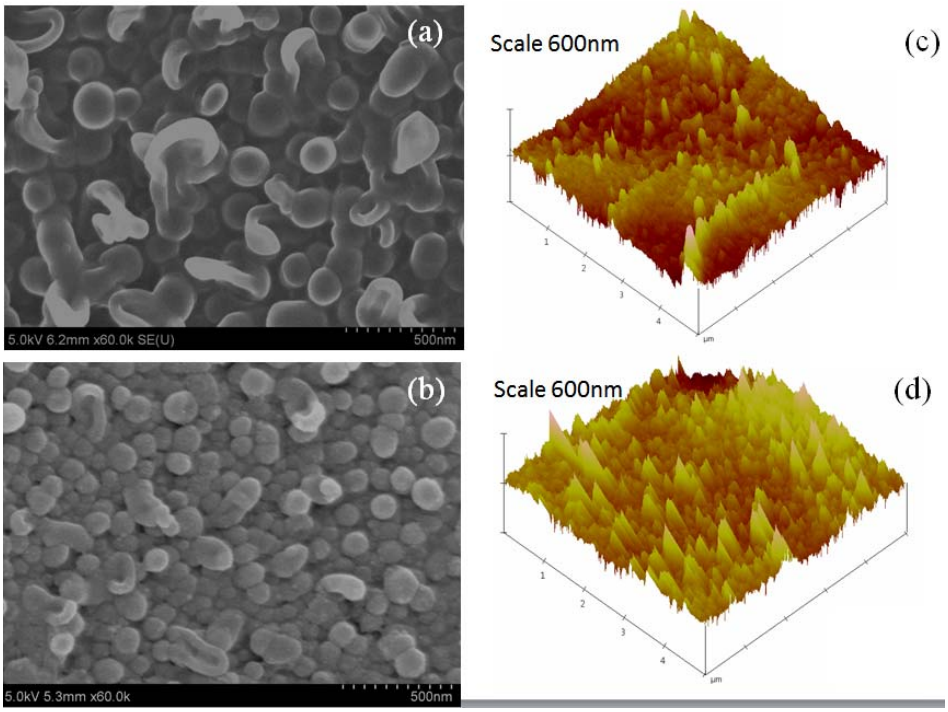

Figure 8.2. SEM and AFM images of membrane surfaces (a) PA membrane surface image, (b) Zeolite modified PA membrane surface, (c)AFM image of PA membrane surface, and (d) AFM image of zeolite modified PA membrane surface.

X-ray photoelectron spectroscopy (XPS) data of the membrane surfaces of the PA membrane and zeolite modified PA membranes are presented in Figure 8.3. As shown in Figure 3a, significant energy peaks were observed for both the PA surface and the zeolite modified PAsurface. These were attributed to carbon, oxygen, and nitrogen (Figure 8.3a). Among these, carbon was the most abundant element (Figure 8.3b and 8.3c), consistent with the chemistry of the membrane active layer. The spectra related to the zeolite modified PA membrane surface showed the appearance of energy peaks associated with silicon and aluminum (Figure 8.3a), which confirm the presence of the silica-aluminum based zeolite nanoparticles at the surfaces.

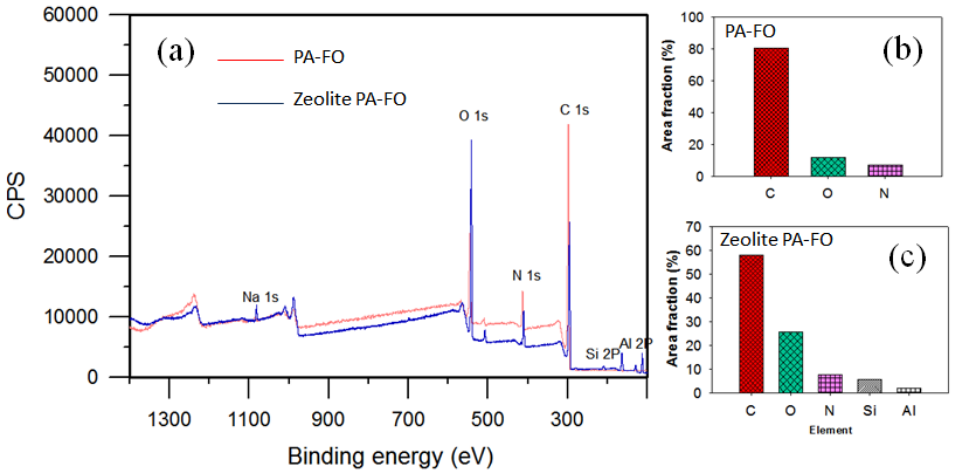

Figure 8.3. XPS spectra of the surface of the PA membrane and the zeolite modified PA membrane. (a) XPA survey scans of PA membrane (red) and of zeolite functionalized PA membrane, (b) Element fractions of carbon, oxygen, and nitrogen relative to the sum of all elements at the surface of PA membrane, and (c) Element fractions of carbon, oxygen, nitrogen, silica and aluminum relative to the sum of all elements at the surface of PA membrane.

8.4.2. Effects of zeolite modification on membrane performance

The pure water permeability of the PA membrane and the zeolite-FO were shown in Figure 8.4. The feed solution used for testing was DI water. Three draw solutions were tested including 1.5 M, 4 M, and 5 M. As shown in Figure 8.4, the zeolite modified PA membrane showed slightly higher flux. This is probably due to the effects of increased hydrophilicity from the zeolite grafting. The PA membrane surface is relatively hydrophilic with a water contact angle of around 61 ± 4°, which was measured with DI water (~40 µL) under ambient conditions using a KRUSS G10 Goniometer (Matthews, NC). The zeolite modified PA membrane has a water contact angle of 31 ± 4°.

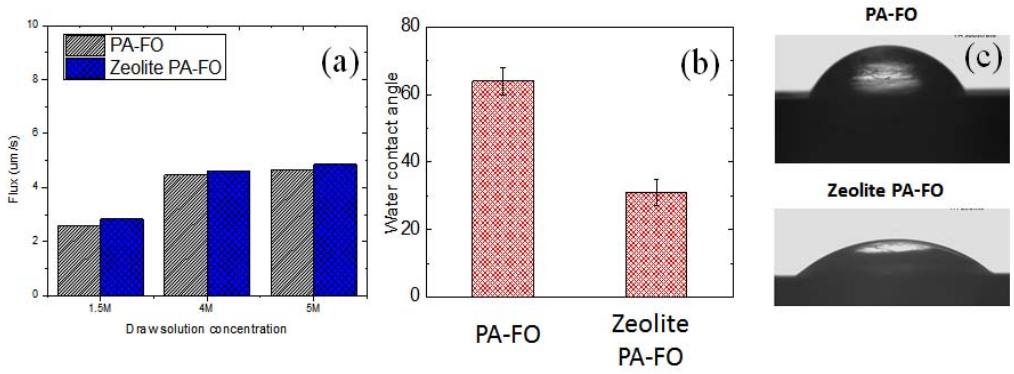

Figure 8.4. Zeolite functionalization increased membrane surface hydrophilicity and membrane permeate flux. (a) Membrane flux in FO mode, (b) water contact angle measured on membrane surface, and (c) representative water contact angle images,

8.4.3 Effects of zeolite modification on antifouling properties

Effects of zeolite modification on initial stage bacteria deposition and release

The bacterial deposition behaviors on the TFC-FO and zeolite TFC-FO membranes, determined from deposition and rinsing experiments, were presented in Figure 7. For both the TFC-FO and zeolite TFC-FO, the bacteria density on membrane surface increases linearly with time. The deposition rate on the TFC-FO membranes was higher than that on the zeolite TFC-FO membrane. And 50% of the deposited bacteria can be removed by physical rinsing. This observation indicates that the interaction between bacteria and zeolite TFC-FO membrane is much weaker than that of the TFC-FO membrane. In FO system with steady cross-flow rate, the deposition of bacterial cells on the membrane surface was determined by the combination of permeation drag force resulting from the permeate flow and the electrostatic double layer

interactions between the bacteria and the membrane surface at close distance. The permeation drag force for the two experiments was kept the same by adjusting same permeate flux. However, the electrostatic interactions between the bacteria and the two membranes are much different. The TFC-FO membrane is negatively charged in neutral environment and bacteria cells carry negative charge as well. Calcium bridging between carboxylic surface functional groups and the extracellular substances enhanced bacteria adhesion and results in an irreversible deposition. For the zeolite TFC-FO membranes, zeolite nanoparticles were introduced together with the superhydrophilic ligands with amine functionalities instead of carboxylic moieties [166].

The chance of irreversible deposition was much reduced due to the decreased carboxylic functional density and subsequent effects of calcium bridging. Furthermore, the hydration layer introduced by zeolite nanoparticles surface also resists the adsorption of EPS substances to the membrane surface. Thus the modified surface functionalities and surface hydration layer increased the antibiofouling resistance of the zeolite TFC-FO membrane.

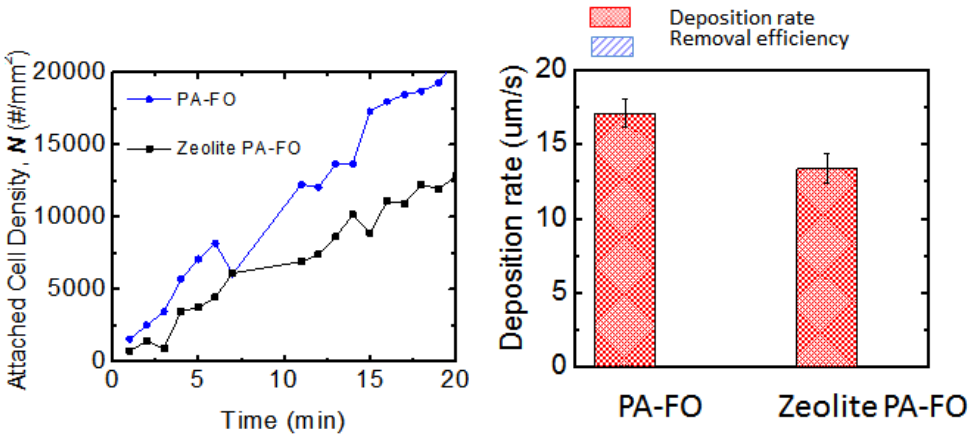

Figure 8.5. Comparison of attached bacterial cell deposition and release on different membrane materials. (a) Density of attached bacteria cell on membrane surface during attachment, and (b) bacteria deposition rates during attachment experiment (red) and bacteria release. The operational conditions for the attachment experiment were: 4M NaCl solution as the draw solution and 100 mM NaCl as the feed solution (which resulted in a permeate flux of 3.5 µm/s). The feed solution pH was adjusted to 7.0 by adding NaOH. Bacterial concentration in the feed solution was 1x106 *E.coli* K12 CFU/ml. 1 mM calcium was added to feed solution. A cross-flow rate of 100 mL/min was maintained for attachment experiment. The operational conditions for the rinsing experiments were: 100 mM NaCl as draw and feed solutions, 1 x 106 *E. coli* K12 CFU/ml was in feed solution and a cross-flow rate of 1000 mL/min. The two sets of experiments were conducted with different membrane materials including PA membrane and zeolite modified PA membrane.

Effects of zeolite modification on alginate fouling

Fouling behavior of the PA and zeolite modified PA membranes were investigated with alginate as a model organic foulant. Experiments were carried out for 24 hours and were followed by physical cleaning with the addition of air bubbles to enhance the hydrodynamic shear in the feed channel. The results of duplicate runs for the PA and zeolite modified PA membranes are summarized in Figure 8.6. 5 M NaCl was used as draw solution in both experiments; the feed solution's total ionic strength was kept at 0.02 mM by adding NaCL and 1 mM CaCl2 was added. A high foulant concentration (200

mg/L) was used to accelerate the fouling rate. Figure 8.6 showed the results of membrane flux declines caused by alginate fouling. A small flux decline is observed for the zeolite modified PA membrane. In contrast, the flux decline for the PA membrane drops quickly even at the beginning of the experiment. This observation was attributed to the complexity of the bridging mechanisms between the alginate molecules and the carboxylic functional groups on the surface of the PA membrane and in the presence of calcium ions which results in a dense and cross-linked alginate gel layer on the membrane's surface. The zeolite modified PA membrane exhibited a much slower flux decline than the PA membranes due to the reduced density of carboxylic functional groups. This slower flux decline suggested that the zeolite modified PA membranes may be more resistant to fouling than the PA membranes.

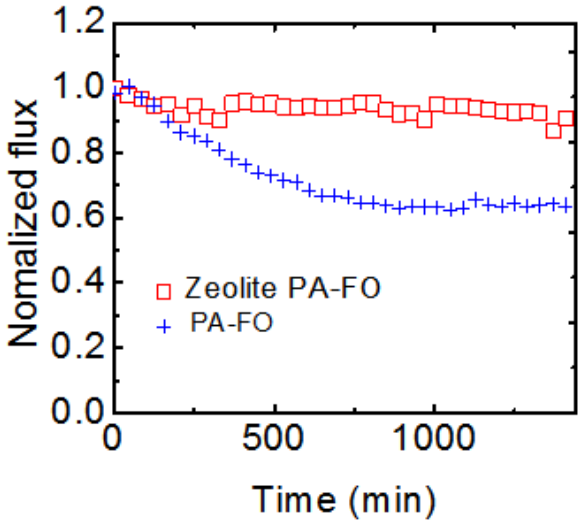

Figure 8.6. Comparison of membrane flux declines during organic fouling experiments with different membrane materials including the PA membrane and the zeolite modified PA membrane. Experimental conditions are: 5 M NaCl as draw solution in both experiments; the feed solution total ionic strength kept at 0.02 mM by adding NaCL and 1 mM CaCl2; temperature of 20 ± 1 oC; cross-flow rate of 8.5 cm/s; and, 200mg/L sodium alginate used as the organic foulant.

8.5 Concluding Remarks

We successfully grafted zeolite nanoparticles onto a polyamide forward osmosis membrane resulting in more hydrophilic surface. The zeolite modified membrane exhibits improved resistance to bacterial adhesion and organic fouling.

8.6 Acknowledgements

The authors are grateful for Dr Dong xia Liu and Ph.D student Laleh Emdadi for kindly provding us the zeolite nanoparticles. This material is based upon work supported by the National Science Foundation under Grant No. CBET-1034158. In addition, the first author is partially supported by an NWRI-

AMTA (National Water Research Institute – American Membrane Technology Association) Fellowship for Membrane Technology. These supports are gratefully acknowledged.

Chapter 9: Conclusions and Recommendations

9.1 Conclusions

This dissertation work investigated the fouling behavior of two types of FO membrane including a CTA-FO membrane and a PA-FO membrane and developed effective surface modification strategies to improve membrane antifouling properties. FO membrane fouling behavior was analyzed dynamically using a lab-scale system. The foulant-membrane interactions and fouling layer properties were characterized at microscopic level to help provide critical information to explain FO membrane fouling. Atomic force measurement and molecular simulation were combined to understand the foulant-foulant and foulant-membrane interactions at molecular level.

A synergistic effect between alginate fouling and gypsum scaling was observed in the fouling experiment to study the combined organic and inorganic fouling of CTA-FO membranes using alginate and gypsum as model foulants (Chapter 3). That is, the coexisting foulants resulted in more severe flux decline than the algebraic sum of flux declines caused by individual foulants. It was found that this synergistic effect was mainly due to the aggravated gypsum scaling in the presence of alginate molecules. Analysis of flux decline results and SEM images indicate that alginate molecules act as large nuclei in gypsum crystal growth, thus significantly increasing the size of gypsum crystal and shortening the initiation time for crystallization. It is also revealed that the dominating scaling mechanism switches from bulk crystallization (in the absence of

alginate) to surface/heterogeneous crystallization (in the presence of alginate).

The adsorption of organic foulants on CTA-FO membrane surfaces had significant effects on subsequent gypsum scaling in FO membrane process (Chapter 4). The absorbed organic macromolecules significantly changed the membrane flux-decline behavior under gypsum scaling: organic macromolecules (AHA and alginate) with a high density of carboxylate functional groups led to increased gypsum crystal size, shortened crystal nucleation time, and resulted in severe flux decline; BSA with its low carboxylate density did not show any significant effects on gypsum scaling.

The results of biofouling experiments demonstrated that direct microscopic observation is a useful tool to study initial bacteria deposition on FO membrane surfaces (Chapter 5). For the CTA-FO membrane, the initial microbial deposition rate is relatively slow and more than 50% cells deposited on the FO membrane surface can be easily removed by simultaneously increasing crow-flow rate and stopping permeate flux. This high removal efficiency indicates a weak bond between bacteria and CTA membrane surface. Membrane surface properties such as hydrophilicity played an important role in bacteria deposition. Polydopamine coating on the CTA-FO membrane further increased surface hydrophilicity and reduced biofouling.

The biofouling of a lab-synthesized polyamide (PA) membrane was also studied in FO membrane process (Chapter 6). Solution pH and divalent ions such as calcium ions demonstrated significant effects on bacteria deposition rate.

Integrated results from atomic force measurements and molecular simulations suggested that the electrostatic force between bacteria and membrane surface played an important role in controlling the initial deposition of bacterial cells onto the PA membrane.

The adsorption and viscoelastic structure properties of alginate layer grow on a polyamide sensor surface as a function of ionic strength and the presence of calcium ions are monitored by quartz crystal microbalance with dissipation (QCM-D) (Chapter 7). The results from this part of study shows that in the absence of calcium ions, alginate adsorption behavior is strongly influenced by charge screening between the negatively charged carboxyl functional groups of the alginate molecules and membrane surfaces. Enhanced alginate adsorption rate is observed as ionic strength is increased. However the charge screening effects at different ionic strengths have negligible effects on PA-FO membrane fouling. The presence of calcium ions induces the formation of a thick and dense layer via the bridging effects between alginate -alginate and alginate-membrane surfaces and significantly changed membrane fouling behavior.

In chapter 8, a zeolite-modified PA membrane was successfully fabricated and its antifouling performance was thoroughly investigated in FO membrane process. Amine-functionalized zeolite nanoparticles were irreversibly grafted onto PA membrane surface by covalent binding. The membrane surface hydrophilicity was greatly increased by the zeolite nanoparticles. The zeolite-modified membrane exhibits enhanced fouling-resistance to bacteria adhesion and organic fouling.

9.2 Key Contributions

The dissertation work provided insights into the fouling behaviors of two types of FO membranes, i.e., a commercial CTA-FO membrane and a lab-synthesized PA-FO membrane with various types of fouling, including organic fouling, scaling, biofouling, and combined fouling. A more systematic and fundamental understanding of FO membrane fouling mechanisms was achieved by characterizing the foulant-foulant and foulant-membrane interactions in FO membrane process. Novel surface modification strategies using biomimetic polymers (polydopamine) or hydrophilic zeolite nanoparticles were successfully developed to mitigate FO membrane fouling.

The specific contributions are listed below:

- Gaining an understanding of the influence of alginate on the gypsum crystallization kinetics and scaling behavior.
- Identifying how alginate, bovine serum albumin, and humic acid affect the scaling behavior of gypsum in FO process.
- Demonstrating that the electrostatic interaction between bacteria and membrane surface is the dominant factor in the initial stage of biofouling for both CTA-FO and PA-FO membranes.
- Developing a QCM-D method for quantitatively characterization of foulant adsorption on polyamide membrane surfaces.
- Successfully fabricating a PA-FO membrane with relatively high water permeability and salt rejection.
- Developing an effective surface modification strategy of grafting zeolite nanoparticles onto the PA membrane surface to successfully mitigate FO membrane fouling.

9.3 Future Work

Following the investigations described in this dissertation, a number of projects could be taken up, including:

- Further investigation on biofouling mechanisms of CTA-FO and PA-FO membranes. This dissertation work investigated the effects of solution chemistry on initial stage bacterial deposition and release in FO process. Further study on role of extracellular polymeric substances (EPS), bacteria eletromobility and membrane surface charge will give more insights to the biofouling mechanisms. Furthermore, long-term befouling experiments will provide more information for biofilm formation in FO process.
- Fouling study and fouling control strategies development in pressure retarded osmosis (PRO) process. PRO process share similar working mechanism as FO and use the same membrane as FO process. However the fouling propensity is much severe. Fouling study on PRO process is very limited. The fouling investigation method developed in this study can be immediately applied to the fouling study in PRO process.
- Fabrication of nanocomposite PA-FO membrane with different types of nano particles. The method of using covalent binding between carboxylate functional groups on membrane surfaces and amine functionalized nanoparticles is suggested to be reliable and effective. This method can be further explored with other types of functionalized nanoparticles such as nanosilver, carbon nanotube, and titanium dioxide nanoparticles to tailor the properties of membrane surface and improve fouling resistance .
- QCM-D study on polyamide membrane membrane surface modification and foulant on polyamide membrane surface. This study developed a protocol for polyamide sensor coating. The polyamide coated sensor strongly mimics the real membrane surface. The degree of coating and grafting on polyamide membrane surface can be monitored at nanoscale level. The information of initial foulant adsorption and foulant layer growth on membrane surface can

be obtained from QCM-D study as well.

References

[1] Water in a changing world, in: The united nations world water development report, (WWDR3). , World Water Forum, 2009.

[2] H. Ashraf, Experts gather to discuss water crisis that the world is ignoring, LANCET, 361 (2003) 935-935.

[3] S. Kanae, Global warming and the water crisis, J Health Sci, 55 (2009) 860-864.

[4] C. Charcosset, A review of membrane processes and renewable energies for desalination, Desalination, 245 (2009) 214-231.

[5] L.R.E. James E. Miller, Forward osmosis: a new approach to water purification and desalination, in, Sandia National Laboratories, Albuquerque, New Mexico 87185 and Livermore, California 94550, 2006.

[6] Dynamic growth in water reuse and desalination, in: World Water Reuse and Desalination WEF Publishing UK Ltd, WEF Head Office, 2010.

[7] D. Li, X.Y. Zhang, G.P. Simon, H.T. Wang, Forward osmosis desalination using polymer hydrogels as a draw agent: Influence of draw agent, feed solution and membrane on process performance, Water Res, 47 (2013) 209-215.

[8] J. Schrier, Ethanol concentration by forward osmosis with solar-regenerated draw solution, Sol Energy, 86 (2012) 1351-1358.

[9] J.R. McCutcheon, R.L. McGinnis, M. Elimelech, Desalination by ammonia-carbon dioxide forward osmosis: Influence of draw and feed solution concentrations on process performance, J Membrane Sci, 278 (2006) 114-123.

[10] S.C. Low, Preliminary studies of seawater desalination using forward osmosis, Desalin Water Treat, 7 (2009) 41-46.

[11] M. Elimelech, J.R. McCutcheon, R.L. McGinnis, A novel ammonia-carbon dioxide forward (direct) osmosis desalination process, Desalination, 174 (2005) 1-11.

[12] T.Y. Cath, A.E. Childress, M. Elimelech, Forward osmosis: Principles, applications, and recent developments, J Membrane Sci, 281 (2006) 70-87.

[13] E.G. Beaudry, K.A. Lampi, Membrane Technology for Direct-Osmosis Concentration of Fruit Juices, Food Technol-Chicago, 44 (1990) 121-121.

[14] R.V. Linares, V. Yangali-Quintanilla, Z.Y. Li, G. Amy, NOM and TEP fouling of a forward osmosis (FO) membrane: Foulant identification and cleaning, J Membrane Sci, 421 (2012) 217-224.

[15] E. Arkhangelsky, F. Wicaksana, C.Y. Tang, A.A. Al-Rabiah, S.M. Al-Zahrani, R. Wang, Combined organic-inorganic fouling of forward osmosis hollow fiber membranes, Water Res, 46 (2012) 6329-6338.

[16] Y.L. Liu, B.X. Mi, Combined fouling of forward osmosis membranes: Synergistic foulant interaction and direct observation of fouling layer formation, J Membrane Sci, 407 (2012) 136-144.

[17] S.R. Qi, C.Q. Qiu, Y. Zhao, C.Y.Y. Tang, Double-skinned forward osmosis membranes based on layer-by-layer assembly-FO performance and fouling behavior, J Membrane Sci, 405 (2012) 20-29.

[18] C. Boo, S. Lee, M. Elimelech, Z.Y. Meng, S. Hong, Colloidal fouling in forward osmosis: Role of reverse salt diffusion, J Membrane Sci, 390 (2012) 277-284.

[19] Z.Y. Li, V. Yangali-Quintanilla, R. Valladares-Linares, Q.Y. Li, T. Zhan, G. Amy, Flux patterns and membrane fouling propensity during desalination of seawater by forward osmosis, Water Res, 46 (2012) 195-204.

[20] S. Zou, Y.S. Gu, D.Z. Xiao, C.Y.Y. Tang, The role of physical and chemical parameters on forward osmosis membrane fouling during algae separation, J Membrane Sci, 366 (2011) 356-362.

[21] S. Lee, C. Boo, M. Elimelech, S. Hong, Comparison of fouling behavior in forward osmosis (FO) and reverse osmosis (RO), J Membrane Sci, 365 (2010) 34-39.

[22] Y.N. Wang, F. Wicaksana, C.Y. Tang, A.G. Fane, Direct Microscopic Observation of Forward Osmosis Membrane Fouling, Environ Sci Technol, 44 (2010) 7102-7109.

[23] C.Y.Y. Tang, Q.H. She, W.C.L. Lay, R. Wang, A.G. Fane, Coupled effects of internal concentration polarization and fouling on flux behavior of forward osmosis membranes during humic acid filtration, J Membrane Sci, 354 (2010) 123-133.

[24] B.X. Mi, M. Elimelech, Organic fouling of forward osmosis membranes: Fouling reversibility and cleaning without chemical reagents, J Membrane Sci, 348 (2010) 337-345.

[25] W.C.L. Lay, T.H. Chong, C.Y.Y. Tang, A.G. Fane, J.S. Zhang, Y. Liu, Fouling propensity of forward osmosis: investigation of the slower flux decline phenomenon, Water Sci Technol, 61 (2010) 927-936.

[26] A. Achilli, T.Y. Cath, E.A. Marchand, A.E. Childress, The forward osmosis membrane bioreactor: A low fouling alternative to MBR processes, Desalination, 239 (2009) 10-21.

[27] B. Mi, M. Elimelech, Chemical and physical aspects of organic fouling of forward osmosis membranes, J Membrane Sci, 320 (2008) 292-302.

[28] E.R. Cornelissen, D. Harmsen, K.F. de Korte, C.J. Ruiken, J.J. Qin, H. Oo, L.P. Wessels, Membrane fouling and process performance of forward osmosis membranes on activated sludge, J Membrane Sci, 319 (2008) 158-168.

[1] E.J. McAdam, S.J. Judd, A review of membrane bioreactor potential for nitrate removal from drinking water, Desalination, 196 (2006) 135-148.

[2] B. Van der Bruggen, C. Vandecasteele, T. Van Gestel, W. Doyen, R. Leysen, A review of pressure-driven membrane processes in wastewater treatment and drinking water production, Environ Prog, 22 (2003) 46-56.

[3] G.R. Botha, R.D. Sanderson, C.A. Buckley, Brief Historical Review of Membrane-Development and Membrane Applications in Waste-Water Treatment in Southern Africa, Water Sci Technol, 25 (1992) 1-4.

[4] D.W. Green, R.H. Perry, Perry's Chemical Engineers' Handbook (8th Edition), in, McGraw-Hill, 2008.

[5] C.D. Moody, Forward osmosis extractors: theory, feasibility and design optimization, University of Arizona., 1977.

[6] L. Malaeb, G.M. Ayoub, Reverse osmosis technology for water treatment: State of the art review, Desalination, 267 (2011) 1-8.

[7] M.A. Alghoul, P. Poovanaesvaran, K. Sopian, M.Y. Sulaiman, Review of brackish water reverse osmosis (BWRO) system designs, Renew Sust Energ Rev, 13 (2009) 2661-2667.

[8] H.I. Shaban, Reverse-Osmosis Membranes for Seawater Desalination State-of-the-Art, Separ Purif Method, 19 (1990) 121-131.

[9] L.F. Comb, Going Forward with Reverse-Osmosis, Chem Eng-New York, 101 (1994) 90-92.

[10] C. Fritzmann, J. Lowenberg, T. Wintgens, T. Melin, State-of-the-art of reverse osmosis desalination, Desalination, 216 (2007) 1-76.

[11] Dynamic growth in water reuse and desalination, in: World Water Reuse and Desalination WEF Publishing UK Ltd, WEF Head Office, 2010.

[12] M.H. Li, Reducing specific energy consumption in Reverse Osmosis (RO) water desalination: An analysis from first principles, Desalination, 276 (2011) 128-135.

[13] Y.C. Kim, S.J. Park, I.S. Park, Change of energy consumption through the adjustment of feed flow rate in RO membrane process, Desalin Water Treat, 9 (2009) 131-135.

[14] S.A. Avlonitis, K. Kouroumbas, N. Vlachakis, Energy consumption and membrane replacement cost for seawater RO desalination plants, Desalination, 157 (2003) 151-158.

[15] T. Manth, M. Gabor, E. Oklejas, Minimizing RO energy consumption under variable conditions of operation, Desalination, 157 (2003) 9-21.

[16] M.A. Darwish, Critical Comparison between Energy-Consumption in Large Capacity Reverse-Osmosis (Ro) and Multistage Flash (Msf) Seawater Desalting Plants, Desalination, 63 (1987) 143-161.

[17] T. Valencia Rodriguez, A.M. Rojas, C.A. Campos, L.N. Gerschenson, Effect of osmotic dehydration on the quality of air-dried Porphyra, Lebensmittel-Wissenschaft + [i.e. und] Technologie. Food science + technology. Science + technologie alimentaire, 36 (2003) 415-422.

[18] T. Cath, Osmotically and thermally driven membrane processes for enhancement of water recovery in desalination processes, Desalin Water Treat, 15 (2010) 279-286.

[19] T. Cath, A. Childress, M. Elimelech, Forward osmosis: Principles, applications, and recent developments, J MEMBRANE SCI, 281 (2006) 70-87.

[20] A. Achilli, T. Cath, E. Marchand, A. Childress, The forward osmosis membrane bioreactor: A low fouling alternative to MBR processes, Desalination, 239 (2009) 10-21.

[21] C.D. Moody, J.O. Kessler, Forward Osmosis Extractors, Desalination, 18 (1976) 283-295.

[22] I. Goosens, A. Vanhaute, Use of Direct Osmosis Tests as Complementary Experiments to Determine the Water and Salt Permeabilities of Reinforced Cellulose-Acetate Membranes, Desalination, 26 (1978) 299-308.

[23] T.V. Knyazkova, A.A. Kavitskaya, L.A. Kulsky, Formation of the Dynamic Membranes in the Process of Direct Osmosis, Dopovidi Akademii Nauk Ukrainskoi Rsr Seriya B-Geologichni Khimichni Ta Biologichni Nauki, (1979) 33-35.

[24] R.E. Kravath, J.A. Davis, Desalination of Sea-Water by Direct Osmosis, Desalination, 16 (1975) 151-155.

[25] J.O. Kessler, C.D. Moody, Drinking-Water from Sea-Water by Forward Osmosis, Desalination, 18 (1976) 297-306.

[26] C.R. Lerici, M. Dallarosa, G. Pinnavaia, Direct Osmosis as a Parameter for the Drying of Fruit, Industrie Alimentari, 22 (1983) 500-500.

[27] E.G. Beaudry, K.A. Lampi, Membrane Technology for Direct-Osmosis Concentration of Fruit Juices, Food Technology, 44 (1990) 121-121.

[28] C. Severini, S. Pizzirani, M. Anese, C.R. Lerici, Use of Ethanol-Added Syrups in Food Vegetable Concentration by Direct Osmosis, Industrie Alimentari, 32 (1993) 1220-1222.

[29] B.R. Babu, N.K. Rastogi, K. Raghavarao, Effect of process parameters on transmembrane flux during direct osmosis, J MEMBRANE SCI, 280 (2006) 185-194.

[30] E.M. Garcia-Castello, J.R. McCutcheon, M. Elimelech, Performance evaluation of sucrose concentration using forward osmosis, J MEMBRANE SCI, 338 (2009) 61-66.

[31] Q. Yang, K.Y. Wang, T.S. Chung, A novel dual-layer forward osmosis membrane for protein enrichment and concentration, Sep Purif Technol, 69 (2009) 269-274.

[32] J.R. McCutcheon, R.L. McGinnis, M. Elimelech, A novel ammonia—carbon dioxide forward (direct) osmosis desalination process, Desalination, 174 (2005) 1-11.

[33] R.A. Khaydarov, R.R. Khaydarov, Solar powered direct osmosis desalination, Desalination, 217 (2007) 225-232.

[34] S.C. Low, Preliminary studies of seawater desalination using forward osmosis, Desalin Water Treat, 7 (2009) 41-46.

[35] O.A. Bamaga, A. Yokochi, E.G. Beaudry, Application of forward osmosis in pretreatment of seawater for small reverse osmosis desalination units, Desalin Water Treat, 5 (2009) 183-191.

[36] Y.J. Choi, J.S. Choi, H.J. Oh, S. Lee, D.R. Yang, J.H. Kim, Toward a combined system of forward osmosis and reverse osmosis for seawater desalination, Desalination, 247 (2009) 239-246.

[37] J.S. Choi, H. Kim, S. Lee, T.M. Hwang, H. Oh, D.R. Yang, J.H. Kim, Theoretical investigation of hybrid desalination system combining reverse osmosis and forward osmosis, Desalin Water Treat, 15 (2010) 114-120.

[38] T.Y. Cath, D. Adams, A.E. Childress, Membrane contactor processes for wastewater reclamation in space II. Combined direct osmosis, osmotic distillation,

and membrane distillation for treatment of metabolic wastewater, J MEMBRANE SCI, 257 (2005) 111-119.

[39] T.Y. Cath, S. Gormly, E.G. Beaudry, M.T. Flynn, V.D. Adams, A.E. Childress, Membrane contactor processes for wastewater reclamation in space Part I. Direct osmotic concentration as pretreatment for reverse osmosis, J MEMBRANE SCI, 257 (2005) 85-98.

[40] E.R. Cornelissen, D. Harmsen, K.F. de Korte, C.J. Ruiken, J.J. Qin, H. Oo, L.P. Wessels, Membrane fouling and process performance of forward osmosis membranes on activated sludge, J MEMBRANE SCI, 319 (2008) 158-168.

[41] R.W. Holloway, A.E. Childress, K.E. Dennett, T.Y. Cath, Forward osmosis for concentration of anaerobic digester centrate, Water Res, 41 (2007) 4005-4014.

[42] S. Loeb, Mccutcha.Jw, Electrolytic Additives in Casting Solutions for Cellulose Acetate Desalination Membranes, Ind Eng Chem Prod Rd, 4 (1965) 114-&.

[43] J.R. McCutcheon, M. Elimelech, Influence of concentrative and dilutive internal concentration polarization on flux behavior in forward osmosis, J Membrane Sci, 284 (2006) 237-247.

[44] J.R. McCutcheon, M. Elimelech, Influence of membrane support layer hydrophobicity on water flux in osmotically driven membrane processes, J MEMBRANE SCI, 318 (2008) 458-466.

[45] R.J. Salter, Forward osmosis, Water Conditioning & Purification, 48 (2006) 36-38.

[46] S.R. Chou, L. Shi, R. Wang, C.Y.Y. Tang, C.Q. Qiu, A.G. Fane, Characteristics and potential applications of a novel forward osmosis hollow fiber membrane, Desalination, 261 (2010) 365-372.

[47] N.Y. Yip, A. Tiraferri, W.A. Phillip, J.D. Schiffman, M. Elimelech, High Performance Thin-Film Composite Forward Osmosis Membrane, Environ Sci Technol, 44 (2010) 3812-3818.

[48] A. Tiraferri, N.Y. Yip, W.A. Phillip, J.D. Schiffman, M. Elimelech, Relating performance of thin-film composite forward osmosis membranes to support layer formation and structure, J MEMBRANE SCI, 367 (2011) 340-352.

[49] N.Y. Yip, A. Tiraferri, W.A. Phillip, J.D. Schiffrnan, L.A. Hoover, Y.C. Kim, M. Elimelech, Thin-Film Composite Pressure Retarded Osmosis Membranes for Sustainable Power Generation from Salinity Gradients, Environ Sci Technol, 45 (2011) 4360-4369.

[50] J. Wei, C.Q. Qiu, C.Y.Y. Tang, R. Wang, A.G. Fane, Synthesis and characterization of flat-sheet thin film composite forward osmosis membranes, J MEMBRANE SCI, 372 (2011) 292-302.

[51] N. Widjojo, T.S. Chung, M. Weber, C. Maletzko, V. Warzelhan, The role of sulphonated polymer and macrovoid-free structure in the support layer for thin-film composite (TFC) forward osmosis (FO) membranes, J MEMBRANE SCI, 383 (2011) 214-223.

[52] A. Sweity, W. Ying, S. Belfer, G. Oron, M. Herzberg, pH effects on the adherence and fouling propensity of extracellular polymeric substances in a membrane bioreactor, J Membrane Sci, 378 (2011) 186-193.

[53] X.X. Song, Z.Y. Liu, D. Sun, Nano Gives the Answer: Breaking the Bottleneck of Internal Concentration Polarization with a Nanofiber Composite Forward Osmosis Membrane for a High Water Production Rate, Adv Mater, 23 (2011) 3256-+.

[54] S. Zhang, K.Y. Wang, T.S. Chung, Y.C. Jean, H.M. Chen, Molecular design of the cellulose ester-based forward osmosis membranes for desalination, Chem Eng Sci, 66 (2011) 2008-2018.

[55] Y. Yu, S. Seo, I.C. Kim, S. Lee, Nanoporous polyethersulfone (PES) membrane with enhanced flux applied in forward osmosis process, J MEMBRANE SCI, 375 (2011) 63-68.

[56] S.C. Yu, X.S. Liu, J.Q. Liu, D.H. Wu, M.H. Liu, C.J. Gao, Surface modification of thin-film composite polyamide reverse osmosis membranes with thermo-responsive polymer (TRP) for improved fouling resistance and cleaning efficiency, Sep Purif Technol, 76 (2011) 283-291.

[57] S. Phuntsho, H.K. Shon, S. Hong, S. Lee, S. Vigneswaran, A novel low energy fertilizer driven forward osmosis desalination for direct fertigation: Evaluating the performance of fertilizer draw solutions, J Membrane Sci, 375 (2011) 172-181.

[58] J.R. McCutcheon, R.L. McGinnis, M. Elimelech, A novel ammonia-carbon dioxide forward (direct) osmosis desalination process, Desalination, 174 (2005) 1-11.

[59] J.R. McCutcheon, R.L. McGinnis, M. Elimelech, Desalination by ammonia-carbon dioxide forward osmosis: Influence of draw and feed solution concentrations on process performance, J Membrane Sci, 278 (2006) 114-123.

[60] R.L. McGinnis, M. Elimelech, Energy requirements of ammonia-carbon dioxide forward osmosis desalination, Desalination, 207 (2007) 370-382.

[61] L.L. J.O. Samer adham, Manish Kumar, Dewatering reverse osmosis concentrate from water reuse applications using forward osmosis, WaterReuse foundation, (2009).

[62] P.L. Hansen, J.A. Cohen, R. Podgornik, V.A. Parsegian, Osmotic properties of poly(ethylene glycols): Quantitative features of brush and bulk scaling laws, Biophys J, 84 (2003) 350-355.

[63] M.M. Ling, T.S. Chung, Novel dual-stage FO system for sustainable protein enrichment using nanoparticles as intermediate draw solutes, J MEMBRANE SCI, 372 (2011) 201-209.

[64] M.M. Ling, K.Y. Wang, T.S. Chung, Highly Water-Soluble Magnetic Nanoparticles as Novel Draw Solutes in Forward Osmosis for Water Reuse, Ind Eng Chem Res, 49 (2010) 5869-5876.

[65] T.A. Zangle, A. Mani, J.G. Santiago, Theory and experiments of concentration polarization and ion focusing at microchannel and nanochannel interfaces, Chem Soc Rev, 39 (2010) 1014-1035.

[66] M. Elimelech, S. Bhattacharjee, A novel approach for modeling concentration polarization in crossflow membrane filtration based on the equivalence of osmotic pressure model and filtration theory, J MEMBRANE SCI, 145 (1998) 223-241.

[67] L.F. Song, M. Elimelech, Theory of Concentration Polarization in Cross-Flow Filtration, J Chem Soc Faraday T, 91 (1995) 3389-3398.

[68] G.A. Denisov, Theory of Concentration Polarization in Cross-Flow Ultrafiltration - Gel-Layer Model and Osmotic-Pressure Model, J MEMBRANE SCI, 91 (1994) 173-187.

[69] J.R. McCutcheon, M. Elimelech, Modeling water flux in forward osmosis: Implications for improved membrane design, Aiche Journal, 53 (2007) 1736-1744.

[70] S.A.F. Zhao, L.D. Zou, Relating solution physicochemical properties to internal concentration polarization in forward osmosis, J MEMBRANE SCI, 379 (2011) 459-467.

[71] G.T. Gray, J.R. McCutcheon, M. Elimelech, Internal concentration polarization in forward osmosis: role of membrane orientation, Desalination, 197 (2006) 1-8.

[72] S. Loeb, L. Titelman, E. Korngold, J. Freiman, Effect of porous support fabric on osmosis through a Loeb-Sourirajan type asymmetric membrane, J Membrane Sci, 129 (1997) 243-249.

[73] G. Li, X.M. Li, Y. Liu, D. Wang, T. He, C.J. Gao, Forward Osmosis and Concentration Polarization, Prog Chem, 22 (2010) 812-821.

[74] G.D. Mehta, S. Loeb, Performance of Permasep B-9 and B-10 Membranes in Various Osmotic Regions and at High Osmotic Pressures, J MEMBRANE SCI, 4 (1979) 335-349.

[75] E.M.V. Hoek, M. Elimelech, Cake-enhanced concentration polarization: A new fouling mechanism for salt-rejecting membranes, Environ Sci Technol, 37 (2003) 5581-5588.

[76] T.H. Chong, F.S. Wong, A.G. Fane, Implications of critical flux and cake enhanced osmotic pressure (CEOP) on colloidal fouling in reverse osmosis: Experimental observations, J MEMBRANE SCI, 314 (2008) 101-111.

[77] T.H. Chong, A.G. Fane, Implications of critical flux and cake enhanced osmotic pressure (CEOP) on colloidal fouling in reverse osmosis: Modeling approach, Desalin Water Treat, 8 (2009) 68-90.

[78] L.N. Sim, Y. Ye, V. Chen, A.G. Fane, Investigations of the coupled effect of cake-enhanced osmotic pressure and colloidal fouling in RO using crossflow sampler-modified fouling index ultrafiltration, Desalination, 273 (2011) 184-196.

[79] K. Nath, Membrane separation processes, Prentice-Hall of India, New Delhi, 2008.

[80] S.J. Judd, D.F. Ayala, V. Ferre, Membrane life estimation in full-scale immersed membrane bioreactors, J MEMBRANE SCI, 378 (2011) 95-100.

[81] S.H. Moon, P.V.X. Hung, S.H. Cho, J.J. Woo, Behaviors of commercialized seawater reverse osmosis membranes under harsh organic fouling conditions, Desalin Water Treat, 15 (2010) 48-53.

[82] S.S. Mitra, A.R. Thomas, G.T. Gang, Evaluation and characterization of seawater RO membrane fouling, Desalination, 247 (2009) 94-107.

[83] J.E. Kilduff, M. Taniguchi, G. Belfort, Modes of natural organic matter fouling during ultrafiltration, Environ Sci Technol, 37 (2003) 1676-1683.

[84] V. Chen, E.K. Lee, A.G. Fane, Natural organic matter (NOM) fouling in low pressure membrane filtration - effect of membranes and operation modes, Desalination, 218 (2008) 257-270.

[85] J.H. Kim, M. Moonkhum, Y.G. Lee, Y.S. Lee, Review of seawater natural organic matter fouling and reverse osmosis transport modeling for seawater reverse osmosis desalination, Desalin Water Treat, 15 (2010) 92-107.

[86] S.K. Hong, M. Elimelech, Chemical and physical aspects of natural organic matter (NOM) fouling of nanofiltration membranes, J MEMBRANE SCI, 132 (1997) 159-181.

[87] T.R. Holm, Metal Complexation by Natural Organic-Matter in Ground-Water, Abstr Pap Am Chem S, 196 (1988) 89-Geoc.

[88] C. Jucker, M.M. Clark, Adsorption of Aquatic Humic Substances on Hydrophobic Ultrafiltration Membranes, J MEMBRANE SCI, 97 (1994) 37-52.

[89] K. Preston, D. Lantagne, N. Kotlarz, K. Jellison, Turbidity and chlorine demand reduction using alum and moringa flocculation before household chlorination in developing countries, J Water Health, 8 (2010) 60-70.

[90] B. Mi, M. Elimelech, Chemical and physical aspects of organic fouling of forward osmosis membranes, J Membrane Sci, 320 (2008) 292-302.

[91] B.X. Mi, M. Elimelech, Organic fouling of forward osmosis membranes: Fouling reversibility and cleaning without chemical reagents, J MEMBRANE SCI, 348 (2010) 337-345.

[92] C.A.C. van de Lisdonk, J.A.M. van Paassen, J.C. Schippers, Monitoring scaling in nanofiltration and reverse osmosis membrane systems, Desalination, 132 (2000) 101-108.

[93] S.F.E. Boerlage, M.D. Kennedy, I. Bremere, G.J. Witkamp, J.P. Van der Hoek, J.C. Schippers, The scaling potential of barium sulphate in reverse osmosis systems, J MEMBRANE SCI, 197 (2002) 251-268.

[94] A. Al-Rammah, The application of acid free antiscalant to mitigate scaling in reverse osmosis membranes, Desalination, 132 (2000) 83-87.

[95] S. Seewoo, R. Van Hille, A. Lewis, Aspects of gypsum precipitation in scaling waters, Hydrometallurgy, 75 (2004) 135-146.

[96] P. Dydo, M. Turek, J. Ciba, K. Wandachowicz, J. Misztal, The nucleation kinetic aspects of gypsum nanofiltration membrane scaling, Desalination, 164 (2004) 41-52.

[97] Y.A. Le Gouellec, M. Elimelech, Calcium sulfate (gypsum) scaling in nanofiltration of agricultural drainage water, J MEMBRANE SCI, 205 (2002) 279-291.

[98] B.X. Mi, M. Elimelech, Gypsum Scaling and Cleaning in Forward Osmosis: Measurements and Mechanisms, Environ Sci Technol, 44 (2010) 2022-2028.

[99] H.C. Flemming, Biofouling in water systems - cases, causes and countermeasures, Appl Microbiol Biot, 59 (2002) 629-640.

[100] Y. Baek, J. Yu, S.H. Kim, S. Lee, J. Yoon, Effect of surface properties of reverse osmosis membranes on biofouling occurrence under filtration conditions, J Membrane Sci, 382 (2011) 91-99.

[101] J. Lee, I.S. Kim, Microbial community in seawater reverse osmosis and rapid diagnosis of membrane biofouling, Desalination, 273 (2011) 118-126.

[102] C.M. Pang, W.T. Liu, Community structure analysis of reverse osmosis membrane biofilms and the significance of Rhizobiales bacteria in biofouling, Environ Sci Technol, 41 (2007) 4728-4734.

[103] H.F. Ridgway, A. Kelly, C. Justice, B.H. Olson, MICROBIAL FOULING OF REVERSE-OSMOSIS MEMBRANES USED IN ADVANCED WASTEWATER-TREATMENT TECHNOLOGY - CHEMICAL, BACTERIOLOGICAL, AND ULTRASTRUCTURAL ANALYSES, Appl Environ Microb, 45 (1983) 1066-1084.

[104] M. Herzberg, M. Elimelech, Biofouling of reverse osmosis membrane: Mechanisms and performance, Abstr Pap Am Chem S, 232 (2006) 541-541.

[105] H. Brouwer, K. Meesters, J. van Groenestijn, Biofouling control in reverse osmosis membranes using rapid biofiltration technology, Desalination, 199 (2006) 15-17.

[106] H.C. Flemming, Reverse osmosis membrane biofouling, Exp Therm Fluid Sci, 14 (1997) 382-391.

[107] R.P. Carnahan, L. Bolin, W. Suratt, Biofouling of Pvd-1 Reverse-Osmosis Elements in the Water-Treatment Plant of the City of Dunedin, Florida, Desalination, 102 (1995) 235-244.

[108] M. Herzberg, Osmotic effects of biofouling in reverse osmosis (RO) processes: Physical and physiological measurements and mechanisms, Desalin Water Treat, 15 (2010) 287-291.

[109] M.M.T. Khan, P.S. Stewart, D.J. Moll, W.E. Mickols, M.D. Burr, S.E. Nelson, A.K. Camper, Assessing biofouling on polyamide reverse osmosis (RO) membrane surfaces in a laboratory system, J Membrane Sci, 349 (2010) 429-437.

[110] S. Kappachery, D. Paul, J. Yoon, J.H. Kweon, Vanillin, a potential agent to prevent biofouling of reverse osmosis membrane, Biofouling, 26 (2010) 667-672.

[111] C.K. Ho, S.J. Altman, H.D.T. Jones, S.S. Khalsa, L.K. McGrath, P.G. Clem, Analysis of micromixers to reduce biofouling on reverse-osmosis membranes, Environ Prog, 27 (2008) 195-203.

[112] M. Herzberg, D. Berry, A.M. Briones, L. Raskin, M. Elimelech, ENVR 65-Impact of microfiltration on biofouling of reverse osmosis membranes, Abstr Pap Am Chem S, 235 (2008).

[113] T.R.R. Pintelon, S.A. Creber, D.A.G. von der Schulenburg, M.L. Johns, Validation of 3D Simulations of Reverse Osmosis Membrane Biofouling, Biotechnol Bioeng, 106 (2010) 677-689.

[114] A.G. Fane, C.J.D. Fell, R.M. Mcdonogh, Colloidal Effects in Ultrafiltration and Reverse-Osmosis, Abstr Pap Am Chem S, 188 (1984) 128-INDE.

[115] M.T. Brunelle, Colloidal Fouling of Reverse-Osmosis Membranes, Desalination, 32 (1980) 127-135.

[116] C. Park, Y.H. Lee, S. Lee, S. Hong, Effect of cake layer structure on colloidal fouling in reverse osmosis membranes, Desalination, 220 (2008) 335-344.

[117] R.J. Hunter, Introduction to modern colloid science / Robert J. Hunter, Oxford University Press, Oxford, England ; New York ; Melbourne :, 1993.

[118] H.Y. Ng, M. Elimelech, Influence of colloidal fouling on rejection of trace organic contaminants by reverse osmosis, J MEMBRANE SCI, 244 (2004) 215-226.

[119] E.M.V. Hoek, A.S. Kim, M. Elimelech, Influence of crossflow membrane filter geometry and shear rate on colloidal fouling in reverse osmosis and nanofiltration separations, Environ Eng Sci, 19 (2002) 357-372.

[120] E.M. Vrijenhoek, S. Hong, M. Elimelech, Influence of membrane surface properties on initial rate of colloidal fouling of reverse osmosis and nanofiltration membranes, J Membrane Sci, 188 (2001) 115-128.

[121] E.M. Vrijenhoek, M. Elimelech, S.K. Hong, Influence of membrane properties, solution chemistry, and hydrodynamics on colloidal fouling of reverse osmosis and nanofiltration membranes., Abstr Pap Am Chem S, 220 (2000) U322-U322.

[122] X.H. Zhu, M. Elimelech, Colloidal fouling of reverse osmosis membranes: measurements and fouling mechanisms, Environ Sci Technol, 31 (1997) 3654-3662.

[123] M. Elimelech, X.H. Zhu, A.E. Childress, S.K. Hong, Role of membrane surface morphology in colloidal fouling of cellulose acetate and composite aromatic polyamide reverse osmosis membranes, J Membrane Sci, 127 (1997) 101-109.

[124] M. Herzberg, M. Elimelech, Biofouling of reverse osmosis membranes: Role of biofilm-enhanced osmotic pressure, J Membrane Sci, 295 (2007) 11-20.

[125] G.D. Kang, M. Liu, B. Lin, Y.M. Cao, Q. Yuan, A novel method of surface modification on thin-film composite reverse osmosis membrane by grafting poly(ethylene glycol), Polymer, 48 (2007) 1165-1170.

[126] X.Y. Wei, Z. Wang, J. Chen, J.X. Wang, S.C. Wang, A novel method of surface modification on thin-film-composite reverse osmosis membrane by grafting hydantoin derivative, J Membrane Sci, 346 (2010) 152-162.

[127] C. Grossmann, K.H. Johannsen, Methods for the Determination of the Portion of Allowable Colloid in Raw Solutions from Their Treatment in Reverse-Osmosis Plants, Chem Tech-Leipzig, 34 (1982) 544-544.

[128] S.Y. Wu, J. Xing, C. Zheng, G.F. Xu, G.D. Zheng, J.P. Xu, Plasma modification of aromatic polyamide reverse osmosis composite membrane surface, J Appl Polym Sci, 64 (1997) 1923-1926.

[129] W.H. Zhou, C.H. Lu, X.C. Guo, F.R. Chen, H.H. Yang, X.R. Wang, Mussel-inspired molecularly imprinted polymer coating superparamagnetic nanoparticles for protein recognition, J Mater Chem, 20 (2010) 880-883.

[130] C.E. Brubaker, W. Lo, H. Kissler, D.B. Kaufman, P.B. Messersmith, Characterization and biocompatibility of a mussel-inspired PEG-based adhesive, Abstr Pap Am Chem S, 238 (2009).

[131] S. Kasemset, A. Lee, D.J. Miller, B.D. Freeman, M.M. Sharma, Effect of polydopamine deposition conditions on fouling resistance, physical properties, and permeation properties of reverse osmosis membranes in oil/water separation, J Membrane Sci, 425 (2013) 208-216.

[132] J.T. Arena, B. McCloskey, B.D. Freeman, J.R. McCutcheon, Surface modification of thin film composite membrane support layers with polydopamine: Enabling use of reverse osmosis membranes in pressure retarded osmosis, J Membrane Sci, 375 (2011) 55-62.

[133] B.D. McCloskey, H.B. Park, H. Ju, B.W. Rowe, D.J. Miller, B.J. Chun, K. Kin, B.D. Freeman, Influence of polydopamine deposition conditions on pure water flux and foulant adhesion resistance of reverse osmosis, ultrafiltration, and microfiltration membranes, Polymer, 51 (2010) 3472-3485.

[134] K. Sun, L.S. Song, Y.Y. Xie, D.B. Liu, D. Wang, Z. Wang, W.S. Ma, J.S. Zhu, X.Y. Jiang, Using Self-Polymerized Dopamine to Modify the Antifouling Property of Oligo(ethylene glycol) Self-Assembled Monolayers and Its Application in Cell Patterning, Langmuir, 27 (2011) 5709-5712.

[135] M. Zheng, Y. Zhou, Y. Chen, Y.W. Tang, T.H. Lu, Electrochemical behavior of dopamine in the presence of phosphonate and the determination of dopamine at phosphonate modified zirconia films electrode with highly antifouling capability, Electrochim Acta, 55 (2010) 4789-4798.

[136] Z.D. Chen, T. Nagaoka, Selective determination of dopamine based on a self-assembled monolayer electrode with antifouling activity on protein adsorption, Bunseki Kagaku, 53 (2004) 1321-1324.

[137] T.A. Saleh, V.K. Gupta, Synthesis and characterization of alumina nano-particles polyamide membrane with enhanced flux rejection performance, Sep Purif Technol, 89 (2012) 245-251.

[138] M. Fathizadeh, A. Aroujalian, A. Raisi, Effect of added NaX nano-zeolite into polyamide as a top thin layer of membrane on water flux and salt rejection in a reverse osmosis process, J Membrane Sci, 375 (2011) 88-95.

[139] E.S. Kim, B.L. Deng, Fabrication of polyamide thin-film nano-composite (PA-TFN) membrane with hydrophilized ordered mesoporous carbon (H-OMC) for water purifications, J Membrane Sci, 375 (2011) 46-54.

[140] A. Tiraferri, C.D. Vecitis, M. Elimelech, Covalent Binding of Single-Walled Carbon Nanotubes to Polyamide Membranes for Antimicrobial Surface Properties, Acs Appl Mater Inter, 3 (2011) 2869-2877.

[141] C. Lee, S. Baik, Vertically-aligned carbon nano-tube membrane filters with superhydrophobicity and superoleophilicity, Carbon, 48 (2010) 2192-2197.

[142] S.S. Madaeni, T.A. Arbatan, Preparation and Characterization of Microfiltration Membrane Embedded with Silver Nano-Particles, Iran J Chem Chem Eng, 29 (2010) 105-111.

[143] J.H. Li, X.S. Shao, Q. Zhou, M.Z. Li, Q.Q. Zhang, The double effects of silver nanoparticles on the PVDF membrane: Surface hydrophilicity and antifouling performance, Appl Surf Sci, 265 (2013) 663-670.

[144] Y. Liu, E. Rosenfield, M. Hu, B. Mi, Direct Observation of Bacterial Deposition on and Detachment from Nanocomposite Membranes Embedded with Silver Nanoparticles, Water Res.

[145] A. Tiraferri, Y. Kang, E.P. Giannelis, M. Elimelech, Superhydrophilic Thin-Film Composite Forward Osmosis Membranes for Organic Fouling Control: Fouling Behavior and Antifouling Mechanisms, Environ Sci Technol, 46 (2012) 11135-11144.

[146] A. Tiraferri, Y. Kang, E.P. Giannelis, M. Elimelech, Highly Hydrophilic Thin-Film Composite Forward Osmosis Membranes Functionalized with Surface-Tailored Nanoparticles, Acs Appl Mater Inter, 4 (2012) 5044-5053.

[147] A. Tiraferri, Y. Wang, E.P. Giannelis, M. Elimelech, Binding silver and silica nanoparticles to polymeric membrane surface for novel antibiofouling properties, Abstr Pap Am Chem S, 242 (2011).

[148] M. Kazemimoghadam, Preparation of nanopore HS zeolite membranes for reverse osmosis processes, Desalin Water Treat, 30 (2011) 51-57.

[149] X.Y. Qu, H. Dong, Q. Ye, L. Zhang, Z.J. Zhou, H.L. Chen, Improvement of the zeolite-polyamide nanocomposite reverse osmosis membrane for desalination, Abstr Pap Am Chem S, 239 (2010).

[150] E.M. Flanigen, Review and New Perspectives in Zeolite Crystallization, Adv Chem Ser, (1973) 119-139.

[151] X.J. Yin, G.S. Zhu, Z.Y. Wang, N.L. Yue, S.L. Qiu, Zeolite P/NaX composite membrane for gas separation, Micropor Mesopor Mat, 105 (2007) 156-162.

[152] D. Sen, H. Kalipcilar, L. Yilmaz, Development of zeolite filled polycarbonate mixed matrix gas separation membranes, Desalination, 200 (2006) 222-224.

[153] Z. Huang, Y. Li, R. Wen, M.M. Teoh, S. Kulprathipanja, Enhanced gas separation properties by using nanostructured PES-zeolite 4A mixed matrix membranes, J Appl Polym Sci, 101 (2006) 3800-3805.

[154] L.G. Lin, Y.H. Zhang, H. Li, Pervaporation and sorption behavior of zeolite-filled polyethylene glycol hybrid membranes for the removal of thiophene species, J Colloid Interf Sci, 350 (2010) 355-360.

[155] M. Kazemimoghadam, T. Mohammadi, The pilot-scale pervaporation plant using tubular-type module with nano pore zeolite membrane, Desalination, 255 (2010) 196-199.

[156] W. Jia, S. Murad, Molecular dynamics simulations of gas separations using faujasite-type zeolite membranes, J Chem Phys, 120 (2004) 4877-4885.

[157] L.X. Li, J.H. Dong, T.M. Nenoff, R. Lee, Desalination by reverse osmosis using MFI zeolite membranes, J Membrane Sci, 243 (2004) 401-404.

[158] M.E. Lydon, K.A. Unocic, T.H. Bae, C.W. Jones, S. Nair, Structure-Property Relationships of Inorganically Surface-Modified Zeolite Molecular Sieves for Nanocomposite Membrane Fabrication, J Phys Chem C, 116 (2012) 9636-9645.

[159] C.P. Leo, N.H.A. Kamil, M.U.M. Junaidi, S.N.M. Kamal, A.L. Ahmad, The potential of SAPO-44 zeolite filler in fouling mitigation of polysulfone ultrafiltration membrane, Sep Purif Technol, 103 (2013) 84-91.

[160] A. Ivan, D.L. Ghindeanu, V. Danciulescu, A. Raducu, A.C. Nechifor, Composite polyaniline-zeolite membrane material for wastewater ultrafiltration, Optoelectron Adv Mat, 6 (2012) 1134-1138.

[161] F.Q. Mir, A. Shukla, Negative Rejection of NaCl in Ultrafiltration of Aqueous Solution of NaCl and KCl Using Socialite Octahydrate Zeolite-Clay Charged Ultrafiltration Membrane, Ind Eng Chem Res, 49 (2010) 6539-6546.

[162] S. Malamis, E. Katsou, M. Stylianou, K.J. Haralambous, M. Loizidou, Copper removal from sludge permeate with ultrafiltration membranes using zeolite, bentonite and vermiculite as adsorbents, Water Sci Technol, 61 (2010) 581-589.

[163] R.L. Han, S.H. Zhang, C. Liu, Y.T. Wang, X.G. Jian, Effect of NaA zeolite particle addition on poly(phthalazinone ether sulfone ketone) composite ultrafiltration (UF) membrane performance, J Membrane Sci, 345 (2009) 5-12.

[164] N. Ma, J. Wei, R.H. Liao, C.Y.Y. Tang, Zeolite-polyamide thin film nanocomposite membranes: Towards enhanced performance for forward osmosis, J Membrane Sci, 405 (2012) 149-157.

[165] B.H. Jeong, E.M.V. Hoek, Y.S. Yan, A. Subramani, X.F. Huang, G. Hurwitz, A.K. Ghosh, A. Jawor, Interfacial polymerization of thin film nanocomposites: A new concept for reverse osmosis membranes, J Membrane Sci, 294 (2007) 1-7.

[1] M.A. Shannon, P.W. Bohn, M. Elimelech, J.G. Georgiadis, B.J. Mariñas, and A.M. Mayes, Science and technology for water purification in the coming decades, Nature 452 (2008), 301-310.

[2] S. Kanae, Global warming and the water crisis, J. Health. Sci. 55 (2009) 860-864.

[3] C. Charcosset, A review of membrane processes and renewable energies for desalination, Desalination 245 (2009) 214-231.

[4] L.R.E. James, E. Miller, Forward Osmosis: A new approach to water purification and desalination, Sandia National Laboratories, Albuquerque, New Mexico and Livermore, California, 2006.

[5] R.L. McGinnis, M. Elimelech, Energy requirements of ammonia-carbon dioxide forward osmosis membrane desalination, Desalination, 207 (2007) 370-382.

[6] T. Cath, Osmotically and thermally driven membrane processes for enhancement of water recovery in desalination processes, Desalin Water Treatment, 15 (2010) 279-286.

[7] T. Cath, A. Childress, M. Elimelech, Forward osmosis: Principles, applications, and recent developments, J. Membrane. Sci. 281 (2006) 70-87.

[8] A. Achilli, T. Cath, E. Marchand, A. Childress, The forward osmosis membrane bioreactor: A low fouling alternative to MBR processes, Desalination 239 (2009) 10-21.

[9] I. Escobar, E. Hoek, C. Gabelich, F. DiGiano, Y. Le Gouellec, P. Berube, K. Howe, J. Allen, K. Atasi, M. Benjamin, P. Brandhuber, J. Brant, Y. Chang, M. Chapman, A. Childress, W. Conlon, T. Cooke, I. Crossley, G. Crozes, P. Huck, S. Kommineni, J. Jacangelo, A. Karimi, J. Kim, D. Lawler, Q. Li, L. Schideman, S. Sethi, J. Tobiason, T. Tseng, S. Veerapanemi, A. Zander, A.M.T.R. Comm,Committee Report: Recent advances and research needs in membrane fouling, J. Am. Water Works Ass. 97 (2005) 79-89.

[10] Q. Li, M. Elimelech, Revealing the mechanisms of organic fouling and chemical cleaning of nanofiltration membranes., Abstr. Pap. Am. Chem. Soc. 226 (2003) U506-U507.

[11] C. Bellona, M. Marts, J. Drewes, The effect of organic membrane fouling on the properties and rejection characteristics of nanofiltration membranes, Sep. Purif. Technol. 74 (2010) 44-54.

[12] S. Kang, A. Subramani, E. Hoek, M. Deshusses, M. Matsumoto, Direct observation of biofouling in cross-flow microfiltration: mechanisms of deposition and release, J Membrane Sci. 244 (2004) 151-165.

[13] M. Herzberg, S. Kang, M. Elimelech, Role of extracellular polymeric substances (EPS) in biofouling of reverse osmosis membranes, Environ. Sci. Technol. 43 (2009) 4393-4398.

[14] X. Zhu, M. Elimelech, Colloidal fouling of reverse osmosis membranes: Measurements and fouling mechanisms, Environ. Sci. Technol. 31 (1997) 3654-3662.

[15] E. Vrijenhoek, S. Hong, M. Elimelech, Influence of membrane surface properties on initial rate of colloidal fouling of reverse osmosis and nanofiltration membranes, J. Membrane. Sci. 188 (2001) 115-128.

[16] R. Holloway, A. Childress, K. Dennett, T. Cath, Forward osmosis for concentration of anaerobic digester centrate, Water. Res. 41 (2007) 4005-4014.

[17] B. Mi, M. Elimelech, Chemical and physical aspects of organic fouling of forward osmosis membranes, J Membrane Sci., 320 (2008) 292-302.

[18] B. Mi, M. Elimelech, Gypsum scaling and cleaning in forward osmosis: measurements and mechanisms, Environ. Sci. Technol. 44 (2010) 2022-2028.

[19] B. Mi, M. Elimelech, Organic fouling of forward osmosis membranes: Fouling reversibility and cleaning without chemical reagents, J. Membrane. Sci. 348 (2010) 337-345.

[20] C. Tang, Q. She, W. Lay, R. Wang, A. Fane, Coupled effects of internal concentration polarization and fouling on flux behavior of forward osmosis membranes during humic acid filtration, J. Membrane. Sci. 354 (2010) 123-133.

[21] S. Lee, J. Cho, M. Elimelech, Combined influence of natural organic matter (NOM) and colloidal particles on nanofiltration membrane fouling, J. Membrane. Sci. 262 (2005) 27-41.

[22] Q. Li, M. Elimelech, Synergistic effects in combined fouling of a loose nanofiltration membrane by colloidal materials and natural organic matter, J. Membrane. Sci. 278 (2006) 72-82.

[23] C. Law, X. Li, Q. Li, The combined colloid-organic fouling on nanofiltration membrane for wastewater treatment and reuse, Sep. Sci. Technol. 45 (2010) 935-940.

[24] C. Jarusutthirak, S. Mattaraj, R. Jiraratananon, Influence of inorganic scalants and natural organic matter on nanofiltration membrane fouling, J. Membrane. Sci. 287 (2007) 138-145.

[25] S. Lee, M. Elimelech, Relating organic fouling of reverse osmosis membranes to intermolecular adhesion forces, Environ. Sci. Technol. 40 (2006) 980-987.

[26] Q. Li, M. Elimelech, Organic fouling and chemical cleaning of nanofiltration membranes: Measurements and mechanisms, Environ. Sci. Technol. 38 (2004) 4683-4693.

[27] S. Lee, M. Elimelech, Salt cleaning of organic-fouled reverse osmosis membranes, Water. Res. 41 (2007) 1134-1142.

[28] D. Hatziantoniou, J. Howell, Influence of the properties and characteristics of sugar-beet pulp extract on its fouling and rejection behaviour during membrane filtration, Desalanation 148 (2002) 67-72.

[29] Image J. in: http://rsbweb.nih.gov/ij/

[1] S.C. Low, Preliminary studies of seawater desalination using forward osmosis, Desalin Water Treat, 7 (2009) 41-46.

[2] M. Elimelech, J.R. McCutcheon, R.L. McGinnis, A novel ammonia-carbon dioxide forward (direct) osmosis desalination process, Desalination, 174 (2005) 1-11.

[3] G. Han, T.S. Chung, M. Toriida, S. Tamai, Thin-film composite forward osmosis membranes with novel hydrophilic supports for desalination, J Membrane Sci, 423 (2012) 543-555.

[4] J.R. McCutcheon, R.L. McGinnis, M. Elimelech, Desalination by ammonia-carbon dioxide forward osmosis: Influence of draw and feed solution concentrations on process performance, J Membrane Sci, 278 (2006) 114-123.

[5] S. Phuntsho, H.K. Shon, S. Hong, S. Lee, S. Vigneswaran, A novel low energy fertilizer driven forward osmosis desalination for direct fertigation: Evaluating the performance of fertilizer draw solutions, J Membrane Sci, 375 (2011) 172-181.

[6] D.L. Shaffer, N.Y. Yip, J. Gilron, M. Elimelech, Seawater desalination for agriculture by integrated forward and reverse osmosis: Improved product water quality for potentially less energy, J Membrane Sci, 415 (2012) 1-8.

[7] T.Y. Cath, A.E. Childress, M. Elimelech, Forward osmosis: Principles, applications, and recent developments, J Membrane Sci, 281 (2006) 70-87.

[8] C.M. Werner, B.E. Logan, P.E. Saikaly, G.L. Amy, Wastewater treatment, energy recovery and desalination using a forward osmosis membrane in an air-cathode microbial osmotic fuel cell, J Membrane Sci, 428 (2013) 116-122.

[9] E.G. Beaudry, K.A. Lampi, Membrane Technology for Direct-Osmosis Concentration of Fruit Juices, Food Technol-Chicago, 44 (1990) 121-121.

[10] V. Sant'Anna, L.D.F. Marczak, I.C. Tessaro, Membrane concentration of liquid foods by forward osmosis: Process and quality view, J Food Eng, 111 (2012) 483-489.

[11] A.E. Childress, A. Achilli, T.Y. Cath, E.A. Marchand, The forward osmosis membrane bioreactor: A low fouling alternative to MBR processes, Desalination, 239 (2009) 10-21.

[12] S.J. Judd, D.F. Ayala, V. Ferre, Membrane life estimation in full-scale immersed membrane bioreactors, Journal of Membrane Science, 378 (2011) 95-100.

[13] S.S. Mitra, A.R. Thomas, G.T. Gang, Evaluation and characterization of seawater RO membrane fouling, Desalination, 247 (2009) 94-107.

[14] J.E. Kilduff, M. Taniguchi, G. Belfort, Modes of natural organic matter fouling during ultrafiltration, Environmental Science & Technology, 37 (2003) 1676-1683.

[15] V. Chen, E.K. Lee, A.G. Fane, Natural organic matter (NOM) fouling in low pressure membrane filtration - effect of membranes and operation modes, Desalination, 218 (2008) 257-270.

[16] J.H. Kim, M. Moonkhum, Y.G. Lee, Y.S. Lee, Review of seawater natural organic matter fouling and reverse osmosis transport modeling for seawater reverse osmosis desalination, Desalination and Water Treatment, 15 (2010) 92-107.

[17] Y. Liu, B. Mi, Combined fouling of forward osmosis membranes: Synergistic foulant interaction and direct observation of fouling layer formation, J. Membr. Sci., 407 (2012) 136-144.

[18] B. Mi, M. Elimelech, Chemical and physical aspects of organic fouling of forward osmosis membranes, J Membrane Sci, 320 (2008) 292-302.

[19] B.X. Mi, M. Elimelech, Organic fouling of forward osmosis membranes: Fouling reversibility and cleaning without chemical reagents, J Membrane Sci, 348 (2010) 337-345.

[20] G.A. Denisov, Theory of Concentration Polarization in Cross-Flow Ultrafiltration - Gel-Layer Model and Osmotic-Pressure Model, Journal of Membrane Science, 91 (1994) 173-187.

[21] S. Seewoo, R. Van Hille, A. Lewis, Aspects of gypsum precipitation in scaling waters, Hydrometallurgy, 75 (2004) 135-146.

[22] P. Dydo, M. Turek, J. Ciba, K. Wandachowicz, J. Misztal, The nucleation kinetic aspects of gypsum nanofiltration membrane scaling, Desalination, 164 (2004) 41-52.

[23] Y.A. Le Gouellec, M. Elimelech, Calcium sulfate (gypsum) scaling in nanofiltration of agricultural drainage water, Journal of Membrane Science, 205 (2002) 279-291.

[24] A. Rahardianto, B.C. Mccool, Y. Cohen, Reverse osmosis desalting of inland brackish water of high gypsum scaling propensity: Kinetics and mitigation of membrane mineral scaling, Environmental Science & Technology, 42 (2008) 4292-4297.

[25] B.X. Mi, M. Elimelech, Gypsum Scaling and Cleaning in Forward Osmosis: Measurements and Mechanisms, Environ Sci Technol, 44 (2010) 2022-2028.

[26] S.K. Hong, M. Elimelech, Chemical and physical aspects of natural organic matter (NOM) fouling of nanofiltration membranes, Journal of Membrane Science, 132 (1997) 159-181.

[27] Y. Liu, E. Rosenfield, M. Hu, B. Mi, Direct observation of bacterial deposition on and detachment from nanocomposite membranes embedded with silver nanoparticles, Water Res, 47 (2013) 2949-2958.

[28] A.J. de Kerchove, M. Elimelech, Structural growth and viscoelastic properties of adsorbed alginate layers in monovalent and divalent salts, Macromolecules, 39 (2006) 6558-6564.

[29] G. Sauerbrey, Verwendung Von Schwingquarzen Zur Wagung Dunner Schichten Und Zur Mikrowagung, Z Phys, 155 (1959) 206-222.

[30] F. Höök, M. Rodahl, P. Brzezinski, B. Kasemo, Energy Dissipation Kinetics for Protein and Antibody−Antigen Adsorption under Shear Oscillation on a Quartz Crystal Microbalance, Langmuir, 14 (1998) 729-734.

[31] C. Kößlinger, S. Drost, F. Aberl, H. Wolf, S. Koch, P. Woias, A quartz crystal biosensor for measurement in liquids, Biosensors and Bioelectronics, 7 (1992) 397-404.

[32] A.E. Contreras, Z. Steiner, J. Miao, R. Kasher, Q. Li, Studying the Role of Common Membrane Surface Functionalities on Adsorption and Cleaning of Organic Foulants Using QCM-D, Environ Sci Technol, 45 (2011) 6309-6315.

[33] R.W. Field, D. Wu, J.A. Howell, B.B. Gupta, Critical flux concept for microfiltration fouling, J Membrane Sci, 100 (1995) 259-272.

[34] J.S. Vrouwenvelder, J.A.M. van Paassen, J.M.C. van Agtmaal, M.C.M. van Loosdrecht, J.C. Kruithof, A critical flux to avoid biofouling of spiral wound nanofiltration and reverse osmosis membranes: Fact or fiction?, J Membrane Sci, 326 (2009) 36-44.

[35] S. Zou, Y. Gu, D. Xiao, C.Y. Tang, The role of physical and chemical parameters on forward osmosis membrane fouling during algae separation, J Membrane Sci, 366 (2011) 356-362.

[36] S. Zou, Y.-N. Wang, F. Wicaksana, T. Aung, P.C.Y. Wong, A.G. Fane, C.Y. Tang, Direct microscopic observation of forward osmosis membrane fouling by microalgae: Critical flux and the role of operational conditions, J Membrane Sci, 436 (2013) 174-185.

[37] P. Sikorski, F. Mo, G. Skjak-Braek, B.T. Stokke, Evidence for egg-box-compatible interactions in calcium-alginate gels from fiber X-ray diffraction, Biomacromolecules, 8 (2007) 2098-2103.

[38] L. Li, Y. Fang, R. Vreeker, I. Appelqvist, E. Mendes, Reexamining the egg-box model in calcium-alginate gels with X-ray diffraction, Biomacromolecules, 8 (2007) 464-468.

[39] G.R.M. G. R. Aiken, R. L. Wershaw, P. MacCarthy, Humic substances in soil, sediment, and water : geochemistry, isolation, and characterization / edited by George R. Aiken ... [et al.], Wiley, New York :, 1985.

[40] F.J. Stevenson, Humus chemistry: genesis, composition, reactions, in, John Wiley and Sons, canada, 1994.

[41] P.J.M. Anđelković Tatjana, Purenović Milovan M., Anđelković Darko, Destabilization and aggregation of aqueous humic acids solution by metal ions, in: Physics, Chemistry and Technology, 2004, pp. 79-85.

[42] M.M.T. Khan, P.S. Stewart, D.J. Moll, W.E. Mickols, M.D. Burr, S.E. Nelson, A.K. Camper, Assessing biofouling on polyamide reverse osmosis (RO) membrane surfaces in a laboratory system, J Membrane Sci, 349 (2010) 429-437.

[43] W.S. Ang, M. Elimelech, Protein (BSA) fouling of reverse osmosis membranes: Implications for wastewater reclamation, Journal of Membrane Science, 296 (2007) 83-92.

[44] M.L. Ferrer, R. Duchowicz, B. Carrasco, J.G. de la Torre, A.U. Acuna, The conformation of serum albumin in solution: A combined phosphorescence depolarization-hydrodynamic modeling study, Biophys J, 80 (2001) 2422-2430.

[45] E.M.V. Hoek, M. Elimelech, Cake-enhanced concentration polarization: A new fouling mechanism for salt-rejecting membranes, Environmental Science & Technology, 37 (2003) 5581-5588.

[46] T.H. Chong, F.S. Wong, A.G. Fane, The effect of imposed flux on biofouling in reverse osmosis: Role of concentration polarisation and biofilm enhanced osmotic pressure phenomena, J Membrane Sci, 325 (2008) 840-850.

[47] T.H. Chong, A.G. Fane, Implications of critical flux and cake enhanced osmotic pressure (CEOP) on colloidal fouling in reverse osmosis: Modeling approach, Desalination and Water Treatment, 8 (2009) 68-90.

[48] L.N. Sim, Y. Ye, V. Chen, A.G. Fane, Investigations of the coupled effect of cake-enhanced osmotic pressure and colloidal fouling in RO using crossflow sampler-modified fouling index ultrafiltration, Desalination, 273 (2011) 184-196.

[1] T.Y. Cath, A.E. Childress, M. Elimelech, Forward osmosis: Principles, applications, and recent developments, J Membrane Sci, 281 (2006) 70-87.

[2] J.C. Su, S. Zhang, M.M. Ling, T.S. Chung, Forward osmosis: an emerging technology for sustainable supply of clean water, Clean Technol Envir, 14 (2012) 507-511.

[3] J.J. Qin, W.C.L. Lay, K.A. Kekre, Recent developments and future challenges of forward osmosis for desalination: a review, Desalin Water Treat, 39 (2012) 123-136.

[4] T.S. Chung, S. Zhang, K.Y. Wang, J.C. Su, M.M. Ling, Forward osmosis processes: Yesterday, today and tomorrow, Desalination, 287 (2012) 78-81.

[5] L.A. Hoover, W.A. Phillip, A. Tiraferri, N.Y. Yip, M. Elimelech, Forward with Osmosis: Emerging Applications for Greater Sustainability, Environ Sci Technol, 45 (2011) 9824-9830.

[6] S.C. Low, Preliminary studies of seawater desalination using forward osmosis, Desalin Water Treat, 7 (2009) 41-46.

[7] S.F. Zhao, L.D. Zou, D. Mulcahy, Brackish water desalination by a hybrid forward osmosis-nanofiltration system using divalent draw solute, Desalination, 284 (2012) 175-181.

[8] J.R. McCutcheon, R.L. McGinnis, M. Elimelech, Desalination by ammonia-carbon dioxide forward osmosis: Influence of draw and feed solution concentrations on process performance, J Membrane Sci, 278 (2006) 114-123.

[9] K. Lutchmiah, E.R. Cornelissen, D.J.H. Harmsen, J.W. Post, K. Lampi, H. Ramaekers, L.C. Rietveld, K. Roest, Water recovery from sewage using forward osmosis, Water Sci Technol, 64 (2011) 1443-1449.

[10] C.M. Werner, B.E. Logan, P.E. Saikaly, G.L. Amy, Wastewater treatment, energy recovery and desalination using a forward osmosis membrane in an air-cathode microbial osmotic fuel cell, J Membrane Sci, 428 (2013) 116-122.

[11] F. Zhang, K.S. Brastad, Z. He, Integrating Forward Osmosis into Microbial Fuel Cells for Wastewater Treatment, Water Extraction and Bioelectricity Generation, Environ Sci Technol, 45 (2011) 6690-6696.

[12] O.A. Bamaga, A. Yokochi, E.G. Beaudry, Application of forward osmosis in pretreatment of seawater for small reverse osmosis desalination units, Desalin Water Treat, 5 (2009) 183-191.

[13] C. Aydiner, S. Topcu, C. Tortop, F. Kuvvet, D. Ekinci, N. Dizge, B. Keskinler, A novel implementation of water recovery from whey: "forward-reverse osmosis" integrated membrane system, Desalin Water Treat, 51 (2013) 786-799.

[14] Y.J. Choi, J.S. Choi, H.J. Oh, S. Lee, D.R. Yang, J.H. Kim, Toward a combined system of forward osmosis and reverse osmosis for seawater desalination, Desalination, 247 (2009) 239-246.

[15] D.L. Shaffer, N.Y. Yip, J. Gilron, M. Elimelech, Seawater desalination for agriculture by integrated forward and reverse osmosis: Improved product water quality for potentially less energy, J Membrane Sci, 415 (2012) 1-8.

[16] M.A. Saad, Early discovery of RO membrane fouling and real-time monitoring of plant performance for optimizing cost of water, Desalination, 165 (2004) 183-191.

[17] N.T. Hancock, P. Xu, D.M. Heil, C. Bellona, T.Y. Cath, Comprehensive Bench- and Pilot-Scale Investigation of Trace Organic Compounds Rejection by Forward Osmosis, Environ Sci Technol, 45 (2011) 8483-8490.

[18] B.X. Mi, M. Elimelech, Organic fouling of forward osmosis membranes: Fouling reversibility and cleaning without chemical reagents, J Membrane Sci, 348 (2010) 337-345.

[19] B. Mi, M. Elimelech, Chemical and physical aspects of organic fouling of forward osmosis membranes, J Membrane Sci, 320 (2008) 292-302.

[20] C. Boo, S. Lee, M. Elimelech, Z.Y. Meng, S. Hong, Colloidal fouling in forward osmosis: Role of reverse salt diffusion, J Membrane Sci, 390 (2012) 277-284.

[21] B.X. Mi, M. Elimelech, Gypsum Scaling and Cleaning in Forward Osmosis: Measurements and Mechanisms, Environ Sci Technol, 44 (2010) 2022-2028.

[22] E. Arkhangelsky, F. Wicaksana, C.Y. Tang, A.A. Al-Rabiah, S.M. Al-Zahrani, R. Wang, Combined organic-inorganic fouling of forward osmosis hollow fiber membranes, Water Res, 46 (2012) 6329-6338.

[23] E. Arkhangelsky, F. Wicaksana, S.R. Chou, A.A. Al-Rabiah, S.M. Al-Zahrani, R. Wang, Effects of scaling and cleaning on the performance of forward osmosis hollow fiber membranes, J Membrane Sci, 415 (2012) 101-108.

[24] J.S. Zhang, W.L.C. Loong, S.R. Chou, C.Y. Tang, R. Wang, A.G. Fane, Membrane biofouling and scaling in forward osmosis membrane bioreactor, J Membrane Sci, 403 (2012) 8-14.

[25] A. Achilli, T.Y. Cath, E.A. Marchand, A.E. Childress, The forward osmosis membrane bioreactor: A low fouling alternative to MBR processes, Desalination, 239 (2009) 10-21.

[26] S.T. Kang, A. Subramani, E.M.V. Hoek, M.A. Deshusses, M.R. Matsumoto, Direct observation of biofouling in cross-flow microfiltration: mechanisms of deposition and release, J Membrane Sci, 244 (2004) 151-165.

[27] E.M.V. Hoek, Direct observation of biofouling in environmental membrane processes., Abstr Pap Am Chem S, 228 (2004) U614-U614.

[28] Y.L. Liu, B.X. Mi, Combined fouling of forward osmosis membranes: Synergistic foulant interaction and direct observation of fouling layer formation, J Membrane Sci, 407 (2012) 136-144.

[29] M. Herzberg, M. Elimelech, Biofouling of reverse osmosis membranes: Role of biofilm-enhanced osmotic pressure, J Membrane Sci, 295 (2007) 11-20.

[1] A. Tiraferri, N.Y. Yip, W.A. Phillip, J.D. Schiffman, M. Elimelech, Relating performance of thin-film composite forward osmosis membranes to support layer formation and structure, J Membrane Sci, 367 (2011) 340-352.

[2] N.Y. Yip, A. Tiraferri, W.A. Phillip, J.D. Schiffman, M. Elimelech, High Performance Thin-Film Composite Forward Osmosis Membrane, Environ Sci Technol, 44 (2010) 3812-3818.

[3] P. Sukitpaneenit, T.S. Chung, High Performance Thin-Film Composite Forward Osmosis Hollow Fiber Membranes with Macrovoid-Free and Highly Porous Structure for Sustainable Water Production, Environ Sci Technol, 46 (2012) 7358-7365.

[4] N. Ma, J. Wei, R.H. Liao, C.Y.Y. Tang, Zeolite-polyamide thin film nanocomposite membranes: Towards enhanced performance for forward osmosis, J Membrane Sci, 405 (2012) 149-157.

[5] H.C. Flemming, Biofouling in water systems - cases, causes and countermeasures, Appl Microbiol Biot, 59 (2002) 629-640.

[6] Y. Baek, J. Yu, S.H. Kim, S. Lee, J. Yoon, Effect of surface properties of reverse osmosis membranes on biofouling occurrence under filtration conditions, J Membrane Sci, 382 (2011) 91-99.

[7] J. Lee, I.S. Kim, Microbial community in seawater reverse osmosis and rapid diagnosis of membrane biofouling, DESALINATION, 273 (2011) 118-126.

[8] R.P. Schneider, L.M. Ferreira, P. Binder, E.M. Bejarano, K.P. Goes, E. Slongo, C.R. Machado, G.M.Z. Rosa, Dynamics of organic carbon and of bacterial populations in a conventional pretreatment train of a reverse osmosis unit experiencing severe biofouling, J Membrane Sci, 266 (2005) 18-29.

[9] J.L. Rand, R. Hofmann, M.Z.B. Alam, C. Chauret, R. Cantwell, R.C. Andrews, G.A. Gagnon, A field study evaluation for mitigating biofouling with chlorine dioxide or chlorine integrated with UV disinfection, Water Res, 41 (2007) 1939-1948.

[10] M. Herzberg, M. Elimelech, Biofouling of reverse osmosis membrane: Mechanisms and performance, Abstr Pap Am Chem S, 232 (2006) 541-541.

[11] H. Brouwer, K. Meesters, J. van Groenestijn, Biofouling control in reverse osmosis membranes using rapid biofiltration technology, DESALINATION, 199 (2006) 15-17.

[12] H.C. Flemming, Reverse osmosis membrane biofouling, Exp Therm Fluid Sci, 14 (1997) 382-391.

[13] R.P. Carnahan, L. Bolin, W. Suratt, Biofouling of Pvd-1 Reverse-Osmosis Elements in the Water-Treatment Plant of the City of Dunedin, Florida, DESALINATION, 102 (1995) 235-244.

[14] B. Gottenbos, H.C. van der Mei, H.J. Busscher, [38] Models for studying initial adhesion and surface growth in biofilm formation on surfaces, in: J.D. Ron (Ed.) Methods in Enzymology, Academic Press, 1999, pp. 523-534.

[15] S. Kappachery, D. Paul, J. Yoon, J.H. Kweon, Vanillin, a potential agent to prevent biofouling of reverse osmosis membrane, Biofouling, 26 (2010) 667-672.

[16] M. Herzberg, Osmotic effects of biofouling in reverse osmosis (RO) processes: Physical and physiological measurements and mechanisms, Desalin Water Treat, 15 (2010) 287-291.

[17] M.M.T. Khan, P.S. Stewart, D.J. Moll, W.E. Mickols, M.D. Burr, S.E. Nelson, A.K. Camper, Assessing biofouling on polyamide reverse osmosis (RO) membrane surfaces in a laboratory system, J MEMBRANE SCI, 349 (2010) 429-437.

[18] C.K. Ho, S.J. Altman, H.D.T. Jones, S.S. Khalsa, L.K. McGrath, P.G. Clem, Analysis of micromixers to reduce biofouling on reverse-osmosis membranes, Environ Prog, 27 (2008) 195-203.

[19] M. Herzberg, D. Berry, A.M. Briones, L. Raskin, M. Elimelech, ENVR 65-Impact of microfiltration on biofouling of reverse osmosis membranes, Abstr Pap Am Chem S, 235 (2008).

[20] J.S. Zhang, W.L.C. Loong, S.R. Chou, C.Y. Tang, R. Wang, A.G. Fane, Membrane biofouling and scaling in forward osmosis membrane bioreactor, J Membrane Sci, 403 (2012) 8-14.

[21] E.R. Cornelissen, D. Harmsen, K.F. de Korte, C.J. Ruiken, J.-J. Qin, H. Oo, L.P. Wessels, Membrane fouling and process performance of forward osmosis membranes on activated sludge, J Membrane Sci, 319 (2008) 158-168.

[22] A. Achilli, T.Y. Cath, E.A. Marchand, A.E. Childress, The forward osmosis membrane bioreactor: A low fouling alternative to MBR processes, Desalination, 239 (2009) 10-21.

[23] W.C.L. Lay, Q. Zhang, J. Zhang, D. McDougald, C. Tang, R. Wang, Y. Liu, A.G. Fane, Study of integration of forward osmosis and biological process: Membrane performance under elevated salt environment, Desalination, 283 (2011) 123-130.

[24] Y.L. Liu, B.X. Mi, Combined fouling of forward osmosis membranes: Synergistic foulant interaction and direct observation of fouling layer formation, J Membrane Sci, 407 (2012) 136-144.

[25] G. Sezonov, D. Joseleau-Petit, R. D'Ari, Escherichia coli physiology in Luria-Bertani broth, J Bacteriol, 189 (2007) 8746-8749.

[26] M. Herzberg, M. Elimelech, Biofouling of reverse osmosis membranes: Role of biofilm-enhanced osmotic pressure, J Membrane Sci, 295 (2007) 11-20.

[27] M. Herzberg, S. Kang, M. Elimelech, Role of extracellular polymeric substances (EPS) in biofouling of reverse osmosis membranes, Environ Sci Technol, 43 (2009) 4393-4398.

[28] A. Ramesh, D.J. Lee, J.Y. Lai, Membrane biofouling by extracellular polymeric substances or soluble microbial products from membrane bioreactor sludge, Appl Microbiol Biot, 74 (2007) 699-707.

[29] S. Lee, M. Elimelech, Relating organic fouling of reverse osmosis membranes to intermolecular adhesion forces, Environ Sci Technol, 40 (2006) 980-987.

[30] Q.L. Li, M. Elimelech, Organic fouling and chemical cleaning of nanofiltration membranes: Measurements and mechanisms, Environ Sci Technol, 38 (2004) 4683-4693.

[31] B.X. Mi, M. Elimelech, Organic fouling of forward osmosis membranes: Fouling reversibility and cleaning without chemical reagents, J Membrane Sci, 348 (2010) 337-345.

[32] B. Mi, M. Elimelech, Chemical and physical aspects of organic fouling of forward osmosis membranes, J Membrane Sci, 320 (2008) 292-302.

[33] Y. Liu, E. Rosenfield, M. Hu, B. Mi, Direct Observation of Bacterial Deposition on and Detachment from Nanocomposite Membranes Embedded with Silver Nanoparticles, Water Res.

[34] C.Y.Y. Tang, Y.N. Kwon, J.O. Leckie, Effect of membrane chemistry and coating layer on physiochemical properties of thin film composite polyamide RO and

NF membranes I. FTIR and XPS characterization of polyamide and coating layer chemistry, Desalination, 242 (2009) 149-167.

[35] V. Freger, J. Gilron, S. Belfer, TFC polyamide membranes modified by grafting of hydrophilic polymers: an FT-IR/AFM/TEM study, J Membrane Sci, 209 (2002) 283-292.

[36] P.S. Singh, A.P. Rao, P. Ray, A. Bhattacharya, K. Singh, N.K. Saha, A.V.R. Reddy, Techniques for characterization of polyamide thin film composite membranes, Desalination, 282 (2011) 78-86.

[37] Y.-N. Kwon, J.O. Leckie, Hypochlorite degradation of crosslinked polyamide membranes: II. Changes in hydrogen bonding behavior and performance, J Membrane Sci, 282 (2006) 456-464.

[38] O. Coronell, B.J. Marinas, X.J. Zhang, D.G. Cahill, Quantification of functional groups and modeling of their ionization behavior in the active layer of FT30 reverse osmosis membrane, Environ Sci Technol, 42 (2008) 5260-5266.

[39] O. Coronell, X.J. Zhang, M.I. Gonzalez, D.G. Cahill, B.J. Marinas, ENVR 119-Quantification of functional groups in FT30 (RO) membrane and modeling of their acid/base behavior, Abstr Pap Am Chem S, 235 (2008).

[40] A.E. Childress, M. Elimelech, Effect of solution chemistry on the surface charge of polymeric reverse osmosis and nanofiltration membranes, J Membrane Sci, 119 (1996) 253-268.

[41] S.R. Holmes-Farley, R.H. Reamey, T.J. McCarthy, J. Deutch, G.M. Whitesides, Acid-base behavior of carboxylic acid groups covalently attached at the surface of polyethylene: The usefulness of contact angle in following the ionization of surface functionality, Langmuir, 1 (1985) 725-740.

[42] O. Coronell, B.J. Mariñas, X. Zhang, D.G. Cahill, Quantification of Functional Groups and Modeling of Their Ionization Behavior in the Active Layer of FT30 Reverse Osmosis Membrane, Environ Sci Technol, 42 (2008) 5260-5266.

[43] M. Elimelech, W.H. Chen, J.J. Waypa, Measuring the Zeta (Electrokinetic) Potential of Reverse-Osmosis Membranes by a Streaming Potential Analyzer, Desalination, 95 (1994) 269-286.

[44] A. Tiraferri, M. Elimelech, Direct quantification of negatively charged functional groups on membrane surfaces, J Membrane Sci, 389 (2012) 499-508.

[45] C. Gomez-Suarez, J. Pasma, A.J. van der Borden, J. Wingender, H.C. Flemming, H.J. Busscher, H.C. van der Mei, Influence of extracellular polymeric substances on deposition and redeposition of Pseudomonas aeruginosa to surfaces, Microbiol-Sgm, 148 (2002) 1161-1169.

[46] J. Tourney, B.T. Ngwenya, The effect of ionic strength on the electrophoretic mobility and protonation constants of an EPS-producing bacterial strain, J Colloid Interf Sci, 348 (2010) 348-354.

[47] H. Schott, C.Y. Young, Electrokinetic Studies of Bacteria .1. Effect of Nature, Ionic-Strength, and Ph of Buffer Solutions on Electrophoretic Mobility of Streptococcus-Faecalis and Escherichia-Coli, J Pharm Sci, 61 (1972) 182-&.

[48] J. Li, L.A. McLandsborough, The effects of the surface charge and hydrophobicity of Escherichia coli on its adhesion to beef muscle, Int J Food Microbiol, 53 (1999) 185-193.

[49] H. Takruri, B. Ecanow, Interactions of surfactants with lipoproteins, Journal of Pharmaceutical Sciences, 55 (1966) 979-981.

[50] G.V. Sherbet, M.S. Lakshmi, Characterization of Escherichia-Coli Cell-Surface by Isoelectric Equilibrium Analysis, Biochim Biophys Acta, 298 (1973) 50-58.

[51] M. Elimelech, W.H. Chen, J.J. Waypa, Measuring the zeta (electrokinetic) potential of reverse osmosis membranes by a streaming potential analyzer, Desalination, 95 (1994) 269-286.

[52] I.S. Kim, N. Jang, The effect of calcium on the membrane biofouling in the membrane bioreactor (MBR), Water Res, 40 (2006) 2756-2764.

[53] B.X. Mi, M. Elimelech, Gypsum Scaling and Cleaning in Forward Osmosis: Measurements and Mechanisms, Environ Sci Technol, 44 (2010) 2022-2028.

[54] X.Y. Yuan, liu. Yongseng, Leng. Baoxia, Mi, Molecular Dynamics Simulations of Hydrated Polyamide Membrane and Its Interactions with Alginate Langmuir, Under review (2013).

[55] G. Völgyi, E. Baka, K.J. Box, J.E.A. Comer, K. Takács-Novák, Study of pH-dependent solubility of organic bases. Revisit of Henderson-Hasselbalch relationship, Analytica Chimica Acta, 673 (2010) 40-46.

[1] T.Y. Cath, A.E. Childress, M. Elimelech, Forward osmosis: Principles, applications, and recent developments, J Membrane Sci, 281 (2006) 70-87.

[2] J.R. McCutcheon, R.L. McGinnis, M. Elimelech, Desalination by ammonia-carbon dioxide forward osmosis: Influence of draw and feed solution concentrations on process performance, J Membrane Sci, 278 (2006) 114-123.

[3] J.J. Qin, W.C.L. Lay, K.A. Kekre, Recent developments and future challenges of forward osmosis for desalination: a review, Desalin Water Treat, 39 (2012) 123-136.

[4] S.F. Zhao, L.D. Zou, D. Mulcahy, Brackish water desalination by a hybrid forward osmosis-nanofiltration system using divalent draw solute, Desalination, 284 (2012) 175-181.

[5] V. Yangali-Quintanilla, Z.Y. Li, R. Valladares, Q.Y. Li, G. Amy, Indirect desalination of Red Sea water with forward osmosis and low pressure reverse osmosis for water reuse, Desalination, 280 (2011) 160-166.

[6] S.C. Low, Preliminary studies of seawater desalination using forward osmosis, Desalin Water Treat, 7 (2009) 41-46.

[7] C.R. Martinetti, A.E. Childress, T.Y. Cath, High recovery of concentrated RO brines using forward osmosis and membrane distillation, J Membrane Sci, 331 (2009) 31-39.

[8] P.K. Park, S. Lee, J.S. Cho, J.H. Kim, Full-scale simulation of seawater reverse osmosis desalination processes for boron removal: Effect of membrane fouling, Water Res, 46 (2012) 3796-3804.

[9] M. Moonkhum, Y.G. Lee, Y.S. Lee, J.H. Kim, Review of seawater natural organic matter fouling and reverse osmosis transport modeling for seawater reverse osmosis desalination, Desalin Water Treat, 15 (2010) 92-107.

[10] B.X. Mi, M. Elimelech, Organic fouling of forward osmosis membranes: Fouling reversibility and cleaning without chemical reagents, J Membrane Sci, 348 (2010) 337-345.

[11] S. Lee, C. Boo, M. Elimelech, S. Hong, Comparison of fouling behavior in forward osmosis (FO) and reverse osmosis (RO), J Membrane Sci, 365 (2010) 34-39.

[12] W.C.L. Lay, T.H. Chong, C.Y.Y. Tang, A.G. Fane, J.S. Zhang, Y. Liu, Fouling propensity of forward osmosis: investigation of the slower flux decline phenomenon, Water Sci Technol, 61 (2010) 927-936.

[13] A.E. Contreras, Z. Steiner, J. Miao, R. Kasher, Q.L. Li, Studying the Role of Common Membrane Surface Functionalities on Adsorption and Cleaning of Organic Foulants Using QCM-D (vol 45, pg 6309, 2011), Environ Sci Technol, 46 (2012) 5261-5261.

[14] S.X. Liu, J.T. Kim, Study of adsorption kinetics of surfactants onto polyethersulfone membrane surface using QCM-D, Desalination, 247 (2009) 355-361.

[15] Y.L. Liu, B.X. Mi, Combined fouling of forward osmosis membranes: Synergistic foulant interaction and direct observation of fouling layer formation, J Membrane Sci, 407 (2012) 136-144.

[16] A. Widjaya, T. Hoang, G.W. Stevens, S.E. Kentish, A comparison of commercial reverse osmosis membrane characteristics and performance under alginate fouling conditions, Sep Purif Technol, 89 (2012) 270-281.

[17] T. Hoang, G.W. Stevens, S.E. Kentish, The influence of feed pH on the performance of a reverse osmosis membrane during alginate fouling, Desalin Water Treat, 50 (2012) 220-225.

[18] S. Lee, W.S. Ang, M. Elimelech, Fouling of reverse osmosis membranes by hydrophilic organic matter: implications for water reuse, Desalination, 187 (2006) 313-321.

[19] S. Lee, M. Elimelech, Relating organic fouling of reverse osmosis membranes to intermolecular adhesion forces, Environ Sci Technol, 40 (2006) 980-987.

[1] Water in a changing world, in: The united nations world water development report, (WWDR3). , World Water Forum, 2009.

[2] H. Ashraf, Experts gather to discuss water crisis that the world is ignoring, LANCET, 361 (2003) 935-935.

[3] S. Kanae, Global Warming and the Water Crisis, J HEALTH SCI, 55 (2009) 860-864.

[4] C. Charcosset, A review of membrane processes and renewable energies for desalination, Desalination, 245 (2009) 214-231.

[5] L.R.E. James E. Miller, Forward osmosis: a new approach to water purification and desalination, in, Sandia National Laboratories, Albuquerque, New Mexico 87185 and Livermore, California 94550, 2006.

[6] Dynamic growth in water reuse and desalination, in: World Water Reuse and Desalination WEF Publishing UK Ltd, WEF Head Office, 2010.

[7] D. Li, X.Y. Zhang, G.P. Simon, H.T. Wang, Forward osmosis desalination using polymer hydrogels as a draw agent: Influence of draw agent, feed solution and membrane on process performance, Water Res, 47 (2013) 209-215.

[8] J. Schrier, Ethanol concentration by forward osmosis with solar-regenerated draw solution, Sol Energy, 86 (2012) 1351-1358.

[9] J.R. McCutcheon, R.L. McGinnis, M. Elimelech, Desalination by ammonia-carbon dioxide forward osmosis: Influence of draw and feed solution concentrations on process performance, J Membrane Sci, 278 (2006) 114-123.

[10] S.C. Low, Preliminary studies of seawater desalination using forward osmosis, Desalin Water Treat, 7 (2009) 41-46.

[11] M. Elimelech, J.R. McCutcheon, R.L. McGinnis, A novel ammonia-carbon dioxide forward (direct) osmosis desalination process, Desalination, 174 (2005) 1-11.

[12] T.Y. Cath, A.E. Childress, M. Elimelech, Forward osmosis: Principles, applications, and recent developments, J Membrane Sci, 281 (2006) 70-87.

[13] E.G. Beaudry, K.A. Lampi, Membrane Technology for Direct-Osmosis Concentration of Fruit Juices, Food Technol-Chicago, 44 (1990) 121-121.

[14] R.V. Linares, V. Yangali-Quintanilla, Z.Y. Li, G. Amy, NOM and TEP fouling of a forward osmosis (FO) membrane: Foulant identification and cleaning, J Membrane Sci, 421 (2012) 217-224.

[15] E. Arkhangelsky, F. Wicaksana, C.Y. Tang, A.A. Al-Rabiah, S.M. Al-Zahrani, R. Wang, Combined organic-inorganic fouling of forward osmosis hollow fiber membranes, Water Res, 46 (2012) 6329-6338.

[16] Y.L. Liu, B.X. Mi, Combined fouling of forward osmosis membranes: Synergistic foulant interaction and direct observation of fouling layer formation, J Membrane Sci, 407 (2012) 136-144.

[17] S.R. Qi, C.Q. Qiu, Y. Zhao, C.Y.Y. Tang, Double-skinned forward osmosis membranes based on layer-by-layer assembly-FO performance and fouling behavior, J Membrane Sci, 405 (2012) 20-29.

[18] C. Boo, S. Lee, M. Elimelech, Z.Y. Meng, S. Hong, Colloidal fouling in forward osmosis: Role of reverse salt diffusion, J Membrane Sci, 390 (2012) 277-284.

[19] Z.Y. Li, V. Yangali-Quintanilla, R. Valladares-Linares, Q.Y. Li, T. Zhan, G. Amy, Flux patterns and membrane fouling propensity during desalination of seawater by forward osmosis, Water Res, 46 (2012) 195-204.

[20] S. Zou, Y.S. Gu, D.Z. Xiao, C.Y.Y. Tang, The role of physical and chemical parameters on forward osmosis membrane fouling during algae separation, J Membrane Sci, 366 (2011) 356-362.

[21] S. Lee, C. Boo, M. Elimelech, S. Hong, Comparison of fouling behavior in forward osmosis (FO) and reverse osmosis (RO), J Membrane Sci, 365 (2010) 34-39.

[22] Y.N. Wang, F. Wicaksana, C.Y. Tang, A.G. Fane, Direct Microscopic Observation of Forward Osmosis Membrane Fouling, Environ Sci Technol, 44 (2010) 7102-7109.

[23] C.Y.Y. Tang, Q.H. She, W.C.L. Lay, R. Wang, A.G. Fane, Coupled effects of internal concentration polarization and fouling on flux behavior of forward osmosis membranes during humic acid filtration, J Membrane Sci, 354 (2010) 123-133.

[24] B.X. Mi, M. Elimelech, Organic fouling of forward osmosis membranes: Fouling reversibility and cleaning without chemical reagents, J Membrane Sci, 348 (2010) 337-345.

[25] W.C.L. Lay, T.H. Chong, C.Y.Y. Tang, A.G. Fane, J.S. Zhang, Y. Liu, Fouling propensity of forward osmosis: investigation of the slower flux decline phenomenon, Water Sci Technol, 61 (2010) 927-936.

[26] A. Achilli, T.Y. Cath, E.A. Marchand, A.E. Childress, The forward osmosis membrane bioreactor: A low fouling alternative to MBR processes, Desalination, 239 (2009) 10-21.

[27] B. Mi, M. Elimelech, Chemical and physical aspects of organic fouling of forward osmosis membranes, J Membrane Sci, 320 (2008) 292-302.

[28] E.R. Cornelissen, D. Harmsen, K.F. de Korte, C.J. Ruiken, J.J. Qin, H. Oo, L.P. Wessels, Membrane fouling and process performance of forward osmosis membranes on activated sludge, J Membrane Sci, 319 (2008) 158-168.

[29] E.J. McAdam, S.J. Judd, A review of membrane bioreactor potential for nitrate removal from drinking water, Desalination, 196 (2006) 135-148.

[30] B. Van der Bruggen, C. Vandecasteele, T. Van Gestel, W. Doyen, R. Leysen, A review of pressure-driven membrane processes in wastewater treatment and drinking water production, Environ Prog, 22 (2003) 46-56.

[31] G.R. Botha, R.D. Sanderson, C.A. Buckley, Brief Historical Review of Membrane-Development and Membrane Applications in Waste-Water Treatment in Southern Africa, Water Sci Technol, 25 (1992) 1-4.

[32] D.W. Green, R.H. Perry, Perry's Chemical Engineers' Handbook (8th Edition), in, McGraw-Hill, 2008.

[33] C.D. Moody, Forward osmosis extractors: theory, feasibility and design optimization, University of Arizona., 1977.

[34] L. Malaeb, G.M. Ayoub, Reverse osmosis technology for water treatment: State of the art review, Desalination, 267 (2011) 1-8.

[35] M.A. Alghoul, P. Poovanaesvaran, K. Sopian, M.Y. Sulaiman, Review of brackish water reverse osmosis (BWRO) system designs, Renew Sust Energ Rev, 13 (2009) 2661-2667.

[36] H.I. Shaban, Reverse-Osmosis Membranes for Seawater Desalination State-of-the-Art, Separ Purif Method, 19 (1990) 121-131.

[37] L.F. Comb, Going Forward with Reverse-Osmosis, Chem Eng-New York, 101 (1994) 90-92.

[38] C. Fritzmann, J. Lowenberg, T. Wintgens, T. Melin, State-of-the-art of reverse osmosis desalination, Desalination, 216 (2007) 1-76.

[39] M.H. Li, Reducing specific energy consumption in Reverse Osmosis (RO) water desalination: An analysis from first principles, Desalination, 276 (2011) 128-135.

[40] Y.C. Kim, S.J. Park, I.S. Park, Change of energy consumption through the adjustment of feed flow rate in RO membrane process, Desalin Water Treat, 9 (2009) 131-135.

[41] S.A. Avlonitis, K. Kouroumbas, N. Vlachakis, Energy consumption and membrane replacement cost for seawater RO desalination plants, Desalination, 157 (2003) 151-158.

[42] T. Manth, M. Gabor, E. Oklejas, Minimizing RO energy consumption under variable conditions of operation, Desalination, 157 (2003) 9-21.

[43] M.A. Darwish, Critical Comparison between Energy-Consumption in Large Capacity Reverse-Osmosis (Ro) and Multistage Flash (Msf) Seawater Desalting Plants, Desalination, 63 (1987) 143-161.

[44] T. Valencia Rodriguez, A.M. Rojas, C.A. Campos, L.N. Gerschenson, Effect of osmotic dehydration on the quality of air-dried Porphyra, Lebensmittel-Wissenschaft + [i.e. und] Technologie. Food science + technology. Science + technologie alimentaire, 36 (2003) 415-422.

[45] T. Cath, Osmotically and thermally driven membrane processes for enhancement of water recovery in desalination processes, Desalin Water Treat, 15 (2010) 279-286.

[46] T. Cath, A. Childress, M. Elimelech, Forward osmosis: Principles, applications, and recent developments, J MEMBRANE SCI, 281 (2006) 70-87.

[47] A. Achilli, T. Cath, E. Marchand, A. Childress, The forward osmosis membrane bioreactor: A low fouling alternative to MBR processes, DESALINATION, 239 (2009) 10-21.

[48] C.D. Moody, J.O. Kessler, Forward Osmosis Extractors, Desalination, 18 (1976) 283-295.

[49] I. Goosens, A. Vanhaute, Use of Direct Osmosis Tests as Complementary Experiments to Determine the Water and Salt Permeabilities of Reinforced Cellulose-Acetate Membranes, Desalination, 26 (1978) 299-308.

[50] T.V. Knyazkova, A.A. Kavitskaya, L.A. Kulsky, Formation of the Dynamic Membranes in the Process of Direct Osmosis, Dopovidi Akademii Nauk Ukrainskoi Rsr Seriya B-Geologichni Khimichni Ta Biologichni Nauki, (1979) 33-35.

[51] R.E. Kravath, J.A. Davis, Desalination of Sea-Water by Direct Osmosis, Desalination, 16 (1975) 151-155.

[52] J.O. Kessler, C.D. Moody, Drinking-Water from Sea-Water by Forward Osmosis, Desalination, 18 (1976) 297-306.

[53] C.R. Lerici, M. Dallarosa, G. Pinnavaia, Direct Osmosis as a Parameter for the Drying of Fruit, Industrie Alimentari, 22 (1983) 500-500.

[54] C. Severini, S. Pizzirani, M. Anese, C.R. Lerici, Use of Ethanol-Added Syrups in Food Vegetable Concentration by Direct Osmosis, Industrie Alimentari, 32 (1993) 1220-1222.

[55] B.R. Babu, N.K. Rastogi, K. Raghavarao, Effect of process parameters on transmembrane flux during direct osmosis, J MEMBRANE SCI, 280 (2006) 185-194.

[56] E.M. Garcia-Castello, J.R. McCutcheon, M. Elimelech, Performance evaluation of sucrose concentration using forward osmosis, J MEMBRANE SCI, 338 (2009) 61-66.

[57] Q. Yang, K.Y. Wang, T.S. Chung, A novel dual-layer forward osmosis membrane for protein enrichment and concentration, Sep Purif Technol, 69 (2009) 269-274.

[58] J.R. McCutcheon, R.L. McGinnis, M. Elimelech, A novel ammonia—carbon dioxide forward (direct) osmosis desalination process, Desalination, 174 (2005) 1-11.

[59] R.A. Khaydarov, R.R. Khaydarov, Solar powered direct osmosis desalination, Desalination, 217 (2007) 225-232.

[60] O.A. Bamaga, A. Yokochi, E.G. Beaudry, Application of forward osmosis in pretreatment of seawater for small reverse osmosis desalination units, Desalin Water Treat, 5 (2009) 183-191.

[61] Y.J. Choi, J.S. Choi, H.J. Oh, S. Lee, D.R. Yang, J.H. Kim, Toward a combined system of forward osmosis and reverse osmosis for seawater desalination, Desalination, 247 (2009) 239-246.

[62] J.S. Choi, H. Kim, S. Lee, T.M. Hwang, H. Oh, D.R. Yang, J.H. Kim, Theoretical investigation of hybrid desalination system combining reverse osmosis and forward osmosis, Desalin Water Treat, 15 (2010) 114-120.

[63] T.Y. Cath, D. Adams, A.E. Childress, Membrane contactor processes for wastewater reclamation in space II. Combined direct osmosis, osmotic distillation, and membrane distillation for treatment of metabolic wastewater, J MEMBRANE SCI, 257 (2005) 111-119.

[64] T.Y. Cath, S. Gormly, E.G. Beaudry, M.T. Flynn, V.D. Adams, A.E. Childress, Membrane contactor processes for wastewater reclamation in space Part I. Direct osmotic concentration as pretreatment for reverse osmosis, J MEMBRANE SCI, 257 (2005) 85-98.

[65] R.W. Holloway, A.E. Childress, K.E. Dennett, T.Y. Cath, Forward osmosis for concentration of anaerobic digester centrate, Water Res, 41 (2007) 4005-4014.

[66] S. Loeb, Mccutcha.Jw, Electrolytic Additives in Casting Solutions for Cellulose Acetate Desalination Membranes, Ind Eng Chem Prod Rd, 4 (1965) 114-&.

[67] J.R. McCutcheon, M. Elimelech, Influence of concentrative and dilutive internal concentration polarization on flux behavior in forward osmosis, J Membrane Sci, 284 (2006) 237-247.

[68] J.R. McCutcheon, M. Elimelech, Influence of membrane support layer hydrophobicity on water flux in osmotically driven membrane processes, J MEMBRANE SCI, 318 (2008) 458-466.

[69] R.J. Salter, Forward osmosis, Water Conditioning & Purification, 48 (2006) 36-38.

[70] S.R. Chou, L. Shi, R. Wang, C.Y.Y. Tang, C.Q. Qiu, A.G. Fane, Characteristics and potential applications of a novel forward osmosis hollow fiber membrane, Desalination, 261 (2010) 365-372.

[71] N.Y. Yip, A. Tiraferri, W.A. Phillip, J.D. Schiffman, M. Elimelech, High Performance Thin-Film Composite Forward Osmosis Membrane, Environ Sci Technol, 44 (2010) 3812-3818.

[72] A. Tiraferri, N.Y. Yip, W.A. Phillip, J.D. Schiffman, M. Elimelech, Relating performance of thin-film composite forward osmosis membranes to support layer formation and structure, J Membrane Sci, 367 (2011) 340-352.

[73] N.Y. Yip, A. Tiraferri, W.A. Phillip, J.D. Schiffrnan, L.A. Hoover, Y.C. Kim, M. Elimelech, Thin-Film Composite Pressure Retarded Osmosis Membranes for Sustainable Power Generation from Salinity Gradients, Environ Sci Technol, 45 (2011) 4360-4369.

[74] J. Wei, C.Q. Qiu, C.Y.Y. Tang, R. Wang, A.G. Fane, Synthesis and characterization of flat-sheet thin film composite forward osmosis membranes, J MEMBRANE SCI, 372 (2011) 292-302.

[75] N. Widjojo, T.S. Chung, M. Weber, C. Maletzko, V. Warzelhan, The role of sulphonated polymer and macrovoid-free structure in the support layer for thin-film composite (TFC) forward osmosis (FO) membranes, J MEMBRANE SCI, 383 (2011) 214-223.

[76] A. Sweity, W. Ying, S. Belfer, G. Oron, M. Herzberg, pH effects on the adherence and fouling propensity of extracellular polymeric substances in a membrane bioreactor, J Membrane Sci, 378 (2011) 186-193.

[77] X.X. Song, Z.Y. Liu, D. Sun, Nano Gives the Answer: Breaking the Bottleneck of Internal Concentration Polarization with a Nanofiber Composite Forward Osmosis Membrane for a High Water Production Rate, Adv Mater, 23 (2011) 3256-+.

[78] S. Zhang, K.Y. Wang, T.S. Chung, Y.C. Jean, H.M. Chen, Molecular design of the cellulose ester-based forward osmosis membranes for desalination, Chem Eng Sci, 66 (2011) 2008-2018.

[79] Y. Yu, S. Seo, I.C. Kim, S. Lee, Nanoporous polyethersulfone (PES) membrane with enhanced flux applied in forward osmosis process, J MEMBRANE SCI, 375 (2011) 63-68.

[80] M. Hajipour, M. Soltanieh, M. Yazdanshenas, Investigation of membrane fouling in cross flow microfiltration of non-alcoholic beer and modeling of tubular membrane flow, Desalination, 251 (2010) 20-28.

[81] S. Phuntsho, H.K. Shon, S. Hong, S. Lee, S. Vigneswaran, A novel low energy fertilizer driven forward osmosis desalination for direct fertigation: Evaluating the performance of fertilizer draw solutions, J Membrane Sci, 375 (2011) 172-181.

[82] J.R. McCutcheon, R.L. McGinnis, M. Elimelech, A novel ammonia-carbon dioxide forward (direct) osmosis desalination process, Desalination, 174 (2005) 1-11.

[83] R.L. McGinnis, M. Elimelech, Energy requirements of ammonia-carbon dioxide forward osmosis desalination, Desalination, 207 (2007) 370-382.

[84] L.L. J.O. Samer adham, Manish Kumar, Dewatering reverse osmosis concentrate from water reuse applications using forward osmosis, WaterReuse foundation, (2009).

[85] P.L. Hansen, J.A. Cohen, R. Podgornik, V.A. Parsegian, Osmotic properties of poly(ethylene glycols): Quantitative features of brush and bulk scaling laws, Biophys J, 84 (2003) 350-355.

[86] M.M. Ling, T.S. Chung, Novel dual-stage FO system for sustainable protein enrichment using nanoparticles as intermediate draw solutes, J MEMBRANE SCI, 372 (2011) 201-209.

[87] M.M. Ling, K.Y. Wang, T.S. Chung, Highly Water-Soluble Magnetic Nanoparticles as Novel Draw Solutes in Forward Osmosis for Water Reuse, Ind Eng Chem Res, 49 (2010) 5869-5876.

[88] T.A. Zangle, A. Mani, J.G. Santiago, Theory and experiments of concentration polarization and ion focusing at microchannel and nanochannel interfaces, Chem Soc Rev, 39 (2010) 1014-1035.

[89] M. Elimelech, S. Bhattacharjee, A novel approach for modeling concentration polarization in crossflow membrane filtration based on the equivalence of osmotic pressure model and filtration theory, J MEMBRANE SCI, 145 (1998) 223-241.

[90] L.F. Song, M. Elimelech, Theory of Concentration Polarization in Cross-Flow Filtration, J Chem Soc Faraday T, 91 (1995) 3389-3398.

[91] G.A. Denisov, Theory of Concentration Polarization in Cross-Flow Ultrafiltration - Gel-Layer Model and Osmotic-Pressure Model, J MEMBRANE SCI, 91 (1994) 173-187.

[92] J.R. McCutcheon, M. Elimelech, Modeling water flux in forward osmosis: Implications for improved membrane design, Aiche Journal, 53 (2007) 1736-1744.

[93] S.A.F. Zhao, L.D. Zou, Relating solution physicochemical properties to internal concentration polarization in forward osmosis, J MEMBRANE SCI, 379 (2011) 459-467.

[94] G.T. Gray, J.R. McCutcheon, M. Elimelech, Internal concentration polarization in forward osmosis: role of membrane orientation, Desalination, 197 (2006) 1-8.

[95] S. Loeb, L. Titelman, E. Korngold, J. Freiman, Effect of porous support fabric on osmosis through a Loeb-Sourirajan type asymmetric membrane, J Membrane Sci, 129 (1997) 243-249.

[96] G. Li, X.M. Li, Y. Liu, D. Wang, T. He, C.J. Gao, Forward Osmosis and Concentration Polarization, Prog Chem, 22 (2010) 812-821.

[97] G.D. Mehta, S. Loeb, Performance of Permasep B-9 and B-10 Membranes in Various Osmotic Regions and at High Osmotic Pressures, J MEMBRANE SCI, 4 (1979) 335-349.

[98] E.M.V. Hoek, M. Elimelech, Cake-enhanced concentration polarization: A new fouling mechanism for salt-rejecting membranes, Environmental Science & Technology, 37 (2003) 5581-5588.

[99] T.H. Chong, F.S. Wong, A.G. Fane, Implications of critical flux and cake enhanced osmotic pressure (CEOP) on colloidal fouling in reverse osmosis: Experimental observations, J MEMBRANE SCI, 314 (2008) 101-111.

[100] T.H. Chong, A.G. Fane, Implications of critical flux and cake enhanced osmotic pressure (CEOP) on colloidal fouling in reverse osmosis: Modeling approach, Desalination and Water Treatment, 8 (2009) 68-90.

[101] L.N. Sim, Y. Ye, V. Chen, A.G. Fane, Investigations of the coupled effect of cake-enhanced osmotic pressure and colloidal fouling in RO using crossflow sampler-modified fouling index ultrafiltration, Desalination, 273 (2011) 184-196.

[102] K. Nath, Membrane separation processes, Prentice-Hall of India, New Delhi, 2008.

[103] S.J. Judd, D.F. Ayala, V. Ferre, Membrane life estimation in full-scale immersed membrane bioreactors, J MEMBRANE SCI, 378 (2011) 95-100.

[104] S.H. Moon, P.V.X. Hung, S.H. Cho, J.J. Woo, Behaviors of commercialized seawater reverse osmosis membranes under harsh organic fouling conditions, Desalin Water Treat, 15 (2010) 48-53.

[105] S.S. Mitra, A.R. Thomas, G.T. Gang, Evaluation and characterization of seawater RO membrane fouling, Desalination, 247 (2009) 94-107.

[106] J.E. Kilduff, M. Taniguchi, G. Belfort, Modes of natural organic matter fouling during ultrafiltration, Environmental Science & Technology, 37 (2003) 1676-1683.

[107] V. Chen, E.K. Lee, A.G. Fane, Natural organic matter (NOM) fouling in low pressure membrane filtration - effect of membranes and operation modes, Desalination, 218 (2008) 257-270.

[108] J.H. Kim, M. Moonkhum, Y.G. Lee, Y.S. Lee, Review of seawater natural organic matter fouling and reverse osmosis transport modeling for seawater reverse osmosis desalination, Desalination and Water Treatment, 15 (2010) 92-107.

[109] S.K. Hong, M. Elimelech, Chemical and physical aspects of natural organic matter (NOM) fouling of nanofiltration membranes, Journal of Membrane Science, 132 (1997) 159-181.

[110] T.R. Holm, Metal Complexation by Natural Organic-Matter in Ground-Water, Abstr Pap Am Chem S, 196 (1988) 89-Geoc.

[111] C. Jucker, M.M. Clark, Adsorption of Aquatic Humic Substances on Hydrophobic Ultrafiltration Membranes, J MEMBRANE SCI, 97 (1994) 37-52.

[112] K. Preston, D. Lantagne, N. Kotlarz, K. Jellison, Turbidity and chlorine demand reduction using alum and moringa flocculation before household chlorination in developing countries, J Water Health, 8 (2010) 60-70.

[113] C.A.C. van de Lisdonk, J.A.M. van Paassen, J.C. Schippers, Monitoring scaling in nanofiltration and reverse osmosis membrane systems, Desalination, 132 (2000) 101-108.

[114] S.F.E. Boerlage, M.D. Kennedy, I. Bremere, G.J. Witkamp, J.P. Van der Hoek, J.C. Schippers, The scaling potential of barium sulphate in reverse osmosis systems, J MEMBRANE SCI, 197 (2002) 251-268.

[115] A. Al-Rammah, The application of acid free antiscalant to mitigate scaling in reverse osmosis membranes, Desalination, 132 (2000) 83-87.

[116] S. Seewoo, R. Van Hille, A. Lewis, Aspects of gypsum precipitation in scaling waters, Hydrometallurgy, 75 (2004) 135-146.

[117] P. Dydo, M. Turek, J. Ciba, K. Wandachowicz, J. Misztal, The nucleation kinetic aspects of gypsum nanofiltration membrane scaling, Desalination, 164 (2004) 41-52.

[118] Y.A. Le Gouellec, M. Elimelech, Calcium sulfate (gypsum) scaling in nanofiltration of agricultural drainage water, J MEMBRANE SCI, 205 (2002) 279-291.

[119] B.X. Mi, M. Elimelech, Gypsum Scaling and Cleaning in Forward Osmosis: Measurements and Mechanisms, Environ Sci Technol, 44 (2010) 2022-2028.

[120] H.C. Flemming, Biofouling in water systems - cases, causes and countermeasures, Appl Microbiol Biot, 59 (2002) 629-640.

[121] Y. Baek, J. Yu, S.H. Kim, S. Lee, J. Yoon, Effect of surface properties of reverse osmosis membranes on biofouling occurrence under filtration conditions, J Membrane Sci, 382 (2011) 91-99.

[122] J. Lee, I.S. Kim, Microbial community in seawater reverse osmosis and rapid diagnosis of membrane biofouling, DESALINATION, 273 (2011) 118-126.

[123] C.M. Pang, W.T. Liu, Community structure analysis of reverse osmosis membrane biofilms and the significance of Rhizobiales bacteria in biofouling, Environ Sci Technol, 41 (2007) 4728-4734.

[124] H.F. Ridgway, A. Kelly, C. Justice, B.H. Olson, MICROBIAL FOULING OF REVERSE-OSMOSIS MEMBRANES USED IN ADVANCED WASTEWATER-TREATMENT TECHNOLOGY - CHEMICAL, BACTERIOLOGICAL, AND ULTRASTRUCTURAL ANALYSES, Appl Environ Microb, 45 (1983) 1066-1084.

[125] M. Herzberg, M. Elimelech, Biofouling of reverse osmosis membrane: Mechanisms and performance, Abstr Pap Am Chem S, 232 (2006) 541-541.

[126] H. Brouwer, K. Meesters, J. van Groenestijn, Biofouling control in reverse osmosis membranes using rapid biofiltration technology, Desalination, 199 (2006) 15-17.

[127] H.C. Flemming, Reverse osmosis membrane biofouling, Exp Therm Fluid Sci, 14 (1997) 382-391.

[128] R.P. Carnahan, L. Bolin, W. Suratt, Biofouling of Pvd-1 Reverse-Osmosis Elements in the Water-Treatment Plant of the City of Dunedin, Florida, Desalination, 102 (1995) 235-244.

[129] M. Herzberg, Osmotic effects of biofouling in reverse osmosis (RO) processes: Physical and physiological measurements and mechanisms, Desalin Water Treat, 15 (2010) 287-291.

[130] M.M.T. Khan, P.S. Stewart, D.J. Moll, W.E. Mickols, M.D. Burr, S.E. Nelson, A.K. Camper, Assessing biofouling on polyamide reverse osmosis (RO) membrane surfaces in a laboratory system, J Membrane Sci, 349 (2010) 429-437.

[131] S. Kappachery, D. Paul, J. Yoon, J.H. Kweon, Vanillin, a potential agent to prevent biofouling of reverse osmosis membrane, Biofouling, 26 (2010) 667-672.

[132] C.K. Ho, S.J. Altman, H.D.T. Jones, S.S. Khalsa, L.K. McGrath, P.G. Clem, Analysis of micromixers to reduce biofouling on reverse-osmosis membranes, Environ Prog, 27 (2008) 195-203.

[133] M. Herzberg, D. Berry, A.M. Briones, L. Raskin, M. Elimelech, ENVR 65-Impact of microfiltration on biofouling of reverse osmosis membranes, Abstr Pap Am Chem S, 235 (2008).

[134] T.R.R. Pintelon, S.A. Creber, D.A.G. von der Schulenburg, M.L. Johns, Validation of 3D Simulations of Reverse Osmosis Membrane Biofouling, Biotechnol Bioeng, 106 (2010) 677-689.

[135] A.G. Fane, C.J.D. Fell, R.M. Mcdonogh, Colloidal Effects in Ultrafiltration and Reverse-Osmosis, Abstr Pap Am Chem S, 188 (1984) 128-INDE.

[136] M.T. Brunelle, Colloidal Fouling of Reverse-Osmosis Membranes, Desalination, 32 (1980) 127-135.

[137] C. Park, Y.H. Lee, S. Lee, S. Hong, Effect of cake layer structure on colloidal fouling in reverse osmosis membranes, Desalination, 220 (2008) 335-344.

[138] R.J. Hunter, Introduction to modern colloid science / Robert J. Hunter, Oxford University Press, Oxford, England ; New York ; Melbourne :, 1993.

[139] H.Y. Ng, M. Elimelech, Influence of colloidal fouling on rejection of trace organic contaminants by reverse osmosis, J MEMBRANE SCI, 244 (2004) 215-226.

[140] E.M.V. Hoek, A.S. Kim, M. Elimelech, Influence of crossflow membrane filter geometry and shear rate on colloidal fouling in reverse osmosis and nanofiltration separations, Environ Eng Sci, 19 (2002) 357-372.

[141] E.M. Vrijenhoek, S. Hong, M. Elimelech, Influence of membrane surface properties on initial rate of colloidal fouling of reverse osmosis and nanofiltration membranes, J Membrane Sci, 188 (2001) 115-128.

[142] E.M. Vrijenhoek, M. Elimelech, S.K. Hong, Influence of membrane properties, solution chemistry, and hydrodynamics on colloidal fouling of reverse osmosis and nanofiltration membranes., Abstr Pap Am Chem S, 220 (2000) U322-U322.

[143] X.H. Zhu, M. Elimelech, Colloidal fouling of reverse osmosis membranes: measurements and fouling mechanisms, Environ Sci Technol, 31 (1997) 3654-3662.

[144] M. Elimelech, X.H. Zhu, A.E. Childress, S.K. Hong, Role of membrane surface morphology in colloidal fouling of cellulose acetate and composite aromatic polyamide reverse osmosis membranes, J Membrane Sci, 127 (1997) 101-109.

[145] M. Herzberg, M. Elimelech, Biofouling of reverse osmosis membranes: Role of biofilm-enhanced osmotic pressure, J Membrane Sci, 295 (2007) 11-20.

[146] G.D. Kang, M. Liu, B. Lin, Y.M. Cao, Q. Yuan, A novel method of surface modification on thin-film composite reverse osmosis membrane by grafting poly(ethylene glycol), Polymer, 48 (2007) 1165-1170.

[147] X.Y. Wei, Z. Wang, J. Chen, J.X. Wang, S.C. Wang, A novel method of surface modification on thin-film-composite reverse osmosis membrane by grafting hydantoin derivative, J Membrane Sci, 346 (2010) 152-162.

[148] C. Grossmann, K.H. Johannsen, Methods for the Determination of the Portion of Allowable Colloid in Raw Solutions from Their Treatment in Reverse-Osmosis Plants, Chem Tech-Leipzig, 34 (1982) 544-544.

[149] S.Y. Wu, J. Xing, C. Zheng, G.F. Xu, G.D. Zheng, J.P. Xu, Plasma modification of aromatic polyamide reverse osmosis composite membrane surface, J Appl Polym Sci, 64 (1997) 1923-1926.

[150] W.H. Zhou, C.H. Lu, X.C. Guo, F.R. Chen, H.H. Yang, X.R. Wang, Mussel-inspired molecularly imprinted polymer coating superparamagnetic nanoparticles for protein recognition, J Mater Chem, 20 (2010) 880-883.

[151] C.E. Brubaker, W. Lo, H. Kissler, D.B. Kaufman, P.B. Messersmith, Characterization and biocompatibility of a mussel-inspired PEG-based adhesive, Abstr Pap Am Chem S, 238 (2009).

[152] S. Kasemset, A. Lee, D.J. Miller, B.D. Freeman, M.M. Sharma, Effect of polydopamine deposition conditions on fouling resistance, physical properties, and permeation properties of reverse osmosis membranes in oil/water separation, J Membrane Sci, 425 (2013) 208-216.

[153] J.T. Arena, B. McCloskey, B.D. Freeman, J.R. McCutcheon, Surface modification of thin film composite membrane support layers with polydopamine: Enabling use of reverse osmosis membranes in pressure retarded osmosis, J Membrane Sci, 375 (2011) 55-62.

[154] B.D. McCloskey, H.B. Park, H. Ju, B.W. Rowe, D.J. Miller, B.J. Chun, K. Kin, B.D. Freeman, Influence of polydopamine deposition conditions on pure water flux and foulant adhesion resistance of reverse osmosis, ultrafiltration, and microfiltration membranes, Polymer, 51 (2010) 3472-3485.

[155] K. Sun, L.S. Song, Y.Y. Xie, D.B. Liu, D. Wang, Z. Wang, W.S. Ma, J.S. Zhu, X.Y. Jiang, Using Self-Polymerized Dopamine to Modify the Antifouling Property of Oligo(ethylene glycol) Self-Assembled Monolayers and Its Application in Cell Patterning, Langmuir, 27 (2011) 5709-5712.

[156] M. Zheng, Y. Zhou, Y. Chen, Y.W. Tang, T.H. Lu, Electrochemical behavior of dopamine in the presence of phosphonate and the determination of dopamine at phosphonate modified zirconia films electrode with highly antifouling capability, Electrochim Acta, 55 (2010) 4789-4798.

[157] Z.D. Chen, T. Nagaoka, Selective determination of dopamine based on a self-assembled monolayer electrode with antifouling activity on protein adsorption, Bunseki Kagaku, 53 (2004) 1321-1324.

[158] T.A. Saleh, V.K. Gupta, Synthesis and characterization of alumina nano-particles polyamide membrane with enhanced flux rejection performance, Sep Purif Technol, 89 (2012) 245-251.

[159] M. Fathizadeh, A. Aroujalian, A. Raisi, Effect of added NaX nano-zeolite into polyamide as a top thin layer of membrane on water flux and salt rejection in a reverse osmosis process, J Membrane Sci, 375 (2011) 88-95.

[160] E.S. Kim, B.L. Deng, Fabrication of polyamide thin-film nano-composite (PA-TFN) membrane with hydrophilized ordered mesoporous carbon (H-OMC) for water purifications, J Membrane Sci, 375 (2011) 46-54.

[161] A. Tiraferri, C.D. Vecitis, M. Elimelech, Covalent Binding of Single-Walled Carbon Nanotubes to Polyamide Membranes for Antimicrobial Surface Properties, Acs Appl Mater Inter, 3 (2011) 2869-2877.

[162] C. Lee, S. Baik, Vertically-aligned carbon nano-tube membrane filters with superhydrophobicity and superoleophilicity, Carbon, 48 (2010) 2192-2197.

[163] S.S. Madaeni, T.A. Arbatan, Preparation and Characterization of Microfiltration Membrane Embedded with Silver Nano-Particles, Iran J Chem Chem Eng, 29 (2010) 105-111.

[164] J.H. Li, X.S. Shao, Q. Zhou, M.Z. Li, Q.Q. Zhang, The double effects of silver nanoparticles on the PVDF membrane: Surface hydrophilicity and antifouling performance, Appl Surf Sci, 265 (2013) 663-670.

[165] J. Zhan, Z. Liu, B.G. Wang, F.X. Ding, Modification of a membrane surface charge by a low temperature plasma induced grafting reaction and its application to reduce membrane fouling, Sep Sci Technol, 39 (2004) 2977-2995.

[166] A. Tiraferri, Y. Kang, E.P. Giannelis, M. Elimelech, Superhydrophilic Thin-Film Composite Forward Osmosis Membranes for Organic Fouling Control: Fouling Behavior and Antifouling Mechanisms, Environ Sci Technol, 46 (2012) 11135-11144.

[167] A. Tiraferri, Y. Kang, E.P. Giannelis, M. Elimelech, Highly Hydrophilic Thin-Film Composite Forward Osmosis Membranes Functionalized with Surface-Tailored Nanoparticles, Acs Appl Mater Inter, 4 (2012) 5044-5053.

[168] A. Tiraferri, Y. Wang, E.P. Giannelis, M. Elimelech, Binding silver and silica nanoparticles to polymeric membrane surface for novel antibiofouling properties, Abstr Pap Am Chem S, 242 (2011).

[169] M. Kazemimoghadam, Preparation of nanopore HS zeolite membranes for reverse osmosis processes, Desalin Water Treat, 30 (2011) 51-57.

[170] X.Y. Qu, H. Dong, Q. Ye, L. Zhang, Z.J. Zhou, H.L. Chen, Improvement of the zeolite-polyamide nanocomposite reverse osmosis membrane for desalination, Abstr Pap Am Chem S, 239 (2010).

[171] E.M. Flanigen, Review and New Perspectives in Zeolite Crystallization, Adv Chem Ser, (1973) 119-139.

[172] X.J. Yin, G.S. Zhu, Z.Y. Wang, N.L. Yue, S.L. Qiu, Zeolite P/NaX composite membrane for gas separation, Micropor Mesopor Mat, 105 (2007) 156-162.

[173] D. Sen, H. Kalipcilar, L. Yilmaz, Development of zeolite filled polycarbonate mixed matrix gas separation membranes, Desalination, 200 (2006) 222-224.

[174] Z. Huang, Y. Li, R. Wen, M.M. Teoh, S. Kulprathipanja, Enhanced gas separation properties by using nanostructured PES-zeolite 4A mixed matrix membranes, J Appl Polym Sci, 101 (2006) 3800-3805.

[175] L.G. Lin, Y.H. Zhang, H. Li, Pervaporation and sorption behavior of zeolite-filled polyethylene glycol hybrid membranes for the removal of thiophene species, J Colloid Interf Sci, 350 (2010) 355-360.

[176] M. Kazemimoghadam, T. Mohammadi, The pilot-scale pervaporation plant using tubular-type module with nano pore zeolite membrane, Desalination, 255 (2010) 196-199.

[177] W. Jia, S. Murad, Molecular dynamics simulations of gas separations using faujasite-type zeolite membranes, J Chem Phys, 120 (2004) 4877-4885.

[178] L.X. Li, J.H. Dong, T.M. Nenoff, R. Lee, Desalination by reverse osmosis using MFI zeolite membranes, J Membrane Sci, 243 (2004) 401-404.

[179] M.E. Lydon, K.A. Unocic, T.H. Bae, C.W. Jones, S. Nair, Structure-Property Relationships of Inorganically Surface-Modified Zeolite Molecular Sieves for Nanocomposite Membrane Fabrication, J Phys Chem C, 116 (2012) 9636-9645.

[180] C.P. Leo, N.H.A. Kamil, M.U.M. Junaidi, S.N.M. Kamal, A.L. Ahmad, The potential of SAPO-44 zeolite filler in fouling mitigation of polysulfone ultrafiltration membrane, Sep Purif Technol, 103 (2013) 84-91.

[181] A. Ivan, D.L. Ghindeanu, V. Danciulescu, A. Raducu, A.C. Nechifor, Composite polyaniline-zeolite membrane material for wastewater ultrafiltration, Optoelectron Adv Mat, 6 (2012) 1134-1138.

[182] F.Q. Mir, A. Shukla, Negative Rejection of NaCl in Ultrafiltration of Aqueous Solution of NaCl and KCl Using Socialite Octahydrate Zeolite-Clay Charged Ultrafiltration Membrane, Ind Eng Chem Res, 49 (2010) 6539-6546.

[183] S. Malamis, E. Katsou, M. Stylianou, K.J. Haralambous, M. Loizidou, Copper removal from sludge permeate with ultrafiltration membranes using zeolite, bentonite and vermiculite as adsorbents, Water Sci Technol, 61 (2010) 581-589.

[184] R.L. Han, S.H. Zhang, C. Liu, Y.T. Wang, X.G. Jian, Effect of NaA zeolite particle addition on poly(phthalazinone ether sulfone ketone) composite ultrafiltration (UF) membrane performance, J. Membr. Sci., 345 (2009) 5-12.

[185] N. Ma, J. Wei, R.H. Liao, C.Y.Y. Tang, Zeolite-polyamide thin film nanocomposite membranes: Towards enhanced performance for forward osmosis, J Membrane Sci, 405 (2012) 149-157.

[186] B.H. Jeong, E.M.V. Hoek, Y.S. Yan, A. Subramani, X.F. Huang, G. Hurwitz, A.K. Ghosh, A. Jawor, Interfacial polymerization of thin film nanocomposites: A new concept for reverse osmosis membranes, J. Membr. Sci., 294 (2007) 1-7.

[187] C. Bellona, M. Marts, J. Drewes, The effect of organic membrane fouling on the properties and rejection characteristics of nanofiltration membranes, SEP PURIF TECHNOL, 74 (2010) 44-54.

[188] S. Kang, A. Subramani, E. Hoek, M. Deshusses, M. Matsumoto, Direct observation of biofouling in cross-flow microfiltration: mechanisms of deposition and release, J MEMBRANE SCI, 244 (2004) 151-165.

[189] M. Herzberg, S. Kang, M. Elimelech, Role of extracellular polymeric substances (EPS) in biofouling of reverse osmosis membranes, Environ Sci Technol, 43 (2009) 4393-4398.

[190] X. Zhu, M. Elimelech, Colloidal fouling of reverse osmosis membranes: Measurements and fouling mechanisms, ENVIRON SCI TECHNOL, 31 (1997) 3654-3662.

[191] E. Vrijenhoek, S. Hong, M. Elimelech, Influence of membrane surface properties on initial rate of colloidal fouling of reverse osmosis and nanofiltration membranes, J MEMBRANE SCI, 188 (2001) 115-128.

[192] I. Escobar, E. Hoek, C. Gabelich, F. DiGiano, Y. Le Gouellec, P. Berube, K. Howe, J. Allen, K. Atasi, M. Benjamin, P. Brandhuber, J. Brant, Y. Chang, M. Chapman, A. Childress, W. Conlon, T. Cooke, I. Crossley, G. Crozes, P. Huck, S. Kommineni, J. Jacangelo, A. Karimi, J. Kim, D. Lawler, Q. Li, L. Schideman, S. Sethi, J. Tobiason, T. Tseng, S. Veerapanemi, A. Zander, A.M.T.R. Comm, Committee Report: Recent advances and research needs in membrane fouling, J AM WATER WORKS ASS, 97 (2005) 79-89.

[193] Q. Li, M. Elimelech, Revealing the mechanisms of organic fouling and chemical cleaning of nanofiltration membranes., ABSTR PAP AM CHEM S, 226 (2003) U506-U507.

[194] R. Holloway, A. Childress, K. Dennett, T. Cath, Forward osmosis for concentration of anaerobic digester centrate, WATER RES, 41 (2007) 4005-4014.

[195] B. Mi, M. Elimelech, Gypsum Scaling and Cleaning in Forward Osmosis: Measurements and Mechanisms, ENVIRON SCI TECHNOL, 44 (2010) 2022-2028.

[196] B. Mi, M. Elimelech, Organic fouling of forward osmosis membranes: Fouling reversibility and cleaning without chemical reagents, J MEMBRANE SCI, 348 (2010) 337-345.

[197] C. Tang, Q. She, W. Lay, R. Wang, A. Fane, Coupled effects of internal concentration polarization and fouling on flux behavior of forward osmosis membranes during humic acid filtration, J MEMBRANE SCI, 354 (2010) 123-133.

[198] S. Lee, J. Cho, M. Elimelech, Combined influence of natural organic matter (NOM) and colloidal particles on nanofiltration membrane fouling, J MEMBRANE SCI, 262 (2005) 27-41.

[199] Q. Li, M. Elimelech, Synergistic effects in combined fouling of a loose nanofiltration membrane by colloidal materials and natural organic matter, J MEMBRANE SCI, 278 (2006) 72-82.

[200] C. Law, X. Li, Q. Li, The Combined Colloid-Organic Fouling on Nanofiltration Membrane for Wastewater Treatment and Reuse, SEP SCI TECHNOL, 45 (2010) 935-940.

[201] C. Jarusutthirak, S. Mattaraj, R. Jiraratananon, Influence of inorganic scalants and natural organic matter on nanofiltration membrane fouling, J MEMBRANE SCI, 287 (2007) 138-145.

[202] S. Lee, M. Elimelech, Relating organic fouling of reverse osmosis membranes to intermolecular adhesion forces, ENVIRON SCI TECHNOL, 40 (2006) 980-987.

[203] Q. Li, M. Elimelech, Organic fouling and chemical cleaning of nanofiltration membranes: Measurements and mechanisms, ENVIRON SCI TECHNOL, 38 (2004) 4683-4693.

[204] S. Lee, M. Elimelech, Salt cleaning of organic-fouled reverse osmosis membranes, WATER RES, 41 (2007) 1134-1142.

[205] D. Hatziantoniou, J. Howell, Influence of the properties and characteristics of sugar-beet pulp extract on its fouling and rejection behaviour during membrane filtration, DESALINATION, 148 (2002) 67-72.

[206] G. Han, T.S. Chung, M. Toriida, S. Tamai, Thin-film composite forward osmosis membranes with novel hydrophilic supports for desalination, J Membrane Sci, 423 (2012) 543-555.

[207] D.L. Shaffer, N.Y. Yip, J. Gilron, M. Elimelech, Seawater desalination for agriculture by integrated forward and reverse osmosis: Improved product water quality for potentially less energy, J Membrane Sci, 415 (2012) 1-8.

[208] C.M. Werner, B.E. Logan, P.E. Saikaly, G.L. Amy, Wastewater treatment, energy recovery and desalination using a forward osmosis membrane in an air-cathode microbial osmotic fuel cell, J Membrane Sci, 428 (2013) 116-122.

[209] V. Sant'Anna, L.D.F. Marczak, I.C. Tessaro, Membrane concentration of liquid foods by forward osmosis: Process and quality view, J Food Eng, 111 (2012) 483-489.

[210] A.E. Childress, A. Achilli, T.Y. Cath, E.A. Marchand, The forward osmosis membrane bioreactor: A low fouling alternative to MBR processes, Desalination, 239 (2009) 10-21.

[211] Y. Liu, B. Mi, Combined fouling of forward osmosis membranes: Synergistic foulant interaction and direct observation of fouling layer formation, J MEMBRANE SCI, 407 (2012) 136-144.

[212] A. Rahardianto, B.C. Mccool, Y. Cohen, Reverse osmosis desalting of inland brackish water of high gypsum scaling propensity: Kinetics and mitigation of

membrane mineral scaling, Environmental Science & Technology, 42 (2008) 4292-4297.

[213] Y. Liu, E. Rosenfield, M. Hu, B. Mi, Direct observation of bacterial deposition on and detachment from nanocomposite membranes embedded with silver nanoparticles, Water Res, 47 (2013) 2949-2958.

[214] A.J. de Kerchove, M. Elimelech, Structural growth and viscoelastic properties of adsorbed alginate layers in monovalent and divalent salts, Macromolecules, 39 (2006) 6558-6564.

[215] G. Sauerbrey, Verwendung Von Schwingquarzen Zur Wagung Dunner Schichten Und Zur Mikrowagung, Z Phys, 155 (1959) 206-222.

[216] F. Höök, M. Rodahl, P. Brzezinski, B. Kasemo, Energy Dissipation Kinetics for Protein and Antibody−Antigen Adsorption under Shear Oscillation on a Quartz Crystal Microbalance, Langmuir, 14 (1998) 729-734.

[217] C. Kößlinger, S. Drost, F. Aberl, H. Wolf, S. Koch, P. Woias, A quartz crystal biosensor for measurement in liquids, Biosensors and Bioelectronics, 7 (1992) 397-404.

[218] A.E. Contreras, Z. Steiner, J. Miao, R. Kasher, Q. Li, Studying the Role of Common Membrane Surface Functionalities on Adsorption and Cleaning of Organic Foulants Using QCM-D, Environ Sci Technol, 45 (2011) 6309-6315.

[219] R.W. Field, D. Wu, J.A. Howell, B.B. Gupta, Critical flux concept for microfiltration fouling, J Membrane Sci, 100 (1995) 259-272.

[220] J.S. Vrouwenvelder, J.A.M. van Paassen, J.M.C. van Agtmaal, M.C.M. van Loosdrecht, J.C. Kruithof, A critical flux to avoid biofouling of spiral wound nanofiltration and reverse osmosis membranes: Fact or fiction?, J Membrane Sci, 326 (2009) 36-44.

[221] S. Zou, Y. Gu, D. Xiao, C.Y. Tang, The role of physical and chemical parameters on forward osmosis membrane fouling during algae separation, J Membrane Sci, 366 (2011) 356-362.

[222] S. Zou, Y.-N. Wang, F. Wicaksana, T. Aung, P.C.Y. Wong, A.G. Fane, C.Y. Tang, Direct microscopic observation of forward osmosis membrane fouling by microalgae: Critical flux and the role of operational conditions, J Membrane Sci, 436 (2013) 174-185.

[223] P. Sikorski, F. Mo, G. Skjak-Braek, B.T. Stokke, Evidence for egg-box-compatible interactions in calcium-alginate gels from fiber X-ray diffraction, Biomacromolecules, 8 (2007) 2098-2103.

[224] L. Li, Y. Fang, R. Vreeker, I. Appelqvist, E. Mendes, Reexamining the egg-box model in calcium-alginate gels with X-ray diffraction, Biomacromolecules, 8 (2007) 464-468.

[225] G.R.M. G. R. Aiken, R. L. Wershaw, P. MacCarthy, Humic substances in soil, sediment, and water : geochemistry, isolation, and characterization / edited by George R. Aiken ... [et al.], Wiley, New York :, 1985.

[226] F.J. Stevenson, Humus chemistry: genesis, composition, reactions, in, John Wiley and Sons, canada, 1994.

[227] P.J.M. Anđelković Tatjana, Purenović Milovan M., Anđelković Darko, Destabilization and aggregation of aqueous humic acids solution by metal ions, in: Physics, Chemistry and Technology, 2004, pp. 79-85.

[228] W.S. Ang, M. Elimelech, Protein (BSA) fouling of reverse osmosis membranes: Implications for wastewater reclamation, Journal of Membrane Science, 296 (2007) 83-92.

[229] M.L. Ferrer, R. Duchowicz, B. Carrasco, J.G. de la Torre, A.U. Acuna, The conformation of serum albumin in solution: A combined phosphorescence depolarization-hydrodynamic modeling study, Biophys J, 80 (2001) 2422-2430.

[230] T.H. Chong, F.S. Wong, A.G. Fane, The effect of imposed flux on biofouling in reverse osmosis: Role of concentration polarisation and biofilm enhanced osmotic pressure phenomena, J Membrane Sci, 325 (2008) 840-850.

[231] J.C. Su, S. Zhang, M.M. Ling, T.S. Chung, Forward osmosis: an emerging technology for sustainable supply of clean water, Clean Technol Envir, 14 (2012) 507-511.

[232] J.J. Qin, W.C.L. Lay, K.A. Kekre, Recent developments and future challenges of forward osmosis for desalination: a review, Desalin Water Treat, 39 (2012) 123-136.

[233] T.S. Chung, S. Zhang, K.Y. Wang, J.C. Su, M.M. Ling, Forward osmosis processes: Yesterday, today and tomorrow, Desalination, 287 (2012) 78-81.

[234] L.A. Hoover, W.A. Phillip, A. Tiraferri, N.Y. Yip, M. Elimelech, Forward with Osmosis: Emerging Applications for Greater Sustainability, Environ Sci Technol, 45 (2011) 9824-9830.

[235] S.F. Zhao, L.D. Zou, D. Mulcahy, Brackish water desalination by a hybrid forward osmosis-nanofiltration system using divalent draw solute, Desalination, 284 (2012) 175-181.

[236] K. Lutchmiah, E.R. Cornelissen, D.J.H. Harmsen, J.W. Post, K. Lampi, H. Ramaekers, L.C. Rietveld, K. Roest, Water recovery from sewage using forward osmosis, Water Sci Technol, 64 (2011) 1443-1449.

[237] F. Zhang, K.S. Brastad, Z. He, Integrating Forward Osmosis into Microbial Fuel Cells for Wastewater Treatment, Water Extraction and Bioelectricity Generation, Environ Sci Technol, 45 (2011) 6690-6696.

[238] C. Aydiner, S. Topcu, C. Tortop, F. Kuvvet, D. Ekinci, N. Dizge, B. Keskinler, A novel implementation of water recovery from whey: "forward-reverse osmosis" integrated membrane system, Desalin Water Treat, 51 (2013) 786-799.

[239] M.A. Saad, Early discovery of RO membrane fouling and real-time monitoring of plant performance for optimizing cost of water, Desalination, 165 (2004) 183-191.

[240] N.T. Hancock, P. Xu, D.M. Heil, C. Bellona, T.Y. Cath, Comprehensive Bench- and Pilot-Scale Investigation of Trace Organic Compounds Rejection by Forward Osmosis, Environ Sci Technol, 45 (2011) 8483-8490.

[241] E. Arkhangelsky, F. Wicaksana, S.R. Chou, A.A. Al-Rabiah, S.M. Al-Zahrani, R. Wang, Effects of scaling and cleaning on the performance of forward osmosis hollow fiber membranes, J Membrane Sci, 415 (2012) 101-108.

[242] J.S. Zhang, W.L.C. Loong, S.R. Chou, C.Y. Tang, R. Wang, A.G. Fane, Membrane biofouling and scaling in forward osmosis membrane bioreactor, J Membrane Sci, 403 (2012) 8-14.

[243] V.K.K. Upadhyayula, V. Gadhamshetty, Appreciating the role of carbon nanotube composites in preventing biofouling and promoting biofilms on material surfaces in environmental engineering: A review, Biotechnol Adv, 28 (2010) 802-816.

[244] B.Q. Liao, D.M. Bagley, H.E. Kraemer, G.G. Leppard, S.N. Liss, A review of biofouling and its control in membrane separation bioreactors, Water Environ Res, 76 (2004) 425-436.

[245] J.S. Baker, L.Y. Dudley, Biofouling in membrane systems - A review, Desalination, 118 (1998) 81-89.

[246] S.T. Kang, A. Subramani, E.M.V. Hoek, M.A. Deshusses, M.R. Matsumoto, Direct observation of biofouling in cross-flow microfiltration: mechanisms of deposition and release, J Membrane Sci, 244 (2004) 151-165.

[247] E.M.V. Hoek, Direct observation of biofouling in environmental membrane processes., Abstr Pap Am Chem S, 228 (2004) U614-U614.

[248] Y. Liu, E. Rosenfield, M. Hu, B. Mi, Direct Observation of Bacterial Deposition on and Detachment from Nanocomposite Membranes Embedded with Silver Nanoparticles, Water Res.

[249] S.K. Lower, C.J. Tadanier, M.F. Hochella, Measuring interfacial and adhesion forces between bacteria and mineral surfaces with biological force microscopy, Geochim Cosmochim Ac, 64 (2000) 3133-3139.

[250] A.E. Childress, M. Elimelech, Effects of humics and surfactants on the zeta potential of polymeric reverse osmosis and nanofiltration membranes., Abstr Pap Am Chem S, 212 (1996) 9-Envr.

[251] J. Ryu, S.H. Ku, H. Lee, C.B. Park, Mussel-Inspired Polydopamine Coating as a Universal Route to Hydroxyapatite Crystallization, Adv Funct Mater, 20 (2010) 2132-2139.

[252] H. Lee, S.M. Dellatore, W.M. Miller, P.B. Messersmith, Mussel-inspired surface chemistry for multifunctional coatings, Science, 318 (2007) 426-430.

[253] X.L. Li, L.P. Zhu, J.H. Jiang, Z.A. Yi, B.K. Zhu, Y.Y. Xu, Hydrophilic nanofiltration membranes with self-polymerized and strongly-adhered polydopamine as separating layer, Chinese J Polym Sci, 30 (2012) 152-163.

[254] Y.Y. Xu, X.L. Li, L.P. Zhu, Z.A. Yi, New type hydrophilic nanofiltration membranes based on polydopamine as separating layer, Abstr Pap Am Chem S, 242 (2011).

[255] P. Sukitpaneenit, T.S. Chung, High Performance Thin-Film Composite Forward Osmosis Hollow Fiber Membranes with Macrovoid-Free and Highly Porous Structure for Sustainable Water Production, Environ Sci Technol, 46 (2012) 7358-7365.

[256] R.P. Schneider, L.M. Ferreira, P. Binder, E.M. Bejarano, K.P. Goes, E. Slongo, C.R. Machado, G.M.Z. Rosa, Dynamics of organic carbon and of bacterial populations in a conventional pretreatment train of a reverse osmosis unit experiencing severe biofouling, J Membrane Sci, 266 (2005) 18-29.

[257] J.L. Rand, R. Hofmann, M.Z.B. Alam, C. Chauret, R. Cantwell, R.C. Andrews, G.A. Gagnon, A field study evaluation for mitigating biofouling with chlorine dioxide or chlorine integrated with UV disinfection, Water Res, 41 (2007) 1939-1948.

[258] B. Gottenbos, H.C. van der Mei, H.J. Busscher, [38] Models for studying initial adhesion and surface growth in biofilm formation on surfaces, in: J.D. Ron (Ed.) Methods in Enzymology, Academic Press, 1999, pp. 523-534.

[259] E.R. Cornelissen, D. Harmsen, K.F. de Korte, C.J. Ruiken, J.-J. Qin, H. Oo, L.P. Wessels, Membrane fouling and process performance of forward osmosis membranes on activated sludge, J Membrane Sci, 319 (2008) 158-168.

[260] A. Achilli, T.Y. Cath, E.A. Marchand, A.E. Childress, The forward osmosis membrane bioreactor: A low fouling alternative to MBR processes, Desalination, 239 (2009) 10-21.

[261] W.C.L. Lay, Q. Zhang, J. Zhang, D. McDougald, C. Tang, R. Wang, Y. Liu, A.G. Fane, Study of integration of forward osmosis and biological process: Membrane performance under elevated salt environment, Desalination, 283 (2011) 123-130.

[262] G. Sezonov, D. Joseleau-Petit, R. D'Ari, Escherichia coli physiology in Luria-Bertani broth, J Bacteriol, 189 (2007) 8746-8749.

[263] A. Ramesh, D.J. Lee, J.Y. Lai, Membrane biofouling by extracellular polymeric substances or soluble microbial products from membrane bioreactor sludge, Appl Microbiol Biot, 74 (2007) 699-707.

[264] Q.L. Li, M. Elimelech, Organic fouling and chemical cleaning of nanofiltration membranes: Measurements and mechanisms, Environ Sci Technol, 38 (2004) 4683-4693.

[265] C.Y.Y. Tang, Y.N. Kwon, J.O. Leckie, Effect of membrane chemistry and coating layer on physiochemical properties of thin film composite polyamide RO and NF membranes I. FTIR and XPS characterization of polyamide and coating layer chemistry, Desalination, 242 (2009) 149-167.

[266] V. Freger, J. Gilron, S. Belfer, TFC polyamide membranes modified by grafting of hydrophilic polymers: an FT-IR/AFM/TEM study, J Membrane Sci, 209 (2002) 283-292.

[267] P.S. Singh, A.P. Rao, P. Ray, A. Bhattacharya, K. Singh, N.K. Saha, A.V.R. Reddy, Techniques for characterization of polyamide thin film composite membranes, Desalination, 282 (2011) 78-86.

[268] Y.-N. Kwon, J.O. Leckie, Hypochlorite degradation of crosslinked polyamide membranes: II. Changes in hydrogen bonding behavior and performance, J Membrane Sci, 282 (2006) 456-464.

[269] O. Coronell, B.J. Marinas, X.J. Zhang, D.G. Cahill, Quantification of functional groups and modeling of their ionization behavior in the active layer of FT30 reverse osmosis membrane, Environ Sci Technol, 42 (2008) 5260-5266.

[270] O. Coronell, X.J. Zhang, M.I. Gonzalez, D.G. Cahill, B.J. Marinas, ENVR 119-Quantification of functional groups in FT30 (RO) membrane and modeling of their acid/base behavior, Abstr Pap Am Chem S, 235 (2008).

[271] A.E. Childress, M. Elimelech, Effect of solution chemistry on the surface charge of polymeric reverse osmosis and nanofiltration membranes, J Membrane Sci, 119 (1996) 253-268.

[272] S.R. Holmes-Farley, R.H. Reamey, T.J. McCarthy, J. Deutch, G.M. Whitesides, Acid-base behavior of carboxylic acid groups covalently attached at the surface of polyethylene: The usefulness of contact angle in following the ionization of surface functionality, Langmuir, 1 (1985) 725-740.

[273] O. Coronell, B.J. Mariñas, X. Zhang, D.G. Cahill, Quantification of Functional Groups and Modeling of Their Ionization Behavior in the Active Layer of FT30 Reverse Osmosis Membrane, Environ Sci Technol, 42 (2008) 5260-5266.

[274] M. Elimelech, W.H. Chen, J.J. Waypa, Measuring the Zeta (Electrokinetic) Potential of Reverse-Osmosis Membranes by a Streaming Potential Analyzer, Desalination, 95 (1994) 269-286.

[275] A. Tiraferri, M. Elimelech, Direct quantification of negatively charged functional groups on membrane surfaces, J Membrane Sci, 389 (2012) 499-508.

[276] C. Gomez-Suarez, J. Pasma, A.J. van der Borden, J. Wingender, H.C. Flemming, H.J. Busscher, H.C. van der Mei, Influence of extracellular polymeric substances on deposition and redeposition of Pseudomonas aeruginosa to surfaces, Microbiol-Sgm, 148 (2002) 1161-1169.

[277] J. Tourney, B.T. Ngwenya, The effect of ionic strength on the electrophoretic mobility and protonation constants of an EPS-producing bacterial strain, J Colloid Interf Sci, 348 (2010) 348-354.

[278] H. Schott, C.Y. Young, Electrokinetic Studies of Bacteria .1. Effect of Nature, Ionic-Strength, and Ph of Buffer Solutions on Electrophoretic Mobility of Streptococcus-Faecalis and Escherichia-Coli, J Pharm Sci, 61 (1972) 182-&.

[279] J. Li, L.A. McLandsborough, The effects of the surface charge and hydrophobicity of Escherichia coli on its adhesion to beef muscle, Int J Food Microbiol, 53 (1999) 185-193.

[280] H. Takruri, B. Ecanow, Interactions of surfactants with lipoproteins, Journal of Pharmaceutical Sciences, 55 (1966) 979-981.

[281] G.V. Sherbet, M.S. Lakshmi, Characterization of Escherichia-Coli Cell-Surface by Isoelectric Equilibrium Analysis, Biochim Biophys Acta, 298 (1973) 50-58.

[282] M. Elimelech, W.H. Chen, J.J. Waypa, Measuring the zeta (electrokinetic) potential of reverse osmosis membranes by a streaming potential analyzer, Desalination, 95 (1994) 269-286.

[283] I.S. Kim, N. Jang, The effect of calcium on the membrane biofouling in the membrane bioreactor (MBR), Water Res, 40 (2006) 2756-2764.

[284] X.Y. Yuan, liu. Yongseng, Leng. Baoxia, Mi, Molecular Dynamics Simulations of Hydrated Polyamide Membrane and Its Interactions with Alginate Langmuir, Under review (2013).

[285] G. Völgyi, E. Baka, K.J. Box, J.E.A. Comer, K. Takács-Novák, Study of pH-dependent solubility of organic bases. Revisit of Henderson-Hasselbalch relationship, Analytica Chimica Acta, 673 (2010) 40-46.

[286] V. Yangali-Quintanilla, Z.Y. Li, R. Valladares, Q.Y. Li, G. Amy, Indirect desalination of Red Sea water with forward osmosis and low pressure reverse osmosis for water reuse, Desalination, 280 (2011) 160-166.

[287] C.R. Martinetti, A.E. Childress, T.Y. Cath, High recovery of concentrated RO brines using forward osmosis and membrane distillation, J Membrane Sci, 331 (2009) 31-39.

[288] P.K. Park, S. Lee, J.S. Cho, J.H. Kim, Full-scale simulation of seawater reverse osmosis desalination processes for boron removal: Effect of membrane fouling, Water Res, 46 (2012) 3796-3804.

[289] M. Moonkhum, Y.G. Lee, Y.S. Lee, J.H. Kim, Review of seawater natural organic matter fouling and reverse osmosis transport modeling for seawater reverse osmosis desalination, Desalin Water Treat, 15 (2010) 92-107.

[290] A.E. Contreras, Z. Steiner, J. Miao, R. Kasher, Q.L. Li, Studying the Role of Common Membrane Surface Functionalities on Adsorption and Cleaning of Organic Foulants Using QCM-D (vol 45, pg 6309, 2011), Environ Sci Technol, 46 (2012) 5261-5261.

[291] S.X. Liu, J.T. Kim, Study of adsorption kinetics of surfactants onto polyethersulfone membrane surface using QCM-D, Desalination, 247 (2009) 355-361.

[292] A. Widjaya, T. Hoang, G.W. Stevens, S.E. Kentish, A comparison of commercial reverse osmosis membrane characteristics and performance under alginate fouling conditions, Sep Purif Technol, 89 (2012) 270-281.

[293] T. Hoang, G.W. Stevens, S.E. Kentish, The influence of feed pH on the performance of a reverse osmosis membrane during alginate fouling, Desalin Water Treat, 50 (2012) 220-225.

[294] S. Lee, W.S. Ang, M. Elimelech, Fouling of reverse osmosis membranes by hydrophilic organic matter: implications for water reuse, Desalination, 187 (2006) 313-321.

[295] H. Choi, Y. Kwon, J. Park, S. Hong, T. Tak, Enhancing the anti-fouling property of the SWRO membrane through the surface coating with the styrene-PEGA copolymer, Desalin Water Treat, 15 (2010) 183-189.

[296] R.L. McGinnis, N.T. Hancock, M.S. Nowosielski-Slepowron, G.D. McGurgan, Pilot demonstration of the NH3/CO2 forward osmosis desalination process on high salinity brines, Desalination, 312 (2013) 67-74.

[297] L. Chekli, S. Phuntsho, H.K. Shon, S. Vigneswaran, J. Kandasamy, A. Chanan, A review of draw solutes in forward osmosis process and their use in modern applications, Desalin Water Treat, 43 (2012) 167-184.

[298] D. Violleau, H. Essis-Tome, H. Habarou, J.P. Croue, M. Pontie, Fouling studies of a polyamide nanofiltration membrane by selected natural organic matter: an analytical approach, Desalination, 173 (2005) 223-238.

[299] G. Makdissy, P.M. Huck, M.M. Reid, G.G. Leppard, J. Haberkamp, M. Jekel, S. Peldszus, Investigating the fouling layer of polyamide nanofiltration membranes treating two different natural waters: internal heterogeneity yet converging surface properties, J Water Supply Res T, 59 (2010) 164-178.

[300] B.X. Mi, M. Elimelech, Silica scaling and scaling reversibility in forward osmosis, DESALINATION, 312 (2013) 75-81.

[301] Y.H. Mo, A. Tiraferri, N.Y. Yip, A. Adout, X. Huang, M. Elimelech, Improved Antifouling Properties of Polyamide Nanofiltration Membranes by Reducing the Density of Surface Carboxyl Groups, Environ Sci Technol, 46 (2012) 13253-13261.

[302] Y. Yang, H. Zhang, P. Wang, Q. Zheng, J. Li, The influence of nano-sized TiO2 fillers on the morphologies and properties of PSF UF membrane, J. Membr. Sci., 288 (2007) 231-238.

[303] S. Qiu, L. Wu, X. Pan, L. Zhang, H. Chen, C. Gao, Preparation and properties of functionalized carbon nanotube/PSF blend ultrafiltration membranes, J. Membr. Sci., 342 (2009) 165-172.

[304] Y.N. Yang, H.X. Zhang, P. Wang, Q.Z. Zheng, J. Li, The influence of nano-sized TiO2 fillers on the morphologies and properties of PSFUF membrane, J. Membr. Sci., 288 (2007) 231-238.

[305] L.Y. Ng, C.P. Leo, A.W. Mohammad, Optimizing the Incorporation of Silica Nanoparticles in Polysulfone/Poly(vinyl alcohol) Membranes with Response Surface Methodology, J Appl Polym Sci, 121 (2011) 1804-1814.

[306] S. Aslan, M. Deneufchatel, S. Hashmi, N. Li, L.D. Pfefferle, M. Elimelech, E. Pauthe, P.R. Van Tassel, Carbon nanotube-based antimicrobial biomaterials formed via layer-by-layer assembly with polypeptides, J Colloid Interf Sci, 388 (2012) 268-273.

[307] Y. Liu, E. Rosenfield, M. Hu, B. Mi, Direct Observation of Bacterial Deposition on and Detachment from Nanocomposite Membranes Embedded with Silver Nanoparticles, Water Res, (2013).

[308] S. Aslan, J. Maatta, B.Z. Haznedaroglu, J.P.M. Goodman, L.D. Pfefferle, M. Elimelech, E. Pauthe, M. Sammalkorpi, P.R. Van Tassel, Carbon nanotube bundling: influence on layer-by-layer assembly and antimicrobial activity, Soft Matter, 9 (2013) 2136-2144.

[309] F. Diagne, R. Malaisamy, V. Boddie, R.D. Holbrook, B. Eribo, K.L. Jones, Polyelectrolyte and Silver Nanoparticle Modification of Microfiltration Membranes To Mitigate Organic and Bacterial Fouling, Environ Sci Technol, 46 (2012) 4025-4033.

[310] S.Y. Lee, H.J. Kim, R. Patel, S.J. Im, J.H. Kim, B.R. Min, Silver nanoparticles immobilized on thin film composite polyamide membrane: characterization, nanofiltration, antifouling properties, Polym Advan Technol, 18 (2007) 562-568.

[311] S.L. Yu, W.X. Shi, Y. Lu, J.X. Yang, Characterization and anti-fouling performance of nano-Al2O3/PVDF membrane for Songhua River raw water filtration, Water Sci Technol, 64 (2011) 1892-1897.

[312] M. Kazemimoghadam, T. Mohammadi, A modeling approach based on the Maxwell-Stefan theory for pervaporation using home made nanopore NaA zeolite membranes, Desalination, 281 (2011) 298-305.

[313] A.M.P. McDonnell, D. Beving, A. Wang, W. Chen, Y. Yan, Hydrophilic and Antimicrobial Zeolite Coatings for Gravity-Independent Water Separation, Adv Funct Mater, 15 (2005) 336-340.

[314] D.E. Beving, C.R. O'Neill, Y. Yan, Hydrophilic and antimicrobial low-silica-zeolite LTA and high-silica-zeolite MFI hybrid coatings on aluminum alloys, Micropor Mesopor Mat, 108 (2008) 77-85.

[315] M.L. Lind, A.K. Ghosh, A. Jawor, X. Huang, W. Hou, Y. Yang, E.M.V. Hoek, Influence of Zeolite Crystal Size on Zeolite-Polyamide Thin Film Nanocomposite Membranes, Langmuir, 25 (2009) 10139-10145.

[316] M.L. Lind, B.H. Jeong, A. Subramani, X.F. Huang, E.M.V. Hoek, Effect of mobile cation on zeolite-polyamide thin film nanocomposite membranes, J Mater Res, 24 (2009) 1624-1631.

[317] R. Han, S. Zhang, C. Liu, Y. Wang, X. Jian, Effect of NaA zeolite particle addition on poly(phthalazinone ether sulfone ketone) composite ultrafiltration (UF) membrane performance, J. Membr. Sci., 345 (2009) 5-12.

[318] C.J. Liao, P. Yu, J.Q. Zhao, L.M. Wang, Y.B. Luo, Preparation and characterization of NaY/PVDF hybrid ultrafiltration membranes containing silver ions as antibacterial materials, DESALINATION, 272 (2011) 59-65.

[319] M. Carter, P.S. Ho, Assaying the Energies of Biological Halogen Bonds, Crystal Growth & Design, 11 (2011) 5087-5095.

[320] Y.M. Kim, S.J. Lee, I.J. Kim, Synthesis and characterization of TMA-A zeolite nanocrystals, J Ceram Process Res, 8 (2007) 103-105.